THEORETICAL STUDIES ON CLUSTER COMPOUNDS

by

Zhenyang Lin

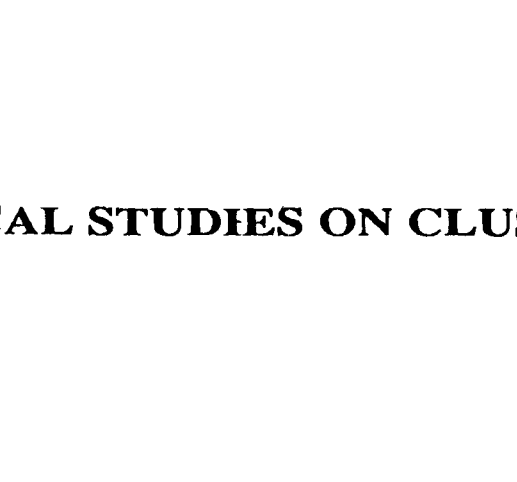
Thesis submitted in part fulfilment of

the requirement for the degree of

Doctor of Philosophy

at the

University of Oxford



St, Hugh's College

Oxford

September 1989

To my wife, Nong, and my parents

Theoretical Studies on Cluster Compounds

Zhenyang Lin — **St. Hugh's College**
Doctor of Philosophy — **Trinity Term 1989**

ABSTRACT

This Thesis describes some theoretical studies on ligated and bare clusters.

Chapter 1 gives a review of the two theoretical models, **Tensor Surface Harmonic Theory (TSH)** and **Jellium Model**, accounting for the electronic structures of ligated and bare clusters. The **Polyhedral Skeletal Electron Pair Theory (PSEPT)**, which correlates the structures and electron counts (total number of valence electrons) of main group and transition metal ligated clusters, is briefly described.

A structural jellium model is developed in **Chapter 2** which accounts for the electronic structures of clusters using a crystal-field perturbation. The zero-order potential we derive is of central-field form, depends on the geometry of the cluster, and has a well-defined relationship to the full nuclear-electron potential. Qualitative arguments suggest that this potential produces different energy level orderings for clusters with a nucleus with large positive charge at the centre of the cluster, enabling the spherical jellium model to be applied to alkali metal clusters seeded with magnesium and zinc. Analysis of the effects of the non-spherical perturbation on the spherical jellium shell structures leads to the conclusion that for a cluster with a closed shell electronic structure a high symmetry arrangement which is approximately or precisely close packed will be preferred. It also provides a basis for rationalising those structures, which have been predicted using *ab initio* calculations, of clusters with incomplete shell electronic configurations

In **Chapter 3**, the geometric conclusions derived in the structural jellium model are developed in more detail. Alkali metal clusters with closed shell electronic configurations according to the jellium model adopt geometries of high symmetry and based on the T_d, O_h and I_h point groups. For high nuclearity clusters alternative high symmetry structures can occur and those which are either the most close packed or spherical are predicted to be the most stable. When the jellium closed shell "magic numbers" coincides with one of these high symmetry structures then the cluster will be particularly stable.

The group theoretical consequences of the Tensor Surface Harmonic Theory are developed in **Chapter 4** for $[ML_2]_n$, $[ML_4]_n$ and $[ML_5]_n$ clusters where either the xz and yz or x^2-y^2 and xy components to L_d^π and L_d^δ do not contribute equally to the bonding. The closed shell requirements for such clusters are defined and the orbital symmetry constraints pertaining to the interconversion of conformers of these clusters are described.

In **Chapter 5** Stone's Tensor Surface Harmonic methodology is applied to high nuclearity transition metal carbonyl cluster compounds with 13-44 metal atoms. Two limiting bonding situations are identified and represented in terms of general electron counting rules. If the radial bonding effects predominate the clusters are characterised by $12n_s+\Delta_i$

valence electrons, where Δ_i is the characteristic electron count of the interstitial moiety. If radial and tangential bonding effects are important then the total number of valence electrons is $12n_s+2(s_s+s_i-1)$, where s_s and s_i are the number of skeletal bonding molecular orbitals associated with surface (s_s) and interstitial (s_i) moieties.

Chapter 6 develops a new theoretical framework to account for the bonding in the high nuclearity ligated clusters with columnar topologies. The wavefunctions of columnar metal clusters can be expressed as an expansion based on the particle on the cylinder problem. This bonding analysis is applied to clusters containing columns of triangles and squares.

In **Chapter 7** the origin of non-bonding orbitals in molecular compounds is reviewed and analysed using general quantum mechanical considerations. A combination of the pairing theorem and a group theoretical analysis leads to a definition of the number of the non-bonding molecular orbitals in co-ordination, polyene and cluster compounds. The non-bonding molecular orbitals have been generated by defining the nodal characteristics of the relevant orbitals and evaluating the solutions under the appropriate boundary conditions. The stereochemical role of non-bonding molecular orbitals in co-ordination compounds is also discussed.

The work described in this Thesis was carried out in the Inorganic Chemistry Laboratory of the University of Oxford from October 1986 to August 1989 under the supervision of Dr. D. Michael P. Mingos. All the work is my own, unless stated to the contrary, and it has not previously been submitted for a degree at this or any other University.

The author's signature has been removed from this version of the thesis.

ACKNOWLEDGEMENTS

I wish to thank my supervisor, Dr. D. Michael P. Mingos, for his invaluable ideas, help, advice and encouragement throughout the past three years.

I am indebted to Drs. Roy L.Johnston and J.F.Halet for offering their guidance and also to Drs. Ian William, Osayi Ezomo, John Jeffrey, Mr. Mike Watson and Mr. Johnathan Machell for their help and friendship in my earlier days. I would like to thank my fellow theoreticians, Drs. Tom Slee, David Wales and Mr. Andy Payne for many stimulating discussions on aspects of theoretical chemistry.

I should also like to thank various members of the Mingos' group, past and present, who have given me so much help. I'd particularly like to thank Mike Watson, David Baghurst, Andy Rohl and Tony Stolberg for proof reading this Thesis; Andy May and Andy Rohl for computer advice; Andy Burrows, Curt Lamberth, Roy Copley, Don Murphy, Jenny Forward and Selina Renolds for their help and friendship.

Finally, I'd like to express my thanks to my wife, Nong Chen, for her love, patience and understanding.

Dr P.A.Cox's comments on the particle on a cylinder problem and the group theoretical aspects of Möbius rings were also most helpful.

List of Publications

1. Lin Zhenyang and D.Michael P.Mingos,
   "Theoretical analysis of cluster compounds with cylindrical topologies",
   J. Organomet. Chem., **399**, 367(1988).

2. D.Michael P.Mingos and Lin Zhenyang,
   "Molecular orbital analysis of some carbonyl cluster compounds with close-packed metallic arrangements",
   J. Organomet. Chem., **341**, 523(1988).

3. D.Michael P.Mingos and Lin Zhenyang,
   "A Theoretical Analysis of High Nuclearity Metal Carbonyl Clusters",
   J. Chem. Soc., Dalton Trans., 1657(1988).

4. D.Michael P.Mingos and Lin Zhenyang,
   "Group theoretical paradigm for defining the non-bonding molecular orbitals",
   New J. Chem., **12**, 787(1988).

5. Roy L.Johnston, Lin Zhenyang and D.Michael P.Mingos,
   "The tensor surface harmonic-equivalent orbital model for bonding in polyhedral cluster molecules",
   New. J. Chem., **13**, 33(1989).

6. D.Michael P.Mingos and Lin Zhenyang,
   "Non-bonding orbitals in co-ordination, hydrocabon and cluster compounds",
   Structure and Bonding, **73**, 1(1989).

7. Tom Slee, Lin Zhenyang and D.Michael P.Mingos
   "Polyhedral Skeletal Electron Pair Theory of Bare Clusters 1: Small Silicon Clusters"
   Inorg. Chem. **28**, 2256(1989).

8. D.Michael P.Mingos and Lin Zhenyang,
   "A group theoretical paradigm for describing the skeletal molecular orbitals of cluster compounds. Part 3."
   Z.Phys.D - Atoms, Molecules and Clusters, **12**, 53(1989).

9. David J.Wales, D.Michael P.Mingos and Lin Zhenyang,
   "Skeletal rearrangements in clusters. 2",
   Inorg. Chem. **28**, 2754(1989).

10. D.Michael P.Mingos and Lin Zhenyang,
"Hybridisation schemes for co-ordination and organometallic compounds",
accepted by <Structure and Bonding>.

11. Lin Zhenyang, Tom Slee and D. Michael P.Mingos
"A Structural Jellium Model of Cluster Electronic Structures"
submitted to Chem. Phys.

12. D.Michael P.Mingos and Lin Zhenyang
"Structural Consequences of the Jellium Model for Alkali Metal Clusters"
Chem. Phys. in press

13. D. Michael P.Mingos and Lin Zhenyang
"Site Prefernce Effects in Heterometallic Clusters"
accepted by Comment on Inorganic Chemistry

14. D.Michael P.Mingos, Tom Slee and Lin Zhenyang
"Bonding Models for Ligated and Bare Clusters"
submitted.

15. David J.Wales, D.Michael P.Mingos, Tom Slee and Lin Zhenyang
"Clusters in Inorganic and Molecular Beam Chemistry, Some Unifying Principles"
submitted

CONTENTS

Chapter 1 Bonding Models in Ligated and Bare Clusters 1

1.1 Introduction 1

1.2 Jellium Model 2

1.3 Polyhedral Skeletal Electron Pair Theory (PSEPT) 5

1.4 Tensor Surface Harmonic (TSH) Theory 8

1.5 Application of TSH Theory 12

1.6 Aims of this Thesis 14

References for Chapter One 16

Chapter 2 A Structural Jellium Model of Cluster Electronic Structure 18

2.1 Introduction 18

2.2 A Structural Spherical Jellium Model 19

2.2.1 The Hamiltonian 19

2.2.2 The Central Field Potential 21

2.2.3 Effect of the Central Field Potential on the Structures of Clusters 26

2.3 First-order Perturbation of the Spherical Jellium Energies 28

2.3.1 The General Aspects of the Splitting of Shells 29

2.3.2 Structures of "Closed Shell" Metal Clusters 32

2.4 Clusters with Incomplete Shell Structures 34

2.4.1 Clusters with Less Than 8 Valence Electrons 34

2.4.2 Clusters with More Than 8 Valence Electrons 39

2.5 Conclusions 46

2.6 Appendix 46

References for Chapter Two 48

Chapter 3 Structural Consequences of the Jellium Model for Alkali Metal Clusters 50

3.1 Introduction 50

3.2 Geometric Conclusions for Alkali Metal Clusters 51

3.3 Orbital Splittings for the Most Close Packed and Spherical Structures 51

3.4 Close Packed and Spherical High Symmetry Structures 55

3.4.1 Close Packed Structures 58

3.4.2 Spherical Geometries 62

3.5 Conclusions 69

References for Chapter Three 70

Chapter 4 A Group Theoretical Paradigm for Describing the Skeletal Molecular Orbitals of Cluster Compounds Deriving From ML_2, ML_4 and ML_5 Fragments 71

4.1 Introduction 71

4.2 ML_2 and ML_4 C_{2v} Fragments 72

4.3 L^{δ} and $\bar{L}^{\delta}$ Inequivalences in ML_5 Fragments 80

References for Chapter Four 92

Chapter 5 A Theoretical Analysis of High Nuclearity Metal Carbonyl Clusters 94

5.1 Introduction 94

5.2 Bonding Analysis 97

5.2.1 The Bonding in High Nuclearity Clusters with One Interstitial Atom 97

5.2.2 The Bonding in High Nuclearity Clusters with a Deltahedral Interstitial Moiety 104

5.2.3 The Bonding in High Nuclearity Clusters with Two or Three Interstitial Atoms 109
5.2.4 The Bonding in High Nuclearity Clusters with More Complex Interstitial Moieties 116
5.3 Conclusions 120
5.4 Appendix 121
References for Chapter Five 122

Chapter 6 Theoretical Analysis of Cluster Compounds with Cylindrical Topologies 124
6.1 Introduction 124
6.2 MO Wavefunctions and Energies for Columnar Clusters 126
6.2.1 MO Wavefunctions 126
6.2.2 MO Energies 128
6.3 Orbital Interactions 131
6.3.1 σ orbitals 131
6.3.2 π Interactions 132
6.3.3 σ and π Mixings 135
6.3.4 d_δ Interactions 141
6.3.5 Discussion 142
6.4 MO Calculations on Cylindrical Clusters 149
6.5 Applications 156
6.6 Summary 156
6.7 Appendix 158
References for Chapter Six 159

Chapter 7 Non-bonding Orbitals in Coordination, Hydrocarbon and Cluster Compounds 161

7.1 Introduction 161

7.2 Non-bonding Orbitals in Molecular and Coordination Compounds, ML_n 164

7.2.1 Expansion of the Ligand Set as Spherical Harmonic Functions 165

7.2.2 The m-n Rule 171

7.2.3 The Pairing Theorem 174

7.2.4 Group Theoretical Aspects 178

7.2.5 The Effects of Geometric Changes 182

7.2.6 More Quantitative Analysis of the Effects of s-p-d Separations ($\alpha_s \neq \alpha_p \neq \alpha_d$) 197

7.2.7 Generation of Non-bonding Orbitals 203

7.2.8 Summary 206

7.3 Non-bonding Orbitals in Hydrocarbons 214

7.3.1 Alternant Hückel Hydrocarbons 214

7.3.2 Alternant Möbius Hydrocarbons 220

7.4 Non-bonding Orbitals in Cluster Compounds 221

7.4.1 Expansion of the Cluster Skeletal Molecular Orbitals in terms of the Tensor Surface Harmonic Functions 221

7.4.2 Pairing Principle and Group Theoretical Aspects 223

7.4.3 Non-bonding Orbitals in closo Deltahedral and Three-connected Cluster Compounds 224

7.4.4 Non-bonding Orbitals in nido Structures 227

7.5 Summary 243

References for Chapter Seven 249

ABBREVIATIONS

L	two electron ligand
R	alkyl group
Me	methyl
Et	ethyl
Pr^i	*iso*-propyl
Bu^t	tertiary-butyl
Ph	phenyl
Cp	η^5-C_5H_5
MO	molecular orbital
hy	hybrid orbital
HOMO	highest occupied molecular orbital
LUMO	lowest unoccupied molecular orbital
SEP	skeletal electron pair
LCAO	linear combination of atomic orbital
TSH	Tensor Surface Harmonic
PSEPT	Polyhedral Skeletal Electron Pair Theory

Chapter 1. Bonding Models in Ligated and Bare Clusters

1.1 Introduction

During the last twenty years, cluster molecules have attracted a great deal of attention in experimental and theoretical investigations because of their potential catalytic applications, both as models for understanding catalytic surfaces[1,2] and as catalysts in their own right.[3] Ligated clusters with up to 44 skeletal metal atoms have been characterised in the solid state using single-crystal X-ray crystallographic techniques.[4,5] This has provided detailed structural information on the geometries and bond lengths associated with both the metal skeleton and the ligand shell. More recently, physicists and chemists have shown an interest in bare clusters produced in molecular beam experiments and probed primarily by mass spectrometry.[6,7]

Theoretically, the studies have concentrated on the relationship between their geometries, their electronic structures and their relative stabilities. For ligated clusters, the geometries of cluster molecules have been systematised by a set of simple rules described collectively as the **Polyhedral Skeletal Electron Pair Theory (PSEPT)** which accounts for the relationship between the skeletal structure and the total number of valence electrons in the clusters.[8] This PSEPT has been successfully underpinned by Stone's **Tensor Surface Harmonic (TSH) Theory.**[9] For bare alkali metal clusters generated in a supersonic expansion with argon carriers, large peaks corresponding to 8, 20, 40, 58 and 92 alkali metal atoms have been observed in mass spectra.[10,11] These magic numbers have been successfully rationalised using the **Spherical Jellium Model**, a simple one-electron spherical potential model.[10]

The success of the TSH theory and the jellium models for

rationalising the bonding in cluster molecules has prompted us to investigate their inter-relationships. Both methods are based on a spherical symmetry approximation and the TSH theory is a combination of LCAO molecular orbital methods and a free electron particle on a sphere model.

1.2 Jellium Model[10]

The "magic numbers" observed in molecular beam experiments are particularly evident in the mass spectral data for alkali metal clusters. The simplest model, which has successfully predicted several of the magic numbers for these clusters by associating these nuclearities with closed-shell electron counts, is the spherical jellium model of Knight et al.[10] This model postulates that the electronic structure of free electron metal clusters may be approximately described by considering only the energies of the valence electrons in a smooth potential, without specific information about the positions of the atomic cores.

Knight and coworkers' original investigation employed a central field potential of the form:[10]

$$V_O(r) = -U_O/\{\exp[(r-r_O)/\varepsilon]+1\}$$

where U_O is the sum of the Fermi energy and the work function of the bulk and r_O is the effective radius of the cluster sphere and assumed to be $r_s N^{1/3}$ (where r_s is the radius of a sphere containing one electron in the bulk). The parameter ε was taken as 1.5au in their calculations. This potential is a finite well with rounded sides, and is illustrated in Figure 1.1.

A crucial feature of the model is the separation of the Schrödinger equation into radial and angular parts, for it is this separation that

yields the shell structure. The angular solutions are the spherical harmonics. The jellium wavefunctions can be written:

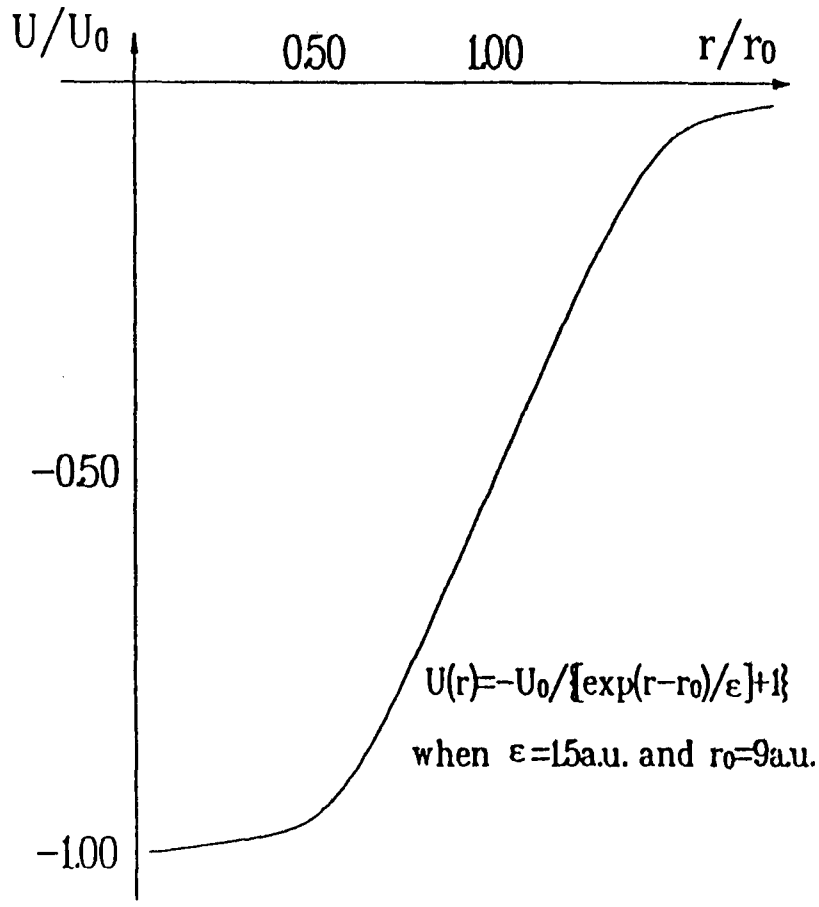


Figure 1.1 Knight's central field potential

$$\psi_{nlm} = f_{nl}(r)Y_{lm}(\theta,\varphi)$$

where $Y_{lm}(\theta,\varphi)$ is a spherical harmonic and $f_{nl}(r)$ depends on the form of the central field potential. The wavefunctions can thus be labelled by a principal quantum number (n) and the angular quantum numbers (l and m). In Knight's calculations, the energy level order for this one-electron model is:

$$1s < 1p < 1d < 2s < 1f < 2p < 1g < 2d < 3s < 1h \ldots$$

(note that for non-coulombic potentials the wavefunctions may be written so that a given n has all positive integers l associated with it). Each shell, specified by n and l, has an orbital degeneracy of $(2l+1)$, the

individual states being labelled by m. Electronic shell closings thus occur at 2, 8, 18, 20, 34, 40, 58, 68, 70, 92, ... Mass spectra revealed larger peaks for masses corresponding to 8, 20, 40, 58 and 92 atoms for neutral sodium and potassium clusters produced in a supersonic expansion with argon carrier gas. All these values are consistent with the spherical jellium model.

There has been debate over the significance and usefulness of the spherical jellium model.[12] Such a simple model does, of course, have several weaknesses and limitations. First, it does not make any predictions concerning the electronic structures of "non-magic number" clusters although the model makes predictions concerning the electronic structure of those clusters with "closed shells". The approximation of a spherical potential leads to stable configurations for closed shells, but not for non-closed shells. We may expect the potential to alter "shape" for non-closed shell clusters. Such a distortion perturbs the electronic energy levels, splitting the high degeneracy associated with spherical symmetry. Such a splitting would be expected to stabilise clusters with partially filled shells. Secondly, the model obviously predicts too many "magic numbers". The electronic closed-shell requirement appears to be necessary, but not sufficient criterion for accounting for the mass spectral data. A third limitation is that the energy level ordering of the jellium model does not fit the observations for several mixed clusters. For example, the MgK_n system[12] shows evidence for a particularly stable cluster at 10 valence electrons: MgK_8.

These limitations have prompted extensions to the original spherical jellium model. Baladron and Alonso[13] replaced the jellium potential with a background positive charge density, of spherical symmetry but varying with radial distance from the centre, in order to explain the electronic

structure of closed-shell clusters such as MgK_8. Clemenger[14] removed the restriction of spherical symmetry, employing a perturbation harmonic oscillator model and allowing one degree of freedom, the ratio of the z force constant k_z to the (degenerate) x and y force constant $k_{x,y}$, to yield oblate ($k_z>k_{x,y}$) and prolate ($k_z<k_{x,y}$) shaped potential wells. We have explored the relationship of the spherical jellium model (and its extension to oblate/prolate shapes) to the crystal field expansion of the nuclear-electron potential, and so clarified the relationship of the jellium model to nuclear configuration. These extensions have extended the scope and removed some of the limitations of the original model, and are discussed in subsequent chapters.

1.3 Polyhedral Skeletal Electron Pair Theory (PSEPT) [8]

A set of rules has been proposed by Mingos and Wade for correlating the structures and electron counts (total number of valence electrons) of main group and transition metal ligated clusters. A brief summary of these rules is given below: (n indicates the number of skeletal atoms in the clusters). Johnston and Mingos have given a more detailed account of the historical development of these rules and their applications.[8]

(1) Main group/transition metal ring compounds have a total of 6n/16n valence electrons.

(2) Main group/transition metal three connected cluster compounds have 5n/15n valence electrons.

(3) If a skeletal transition metal atom occupying a vertex position is replaced by a main group atom then the characteristic number of valence electrons is reduced by 10.

(4) Main group/transition metal four connected clusters are characterised by a total of 4n+2/14n+2 valence electrons, so long as the n vertex atoms lie approximately on a spherical surface.

(5) Main group/transition metal *closo, nido* and *arachno* deltahedral molecules are characterised by $4n+2/14\overset{n}{\underset{\wedge}{+}}2$, 4n+4/14n+4 and 4n+6/14n+6 valence electrons respectively.

(6) The total electron count of a condensed cluster is equal to the sum of the electron counts of the parent clusters minus the electron count characteristic of the $\overset{m}{\underset{\wedge}{\text{co}}}$mon atom, pair of atoms or face of atoms. These characteristic electron counts are 18 for a shared metal vertex, 34 for a shared edge of metal atoms, 48 for a shared metal triangle and 62 for a shared metal square.

A specific case of these condensation rules is the capping principle.

Capping Principle: Edge-bridging a polyhedral cluster results in an increment in the valence electron count by 14 (transition metal). Face-capping results in an increment in the valence electron count by 12 (transition metal).

It should be noted that the difference between main group and transition metal ligated clusters in electron count is 10n when both clusters have$^{\text{the}}$ same skeletal structure. This means that the five d orbitals are not significant for the electron count although they are involved in the metal-metal bonds. This has been explained in terms of the isolobal relationship[15] between AH (A: boron or carbon) and ML_3 (M: transition metal atom; L: ligand) fragments. Both fragments have three frontier fragment orbitals, shown in Figure 1.2, for skeletal bonding for clusters. Except the three frontier fragment orbitals, the occupation of the remaining bonding and non-bonding orbitals leads to 2n electrons for main group fragments and 12n electrons for transition metal fragments. The bonding and non-bonding molecular orbitals derived from the common three frontier orbitals of both main group and

transition metal fragments are defined as the skeletal bonding and non-bonding orbitals. The occupation of these skeletal bonding and non-bonding orbitals leads to the closed-shell electronic requirements for ligated cluster compounds. Alternatively, we can conclude that both main group and transition metal ligated clusters have the same number of skeletal electron pairs as long as they possess the same skeletal geometries. For example, deltahedral (or 4-connected) main group and transition metal clusters are characterised by a total of n+1 skeletal electron pairs and 3-connected clusters by a total of 3n/2 skeletal electron pairs.

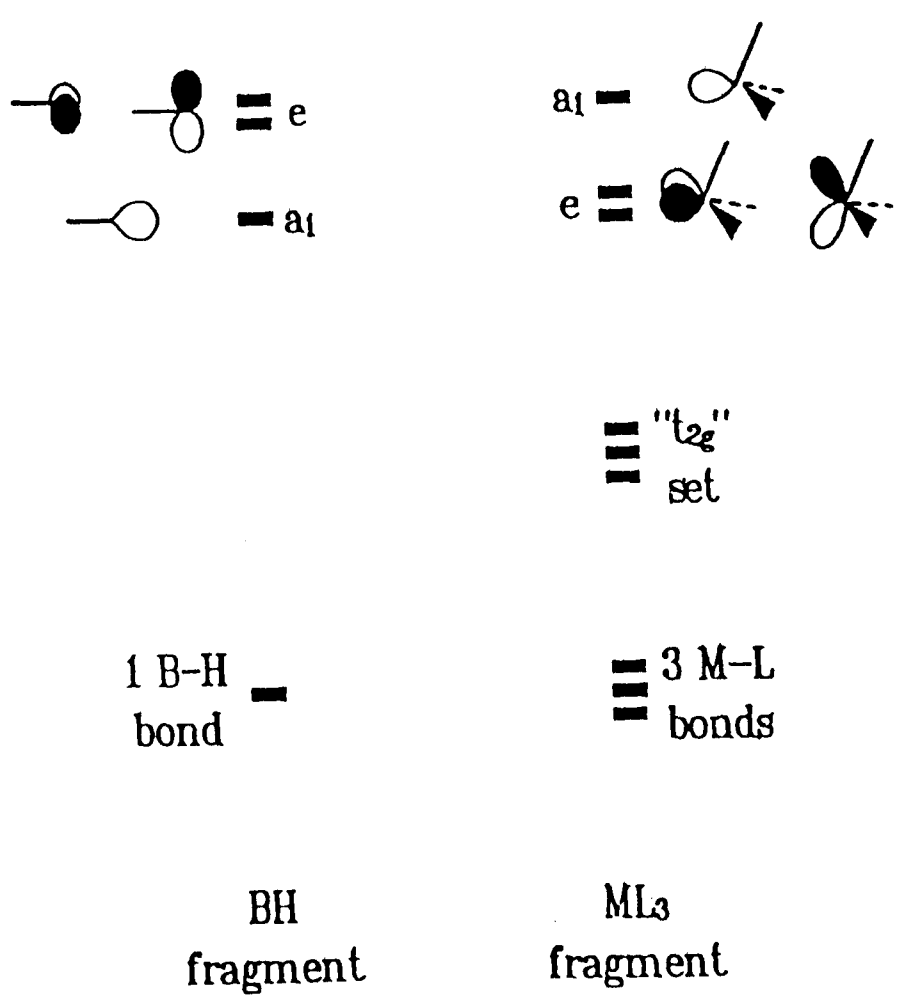


Figure 1.2 Isolobal relationship between BH and ML_3 fragments

1.4 Tensor Surface Harmonic Theory[9]

Recently, an elegant approach to the bonding in clusters has been developed by Stone,[9] whose **Tensor Surface Harmonic Theory** derives cluster molecular orbitals as expansions of scalar, vector and tensor spherical harmonic functions. The molecular orbitals are generated from basis sets with 0(σ), 1(π) and 2(δ) nodes with respect to a radial vector passing through the atoms, as shown in Figure 1.3.

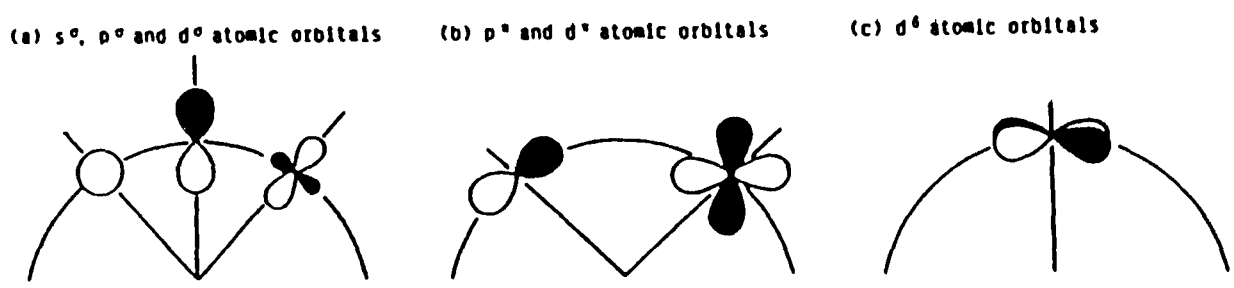


Figure 1.3 σ-, π- and δ- atomic orbitals used in the construction of cluster molecular orbitals.

For a basis set of σ orbitals (see Figure 1.3a), the LCAO can be expressed in terms of a spherical harmonic expansion:

$$\psi^{\sigma}_{LM} = L^{\sigma}_{M} = N \sum_{i} C_{L,M}(\theta_i,\varphi_i)\ \sigma_i$$

(M=0,1c,1s,2c,2s,... and L=S,P,D,...)

where θ_i and φ_i represent the location of the ith skeletal atom in spherical polar coordinates, N is a normalising constant, and C_{LM} is a modified spherical harmonic wavefunction, $C_{L,M}=[4\pi/(2L+1)]^{1/2}Y_{L,M}$. The modified spherical harmonic functions are given in Table 1.1. For those functions with imaginary solutions the real solutions are obtained by taking linear combinations of complementary components, i.e.

$$C_{L,Mc} = (1/2)^{1/2} [(-1)^M C_{L,M} + C_{L,-M}]$$
$$C_{L,Ms} = (1/2)^{1/2} [(-1)^M C_{L,M} - C_{L,-M}]$$

Table 1.1 Polar forms of the modified spherical harmonic functions

C_{lm}	Polar form
C_{00}	1
C_{10}	$\cos\theta$
C_{11c}	$\sin\theta\cos\varphi$
C_{11s}	$\sin\theta\sin\varphi$
C_{20}	$1/2(3\cos^2\theta-1)$
C_{21c}	$(3)^{1/2}\cos\theta\sin\theta\cos\varphi$
C_{21s}	$(3)^{1/2}\cos\theta\sin\theta\sin\varphi$
C_{22c}	$(3/4)^{1/2}\sin^2\theta\cos2\varphi$
C_{22s}	$(3/4)^{1/2}\sin^2\theta\sin2\varphi$
C_{30}	$1/2(5\cos^3\theta-3\cos\theta)$
C_{31c}	$(3/8)^{1/2}\sin\theta(5\cos^2\theta-1)\cos\varphi$
C_{31s}	$(3/8)^{1/2}\sin\theta(5\cos^2\theta-1)\sin\varphi$
C_{32c}	$(15/4)^{1/2}\cos\theta\sin^2\theta\cos2\varphi$
C_{32s}	$(15/4)^{1/2}\cos\theta\sin^2\theta\sin2\varphi$
C_{33c}	$(5/8)^{1/2}\sin^3\theta\cos3\varphi$
C_{33s}	$(5/8)^{1/2}\sin^3\theta\sin3\varphi$

In this fashion the linear combinations are assigned quantum numbers L and M which are related to those which have been defined for the S, P and D functions derived for a particle on a sphere problem.

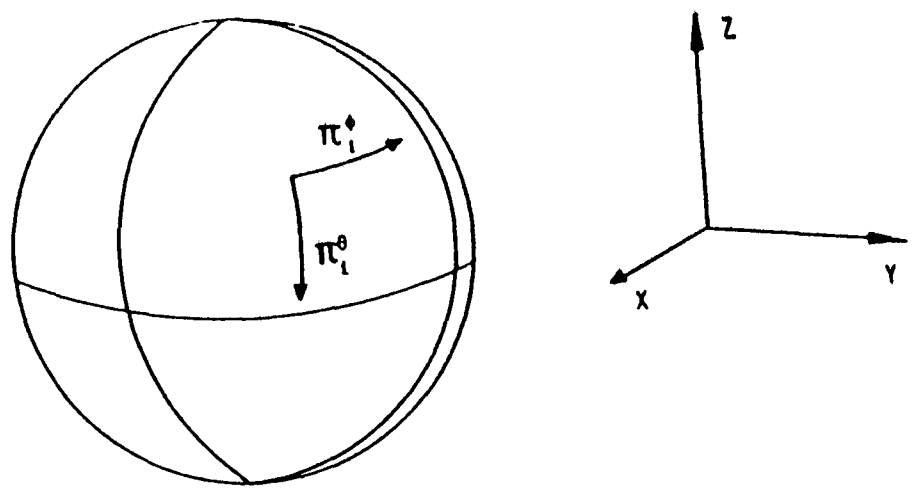


Figure 1.4 Unit vectors on the surface of the cluster sphere

For a basis set of π-orbitals, the LCAO expansions are derived from the sets of π_i^θ and π_i^φ orbitals which are defined in Figure 1.4 (also see Figure 1.3b) and have the following form:

$$\psi^\pi_{LM} = L^\pi_M = N \sum_i [V^\theta_{LM}(\theta_i,\varphi_i)\pi^\theta_i + V^\varphi_{LM}(\theta_i,\varphi_i)\pi^\varphi_i]$$

where (V^θ_{LM}, V^φ_{LM}) are Vector Surface Harmonics. For M>0 the real forms of the Vector Surface Harmonics $V^{\theta,\varphi}_{LMs}/V^{\theta,\varphi}_{LMc}$ are used and listed in Table 1.2. The above L^π wavefunctions are called even parity functions. The corresponding odd parity wavefunctions $\bar{\psi}^\pi_{LM}$ ($\bar{L}^\pi$) are related to $\psi^\pi{}_{LM}$ (L^π) by a 90° anticlockwise rotation of the tangential vectors (π^θ_i, π^φ_i) about the radial vector at each vertex. Therefore, the wavefunctions of $\bar{L}^\pi$ have the following form:

$$\bar{\psi}^\pi{}_{LM} = \bar{L}^\pi_M = N \sum_i [V^\varphi_{LM}(\theta_i,\varphi_i)\pi^\theta_i - V^\theta_{LM}(\theta_i,\varphi_i)\pi^\varphi_i]$$

Table 1.2. Even vector harmonics.

Y_{lm}^{π}	V^{θ} component	V^{φ} component
p_O^{π}	$-\sin\theta$	0
p_{1s}^{π}	$\cos\theta\sin\varphi$	$\cos\varphi$
p_{1c}^{π}	$\cos\theta\cos\varphi$	$-\sin\varphi$
d_O^{π}	$-3/2\sin2\theta$	0
d_{1s}^{π}	$3^{1/2}\cos2\theta\sin\varphi$	$3^{1/2}\cos\theta\cos\varphi$
d_{1c}^{π}	$3^{1/2}\cos2\theta\cos\varphi$	$-3^{1/2}\cos\theta\sin\varphi$
d_{2s}^{π}	$(3/4)^{1/2}\sin2\theta\sin2\varphi$	$3^{1/2}\sin\theta\cos2\varphi$
d_{2c}^{π}	$(3/4)^{1/2}\sin2\theta\cos2\varphi$	$-3^{1/2}\sin\theta\sin2\varphi$
f_O^{π}	$-3/2\sin\theta(5\cos^2\theta-1)$	0
f_{1s}^{π}	$(3/8)^{1/2}\cos\theta(15\cos^2\theta-11)\sin\varphi$	$(3/8)^{1/2}(5\cos^2\theta-1)\cos\varphi$
f_{1c}^{π}	$(3/8)^{1/2}\cos\theta(15\cos^2\theta-11)\cos\varphi$	$-(3/8)^{1/2}(5\cos^2\theta-1)\sin\varphi$
f_{2s}^{π}	$(15/4)^{1/2}\sin\theta(3\cos^2\theta-1)\sin2\varphi$	$(15/4)^{1/2}\sin2\theta\cos2\varphi$
f_{2c}^{π}	$(15/4)^{1/2}\sin\theta(3\cos^2\theta-1)\cos2\varphi$	$-(15/4)^{1/2}\sin2\theta\sin2\varphi$
f_{3s}^{π}	$(3/4)(10)^{1/2}\sin^2\theta\cos\theta\sin3\varphi$	$(3/4)(10)^{1/2}\sin^2\theta\cos3\varphi$
f_{3c}^{π}	$-(3/4)(10)^{1/2}\sin^2\theta\cos\theta\cos3\varphi$	$(3/4)(10)^{1/2}\sin^2\theta\sin3\varphi$

Stone has shown that for deltahedral clusters the L^{π} MOs are generally bonding, and therefore $\bar{L}^{\pi}$ MOs generally antibonding.

$$L_M^{\pi}(\text{bonding}) \underset{\text{operation}}{\overset{\text{parity}}{<\!\text{--------}\!>}} \bar{L}_M^{\pi}(\text{antibonding})$$

For a set of δ atomic orbitals (see Figure 1.3c), the LCAO expansions are derived from the sets of ($d_\theta 2_{-\varphi} 2$, $d_{\theta\varphi}$) orbitals and they have the following form:

$$\psi^{\delta}_{LM} = L^{\delta}_{M} = N \sum_{i} [T^{\theta\theta}_{LM}(\theta_i,\varphi_i) d_\theta 2_{-\varphi} 2(i) + T^{\theta\varphi}_{LM}(\theta_i,\varphi_i) d_{\theta\varphi}(i)]$$

where ($T^{\theta\theta}_{LM}$, $V^{\theta\varphi}_{LM}$) are now Tensor Surface Harmonics.In a similar fashion, the corresponding odd parity wavefunctions $\bar{\psi}^{\delta}_{LM}$ ($\bar{L}^{\delta}$) are related to ψ^{δ}_{LM} (L^{δ}) by a 45° (not 90°) anticlockwise rotation of the tangential δ sets about the radial vector, at each vertex.

By employing the scalar, vector and tensor harmonics, Stone[9] derived the (2n+1) and (7n+1) cluster valence electron pairs for deltahedral main group and transition metal clusters respectively. This aspect will be discussed further in a subsequent section.

1.5 Application of TSH Theory

Many applications of the TSH theory have been developed since 1980 when the TSH theory was first proposed by Stone [9] and a brief summary of these results is given below.

Stone[9] has shown that for deltahedral clusters the L^{π} MOs are generally bonding. The $\bar{L}^{\pi}$ MOs are, therefore, generally antibonding, since the parity inversion operation leads to a reversal of the bonding properties of L^{π} and $\bar{L}^{\pi}$. He used the methodology of Tensor Surface Harmonic theory to derive the n+1 skeletal electron pair rule for deltahedral boranes. Each of the n BH fragments possesses one σ-type sp hybrid, yielding nL^{σ} MOs in total, one of which (S^{σ}) is strongly bonding because it possesses no angular nodes. In addition each fragment has two π-type p orbitals which generate nL^{π} bonding and $n\bar{L}^{\pi}$ antibonding

cluster orbitals. Mixing between L^{σ} and L^{π} orbitals with the same L values results in one bonding combination and one antibonding combination for every matched pair of L^{σ}/L^{π} orbitals. In total, therefore, there are n+1 cluster bonding MOs (S^{σ} and nL^{σ}/L^{π}) since there is no S^{π} orbital. The isolobal relationship between BH and ML_3 fragments leads to the same n+1 skeletal cluster bonding MOs for transition metal clusters because those MOs derived from "t_{2g}" sets of ML_3 fragments are approximately non-bonding.

Athough Stone's methodology was initially applied to *closo*, *nido* and *arachno* deltahedral molecules it has been extended to 3- and 4-connected polyhedral molecules.[16] Like the deltahedral clusters, 4-connected molecules are generally characterised by n+1 skeletal electron pairs (SEP's). 3-connected clusters, however, possess 3n/2 SEP's. This difference is attributed to the occurrence of additional non-bonding orbitals in the 3-connected case. Based on molecular orbital analyses of 3-connected clusters, Johnston and Mingos[16] have shown that in these polyhedra there are (n/2)+2 strongly bonding skeletal molecular orbitals and n-2 approximately non-bonding skeletal molecular orbitals.

Most deltahedral clusters conform to the n+1 skeletal electron pair rule. However, there are a significant number which do not, such as B_4Cl_4, B_8Cl_8 and B_9Cl_9 molecules. These deviations have been rationalised from a combination of group theoretical methods and the paired nature for L^{π} and $\bar{L}^{\pi}$ skeletal molecular orbitals derived from the TSH method.[17,18]

The TSH theory has been used to derive the selection rules of orbital symmetry forbidden crossings in the study of the rearrangements of skeletal atoms of cluster compounds.[19,20] For a DSD (diamond-square-diamond) rearrangement process, it has been concluded that a DSD process in which a mirror plane is retained throughout involves an orbital

crossing and is therefore orbitally "forbidden".[20b]

In addition, the TSH theory has also been used to rationalise the bonding in deltahedral metallaboranes[21] and bispherical[22] and π-donor early transition metal clusters.[23]

1.6 Aims of this Thesis

The success and limitation of the jellium model to alkali metal clusters has prompted us to analyse the reasons for its failure and to develop a new structural jellium model for removing some of the limitations of the original model. The summary above indicates that the TSH theory has been widely and successfully used to rationalise patterns and relationships in the bonding of seemingly disparate ligated cluster molecules of main group and transition metal elements. In this Thesis we investigate its further applications and try to define general patterns of molecular orbitals for coordination and cluster compounds with the aid of the TSH theory and group theoretical principles. A summary of the topics analysed in this Thesis is given below:

1) Developing a new structural jellium model accounting for the electronic structures of alkali metal clusters.
2) Deriving structures for high nuclearity alkali metal clusters from the results of the structural jellium model.
3) Rationalising the MO patterns for clusters derived from ML_2, ML_4 and ML_5 fragments in terms of the TSH theory and group theoretical methods.
4) Using TSH theory to rationalise the electron counting rule of $12n_s+\Delta_i$ for high nuclearity ligated clusters, where n_s is the number of surface skeletal metal atoms and Δ_i is the electron count characteristic of the central atom or cluster lying at the centre of the cluster.

5) Developing a new theoretical framework to account for the electronic structures of high nuclearity ligated clusters with columnar topologies.

6) Defining non-bonding orbitals for coordination, hydrocarbon and cluster compounds.

References for Chapter One

1. B.F.G.Johnson and J.Lewis, *Adv. Inorg. Chem. Radiochem.*, **24**, 225(1981);
   B.F.G.Johnson and J.Lewis, *Phil. Trans. Roy. Soc. London,* **A308**, 5(1982).
2. E.L.Muetterties, T.N.Rhodin, E.Band, C.F.Brucker and W.R.Pretzer, *Chem. Rev.*, **29**, 91(1979);
   E.L.Muetterties and R.M.Wexler, *Survey Prog. Chem.*, **10**, 61(1983).
3. R.Whyman, in "Transition Metal Clusters", (Ed. B.F.G.Johnson) Wiley, New York, Chapter 8, p545 (1981);
   R.Whyman, *Phil. Trans. Roy. Soc. London,* **A308**, 131(1982).
4. "Transition Metal Clusters", (Ed. B.F.G.Johnson) Wiley, New York(1981) and references therein.
5. A.Ceriotti, F.Demartin, G.Longoni, M.Manassero, M.Marchionna, G.Piva and M.Sansoni, *Angew. Chem. Int. Ed. Engl.* **24**, 697(1985).
6. M.M.Kappers, *Chem. Rev.*, **88**, 369(1988).
7. J.C.Phillips, *Chem. Rev.*, **86**, 619(1986).
8. K.Wade, *Adv. Inorg. Chem. Radiochem.*, **18**, 1(1976);
   D.M.P.Mingos, *Chem. Soc. Rev.*, **15**, 31(1986);
   D.M.P.Mingos and R.L.Johnston, *Structure and Bonding,* **68**, 29(1987);
   D.M.P.Mingos and D.J.Wales, "Introduction to Cluster Chemistry", Prentice-Hall, to be pubilished.
9. A.J.Stone, *Mol. Phys.*, **41**, 1339(1980); *Inorg. Chem.*, **20**, 563(1981); *Polyhedron*, **3**, 1229(1984).
10. W.D.Knight, K.Clemenger, W.A.De Heer, W.Saunders, M.Y.Chou and M.L.Cohen, *Phys, Rev. Lett.*, **52**, 2141(1984);
    W.D.Knight, K.Clemenger, W.A.De Heer, W.Saunders, *Sol. State Commun.*, **53**, 445(1985).

11. M.M.Kappes, M.Schür, P.Radi and E.Schumacher, *Chem. Phys. Lett.*, **119**, 11(1985);
M.M.Kappes, M.Schür and E.Schumacher, *J.Phys. Chem.*, **91**, 658(1987).
12. M.M.Kappes, M.Schür, P.Radi and E.Schumacher, *J. Chem. Phys.*, **84**, 1863(1986).
13. C.Baladron and J.Alonso, *Physica B.*, **154**, 73(1988).
14. K.Clemenger, *Phys. Rev.*, **B32**, 1359(1985).
15. R.Hoffmann, Nobel Lecture 1981, *Science* **221**, 995(1981);
R.Hoffmann, *Angew. Chem. Int. Ed. Engl.*, **21**, 711(1982).
16. R.L.Johnston and D.M.P.Mingos, *J. Organomet. Chem.*, **280**, 407(1985);
R.L.Johnston and D.M.P.Mingos, *J. Organomet. Chem.*, **280**, 419(1985).
17. P.W.Fowler, *Polyhedron*, **4**, 2051(1985).
18. R.L.Johnston and D.M.P.Mingos, *Polyhedron*, **5**, 2059(1986).
19. D.M.P.Mingos and R.L.Johnston, *Polyhedron*, **7**, 2437(1988).
20. D.J.Wales and A.J.Stone, *Inorg. Chem.*, **26**, 3845(1987);
D.J.Wales, D.M.P.Mingos and Lin Zhenyang, *Inorg. Chem.*, in press;
D.J.Wales and D.M.P.Mingos, submitted to *Polyhedron*.
21. R.L.Johnston and D.M.P.Mingos, *Inorg. Chem.*, **25**, 3321(1986).
22. R.L.Johnston and D.M.P.Mingos, *J. Chem. Soc. Dalton Trans*, 647(1987);
R.L.Johnston and D.M.P.Mingos, *J. Chem. Soc. Dalton Trans*, 1445(1987).
23. R.L.Johnston and D.M.P.Mingos, *Inorg. Chem.*, **25**, 1661(1986).

Chapter 2. A Structural Jellium Model of Cluster Electronic Structure

2.1 Introduction

Trends in the stabilities of bare clusters as a function of their nuclearity have now been explored for many elements[1]. Mass spectral data, taken under appropriate conditions, have shown large abundances for specific numbers of metal atoms and these have been associated with particularly stable clusters. These "magic numbers" are particularly evident in the mass spectral data for alkali metal clusters[2], noble gases[3], and carbon[4]. In this Chapter we are concerned with the alkali metals. In this group, mass spectra have been reported for Na[5], K[6], LiK_x[7], and Li_xNa_y[8].

Many theoretical studies of alkali metal clusters have been carried out.[1c] The simplest spherical jellium model of Knight et al[5] has successfully predicted several of the magic numbers for alkali metal clusters by associating these nuclearities with closed-shell electronic configurations. More accurate self-consistent jellium calculations have been carried out by Ekardt who investigated the effective potentials, energy levels and charge densities and compared them with the semi-infinite half-space.[9]

Jellium model, although widely used in the solid state physics of simple metals[10], is unfamiliar to most chemists. The crystal-field formalism[11], which was first applied in this context by Upton[12] to explain the effects of the nuclear-electron potential on the electronic shell structures derived from the simple jellium model, allows us to develop the jellium model further and to relate the nuclear-electron potential to Knight's spherical jellium model. This formulation allows simple predictions to be made concerning the shape of small metal

clusters: predictions obviously impossible from Knight's spherical jellium model above.

2.2 A Structural Spherical Jellium Model

The structureless jellium model postulates that "the electronic energy-level structure of free-electron metal clusters may be approximately described by considering only the energies of the valence electrons in a smooth potential, without specific information about the positions of the atomic cores."[13]

Knight et al's original investigation[5] used a central field potential illustrated in Figure 1.1. It is the same form of potential as that used in nuclear physics shell models, where it goes under the name of the Woods-Saxon potential[14], and has no *a priori* justification in the context of clusters.

In the following sections, we reformulate the independent electron model of cluster electronic structure and show how the jellium model is related to more familiar chemical models.

2.2.1 The Hamiltonian

Consider a system composed of a valence electron (charge -e) and N atomic cores with effective charges Ze located on the surface of a sphere with a radius of r_o. By expanding the inverse of the distance between any two points in space in terms of spherical harmonics centred upon the origin of the coordinate system[11,12], we get the following expression for the nuclear-electron potential:

$$V = -\sum_{i=1}^{N} (Z/r_{ie})$$

$$= -4\pi NZ/r_{>} - \sum_{L=1}^{\infty} \sum_{M=-L}^{L} [4\pi Z/(2L+1)] \cdot (r_{<}^{L}/r_{>}^{L+1}) \cdot [\sum_{i=1}^{N} Y_L^M(\theta_i,\varphi_i)^*] \cdot Y_L^M(\theta,\varphi)$$

$$= V_o(r) + V(r,\theta,\varphi) \qquad [1]$$

where $r_{<}$ is the lesser of the distances from the origin to the points i and e. $Y_L^M(\theta_i,\varphi_i)$ and $Y_L^M(\theta,\varphi)$ are spherical harmonics (see Figure 2.1).

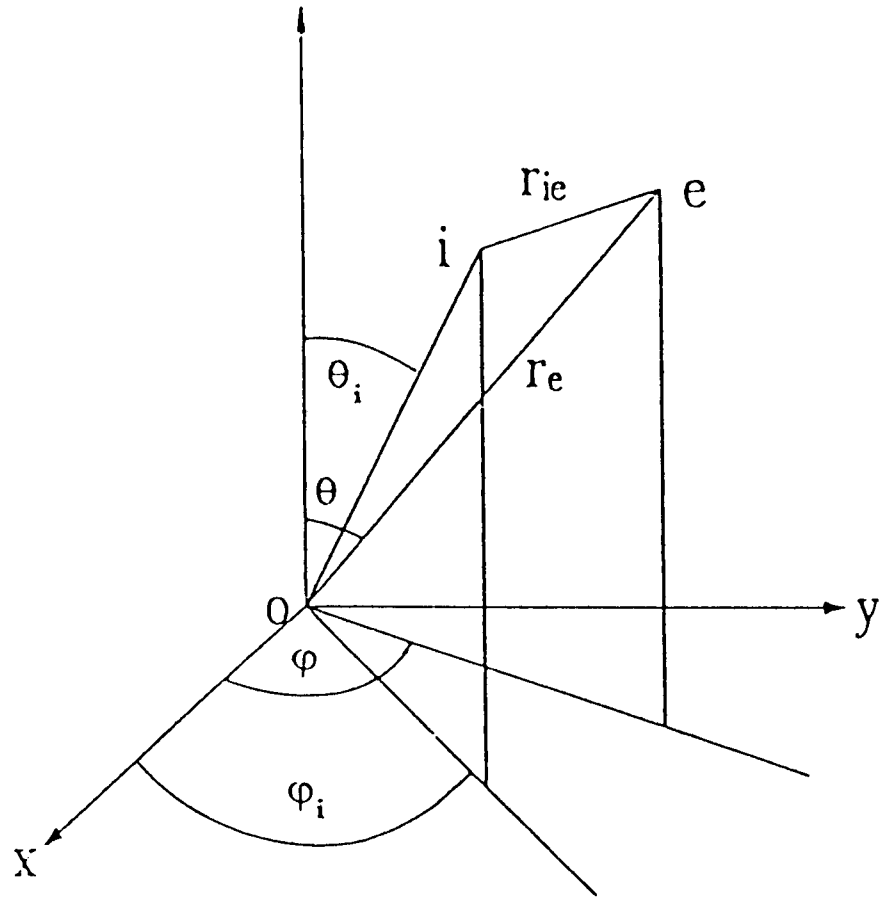


Figure 2.1 The angle θ and φ involved in the expansion of $1/r_{ie}$

This expansion of the potential, and the separation into a spherically symmetric part (V_o) and a non-spherical part (V) that follows from it, is exactly the expansion used in crystal field theory[11,12]. An alternative formulation would employ a nuclear-electron pseudopotential rather than the full (1/r) potential: we discuss the reason we consider such a formulation unnecessary in the present context in the Appendix.

The success of the spherical jellium model for alkali metal mass spectral abundances indicates that in these circumstances it will be valid to treat the non-spherical part $V(r,\theta,\varphi)$ as a perturbation, and to use the solutions of the central field (V_o) problem as the unperturbed cluster wavefunctions. These wavefunctions obviously have the same symmetries and degeneracies as those of Knight's model. Equation [1] allows discussion of situations for which perturbation theory breaks down and the spherical jellium model fails; a point we shall return to below.

2.2.2 The Central Field Potential

Upton has noted the connection between the jellium model and the spherical harmonic expansion of the nuclear-electron potential, but employed a square well and rounded square well as zero-order potentials. In this section, we examine some features of the central field potential $V_o(r)$.

Figure 2.2 shows the potential V_o for the simple case of a single shell of atomic cores placed on a sphere of radius r_o. The potential is just that due to a conducting sphere in classical electrostatics, being constant inside the sphere and falling off as 1/r outside.

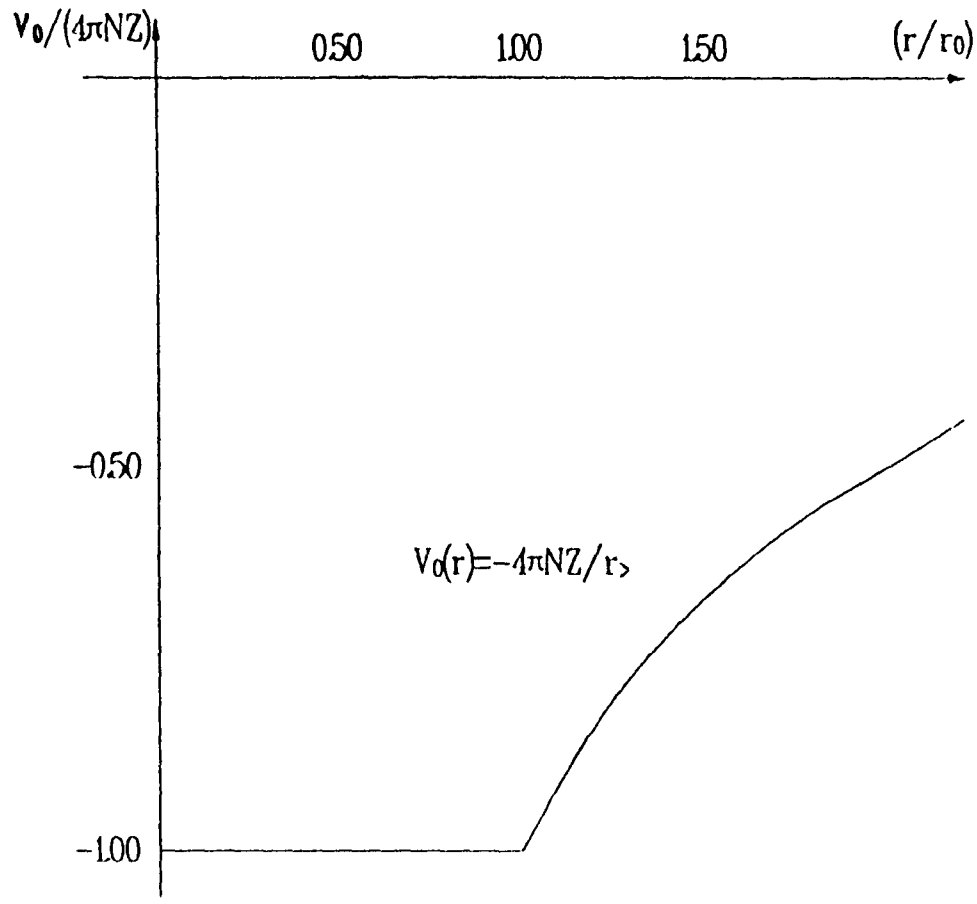


Figure 2.2 The central field potential for a single shell of cores

In a high nuclearity cluster, the nuclear positions can be described in terms of concentric spheres. Now $V_O(r)$ has the form

$$V_O(r) = -4\pi Z \sum_{\mu=0}^{w} (N_\mu / r_>) \qquad [2]$$

where w indicates the number of spheres in the cluster and N_μ atoms in the μth sphere.

Figure 2.3 shows the form of the above potential, where the r_i indicate the radii of successive spheres. The potential is constant inside the innermost sphere, and falls off as 1/r outside the outermost sphere, just as in the single sphere case, but adopts a stepped form

$j_l(kr)$, in the region of constant potential, and hydrogen-like functions R_{nl} in the (1/r) region or regions, joined on to each other by the boundary conditions at the r_i. The energy of such a function is thus the sum of two components, one inside and one outside the radius of the first shell, r_o. For clusters with a large r_o value, a large contribution to the energy will come from the integral over the constant region, while for clusters with small r_o, the hydrogen-like part will be more important. The energy-level ordering will thus be intermediate between the hydrogen-like atom ordering and the ordering of the spherical square well (for which the energies are given solely by integrals of spherical Bessel wavefunctions over regions of constant potential). Figure 2.4 shows a correlation diagram relating the energy levels of the two limits--the wavefunctions are labelled by their particle-in-a-well labels--and this diagram allows us to draw some qualitative conclusions concerning the magic numbers in clusters. We have written a computer program to compute the eigenvalues of the V_o potential for different clusters. The results show that the ordering of the lowest energy orbitals is insensitive to the geometry, being $1s < 1p < 1d < 2s....$, for all non-centred geometries we have investigated.

On Figure 2.4, the Woods-Saxon potential corresponds to a point close to the square well limit, and the spherical harmonic oscillator corresponds to the highly degenerate system as indicated by the level crossings, although neither have the analytic form of our V_o. These models would be expected to fail when there is a nucleus with larger positive charge, such as Mg and Zn, at the centre of the cluster, for in this case the potential will be hydrogen-like, and the energy-level ordering is on the other side of the highly-degenerate harmonic oscillator position on the correlation diagram from the square well.

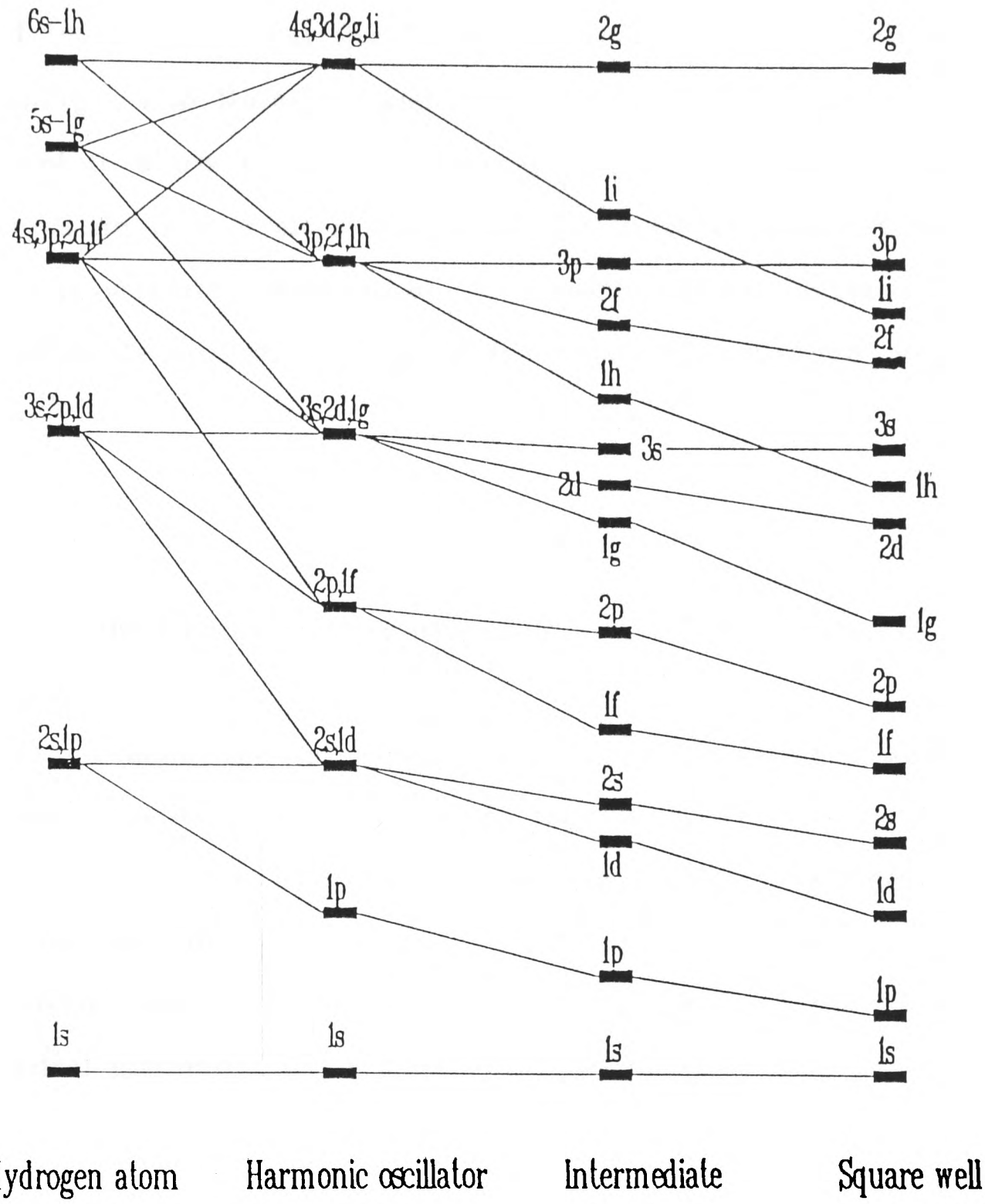


Figure 2.4 A correlation diagram relating energy levels for different central potentials

An experimental observation of this case is that of the alkali metal clusters seeded with magnesium and zinc atoms mentioned above[2b]. Particularly stable clusters are found at K_8Mg and K_8Zn. Knight et al[16] have pointed out that these ten electron species would be closed-shell in the case that the 2s orbital is lowered below the 1d orbital in energy, and Baladron and Alonso have used a background-density model to show this.[17] Ab initio studies[18] suggest that the divalent atoms do indeed sit at the centre of these clusters. A larger electron density was also observed at the centres of those clusters up to 34 atoms when 2s orbital is occupied from the self-consistent jellium calculations.[9]

2.2.3 Effect of the Central Field Potential V_o on the Structures of Clusters

For a given cluster, the radius and depth of the V_o potential well are fixed by the geometry. It is important to recognise that in general the deeper the constant region of V_o the greater the stabilisation energies of the lower lying orbitals.

For a cluster with metal nuclei lying on a single sphere, the adoption of a deltahedral geometry, i.e, a polyhedron with exclusively triangular faces (this is analogous to the well-known covering problem on a spherical surface), minimises the radius of the sphere, and consequently the depth of the V_o potential is maximised.

Adoption of structures with nuclei on more than one sphere also leads to a favorable V_o with a deep constant region inside the innermost sphere. The simplest example of this behaviour is provided by considering two possible structures for a Li_6 cluster both with planar

geometries, namely a hexagon and a triply bridged triangular cluster both with D_{3h} symmetry. From equation [2], the depth of the constant region of V_O for a hexagon is:

$$V_{Oc}(\text{hexagon}) = -4\pi\times6/a = -24(\pi/a)$$

where a is the bond distance between two adjacent atoms. An edge capped triangle has a double shell structure with $r_1=a/(3)^{1/2}$ and $r_2=2a/(3)^{1/2}$. The corresponding value for V_{Oc} is:

$$V_{Oc}(\text{edge capped triangle}) = -4\pi[(3/r_1)+(3/r_2)] = -31.18(\pi/a)$$

Clearly for a 6-electron cluster Li_6 with a planar structure the edge capped structure gives more negative V_{Oc} than the hexagonal one, and therefore is a more stable geometry because a deeper constant region of V_O produces relatively lower 1s and 1p energy levels.

A more complicated three dimensional situation is provided by the three isomers of a 14-atom cluster, i.e. a rhombic dodecahedron (a single sphere with r=1.05a), an octacapped octahedron (a double sphere with $r_1=0.707a$ and $r_2=1.225a$) and a hexacapped cube (a double sphere with $r_1=0.866a$ and $r_2=1.207a$). The following results of V_{Oc} for these three isomers are:

$$V_{Oc}(\text{rhombic dodecahedron}) = -53.32(\pi/a)$$
$$V_{Oc}(\text{octacapped octahedron}) = -60.08(\pi/a)$$
$$V_{Oc}(\text{hexacapped cube}) = -56.84(\pi/a)$$

The deepest constant region of V_O is found for the most close packed octacapped octahedral structure. Therefore, the lowest energy levels of 1s, 1p and 1d orbitals are expected for this structure.

It follows that ***for alkali metal clusters the V_{Oc} terms are maximised by deltahedral structures if the atoms lie on a single sphere, and by close packed or nearly close packed structures based on the most highly***

connected structure on the inner sphere and dual polyhedra on successive spheres if the atoms lie on several spheres. For example, the cube and the octahedron are duals and the structure which maximises V_{Oc} has the octahedron as the inner sphere and the cube as the second sphere, because the former is more highly connected and gives a better coverage of the spherical surface.

To summarise, the V_O central-field potential of the present crystal-field model of clusters is a potential with some similarity to the Woods-Saxon central field potential and also to those potentials calculated by self-consistent jellium model, but which has a well-defined relation to the full nuclear-electron potential of the cluster. It is structure-dependent, and depending on the cluster geometry can yield different energy orderings. This flexibility allows the present model to account for the results of mass spectra of alkali metals seeded with divalent metal atoms. The discussion on the depth of the constant region allows us to conclude that a highly connected structure is preferred for alkali metal clusters.

2.3 First-Order Perturbation of the Spherical Jellium Energies

The magic numbers from mass spectra show that shell structures do exist for alkali metal clusters. The structures of alkali metal clusters are not determined solely by the V_{Oc} term. However, splittings of the shells when they are partially filled are also very important. In order to understand these effects it is necessary to consider the perturbation of the non-spherical $V(r,\theta,\varphi)$ potential on each (nl) shell. This can be achieved by a first-order treatment even though the $V(r,\theta,\varphi)$ term might be quite large.

2.3.1 The general aspects of the splitting of shells

The first-order energy change produced by $V(r,\theta,\varphi)$ can be calculated with the methodology of crystal field theory[11,12]. As an approximation, only splittings within the same (nl) shell are considered. Therefore, only matrix elements $\langle nlm|\, V(r,\theta,\varphi)\,|nlm'\rangle$ will be involved.

$V(r,\theta,\varphi)$ can be expressed as follows:

$$V(r,\theta,\varphi) = \sum_{L,M} V_L^M(r,\theta,\varphi) \qquad [3]$$

The individual terms in the matrix elements of this potential are as follows:

$$\langle nlm|\, V_L^M\,|nlm'\rangle = \frac{-4\pi}{(2L+1)}\left[Z\sum_{i=1}^{N} Y_L^M(\theta_i,\varphi_i)\right]\cdot\langle f_{nl}(r)|\, r_<^L/r_>^{L+1}\,|f_{nl}(r)\rangle\cdot\langle lm|\, LM\,|lm'\rangle$$

$$= F_{nl}\cdot\langle lm|LM|lm'\rangle \qquad [4]$$

where F_{nl} is a function of geometry and number of atoms in the cluster.

Although the spherical harmonic expansion of $V(r,\theta,\varphi)$ is an infinite series, the matrix element above can be reduced to a sum of only a few terms, as

$$\langle nlm|\, LM\,|nlm'\rangle = 0$$

unless $m = M + m'$ and $L = 0, 2, 4, \ldots, 2l$. The requirement that each term in the potential must belong to the totally symmetric representation of the point group provides another restriction on those LM values which appear.

The first-order perturbation produced by $V(r,\theta,\varphi)$ has been discussed by Upton[12] and the following important conclusions have been made:

(1) The jellium model should become progressively less valid as the atomic valency increases. The contribution of $V(r,\theta,\varphi)$ increases linearly with Z.

(2) As cluster size increases and the number of symmetry equivalent (or nearly so) atoms grows, the jellium model should become more valid

regardless of the effective charge Z. This appears mathematically in the perturbing Hamiltonian as the diminution or total absence of contributions for small L. Upton[12] has not, however, considered the implication of the crystal field effects for small clusters with incomplete shells.

The two points above can be directly related to the splitting of shells produced by the non-spherical $V(r,\theta,\varphi)$ potential. A small splitting of shell structures leads to a valid jellium model.

In the extreme limit, we assume that the cluster atoms are evenly distributed on the surface of a single sphere. In this situation, the $V(r,\theta,\varphi)$ term vanishes because the nuclear-electron potential must belong to the totally symmetric representation of the R_{3h} point group. In actual clusters, after a certain nuclearity is reached a new shell is begun. The atoms on the new shell always occupy different angular directions (i.e. different (θ,φ) coordinates) than those on the inner shell. This implies that the effect on the $V(r,\theta,\varphi)$ term from the outer shell cancels some of that from the inner shell although it differs from the inner shell in radius, and the correction may diminish quite rapidly. For example[19], an octacapped octahedron with O_h point group has the perturbing potential $V(r,\theta,\varphi)$ term on d orbitals given by:

$$Cr^4\{Y_4^0(\theta,\varphi)+(5/14)^{1/2}[Y_4^4(\theta,\varphi)+Y_4^{-4}(\theta,\varphi)]\} \qquad [5]$$

C is a constant and can be obtained by adding the constants of a cube $\{-(56/27)(\pi)^{1/2}(qq'/r_c^5)\}$ and an octahedron $\{+(7/3)(\pi)^{1/2}(qq'r/r_o^5)\}$, where r_c and r_o are the radii of the cube and the octahedron respectively, q=Ze and q'=-e, and r is the distance between the electron and the origin. It can be seen that C is substantially decreased by the capping atoms.

In summary, the observation of closed shell electronic structures for alkali metal clusters indicates that the perturbation from $V(r,\theta,\varphi)$ is negligible or, at least, that the splitting of the n*l* shell is not very large. When a cluster has a complete jellium closed shell structure it will adopt a polyhedral geometry based on a high symmetry point group if possible. The adoption of a geometric arrangement which most closely approximates to spherical will be energetically favoured within the approximations of the crystal field model. A similar phenomenon is widespread in co-ordination chemistry where complexes with filled (d^{10}) or high spin half filled (d^5) have T_d and O_h geometries, whereas complexes with incomplete shells have a propensity to show lower symmetry co-ordination polyhedra. Furthermore, it is clear from arguments above that, for clusters with several shells of atoms, complementary angular co-ordinates minimise the splittings of the n*l* shells. Geometrically, this complementarity will be associated with clusters which are close packed or nearly close packed. Therefore, combining the principle derived from the discussion of the V_O term in the above section, we conclude that ***jellium closed shell clusters, e.g. neutral alkali metal clusters with 2, 8, 18, 20, 34, ... atoms, will adopt if possible T_d, O_h and I_h close packed or nearly close packed structures***. When more than one high symmetry structure of this type exists and the metal-metal bonding is relatively weak then such clusters are likely to be in chemical terms "stereochemically non-rigid". To a physicist the clusters may be better described as "liquid-like" or in an "amorphous" state[20].

2.3.2 Structures of "closed shell" metal clusters

Athough no structural information has been experimentally obtained so far, very detailed *ab initio* calculations,[15,18,21] have been carried out a large number of alkali metal clusters with up to 20 atoms, and the results provide detailed information on the optimised geometries.

(1) Clusters with 8 valence electrons

The adoption of the T_d and O_h point groups produces no splitting of the p orbitals. Therefore, clusters with s and p orbitals occupied will adopt these high symmetry structures. Furthermore the V_O terms will be maximised for deltahedral single sphere, or close packed bispherical structures. For example, *ab initio* calculations on Li_8 and Na_8 have indentified a tetracapped tetrahedron with T_d symmetry as the energy minimum[15](a bispherical structure) and for Li_6Mg and Li_6Be a centred (Mg and Be) octahedron has been proposed.[18] Be_4 and Mg_4 are all identified as tetrahedral.[21]

(2) Clusters with 10 valence electrons

Alkali metal clusters seeded with Mg and Zn exhibit a large peak in mass spectroscopy corresponding to the 10 valence electron clusters K_8Mg and K_8Zn. As indicated above, when there is a nucleus at the centre of the clusters, the 2s orbital can be lowered below the 1d orbitals in energy. Therefore these 10-electron clusters correspond to a closed shell electronic structure with the occupations of 1s, 1p and 2s orbitals. The adoption of high symmetry structures is expected. *Ab initio* calculations on Li_8Mg and Li_8Be indicate that the minimum energy structures are centered (Mg and Be) cubes.[22] The cube does not represent the best covering polyhedron, which is a dodecahedron, but the

lower symmetry of the dodecahedron presumably disfavours this structure.

(3) Clusters with 20 valence electrons

Only Li_{20} clusters with the occupation of the 1s, 1p, 1d and 2s orbitals have been studied using *ab initio* calculations.[15c] Two almost isoenergetic T_d structures have been proposed (see Figure 2.5). One is a nearly spherical shape, and the other a tetrahedral fragment derived from the fcc crystal lattice. Both have high symmetry and close packed structures which are consistent with the crystal field analysis.

High symmetry structures have also been proposed for higher nuclearity alkali metal clusters with closed shell electronic structures. These will be discussed in the next Chapter.

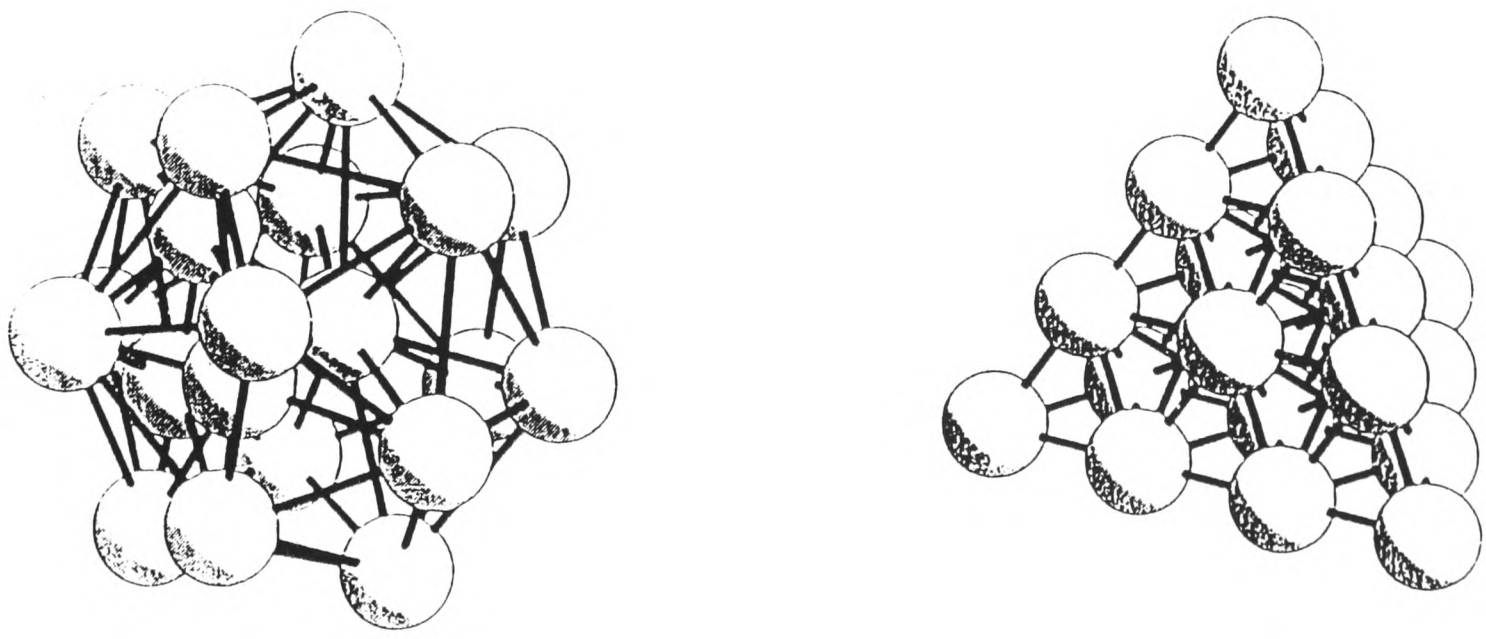


Figure 2.5 Two almost isoenergetic T_d structures for Li_{20} cluster

2.4 Clusters with incomplete shell structures

A cluster with an incomplete jellium p shell will distort in a prolate or oblate fashion to take advantage of the splittings within the subshell. The crystal field analysis is helpful for analysing such splittings and provides a basis for rationalising structures predicted by *ab initio* calculations.

2.4.1 Clusters with less than 8 valence electrons

Clusters with less than 8 valence electrons have an incomplete p shell. Stabilisation energies occur from the splitting of the p orbitals which result from geometric distortions. The only perturbation terms involved in the non-spherical $V(r,\theta,\varphi)$ part are the V_2^M. When the principal axis is of order three or more, only the V_2^O term is needed since the V_2^M term must belong to the totally symmetric representation of the point group considered. The V_2^O perturbation term corresponds to an oblate/prolate distortion of the cluster potential from spherical symmetry. We now show how this term generates "oblate" and "prolate" perturbations, even for clusters with a single shell of atomic cores arranged on a spherical surface.

The sign of the V_2^O term is determined by the sign of the coefficient in equation [4], in fact we can write:

$$\text{sgn}\ \{\ \Delta E(lm)\ \} = \text{sgn}\ \{\ [\ \Sigma\ Y_2^O(\theta_i,\Phi_i)\ ]\cdot\langle lm|LM|lm\rangle\ \}$$

The splitting of p orbitals is shown in Figure 2.6 when $[\Sigma Y_2^O(\theta_i,\Phi_i)]$ (abbreviated as $[\Sigma]$) is positive. In this case the p_O function has the lowest energy. This corresponds to a prolate perturbation. When $[\Sigma]$ is negative, the ordering is reversed, corresponding to an oblate perturbation. In this way the geometry of the cluster, even with all

atomic cores assumed to be at a distance r_o from the centre of the cluster, can be classified as oblate or prolate according to the sign of $[\Sigma]$.

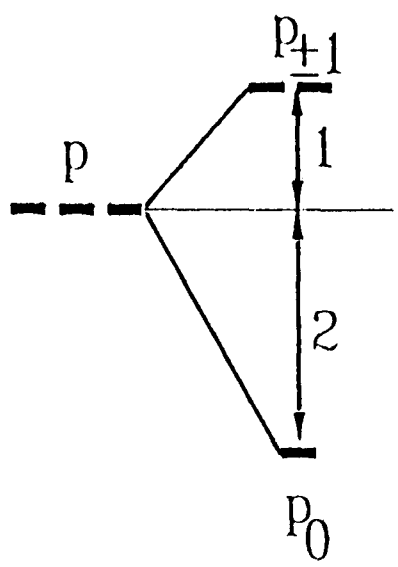


Figure 2.6 The splitting of p orbitals in a prolate perturbation

The sign of $[\Sigma]$ can be easily seen to be positive for a trigonal bipyramid, which is therefore characterised as prolate, zero for a cube or an octahedron which are therefore spherical, and negative for a pentagonal bipyramid which is thus oblate. More examples are listed in Table 2.1.

Table 2.1. Classification of polyhedra according to their oblate/prolate/spherical shape

Nuclearity	Geometry	$(4\pi/5)^{1/2} \sum_{i=1}^{n} Y_2^0(\theta_i,\varphi_i)$	Shape
3	triangle	-3	oblate
4	tetrahedron	0	spherical
4	square	-4	oblate
5	trigonal bipyramid	1	prolate
6	octahedron	0	spherical
6	trigonal prism	1.714	prolate
7	pentagonal bipyramid	-1	oblate
8	cube	0	spherical
8	square antiprism	-1.730	oblate
8	dodecahedron	1.176	prolate
9	tricapped trigonal prism	-1.286	oblate
10	bicapped square antiprism	2.270	prolate
10	pentagonal prism	-2.296	oblate
12	icosahedron	0	spherical

These examples show that the sign of $[\Sigma]$ parallels the actual shape adopted by clusters with equal metal-metal bond lengths: the equatorial nuclei of a pentagonal bipyramid, for example, are at a greater distance from the centre of the cluster than the axial nuclei, while the reverse is the case for the trigonal bipyramid. This occurs because if the V_2^0 term, from the nuclear configuration with all nuclei at r_0, corresponds to an oblate (prolate) perturbation, then a geometrical distortion from the spherical shell of the same oblate (prolate) type will produce a larger perturbation of the same sign. Thus, the present model suggests that for non-closed-shell clusters distortions from a spherical geometry will occur, to yield oblate or prolate geometries.

Clemenger[13] extended the spherical jellium model by adjusting the

potential to take the form of a perturbed harmonic oscillator, which produces the same energy orderings as Knight's potential. The advantage of a harmonic oscillator potential is that it can be rewritten in cartesian form and thus the x,y and z components can be separated. In this way a spheroidal cluster can be modelled by a 3-dimensional harmonic oscillator with a larger (oblate) or smaller (prolate) force constant in the z direction than in the degenerate x and y directions.

In the current framework, we see that results similar to Clemenger's are derived by considering the effects of the $V(r,\theta,\varphi)$ in a first order treatment, just as crystal field theory does in studying the splitting of atomic orbitals in a non-spherical environment. The fact that a first-order treatment is sufficient means that the wavefunctions retain their (n*l*m) labels, even though the $(2l+1)$ degeneracy is lost.

(1) Clusters with 4 valence electrons

From the discussion above, the preferred structures for $1s^2 1p^2$ configurations are those which maximise the V_{Oc} term and also provide the largest prolate splitting of the p shell. The following optimum geometries have been obtained from *ab initio* calculations.[15,18,21]

Li_5^+: trigonal bipyramidal structure.

$BeLi_2$ and $MgLi_2$: linear.

Li_6^{2+}: two tetrahedra sharing an edge.

Na_4 and Li_4: rhombic.

The linear geometries noted for $BeLi_2$ and $MgLi_2$ and the trigonal bipyramid noted for Li_5^+ satisfy these criteria simultaneously since they represent the most satisfactory solutions to the covering problem and are prolate. For Li_6^{2+} the octahedron is the best solution to the covering problem, but does not result in any splitting of the p shell. the observed

structure based on two tetrahedra produces a significant prolate distortion whilst retaining a high degree of connectivity. A trigonal prism produces a prolate distortion, but is not so highly connected and therefore is a less stable structure. Although the rhombic shape calculated for Na_4 and Li_4 can be viewed as either oblate or prolate, it is a distorted square planar structure. In a square planar structure, the p_x and p_y orbitals are degenerate. The distortion leads to a splitting of these two p orbitals, and the stabilisation energy is gained by occupying one of them.

(2) Clusters with 6 valence electrons

Clusters with $1s^2 1p^4$ configurations should adopt an oblate highly connected geometry according to the crystal field analysis. The following results derived from *ab initio* calculations[15,18,21] support this generalisation.

Li_6 and Na_6: two almost isoenergetic structures are proposed. One is a pentagonal pyramid (C_{5v}), and the other a trigonal planar "raft" structure with an atom capping each edge of a central triangle (D_{3h}). Both structures are oblate and also highly connected.

Li_5^-: a centred square planar structure (D_{4h})

Li_7^+: an oblate "squashed" pentagonal bipyramid (D_{5h}).

$AlLi_3$: a centred (Al) trigonal planar structure (D_{3h}).

$BeLi_4$ and $MgLi_4$: a centred (Be, Mg) square planar structure (D_{4h}).

Be_3 and Mg_3: a triangle.

It is apparent that if a heteroatom is present then an oblate

structure with the heteroatom at the origin is always favoured. For homonuclear clusters, centered and bispherical clusters are almost equienergetic.

(3) Clusters with an odd number of valence electrons

From Figure 2.6, it can be proposed that clusters with 3 electrons prefer prolate, 5 electrons either prolate or oblate and 7 electrons oblate geometries. The following *ab initio* results[15,18,21] are in broad agreement with these conclusions.

Li_3: A distorted triangle.

Li_4^+: Triangle with one terminal atom.

Li_5: Planar, triangular lattice.

Li_6^+: Edge-linked tetrahedra.

Li_7: Pentagonal bipyramid.

Li_8^+: Capped pentagonal bipyramid.

$MgLi_5$: An equilateral pentagonal arrangement of Li atoms with Mg at its centre.

$AlLi_4$: A square arrangement of Li atoms with Al slightly above the mid-point.

2.4.2 Clusters with more than 8 valence electrons

The occupations of d orbitals lead to a more complicated problem because the perturbation includes both V_2^M and V_4^M components. The oblate/prolate transformation cannot be simply related to V_2^O term. It is necessary to discuss the splitting of the d shell arising from cubic point groups.

In the crystal field approximation, the non-spherical perturbation

potential on a d shell for clusters with cubic point groups is given by equation [5].

$$C \propto \sum_{i=1}^{n} Y_4^O(\theta_i,\varphi_i)$$

where (θ_i,φ_i) are the angular coordinates of the ith atom on the surface of the sphere with a radius of r_O. Therefore the splitting of the d shell within cubic point groups is determined by the sign of $\sum Y_4^O(\theta_i,\varphi_i)$. The result of splitting is illustrated in Figure 2.7 when $\sum Y_4^O(\theta_i,\varphi_i)$ is positive. When the summation is negative the ordering is reversed. The values of the summation for some specific geometries are given below:

Geometry (n)	$(\pi)^{-1/2} \sum_{i=1}^{n} Y_4^O(\theta_i,\varphi_i)$
Tetrahedron (4)	-2.33
Octahedron (6)	+5.25
Cube (8)	-4.67
Cuboctahedron (12)	-2.63

It can be seen from the table above that the energies of the e_g orbitals are below those of t_{2g} orbitals for an octahedral structure, and the inverse energy orderings occur for the remaining structures. This has been confirmed by Upton's calculations.[12]

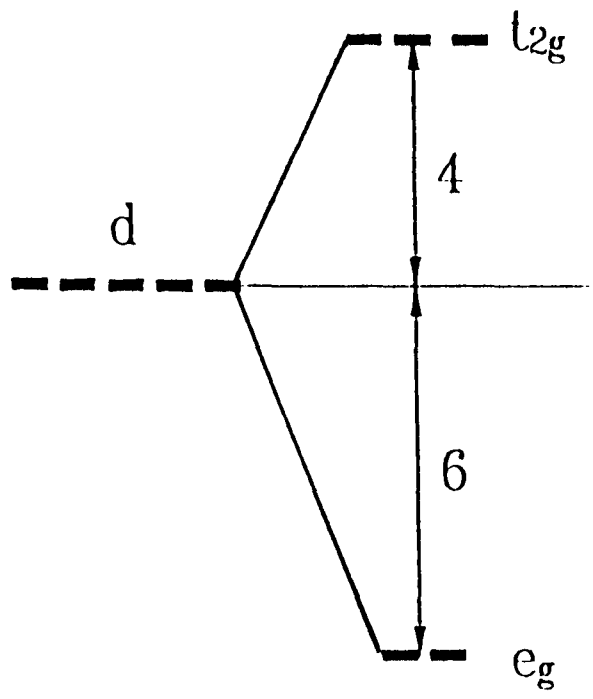


Figure 2.7 The splitting of d orbitals within cubic point groups

It follows that significant d orbital stabilisation energies could result for a cuboctahedron with six electrons occupying the t_{2g} set of the d orbitals. For example, the cluster Li_{13}^- with 14 electrons will adopt a centred cuboctahedral geometry. A smaller splitting of the d shell is expected for the clusters which are bispherical and based on those polyhedra of cubic symmetry. For example, it can be seen from the table above that the opposite sign of the summations for an octahedron and a cube leads to a cancellation when they are combined. A smaller d splitting is expected for a structure derived from a combination of these two polyhedra. Therefore, an octacapped octahedon is not a particularly favourable geometry for the Li_{14} cluster since, although it is close packed, it does not provide a large stabilisation energy for the d sub-shell.

The splitting of the d shell becomes complicated when the clusters possess lower symmetry because the non-spherical perturbed potential now includes not only V_4^M but also V_2^M terms. The splitting cannot be simply defined by one parameter as is the case for clusters with cubic point groups. However the energy orderings of d orbitals with lower symmetry can be estimated using our knowledge of the splittings of d atomic orbitals in transition metal complexes. The perturbation method developed above is exactly the same as that in the crystal field model for coordination compounds except that the electron-nucleus potential is attractive for clusters rather than repulsive. Therefore, the splitting of a d shell in a cluster is an inversion of the splitting of d atomic orbitals in a complex with the ligands in the same arrangement as the cluster vertices. As discussed above, the e_g orbitals are lower in energies than t_{2g} orbitals in an octahedral cluster, which is an inversion of the case observed for an octahedral transition metal complex. Figure 2.8 illustrates the splittings of d shells for some polyhedral clusters together with those for transition metal complexes.

A large cluster can be described as a concentric multi-shell structure. Each shell is viewed as an individual polyhedron. The splitting of the d shell in this cluster can be therefore estimated by the addition of those effects for the individual polyhedra. It can be seen from Figure 2.8 that the trigonal bipyramid and its face-dual, the trigonal prism, have opposite d orbital energy orderings. The same phenomenon is observed for the pentagonal bipyramid and its face dual, the pentagonal prism. From these examples, it can be deduced that a completely capped polyhedron leads to a small splitting of d orbitals, and cannot be an optimum geometry for a cluster with an incomplete d shell electronic

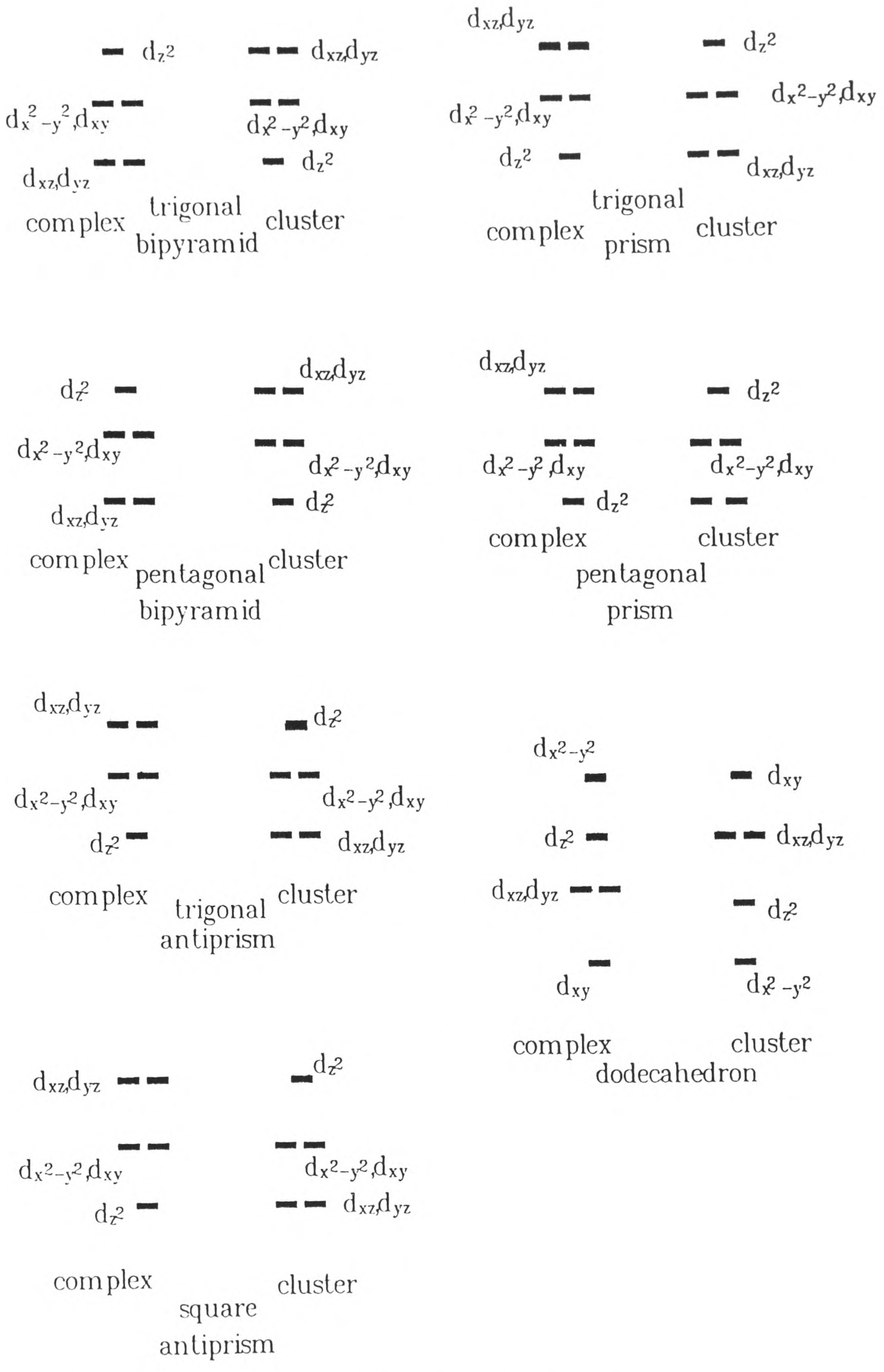


Figure 2.8 The splittings of d shells for some polyhedral clusters together with those for transition metal complexes

structure. However, an incompletely capped polyhedron, in some cases, can result in an increase in the splitting of the d orbitals so that the largest stabilisation energy can be gained for an incomplete d shell electronic structure. Examples illustrating this point are given below.

Li_{10}: This 10 electron cluster has an electronic configuration of $s^2p^6d^2$ A maximum stabilisation of one d orbital is required to provide the maximum stabilisation energy. From Figure 2.8 it can be appreciated that the d_z2 orbital can be stabilised when there are two atoms located on +z and -z directions. Therefore, a dodecahedron capped by two atoms along the +z and -z directions when the S_4 axis is defined as the z axis can be proposed as a candidate for the Li_{10} geometry (D_{2d}).

The energy levels of the d atomic orbitals in a dodecahedral (ML_8) ligand field follow in the order of [23]

$$b_1(d_{xy}) < e(d_{xz}, d_{yz}) < a_1(d_z2) < b_2(d_x2_{-y}2)$$

When two capping atoms are introduced, the d_z2 is destabilised and the energy ordering becomes:

$$b_1(d_{xy}) < e(d_{xz}, d_{yz}) < b_2(d_x2_{-y}2) < a_1(d_z2)$$

As discussed above, the energy ordering of the d shell in a cluster is just an inversion of the d atomic orbitals in a complex. Therefore we expect the splitting of d shell in a bicapped dodecahedral Li_{10} cluster favours the stabilisation of the d_z2 orbital. A tetracapped tetrahedron with two additional atoms located in the +z and -z directions (D_{2d}), which is very close to the one we suggested above, is proposed for Li_{10} cluster from *ab initio* calculations.[15]

Li_{12}: A stabilisation of two d orbitals is now required to obtain a lower energy structure for Li_{12} cluster. From Figure 2.8 it is apparent that a

trigonal antiprism (D_{3d}) cluster (Li_6) produce a lowest e set of d orbitals in the splitting of the d shell. A hexacapped trigonal antiprism, which forms an overlap of two D_{3d} trigonal antiprisms, will enlarge this splitting. Therefore a D_{3d} structure which approximates to two close packed layers can be proposed as a candidate for a Li_{12} cluster.

Li_{14}: An octacapped octahedron is not a good candidate for Li_{14} cluster since it is a complete capped structure and has a small d splitting. We can expect a structure having a_1+e orbitals stabilised for this cluster with 14 electrons. A structure with C_{3v} symmetry is proposed from *ab initio* calculations for this cluster.[15] Assuming the z axis as the C_3 axis, we can describe this structure as a hexacapped trigonal bipyramid linked via a triangle in the -z direction twisted through 60° with respect to the three lower capping atoms. From this structure, the stabilisation of $a_1(d_z2)$ and $e(d_{xz},d_{yz})$ orbitals at the expense of destabilisation of $d_x2_{-y}2$ and d_{xy} orbitals can be expected because the nuclei are located at maxima in the angular parts of the wavefunctions for these orbitals.

Li_{16}: Four d orbitals are occupied for this 16 electron cluster. Two e sets of d orbitals are expected to be stabilised. The same argument as that for Li_{12} cluster can be used for this cluster. An octacapped square antiprism (capping the eight triangular faces) can be proposed since the $e_2(d_x2_{-y}2,d_{xy})$ and $e_3(d_{xz},d_{yz})$ orbitals are stabilised in a square antiprismatic structure.

2.5 Conclusions

The spherical harmonic expansion of the nuclear-electron potential gives insight to the success of jellium approaches in predicting stability trends for alkali metal clusters.[5] Also, it explains why centred clusters such as those of alkali metals seeded with divalent metal atoms exhibit different stability trends to the alkali metals themselves,[17] all within a single framework. The discussion of the depth of the constant region of V_o central field potential also allows us to make some useful generalisations concerning the gross structural features of alkali metal clusters. An analysis of the effects of the non-spherical perturbation of the spherical jellium shell structures enables us to understand qualitatively the success of this model for alkali metal clusters and the reasons for its failure in other situations. In addition we conclude that for a cluster with a closed shell electronic stucture a high symmetry arrangement of atoms which is approximately or precisely close packed is preferred. Consideration of the V_2^o perturbation term allows us to predict the most stable structures for small clusters with incomplete p shells. The discussion of d orbital splittings allows us to propose geometries for clusters with electron counts between 10 and 16.

2.6 Appendix

Throughout this Chapter we have employed the spherical harmonic expansion of the full nuclear-electron potential V_{ne}, where the charge on the nucleus can be replaced by an effective charge in order to take some account of shielding by the core electrons. It may be thought that a pseudopotential formulation would be more appropriate. Our reasons for

preferring to work with the (mathematically simpler) full potential are as follows:

In the regions between the atomic cores, the full potential with an appropriate effective nuclear charge and any sensible local effective potential derived from a pseudopotential formulation will be qualitatively similar: it is only in the regions inside the cores that the difference between the two becomes substantial. In this region, the effective potential is smaller in magnitude than the full potential.

The regions inside the core, where the full potential is quickly changing, have a major contribution from V_L^M where L is large. These terms do not affect the splitting of the shells, as the only components that contribute to the splitting of potential shells of small l are V_L^M components of $L \leq 2l$, and we have only considered the V_2^0 term explicitly. Thus, the major difference between an expansion in spherical harmonics of the full potential and reasonable effective potentials will occur in the high L terms, which do not enter into our model.

preferring to work with the (mathematically simpler) full potential are as follows:

In the regions between the atomic cores, the full potential with an appropriate effective nuclear charge and any sensible local effective potential derived from a pseudopotential formulation will be qualitatively similar: it is only in the regions inside the cores that the difference between the two becomes substantial. In this region, the effective potential is smaller in magnitude than the full potential.

The regions inside the core, where the full potential is quickly changing, have a major contribution from V_L^M where L is large. These terms do not affect the splitting of the shells, as the only components that contribute to the splitting of potential shells of small l are V_L^M components of $L \leq 2l$, and we have only considered the V_2^O term explicitly. Thus, the major difference between an expansion in spherical harmonics of the full potential and reasonable effective potentials will occur in the high L terms, which do not enter into our model.

References for Chapter Two

1. For reviews, see:
   (a) M. M. Kappes, *Chem. Rev.*, 88, (1988), 369.
   (b) J. C .Phillips, *Chem. Rev.*, 86, (1986), 619.
   (c) J. Koutecky, P. Fantucci, *Chem. Rev.*, 86, (1986), 539.
2. (a) M. L. Cohen, M. Y. Chou, W. D. Knight, W. A. de Heer, *J. Phys. Chem*, 91, (1987), 3141.
   (b) M. M. Kappes, M. Schür, P. Radi, E. Schumacher, *J. Chem. Phys.*, 84, (1986), 1863.
3. O. Echt, K. Sattler, E. Recknagel, *Phys. Rev. Lett.* 47, (1981), 1121.
4. H. W. Kroto, J. R. Heath, S. C. O'Brien, R. F. Curl, R. E. Smalley, *Nature*, 318, (1985), 162.
5. W. D. Knight, K. Clemenger, W. A. de Heer, W. Saunders, M. Y. Chou, M. L. Cohen, *Phys. Rev. Lett.* 52, (1984), 2141.
6. W. D. Knight, K. Clemenger, W. A. de Heer, W. Saunders, *Sol. State Commun.*, 53, (1985), 445.
7. M. M. Kappes, M. Schür, P. Radi, E. Schumacher, *Chem. Phys. Lett.*, 119, (1985), 11.
8. M. M. Kappes, M. Schür, E. Schumacher, *J. Phys. Chem.*, 91, (1987), 658.
9. W. Ekardt, *Phys. Rev.* B29, 1558(1984).
10. N. W. Ashcroft, N. D. Mermin, "Solid State Physics", Holt, Rinehart and Winston, New York, 1976, pp. 285 - 288.
11. For crystal field theory, see:
   (a) J. S. Griffith, "Theory of Transition Metal Ions", Cambridge University Press, Cambridge, 1961.

(b) B. L. Silver, "Irreducible Tensor Methods", Academic Press, New York, 1976.

12. T. H. Upton, *Phys. Rev. Lett.*, 56, (1986), 2168; *J. Chem. Phys.*, 86, (1987), 7054.

13. K. Clemenger, *Phys. Rev.*, B32, (1985), 1359.

14. R. D. Woods, D. S. Saxon, *Phys. Rev.*, 95, (1954), 577.

15. (a) I. Boustani, W. Pewestorf, P. Fantucci, V. Bonacic-Koutecky, J. Koutecky, *Phys. Rev.*, B35, (1987), 9437.

(b) V. Bonacic-Koutecky, P. Fantucci, J. Koutecky, *Phys. Rev.*, B37, (1988), 4369.

(c) J. Koutecky, V. Bonacic-Koutecky, I. Boustani, P. Fantucci, in "*Large Finite Systems*", (Ed. J. Jortner et al) p_{303}, Reidel, Dordrecht (1987).

16. W. D. Knight, W. A. de Heer, W. A. Saunders, K. Clemenger, M. Y. Chou, M. L. Cohen, *Chem. Phys. Lett.* 134, (1987), 1.

17. C. Baladron, J. Alonso, *Physica B.*, 154, (1988), 73.

18. B. K. Rao, P. Jena, *Phys. Rev..*, B37, (1988), 2867.

19. M. T. Hutchings, *Sol. State Phys.*, 16, (1964), 227.

20. (a) M. P. Iniguez, J. A. Alonso, L. C. Balbas, *Solid State Commun.*, 57, (1986), 85.

(b) M. Manninen, *Solid State Commun.*, 59, (1986), 281.

21. B. K. Rao, S. N. Khanna, P. Jena, in "Physics and Chemistry of Small Clusters", (Edited by P. Jena, B. K. Rao and S. N. Kanna), p_{369}, Plenum Press, New York and London (1987).

22. W. Pewestorf, V. Bonacic-Koutecky, J. Koutecky, *J. Chem. Phys.*, 89, 5794(1988).

23. R. M. Golding, A. Carrington, *Mol. Phys.* 5, 377(1962).

Chapter 3 Structural Consequences of the Jellium Model for Alkali Metal Clusters

3.1 Introduction

Although the jellium model[1-4] has successfully explained the magic numbers for alkali metal clusters, more sophisticated quantum chemical methods are required to understand the details of the orbital energies, shell structures, ionisation energies and geometries of these clusters. Ab initio calculations have been widely used to study these aspects.[5-7] Such calculations have been carried out on alkali metal clusters with up to 20 atoms and the results have provided detailed information on the geometries and stabilities of lithium clusters and sodium clusters. However, limitations on computing facilities have prevented the application of ab initio calculations to larger systems even when only alkali metals are present.

In Chapter Two, we have developed a structural jellium model which accounts for the electronic structures of clusters using a crystal-field perturbation. The perturbation analysis underlined the geometric consequences for jellium closed shell clusters. In this Chapter these geometric conclusions are developed in more detail.

The magic numbers in clusters of rare gases have been explained in terms of icosahedral close packed geometries, for which the van der Waals' interactions lead to densely packed and nearly spherical geometries corresponding to observed discontinuities at the following numbers of atoms: N=13, 19, 25, 55, 71, 87 and 147 etc.[8] The magic numbers of mixed rare gases have also been explained by the icosahedral close packing of spheres for two kinds of soft sphere.[9] A similar method will be employed in this Chapter.

3.2 Geometric Conclusions for Alkali Metal Clusters

In Chapter Two, we concluded that jellium closed shell alkali metal clusters, i.e. neutral clusters with 2, 8, 20, 34, ... atoms will adopt high symmetry structures with T_d, O_h and I_h symmetries and close packed or nearly close packed spherical geometries.

Satisfying these geometric requirements often leads to several structural possibilities, since the most close packed structure is not necessarily the most spherical structure. The most close packed structure maximises the number of next neighbour resonance integrals and consequently the average energy of n*l* molecular orbitals is lowest. However, such structures do not necessarily minimise the extent of the splittings of the n*l* shells.

3.3 Orbital Splittings for the Most Close Packed and Spherical Structures

The close packed structures maximise the number of inter-atom resonance integrals, but can result in larger splittings of the n*l* shell than spherical structures. In the crystal field approximation, the non-spherical perturbation potential on a D shell for clusters with tetrahedral or octahedral point group is as follows:[10]

$$V = C \cdot r^4 \{ Y_4^0(\theta,\phi) + (5/14)^{1/2} [Y_4^4(\theta,\phi) + Y_4^{-4}(\theta,\phi)] \}$$

where $Y_l^m(\theta,\phi)$ are the spherical harmonics and r the distance between the electron and the origin. C depends on the geometry considered and is given by:

$$C = 4\pi/(9r_O^5) \sum_{i=1}^{N} Y_4^0(\theta_i,\phi_i)$$

where (θ_i,ϕ_i) are the angular coordinates of the ith atom on the surface of a sphere with a radius of r_O. The smaller C is, the smaller the splitting of the D shell is resulted. Calculations of C for a most close

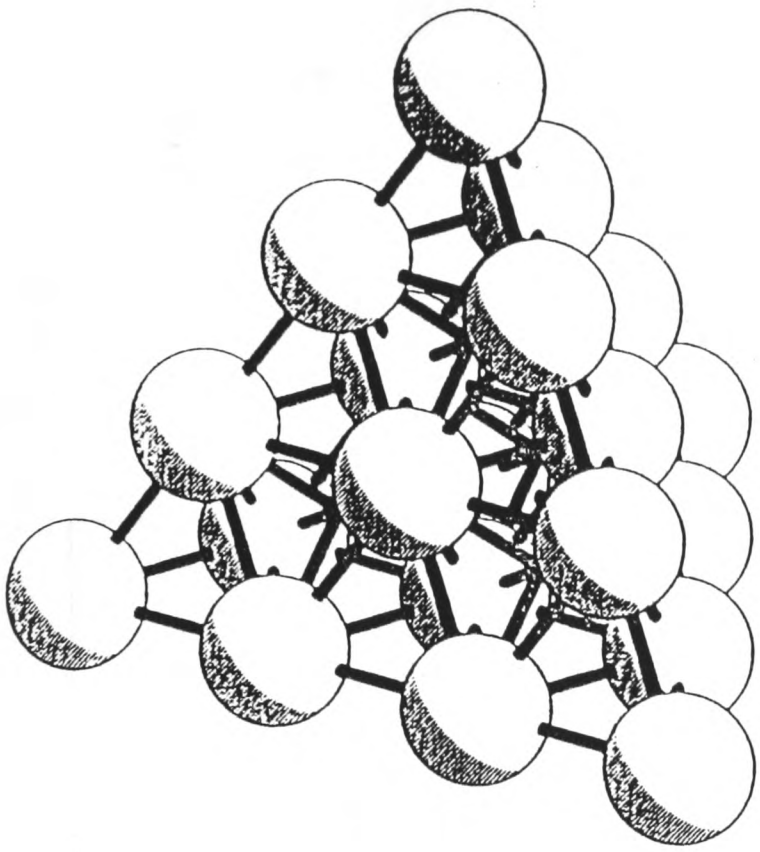
packed (Figure 3.1(a)) and a more spherical (Figure 3.2) structure with 20 alkali metal atoms, which will be discussed later, were carried out. The contribution of the interstitial tetrahedral moiety for both structures is the same and is thus not relevant to the comparision. Only the 16 surface atoms are considered in the following discussion. The contribution of the four atoms located on C_3 axes is defined as C_{tet} for both structures, and is $[-1.04(\pi)^{1/2}/r_{tet}^5]$, where r_{tet} is the distance of the four atoms to the centre of the cluster. The contributions from the remaining 12 atoms located on the mirrors for the close packed (Figure 3.1(a)) and the more spherical (Figure 3.2) structures are:

$$C_{rem}(c.p.) = [1.00(\pi)^{1/2}/r_{rem(c.p.)}^5] \text{ and}$$

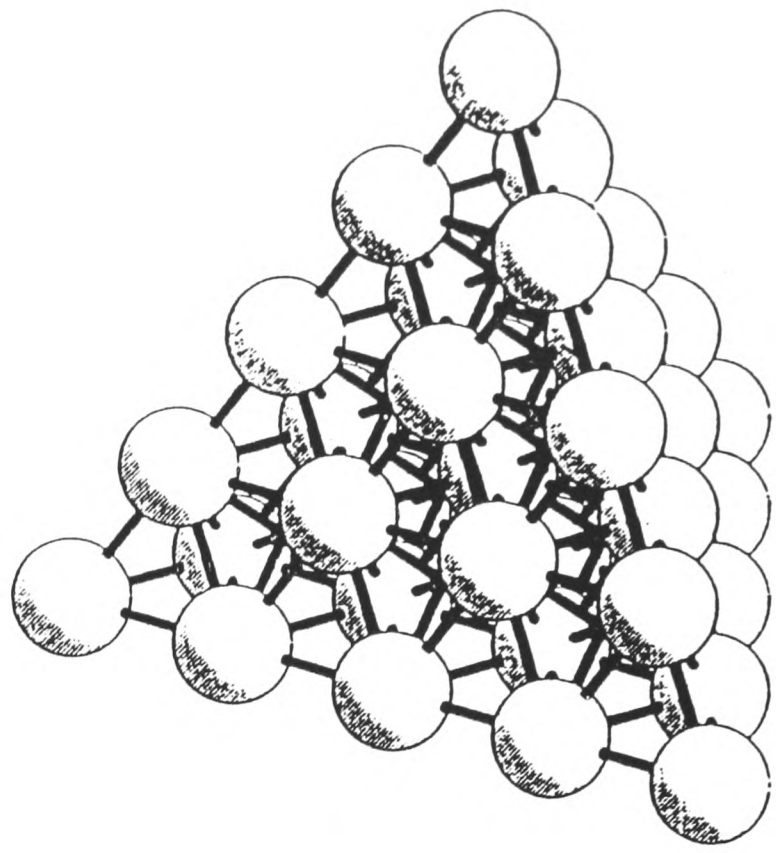
$$C_{rem}(sph) = [1.34(\pi)^{1/2}/r_{rem(sph)}^5]$$

It can be seen that the effect of the remaining 12 atoms opposes that of the tetrahedral atoms for both structures.

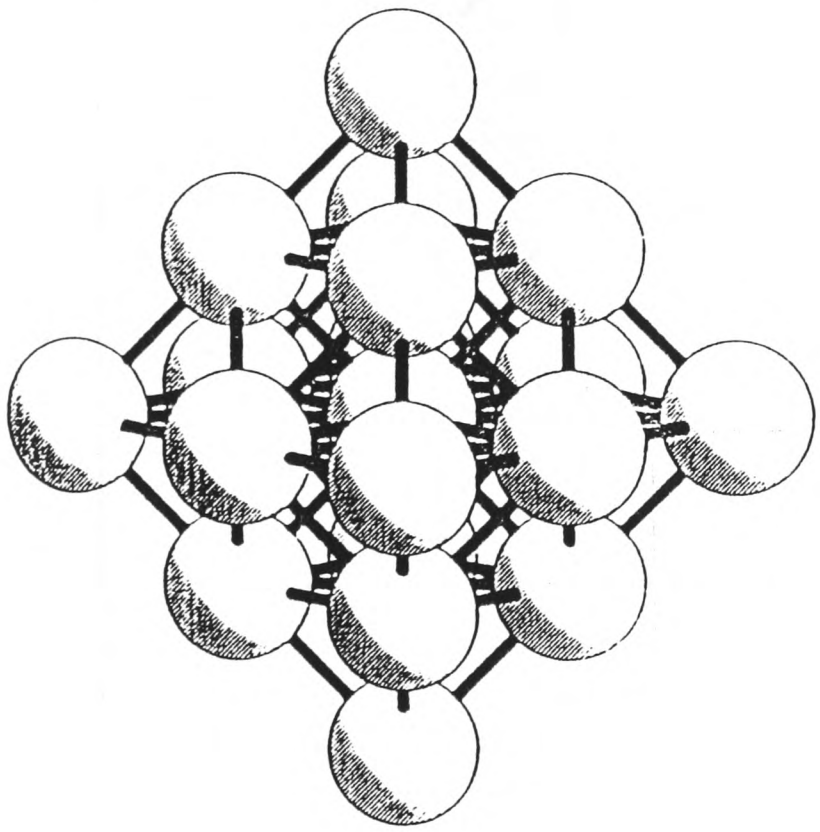
For the close packed structure (Figure 3.1(a)), $r_{tet(c.p.)}=1.17a$ and $r_{rem(c.p.)}=1.84a$ (a is the bond distance between two adjacent atoms). The inequality of $r_{tet(c.p.)}$ and $r_{rem(c.p.)}$ causes a big difference in the contributions from the two sets of atoms. The contribution of the tetrahedral set is only about 10% of that from the remaining set because of the factor of $(1/r_O^5)$ and $C_{tet(c.p.)}$ is negligible compared to $C_{rem(c.p.)}$. Therefore, a larger splitting of the D shell is expected for the close packed structure. In the more spherical structure (Figure 3.2), the cancellation leads to a small C $[0.30(\pi)^{1/2}/r_O^5$, where $r_O=r_{tet(sph)}=r_{rem(sph)}]$. The spherical structure is thus predicted to produce a smaller splitting of the D shell. This prediction is confirmed by the ab initio calculations on the two structures.[7]



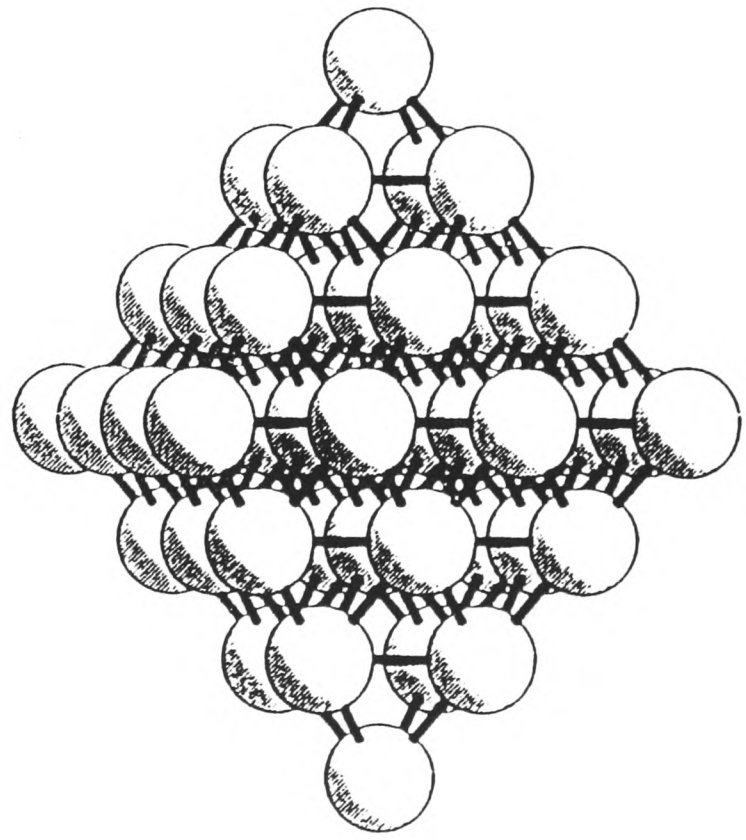
(a)



(b)



(c)



(d)

Figure 3.1 Some specific examples of tetrahedral and octahedral arrangements based on fcc closed packing

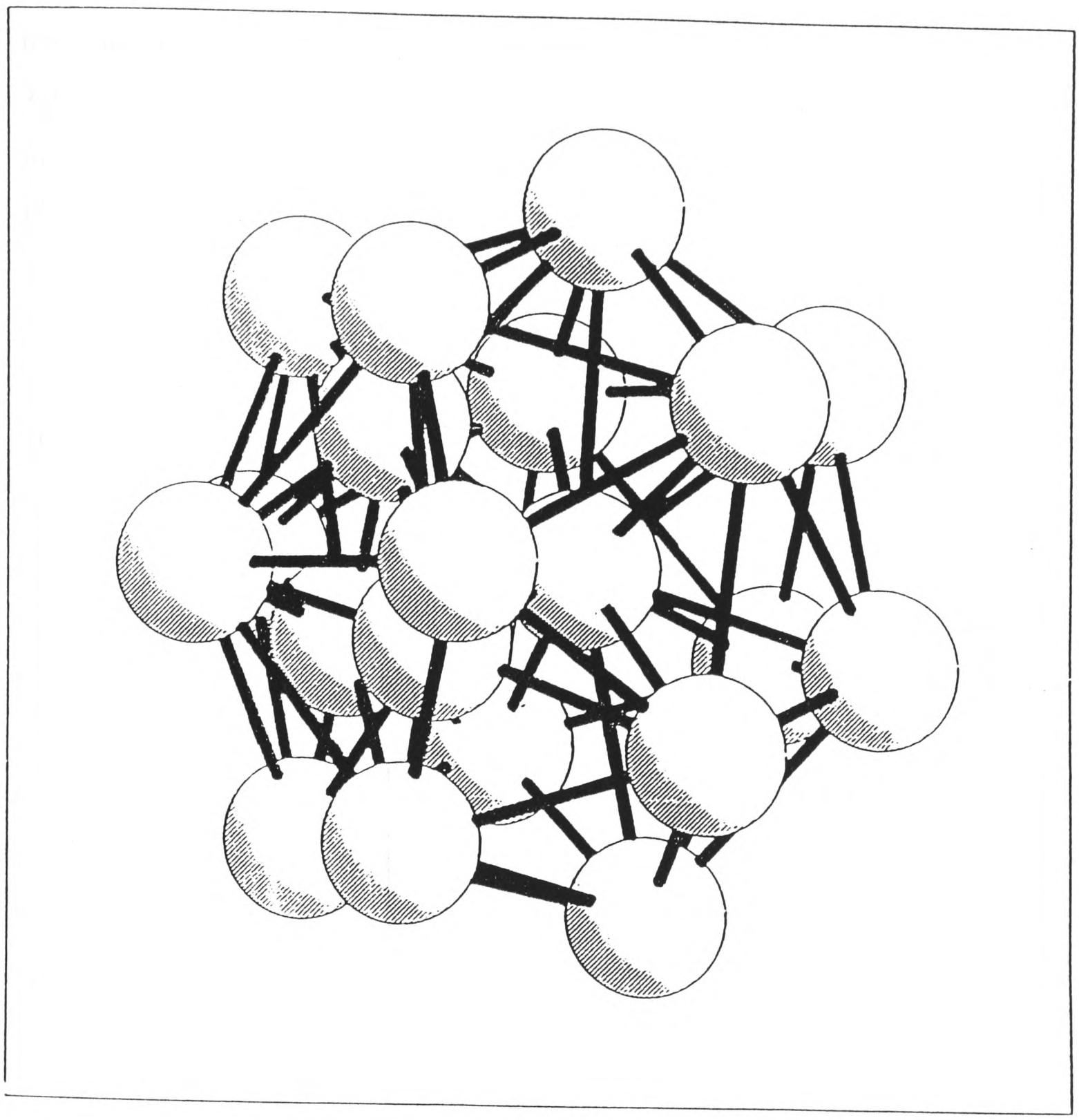


Figure 3.2 A spherical structure with T_d point group for an M_{20} cluster

The same tendency is found from calculations on M_{19}^+ clusters (see Figure 3.1(c)). When C_{oct} is defined as the contribution from the six atoms located on the C_4 axes and C_{rem} from the remaining 12 atoms located on the C_2 axes, $C_{oct}=2.33(\pi)^{1/2}/r_{oct}^5$ and $C_{rem}=-1.17(\pi)^{1/2}/r_{rem}^5$. The cancellation between the two sets of atoms is maximised when $r_{oct}=1.15r_{rem}$. In the close packed structure (Figure 3.1(c)), $r_{oct}=1.414r_{rem}$. A maximum of cancellation can be achieved by moving the atoms located on the C_4 axes towards the centre and moving those on C_2 axes away from the centre along the axes. Therefore, a smaller splitting of the D shell is predicted for a more spherical structure in the M_{19}^+ cluster than for the centred octahedron. In summary, the splitting of electronic shell structures is small for those structures with a more spherical geometry and high symmetry.

3.4 Close Packed and Spherical High Symmetry Structures

We shall focus on T_d, O_h and I_h symmetry structures for alkali metal clusters with closed shell jellium electronic configurations. Tables 3.1, 3.2 and 3.3 summarise the symmetries and the number of atoms in the general and special positions in the T_d, O_h and I_h point groups. The magic numbers associated with the jellium model must coincide with permutations of atoms among these positions. For example, an M_{20} cluster restricted to the T_d, O_h or I_h point groups must result from one of the following permutations.

T_d: $4\,(C_{3v}) + 4\,(C_{3v}) + 12(C_s)$

O_h: $6\,(C_{4v}) + 6\,(C_{4v}) + 8\,(C_{3v})$

$12(C_{2v}) + 8\,(C_{3v})$

I_h: $20(C_{3v})$.

Table 3.1. The symmetry and number of the special and general positions in the tetrahedral point group

symmetry of special position	number of atoms generated	location of atoms on
T_d	1	centre
C_{3v}	4	C_3 axes
C_{2v}	6	C_2 axes
C_s	12	mirrors
C_1	24	general positions

Table 3.2. The symmetry and number of the special and general positions in the octahedral point group

symmetry of special position	number of atoms generated	location of atoms on
O_h	1	centre
C_{4v}	6	C_4 axes
C_{3v}	8	C_3 axes
C_{2v}	12	C_2 axes
C_s	24	mirrors
C_1	48	general positions

Table 3.3. The symmetry and number of the special and general positions in the icosahedral point group

symmetry of special position	number of atoms generated	location of atoms on
I_h	1	centre
C_{5v}	12	C_4 axes
C_{3v}	20	C_3 axes
C_{2v}	30	C_2 axes
C_s	60	mirrors
C_1	120	general positions

Furthermore, these geometries represent composite structures based on tetrahedra ($4C_{3v}$), octahedra ($6C_{4v}$), cubes ($8C_{3v}$), truncated tetrahedra ($12C_s$) and cuboctahedra ($12C_{2v}$).

The most closed packed structure represents the structure with the maximum numbers of nearest atoms and has successive layers of atoms in complementary positions. At the other extreme the most spherical structure is that which has the maximum number of atoms on the outer layer, and has them evenly distributed. Therefore, it is apparent that even for high nuclearity clusters which have closed shell electronic structures, they will have either spherical high symmetry geometries or closed packed or nearly close packed structures. These two geometric requirements restrict the permutational possibilities. For example, for the four possible permutations above for an M_{20} cluster, the first choice is the most preferable since it satisfies the requirements of complementary angular co-ordinates for atoms on successive layers and generates a close packed or nearly close packed structure. For the second

permutation, the location of atoms on two sets of C_{4v} special positions leads to a structure in which two atoms are placed above each other, i.e. in the same radial direction. Structures derived from the third and fourth permutations cannot lead to nearly close packed arrangements because either many atoms (20 or 12) are located on one shell without centre, or a cube (8) is taken as an interstitial moiety. We now look in turn at the close packed and spherical structural possibilities for clusters with closed shell electronic structures.

3.4.1 Close Packed Structures

T_d, O_h and I_h symmetry structures can be only derived from fcc, bcc and icp (icosahedral) close packed arrangements. Those structures derived from the most close packed arrangement (fcc) will be the most preferable since they maximise the number of inter-atom interactions. Therefore, we will focus on the structures derived from the fcc arrangement in the following discussion. However, bcc and icp will also be considered for those structures which cannot be derived from an fcc arrangement.

3.4.1.1 Polyhedra derived from close packed arrangements

The dependence of the number of atoms (N_T) in fcc crystalline-like fragments based on tetrahedral, octahedral and cubic geometries on the number of atoms lying on an equivalent edge (k) (corner atoms included) was formulated in 1960's in the discussion of the statistics of surface atoms and surface sites on metal crystals in catalytic chemistry.[11] Table 3.4 lists the total number of atoms for some values of k and the general expression of N_T as a function of k. Figure 3.1 shows some specific examples. It can be seen from Table 3.4 and Figure 3.1 that the simple tetrahedron and octahedron series are not responsible for the geometries

of the alkali metal clusters with magic numbers, although they possess high symmetries. However, the geometries of clusters with different numbers of atoms with the same symmetries (T_d and O_h) can be derived by capping or truncating these polyhedra. This will be discussed below. The corresponding cubic, octahedral and rhombic dodecahedral polyhedra based on bcc packing are summarised in Table 3.5.

Table 3.4. The dependence of the total number of atoms (N) on the number of atoms (k) on each edge of a tetrahedron, octahedron and cube based on face centred cubic close packing (fcc).

	k=2	k=3	k=4	k=5	general expression
N(tetrahedron)	4	10	20	35	(1/6)k(k+1)(k+2)
N(octahedron)	6	19	44	85	(1/3)k(2k×k+1)
N(cube)	14	63	172	465	k(4k×k-6k+3)

Table 3.5. The dependence of the total number of atoms (N) on the number of atoms (k) on each edge of a cube, octahedron and rhombic dodecahedron based on body centred cubic close packing (bcc).

	k=2	k=3	k=4	k=5	general expression
N(cube)	9	35	72	189	$k^3+(k-1)^3$
N(octahedron)	15	57	143	289	$(1/3)(2k^2+1)(4k-3)$
N(rhombic dodecahedron)	15	65	175	369	$(2k-1)(2k^2-2k+1)$

3.4.1.2 Geometries derived from the fcc close packing arrangements.

Neutral metal clusters

The magic numbers for alkali metal clusters observed in experiments are 8, 20, 40, 58 and 92 atoms. Possible geometries based on close packed arrangements can be deduced from the above discussion.

M_8: The tetra-capped tetrahedron with T_d symmetry represents the geometry of M_8. Ab initio calculations on Li_8 have confirmed that the tetracapped tetrahedron is the most stable geometry.[5]

M_{20}: It can be seen from Table 3.4 and Figure 3.1 that a simple tetrahedron with k=4 is a possible geometry for this cluster. An ab initio calculation has indicated that this structure has the lowest Hartree-Fock energy.[7]

M_{40}: The total number of atoms based on a tetrahedron with k=6 is 56 (see Table 3.3). When a 4-atom tetrahedron is taken away from each corner of this tetrahedron a truncated tetrahedron with 40 atoms is derived (56-4×4).

M_{58}: Taking a vertex away from each corner of a tetrahedron with k=6 and capping each edge of this tetrahedron with one atom generates a geometry of 58 atoms with T_d symmetry (56-4+6).

M_{92}: A tetrahedron with k=7 has 84 atoms. Taking one atom away from each vertex of this tetrahedron and capping each face with 3 atoms leaves a M_{92} cluster with T_d symmetry.

Those clusters with closed shell electronic structures which are not observed as large peaks in the mass spectra, e.g. M_{18}, M_{34}, M_{68} and M_{70} clusters, could have low intensities either because no high symmetry structures (e.g., M_{18}, M_{34} and M_{70} clusters) can be generated, or accidental degeneracies of the energy levels do not lead to a clear definition of the shell structures. The latter factor can be understood

from the following example. In the original discussion of the jellium model,[1] the difference in the total electronic energy between M_N and M_{N+1} clusters, E(N)-E(N+1), was defined as Δ(N). The change in this quantity, Δ(N+1)-Δ(N), was plotted against N. Peaks result when Δ(N+1) increases in a discontinuous fashion, as an energy level is just filled at certain N and the next orbital which is much less stable starts to be occupied in the cluster with N+1 atoms. When 1f orbitals are close to 2p orbitals, the peak of N=34 cannot be observed because Δ(N+1)-Δ(N) is too small to cause a discontinuity.

The alkali metal cluster cations

The magic numbers for cluster cations are those with closed shell electronic structures. The following M_n^+ clusters can be derived using the argument developed above.

M_9^+: Body centred cubic geometry (see Table 3.5) has O_h symmetry.
An ab initio calculation found that the centred square antiprism was the most stable structure. This is because a larger stabilisation energy is gained by the 1s orbital in spite of the destabilisation resulting from the splitting of 1p orbitals during the conversion from body centred cube to centred square antiprism.[5]

M_{19}^+: A simple octahedron with k=3 (see Table 3.4 and Figure 3.1(c)) has a total number of 19 atoms. M_{19}^+ can be also derived from icp close packing (a form of double icosahedron) but is has D_{5h} rather thatn I_h symmetry.

M_{21}^+: Taking one atom away from each vertex of an octahedron with k=3 and capping one atom to each face of the octahedron, a geometry with 21 atoms (O_h) can be derived (19-6+8).

M_{35}^+: A simple tetrahedron with k=5 (see Figure 3.1(b)) has a total of

35 atoms (T_d).

M^+_{41}: Capping one atom on each edge of the above tetrahedron (k=5), a cluster with 41 atoms is generated (35+6). However, this structure is unfavored because the edge-capped atom lies directly above an edge-atom of the tetrahedron.

M^+_{93}: A face capped octahedron with k=5 has a total number of 93 atoms (85+8).

Magic numbers, n=19, 21, 35 and 41 for alkali metal cluster cations generated from the liquid metal ion source (LMIS), have been observed.[12] These magic numbers and the existence of high symmetry geometries to account for their structures contribute to the success of the jellium model.

3.4.2 Spherical Geometries

In the previous Chapter, we concluded that when a cluster has a complete jellium closed shell structure it will adopt a polyhedral geometry based on a high symmetry point group. The adoption of a geometric arrangement which most closely approximates to spherical will minimise the splittings of the n*l* shells. Consequently, alternative possible geometries which not only have high symmetries but also a spherical arrangement can be proposed, which have approximately close packed arrangements of atoms. These spherical geometries can be obtained from those discussed above by assuming that the interstitial atoms are fixed and the surface atoms are allowed to move on the surface of a defined sphere in such a way that the symmetry of the cluster is maintained in the process. Maintaining the symmetry of the cluster simplifies the search for an optimum structure since those atoms lying on

special positions on C_n ($n \geq 2$) axes are fixed (as long as the radius of the sphere is defined) because the atoms located on special positions on C_n axes are not allowed to move away from the rotation axes. Therefore, only those atoms lying on the general positions and the special positions on a mirror are allowed to move. The optimum structure is defined as that where all the surface atoms are most evenly distributed on the surface of the defined sphere. The most evenly distributed structure is, therefore, defined by maximising the sum of all distances between surface atoms. Under this condition, the least repulsion between surface atoms on the sphere is expected and the most evenly "spherical" structure is found. A Fortran program has been written to generate these optimum structures with magic numbers. One chooses the relative orientation of the outer 'sphere' and the interstitial moiety such that no two atoms are placed in the same radial direction. This restricts a random choice in the permutation of the numbers from Tables 3.1, 3.2 and 3.3 to get a magic number. The individual geometries are discussed below.

M_{20}:

Assuming an interstitial 4-atom tetrahedral moiety made of the four face centre atoms of the tetrahedron with k=4 (see Figure 3.1(a)) and allowing the remaining 16 atoms, which include 12 special positions on mirror and 4 on C_3 axes, to move, we find a T_d optimum geometry which is shown in Figure 3.2. When the bond distances between the interstitial atoms are a and the radius of the outer sphere is $1.467a$, the bond distances between the surface atoms are found to be about $1.40a$. This indicates that there is less interaction between the surface atoms and at the Hartree-Fock level this structure is less stable than the close packed alternative. Calculations including correlation appear to invert the relative energies of the two possibilities.[7]

M^{+}_{21}:

An I_h symmetry structure for this cluster can be generated when 20 atoms are located on the C_3 axes of the I_h point group (see Table 3.3) and one atom is placed on the centre.

M^{+}_{35}:

It can be seen from Figure 3.1(b) that the interstitial moiety is a centred cuboctahedron. The remaining 22 surface atoms include 12 special positions on mirrors, 4 on C_3 axes and 6 on C_2 axes. The optimum geometry with T_d point group of the 22 surface atoms is shown in Figure 3.3 (for clarity, the interstitial cuboctahedron has been omitted from the Figure). The radius of the sphere is chosen as $1.73a$ and the distances between surface atoms is about $1.33a$. These ratios are similar to those for the M_{20} cluster.

M_{40}:

When a tetrahedron is taken as the interstitial, the 36 surface atoms are then located on the 12 special mirror positions and 24 on the general positions. The optimum geometry is shown in Figure 3.4, which can be visualised as the superposition of Figures 3.5(a) and 3.5(b). The radius of the polyhedron is $1.8a$ and the distances between surface atoms are found to be about the same as those between the interstitial atoms. The interstitial 4 atom tetrahedron has been omitted from this Figure for reasons of clarity. The atoms in the interstitial tetrahedron are located radially to the centres of the four hexagonal planes (see Figure 3.5(a)).

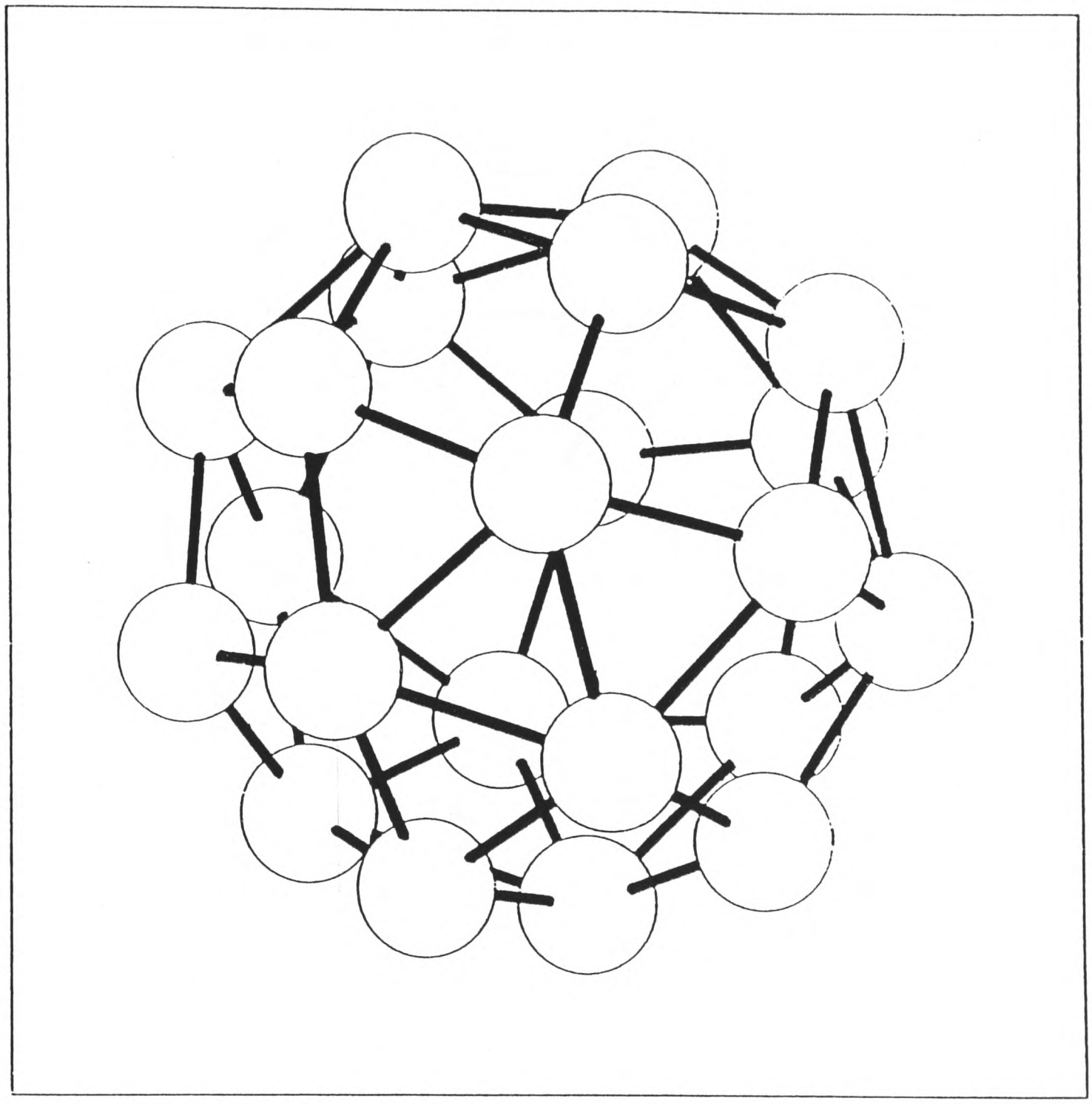


Figure 3.3 The optimum geometry with T_d point group for the M_{35}^+ cluster (the interstitial cuboctahedron is omitted for reasons of clarity)

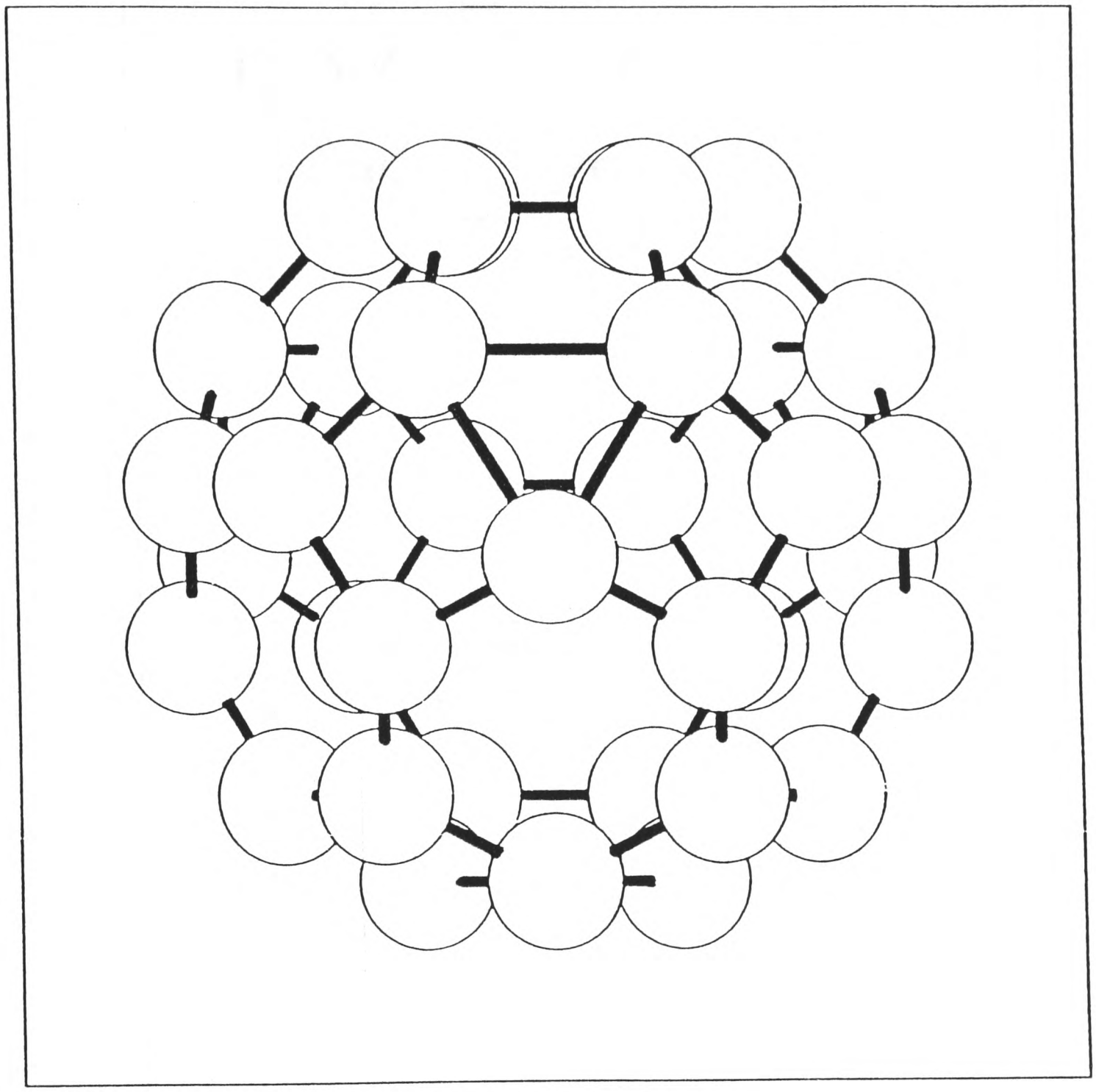
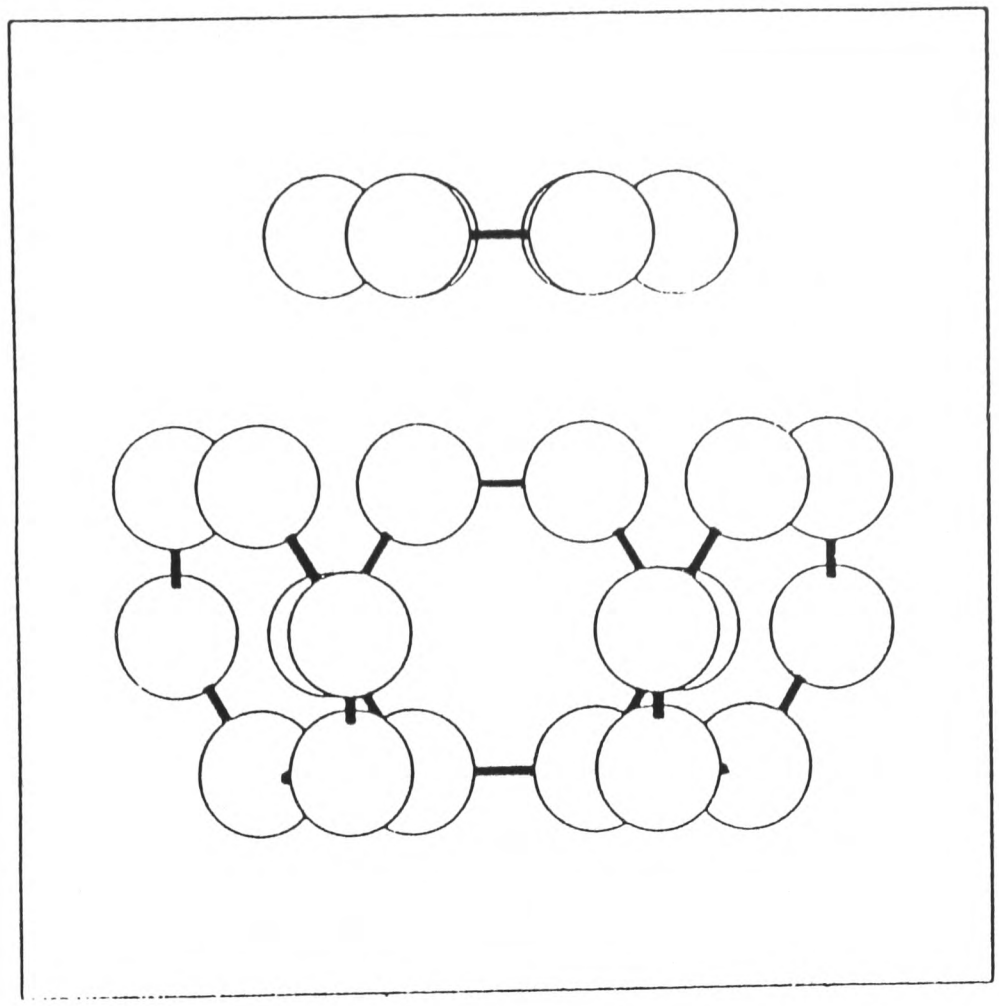
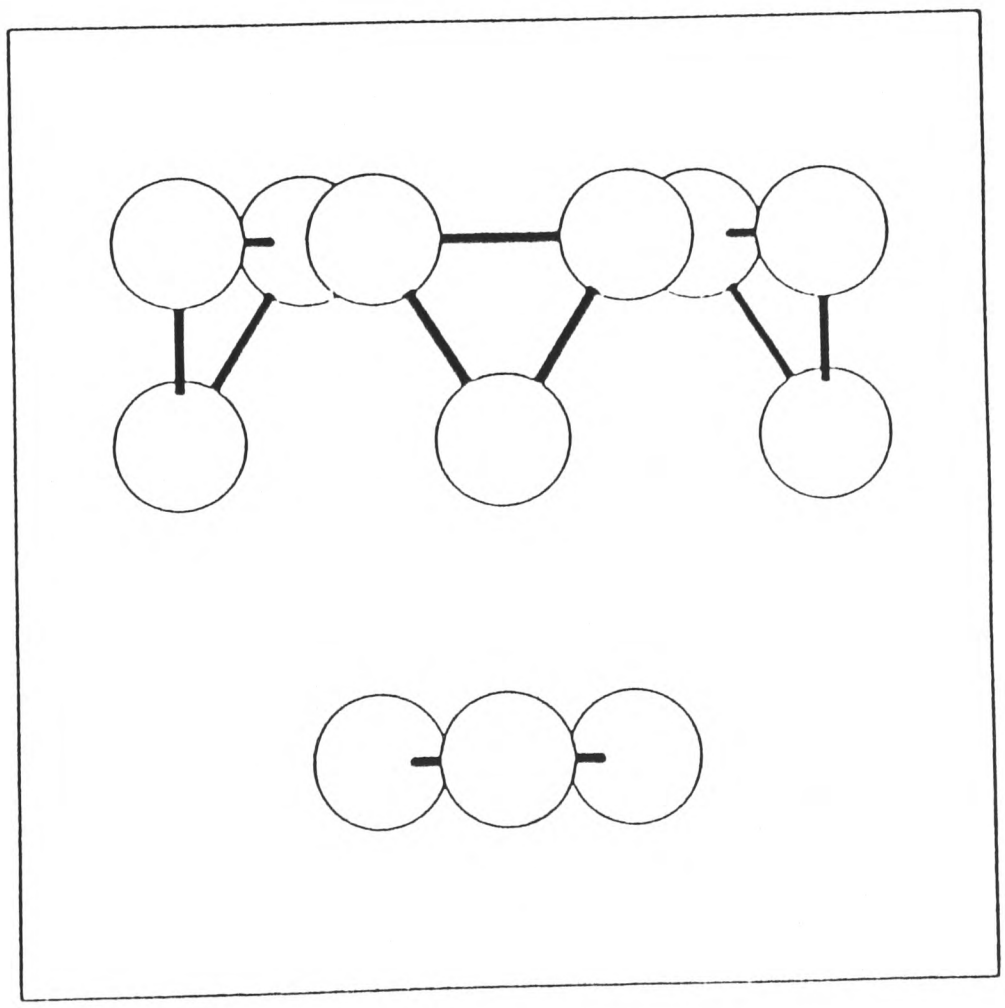


Figure 3.4 The optimum geometry with T_d point group for the M_{40} cluster (the interstitial tetrahedron is omitted for reasons of clarity)



(a)



(b)

Figure 3.5 The two sets of atoms for the optimum structure of the M_{40} cluster (see Figure 3.4)
(a) general positions
(b) special mirror positions

M^+_{41}:

A centred cuboctahedron (13 atoms) is the interstitial moiety and the remaining 28 atoms are located on the general positions (24) and the special positions on C_3 axes (4). A T_d molecule is obtained for the M^+_{41} alkali metal cluster cation.

M_{58}:

A 10-atom tetrahedron with k=3 (see Table 3.4) can be defined as the interstitial moiety for this cluster. The remaining 48 atoms are located on the general positions of the octahedral point group. The combination of the interstitial moiety with T_d symmetry and the surface geometry with O_h point group produces a structure with T_d symmetry.

M_{92}:

A truncated octahedron with k=4 (44-6=38) (see Figure 3.1(d)) is taken as the interstitial moiety and the remaining 54 atoms are placed on the general positions (48) and the special positions (6) on C_4 axes. An O_h symmetry is generated for this cluster.

M^+_{93}:

When a face capped centred icosahedron (1+12+20=33) is taken as the interstitial moiety (see Table 3.3) and the remaining atoms are located on the 60 mirror positions, an I_h symmetry structure is obtained for this cluster.

For other high nuclearity alkali metal clusters with magic numbers, a similar method can be used to generate the possible high symmetry geometries. It depends on the choice of the interstitial moiety and the atoms on the outer sphere. When more atoms need to be considered, more inner spheres can be chosen. This means that more possible structures with high symmetry have to be considered.

3.5 Conclusions

This Chapter provides a general method for generating the geometries of high nuclearity alkali metal clusters with magic numbers according to the jellium model. A theoretical justification for the adoption of high symmetry structures has been given within the framework of molecular orbital and crystal field theories. Clusters which satisfy the magic numbers and can adopt a high symmetry close packed or spherical geometry are predicted to be particularly stable. Clusters with incomplete jellium closed shell electronic structures adopt lower symmetry structures.

References for Chapter Three

1. W.D.Knight, K.Clemenger, W.A.de Heer, W.Saunders, M.Y.Chou, M.L.Cohen, *Phys. Rev. Lett.* 52, (1984), 2141.
2. W.D.Knight, K.Clemenger, W.A.de Heer, W.Saunders, *Sol. State Commun.*, 53, (1985), 445.
3. M.L.Cohen, M.Y.Chou, W.D.Knight, W.A.de Heer, *J. Phys.Chem*, 91, (1987), 3141.
4. C.Baladron, J.Alonso, *Physica B.*, 154, (1988), 73.
5. I.Boustani, W.Pewestorf, P.Fantucci, V.Bonacic-Koutecky, J.Koutecky, *Phys. Rev.*, B35, (1987), 9437.
6. V.Bonacic-Koutecky, P.Fantucci, J.Koutecky, *Phys. Rev.*, B37,(1988), 4369.
7. J.Koutecky, V.Bonacic-Koutecky, I.Boustani, P.Fantucci, in "*Large Finite Systems*", (Ed. J. Jortner et al) p_{303}, D. Reidel Publishing Company (1987).
8. O.Echt, K.Sattler, E.Recknagel, *Phys. Rev. Lett.*, 47, (1981), 1121.
9. G.S.Anagnostatos, *Phys. Lett. A,* 133, (1988), 419.
10. For crystal field theory, see:
    (a) J.S.Griffith, "Theory of Transition Metal Ions", Cambridge University Press, Cambridge, 1961.
    (b) B.L.Silver, "Irreducible Tensor Methods", Academic Press, New York, 1976.
    (c) M.T.Hutchings, *Sol. State Phys.*, 16, (1964), 227.
11. R.Van Hardeveld, F.Hartog, *Surface Science*, 15, (1969), 189.
12. Y.Saito, K.Minami, T.Ishida, T.Noda, *Z. Phys. D*, 11, (1989), 87.

Chapter 4 A Group Theoretical Paradigm for Describing the Skeletal Molecular Orbitals of Cluster Compounds deriving from ML_2, ML_4 and ML_5 fragments

4.1 Introduction

The **Polyhedral Skeletal Electron Pair Theory** has proved to be useful for accounting for the structures of cluster compounds of transition metals and main group atoms.[1,2] The theoretical basis for this approach has been provided by the **Tensor Surface Harmonic Theory** developed initially by Stone [3,4] for deltahedral clusters and subsequently extended to three and four connected, condensed and high nuclearity clusters.[5-8] The group theoretical consequences of the **Tensor Surface Harmonic Theory** have been defined by Ceulemans,[9] Fowler,[10,11] Quinn [12] and Johnston and Mingos.[13-16] These conclusions have been based primarily on the parity relationships which connect L^{π} and $\bar{L}^{\pi}$ molecular orbitals of cluster compounds. The parity relationship is defined as the local rotation of each p_{π} component of a molecular orbital by a rotation of 90° in the same clockwise or counter-clockwise sense. The effect of such a rotation is to convert a bonding molecular orbital (L^{π}) into an equally antibonding molecular orbital ($\bar{L}^{\pi}$). Group theoretically the parity operation is the one dimensional pseudo-scalar representation, Γ_u^o, which is symmetric to all proper operations and antisymmetric to all improper operations. For example, for a tetrahedral cluster the $P^{\pi}(t_2)$ and $\bar{P}^{\pi}(t_1)$ surface molecular orbitals are related by the parity operator, $\hat{P}$, which transforms as a_2 in the tetrahedral point group.

$$t_2 \xrightarrow{\hat{P}} t_1$$

Or, generally Γ_u^O in a point group, i.e.

$$\Gamma(L^{\pi}) \otimes \Gamma_u^O = \Gamma(\bar{L}^{\pi})$$

If the above direct product generates the original representation then the representation is descibed as self-conjugate:

$$\Gamma_A \otimes \Gamma_u^O = \Gamma_A$$

The occurrence of an odd number of self-conjugate representations for a cluster is indicative of non-bonding molecular orbitals and alternative electron counts. For example, in the tetrahedron the e molecular orbitals are self-conjugate:

$$e \otimes \Gamma_u^O = e \otimes a_2 = e$$

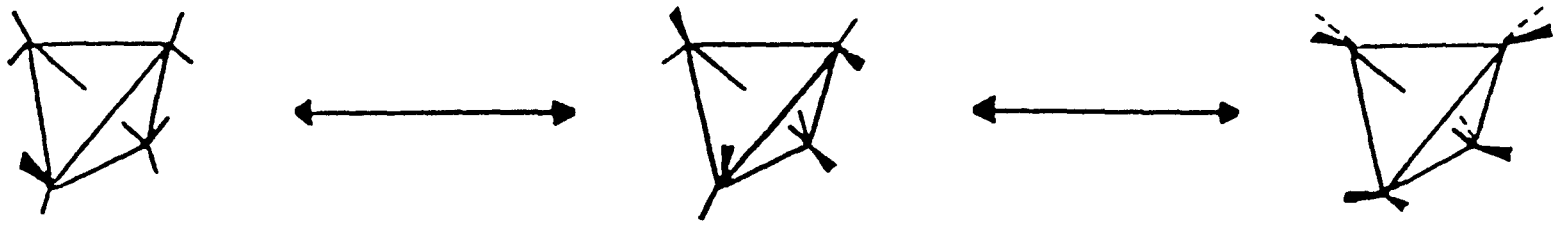
Such a self-conjugate representation must be equally well described as L^{π} and $\bar{L}^{\pi}$ and is consequently non-bonding, i.e. e in tetrahedron is $D^{\pi}/\bar{D}^{\pi}$. These two orbitals remain unoccupied in B_4Cl_4, but are filled in P_4 and C_4R_4.

In a large number of clusters of the transition metals the ligand arrangement around a specific metal atom does not have axial symmetry and therefore the p_{π} orbitals do not comprise a complete set of basis functions. In this Chapter, a group theoretical analysis for clusters based on ML_2 and ML_4 fragments with only one p_{π} component and ML_5 fragments with only one d_{δ} component is presented and used to account for their closed shell requirements.

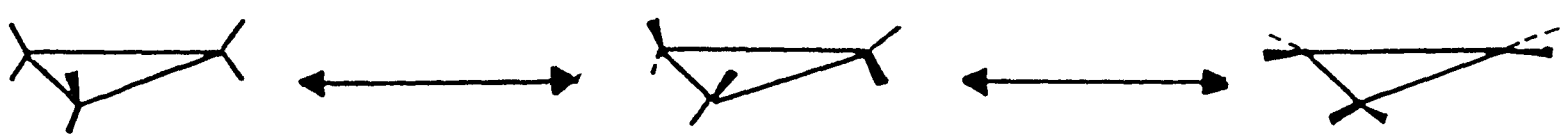
4.2 ML_2 and ML_4 C_{2v} fragments

Evans and Mingos [17,18] have completed semi-empirical molecular orbital calculations on clusters based on ML_2 and ML_4 fragments and these results have been used to confirm the group theoretical arguments developed in this Chapter. In $[ML_2]_n$ clusters the absence of axial symmetry for the ML_2 fragment leads to the possibility of alternative

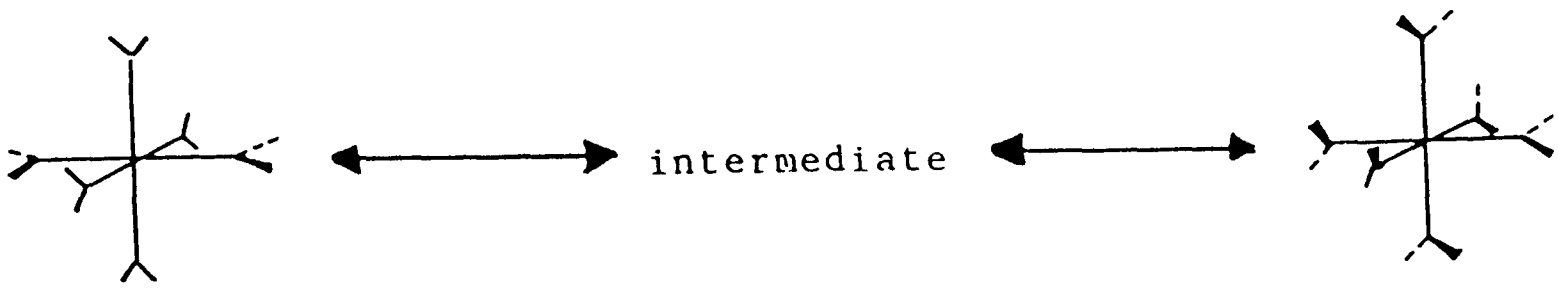
high symmetry conformations. The alternative conformations of this type for tetrahedral and triangular clusters are illustrated in (1) and (3) and (4) and (6). In these instances although the conformations belong to the same point group they represent very different bonding situations. They can be interconverted by simultaneous rotations of the ML_2 fragments by 90° involving intermediates belonging to the pure rotation groups D_2 (2) and D_3 (5) respectively. In contrast the $[ML_2]_6$ clusters illustrated in (7) (T_h point group) and (9) (T_d point group) are converted into each other by simultaneous rotations of the ML_2 fragments by 45° and involve the intermediate (8) belonging to the T pure rotation group, i.e. T_h--->T--->T_d--->T--->T_h. A rotation of 90° leads to an identical geometry, i.e. T_h--->T_h and T_d--->T_d.



D_{2d} (1) D_2 (2) D_{2d} (3)



D_{3h} (4) D_3 (5) D_{3h} (6)



T_h (7) T (8) T_d (9)

For a tetrahedral cluster derived from conical B-H or ML_3 fragments the tangential skeletal molecular orbitals transform as $t_2(P^{\pi})$ bonding, $e(D^{\pi}/\bar{D}^{\pi})$ non-bonding and $t_1(\bar{P}^{\pi})$ antibonding. Table 4.1 summarises the relevant orbital correlations for the descent of symmetry from T_d to D_{2d} to D_2 and also the symmetry properties of the pseudo-scalar parity operator Γ_u^O. In the pure rotation groups C_n, D_n, O and T the parity operator must by definition belong to the totally symmetric representation. Therefore, L^{π} and $\bar{L}^{\pi}$ molecular orbitals must occur in pairs belonging to the same irreducible representations, such that:

$$\Gamma(L^{\pi}) \otimes A = \Gamma(\bar{L}^{\pi}) = \Gamma(L^{\pi})$$

Table 4.1. Correlation for descent in symmetry for T_d--->D_{2d}--->D_2

	T_d	D_{2d}	D_2
$(\bar{P}^{\pi})$	t_1	a_2+e	$b_1+b_2+b_3$
$(D^{\pi}/\bar{D}^{\pi})$	e	a_1+b_1	2a
(P^{π})	t_2	b_2+e	$b_1+b_2+b_3$
Γ_u^O	a_2	b_1	a

For example, in Table 4.1 for D_2 the L^{π} and $\bar{L}^{\pi}$ transform as $2a+2b_1+2b_2+2b_3$. Furthermore, for clusters derived from angular fragments one subset is associated with $L^{\pi}_x/\bar{L}^{\pi}_x$ (or $L^{\pi}_{xz}/\bar{L}^{\pi}_{xz}$ for a transition metal) and the other with $L^{\pi}_y/\bar{L}^{\pi}_y$ (or $L^{\pi}_{yz}/\bar{L}^{\pi}_{yz}$). The x and xz orbitals are defined locally to lie in the angular ML_2 plane. An alternative proof of this generalisation is based on Quinn's relationship:[12]

$$\Gamma(\pi_x) + \Gamma(\pi_y) = \Gamma(\sigma) \otimes \Gamma(z) + \Gamma(\sigma) \otimes \Gamma(R_z)$$

Since both z and R_z transform in an identical fashion in the rotational groups pairs of matching L^{π}_x and L^{π}_y representations are generated.

If the fragments retained axial symmetry the resultant L^{π}_x and L^{π}_y molecular orbitals would mix extensively and regenerate molecular orbitals which closely resembled those in the parent tetrahedron. In angular ML_2 and ML_4 fragments the xz and yz components not only have different symmetry characteristics, but also very different bonding capabilities.[17,18] Molecular orbital calculations have shown that the spectrum of tangential skeletal molecular orbitals is dominated by the xz component. The yz components give rise to a narrow spectrum of bonding, non-bonding and antibonding molecular orbitals which are completely filled by 2n electrons in a $[ML_2]_n$ cluster and have a neutral effect on the bonding requirements of the cluster.

For the D_{2d} geometries illustrated in (1) and (3) the tangential skeletal molecular orbitals derived from xz give rise to the following components:

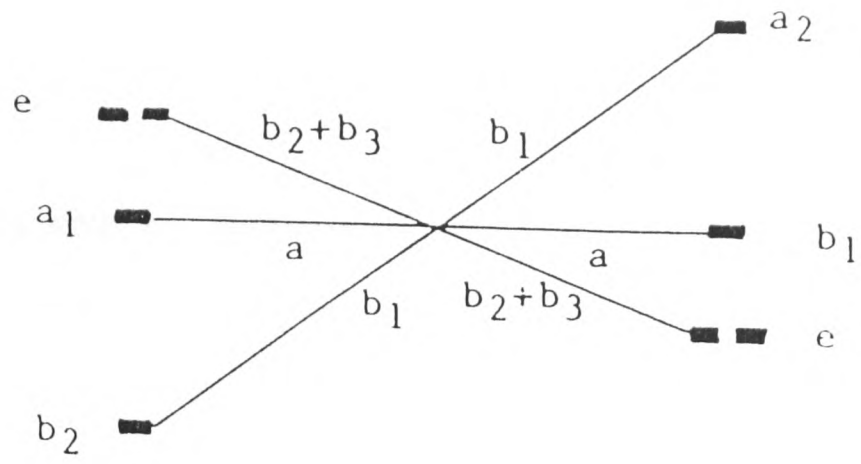
T_d	(1)	(3)
t_1	$e(\bar{L}^{\pi}_{xz})$	$a_2(\bar{L}^{\pi}_{xz})$
e	$a_1(L^{\pi}_{xz}/\bar{L}^{\pi}_{xz})$	$b_1(L^{\pi}_{xz}/\bar{L}^{\pi}_{xz})$
t_2	$b_2(L^{\pi}_{xz})$	$e(L^{\pi}_{xz})$

In D_{2d} Γ^{o}_{u} transforms as b_1 and leads to the following relationships:

$$e \otimes \Gamma^{o}_{u} = e$$
$$b_2 \otimes \Gamma^{o}_{u} = a_2$$
$$a_1 \otimes \Gamma^{o}_{u} = b_1$$

Therefore, the parity operation has the effect of transforming a bonding skeletal molecular orbital in (1) into an antibonding skeletal molecular orbital in (3). Each conformation has one component of the original non-bonding e molecular orbitals and they are also related by the parity transformation. The resultant spectra of molecular orbitals are summarised in Figure 4.1a. The results are in complete agreement with the molecular orbital calculations reported previously.[17] The conformation (3) is clearly the more stable and is associated with 3 $(e+b_1)$ bonding and non-bonding L^{π}_{xz} skeletal bonding molecular orbitals. Since the tetrahedron generally has 5 L^{π} bonding and non-bonding skeletal molecular orbitals it follows that $[ML_2]_4$ clusters will be associated with 56 rather than 60 valence electrons. $[Pt_4(\mu_3\text{-}H)_4(PPr^{i}_{2}Ph)_4]$ with 56 valence electrons provides an example of such a cluster compound.[17]

It is also apparent from Figure 4.1 that the interconversion (1) ---> (3) through (2) is an orbitally forbidden process [19] when the spectrum of L^{π}_{xz} molecular orbitals is filled with 2 to 6 valence electrons. Furthermore, the a, b_1, b_2 and b_3 molecular orbitals in the intermediate D_2 geometry must be approximately non-bonding.

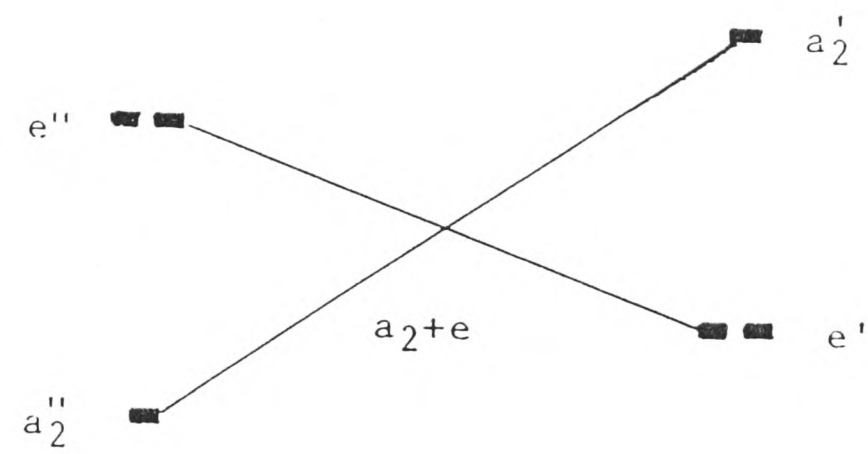


vertical p_π orbials (along the principal axis)

horizontal p_π orbitals (perpendicular to the principal axis)

(1) (2) (3)

(a)



vertical p_π orbitals (perpendicular to the triangle plane)

horizontal p_π orbitals (lying on the triangle plane)

(4) (5) (6)

(b)

Figure 4.1 The correlation diagrams of L^π's (a) for (1), (2) and (3) and (b) for (4), (5) and (6).

Similar arguments can be developed for the interconversion of the two D_{3h} conformations of a triangular cluster (**4**) and (**6**) through the D_3 intermediate (**5**). The relevant orbital correlation diagram is illustrated in Figure 4.1b, and the orbital correlations are summarised in Table 4.2. The more stable conformer is (**6**) since this is associated with 2 bonding skeletal molecular orbitals of e′ symmetry. This conformation is observed in the 48 electron clusters $M_3(CO)_{12}$ (M=Ru or Os)[20] and the 42 electron platinum cluster $[Pt_3(\mu_3\text{-}H)_3H_3(PPr^i_2Ph)_3]$.[21] The interconversion of (**4**) to (**6**) through a D_3 intermediate is once again a symmetry forbidden process.

Table 4.2. Correlation for D_{3h}--->D_3

	D_{3h}	D_3
(P^{π})	$e''+a_2'$	$e+a_2$
(P^{π})	$a_2''+e'$	a_2+e
Γ_u^O	a_1''	a_1

The following general points emerge from the analysis discussed above.

1. The bonding, non-bonding and antibonding components for the two conformations of $[ML_2]_n$, which are related by 90° rotations of the ML_2 fragments, correlate with the L^{π} and $\bar{L}^{\pi}$ skeletal molecular orbitals of a $[ML_3]_n$ cluster only when they are taken together.
2. The molecular orbitals of one conformer are one subset of the $L^{\pi}/\bar{L}^{\pi}$ spectrum and are not related by the parity operator Γ_u^O.

3. The parity operator does relate the molecular orbitals of the conformers A and B in the following manner:

$$\Gamma^{A(bonding)}(L^{\pi}) \otimes \Gamma_u^0 \quad \text{------>} \quad \Gamma^{B(antibonding)}(\bar{L}^{\pi})$$

$$\Gamma^{A(non\text{-}bonding)}(L^{\pi}/\bar{L}^{\pi}) \otimes \Gamma_u^0 \quad \text{------>} \quad \Gamma^{B(non\text{-}bonding)}(L^{\pi}/\bar{L}^{\pi})$$

For example, for (1) and (3)

$$b_2^{(1)} \otimes \Gamma_u^0 = a_2^{(3)}$$
$$a_1^{(1)} \otimes \Gamma_u^0 = b_1^{(3)}$$
$$e^{(1)} \otimes \Gamma_u^0 = e^{(3)}$$

4. Since the parity operator does not relate bonding and antibonding molecular orbitals within the same conformer these clusters do not have a symmetrical spread of molecular orbitals, and the more stable conformer is that which has the larger number of bonding molecular orbitals, i.e. (3) for $[ML_2]_4$ and (6) for $[ML_2]_3$.

5. The interconversion of the conformers by a simultaneous rotation of the angular fragments is a symmetry forbidden process.

In contrast the octahedral clusters (7) and (9) are converted into themselves by simultaneous rotations of the ML_2 fragments by 90°. The parent octahedral cluster is characterised by $t_{2g}(D^{\pi})$ and $t_{1u}(P^{\pi})$ bonding and $t_{1g}(\bar{P}^{\pi})$ and $t_{2u}(\bar{D}^{\pi})$ antibonding skeletal molecular orbitals. The relevant orbital correlations in O_h, T, T_h and T_d are given in Table 4.3. The two equivalent conformations of (7) are characterised by the following components of the octahedral molecular orbitals.

O_h	(7)	(7)	(9)	(9)
t_{2u}				
t_{1g}	t_g	t_g	t_1	t_1
t_{1u}	t_u	t_u	t_2	t_2
t_{2g}				

Table 4.3. Correlation for descent in symmetry O_h-->T_h-->T_d-->T

	O_h	T_h	T_d	T
(D^{π})	t_{2u}	t_u	t_1	t
(P^{π})	t_{1g}	t_g	t_1	t
(P^{π})	t_{1u}	t_u	t_2	t
(D^{π})	t_{2g}	t_g	t_2	t
Γ_u^o	a_{1u}	a_u	a_2	a_1

Since the conformations are identical the parity operator does now relate the bonding and antibonding skeletal molecular orbitals in one conformer:

$$t_u^{(7)} \otimes \Gamma_u^o = t_g^{(7)}$$

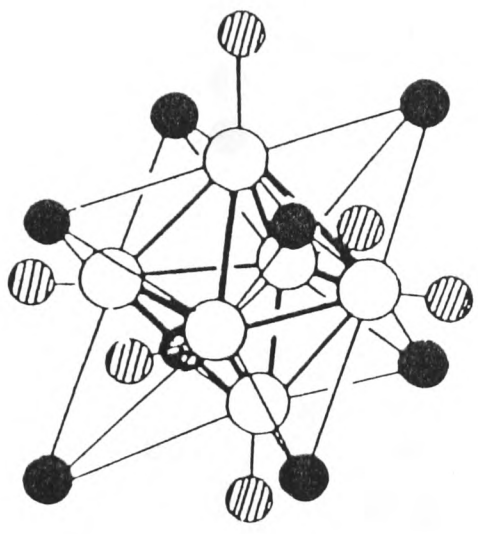
$$t_2^{(9)} \otimes \Gamma_u^o = t_1^{(9)}$$

Furthermore the intermolecular rearrangement of (7) into (9) and then into itself is now a symmetry allowed process. It follows also from the above analysis that deltahedral clusters based on ML_2 fragments (except the tetrahedron) will be characterised by n/2+1 bonding skeletal molecular orbitals if they have two identical conformers related by 90° rotations.

4.3 L^{δ} and $\bar{L}^{\delta}$ Inequivalences in ML_5 Fragments

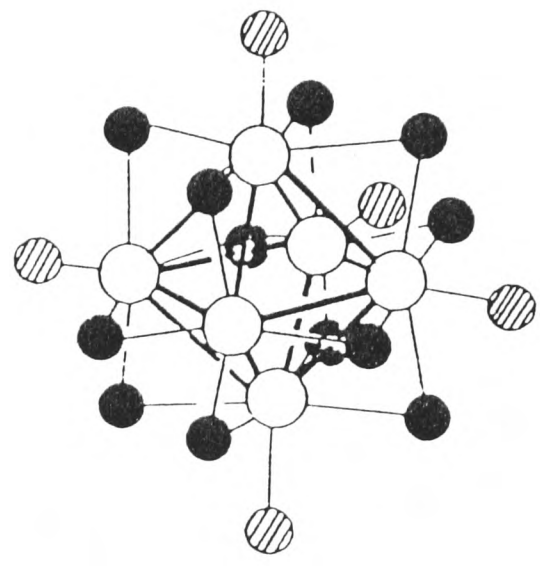
The halide and sulfide clusters of niobium, tantalum, molybdenum and tungsten in their lower oxidation states,[22] e.g. $[M_6(\mu_3\text{-Cl})_8L_6]$ (10) and $[M_6(\mu_2\text{-Cl})_{12}L_6]$ (11), provide examples of clusters based on the ML_5 fragments. The bonding in these clusters has been studied by

Ceulemans and Fowler,[23] and Johnston and Mingos [24] independently within the framework of Stone's tensor surface harmonic theory (TSH). Ceulemans and Fowler's analysis is based on ML_5 fragments with four effective valence orbitals. They also noted the parity relationship between the d_δ orbital pattern of face-bridged cluster (**10**) and that of the edge-bridged cluster (**11**). In this section, the group theoretical analyses for the octahedral clusters (**10**) and (**11**) are extended to their nido and arachno derivatives. Figure 4.2 illustates the structures of closo, nido and arachno chloride-bridged clusters based on (**10**) and (**11**).



$[M_6Cl_8L_6]^{4+}$ (M-Mo or W)

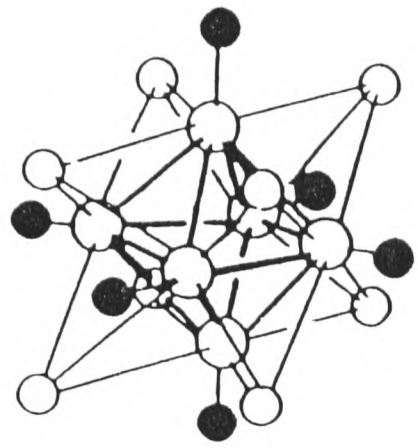
(**10**)



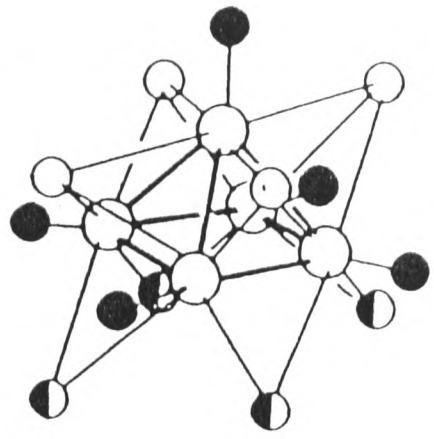
$[M_6Cl_{12}L_6]^{2+}$ (M-Nb or Ta)

(**11**)

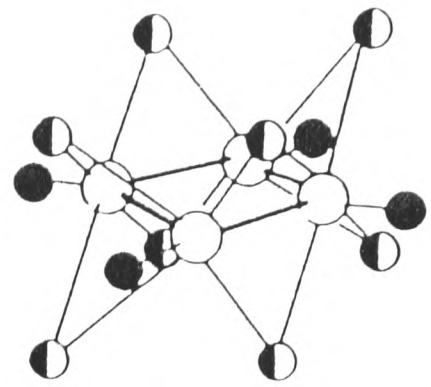
(a)



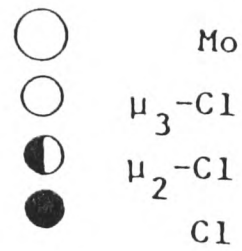
$[Mo_6Cl_{14}]$



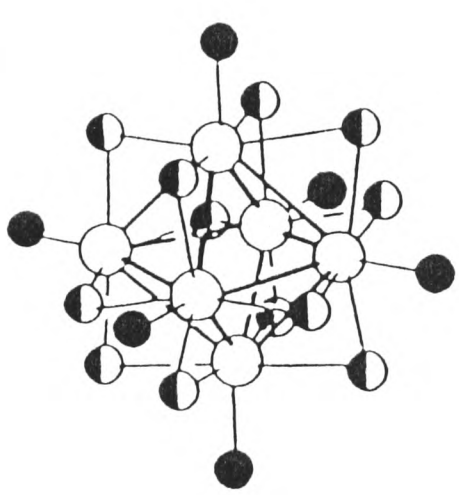
$[Mo_5Cl_{13}]$



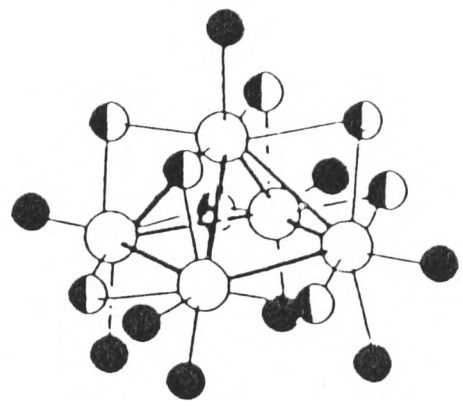
$[Mo_4Cl_{12}]$



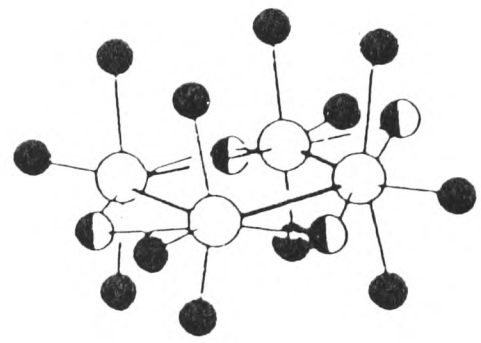
(b)



$[Mo_6Cl_{18}]$



$[Mo_5Cl_{17}]$



$[Mo_4Cl_{16}]$

Figure 4.2 closo, nido and arachno chloride-bridged clusters based on (a) $[Mo_6Cl_8L_6]$ (**10**) and (b) $[Mo_6Cl_{12}L_6]$ (**11**)

The molecular orbital diagram for an ML_5 fragment is shown in Figure 4.3. The frontier fragment orbitals are hy(σ) and the "t_{2g}" set. In carbonyl clusters, the "t_{2g}" orbitals usually are core-like because of the strong stabilisation by CO π^* vacant orbitals. In the π-donor clusters, e.g. sulfide- and chloride-bridged clusters, the "t_{2g}" orbitals are more important for the metal-metal interactions. The three "t_{2g}" orbitals are divided into a d_π pair and one d_δ component. The molecular orbitals derived from the interactions of hy(σ) and d_π pair of the ML_5 fragments are entirely equivalent to those derived from the interactions of the three frontier orbitals of $M(CO)_3$ fragments, and is independent of the arrangement of ligands. In contrast, the d_δ-d_δ interactions depend greatly on the arrangement of ligands.

In a local coordinate frame, the ML_5 fragment in (**10**) appears to be rotated through 45° about the radial vector relative to the ML_5 fragment in (**11**). The single d_δ component is defined as $\delta(x^2-y^2)$ for the ML_5 fragments in (**10**) and $\delta(xy)$ for those in (**11**). In the TSH theory L_d^δ(bonding) is related to L_d^δ(antibonding) by a local rotation of 45° at each vertex about the radial vector.

$$L^\delta \xrightarrow{\hat{P}} \bar{L}^\delta$$

Therefore, the d_δ orbital pattern in (**10**) can be related by the parity operation to that in (**11**). In a similar manner to that discussed above for ML_2 fragments, i.e.

$$L_d^\delta(\text{face-bridged cluster}) \xrightarrow{\hat{P}} \bar{L}_d^\delta(\text{edge-bridged cluster})$$

$$\text{Bonding} \xrightarrow{\hat{P}} \text{Antibonding}$$

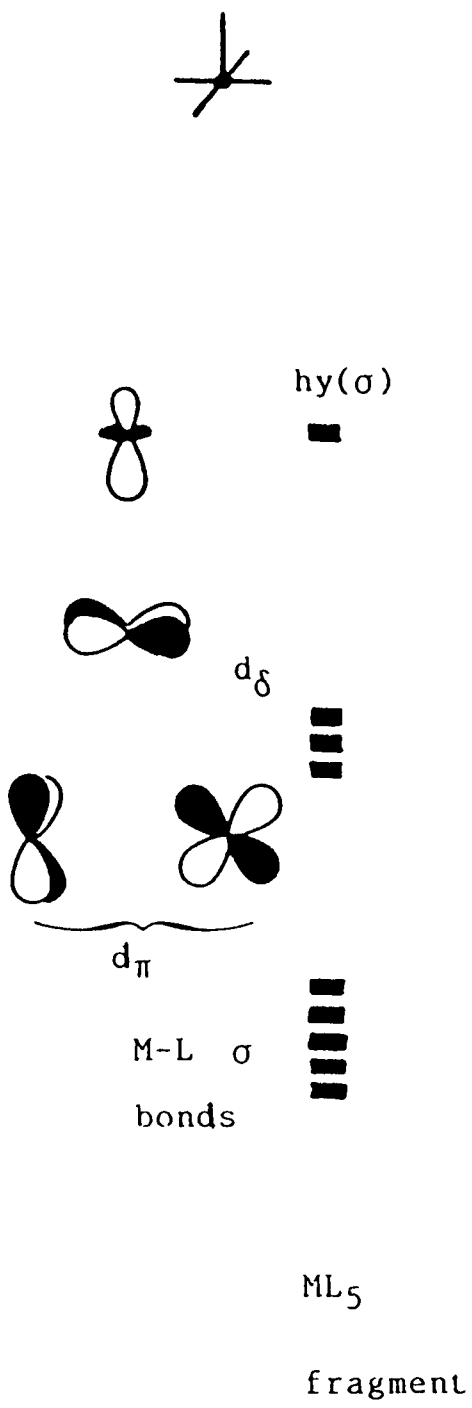


Figure 4.3 The MO level diagram of ML_5 fragment.

An intermediate structure between the face- and edge-bridged clusters belongs to the pure rotation point group O, where the parity operator transforms according to the totally symmetric representation. The linear combinations of the d_δ components are therefore $2a_2+2e+2t_2$. The following correlation is thereby established for the octahedral clusters:

O_h	O	O_h
$(a_{2g}+e_g+t_{2u})$ <--------	(a_2+e+t_2)	--------> $(a_{2u}+e_u+t_{2g})$
face-bridged	single d_δ component	edge-bridged
(<u>10</u>) $d_{x^2-y^2}$	$d_{x^2-y^2}$ or d_{xy}	(<u>11</u>) d_{xy}

In the octahedral point group the parity operator transforms as a_{1u} and relates the L_d^δ and $\bar{L}_d^\delta$ orbitals in the following fashion:

$$a_{2g} \otimes \Gamma_u^O \text{ ----> } a_{2u}$$
$$e_g \otimes \Gamma_u^O \text{ ----> } e_u$$
$$t_{2u} \otimes \Gamma_u^O \text{ ----> } t_{2g}$$

The results of the molecular orbital calculations of Johnston and Mingos [24] which are reproducd in Figures 4.4, 4.5 and 4.6 confirm the argument derived above. In these figures, the MO levels in the left side show the results for (<u>10</u>) and its <u>nido</u>, <u>arachno</u> derivatives and those in the right side are the results of (<u>11</u>) and its corresponding derivatives (see Figure 4.2). It also can be seen that the L_d^π and $\bar{L}_d^\pi$ pattern is entirely equivalent to the L_{pd}^π and $\bar{L}_{pd}^\pi$ pattern derived for $M(CO)_3$ fragments.

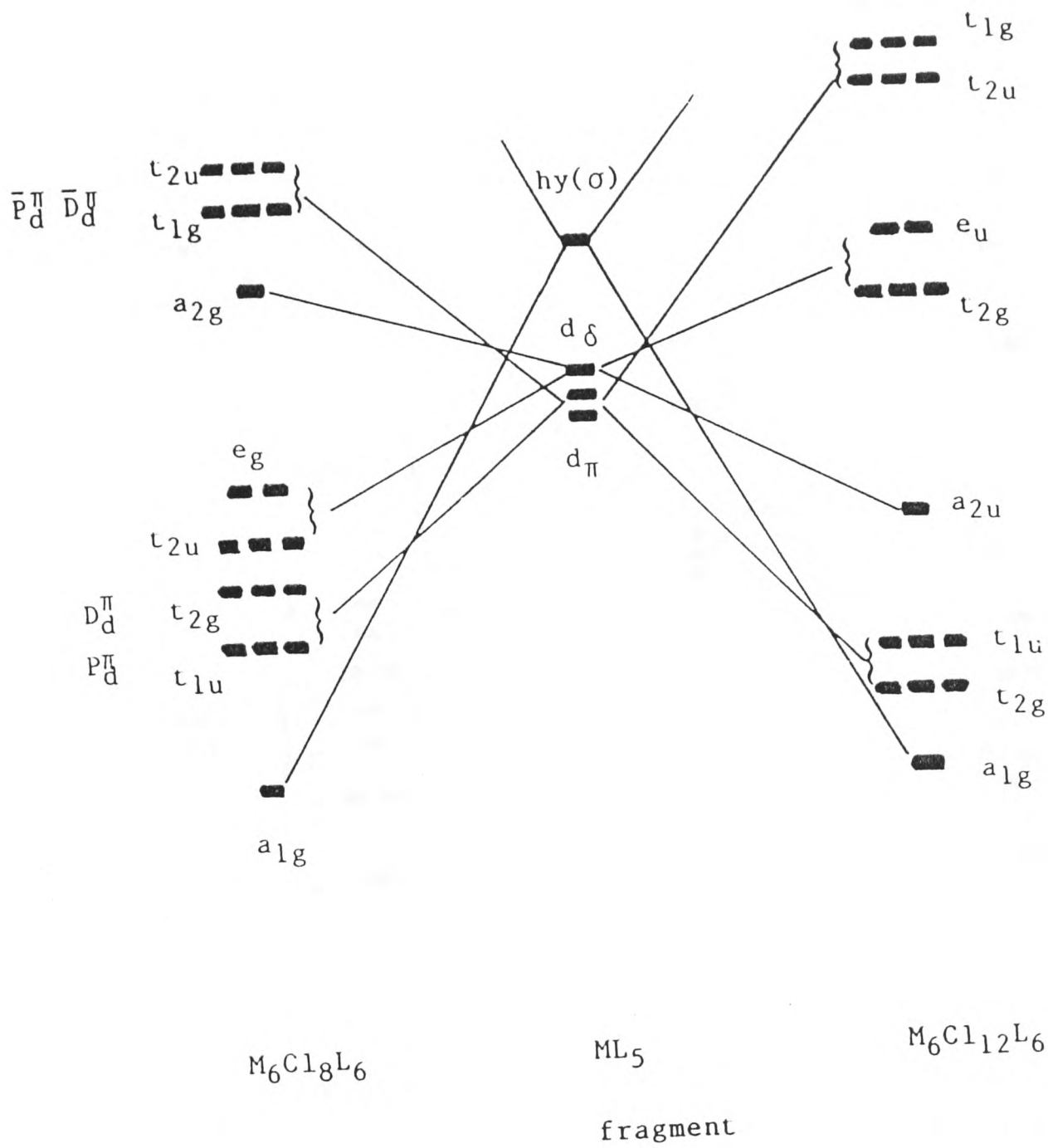


Figure 4.4 The correlation MO diagram of (10) and (11)

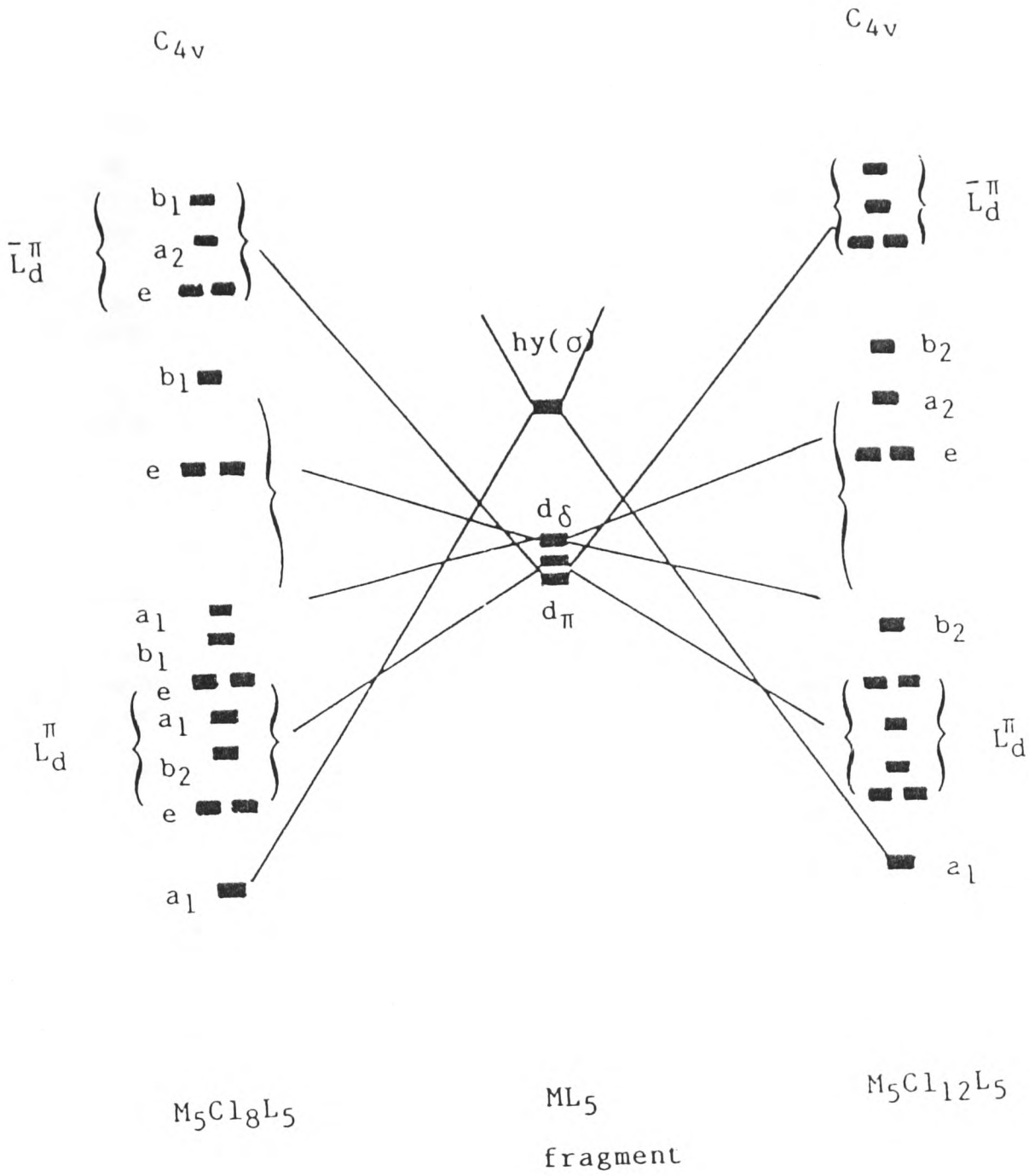


Figure 4.5 the correlation MO diagram of the nido chloride bridged clusters derived from (**10**) and (**11**).

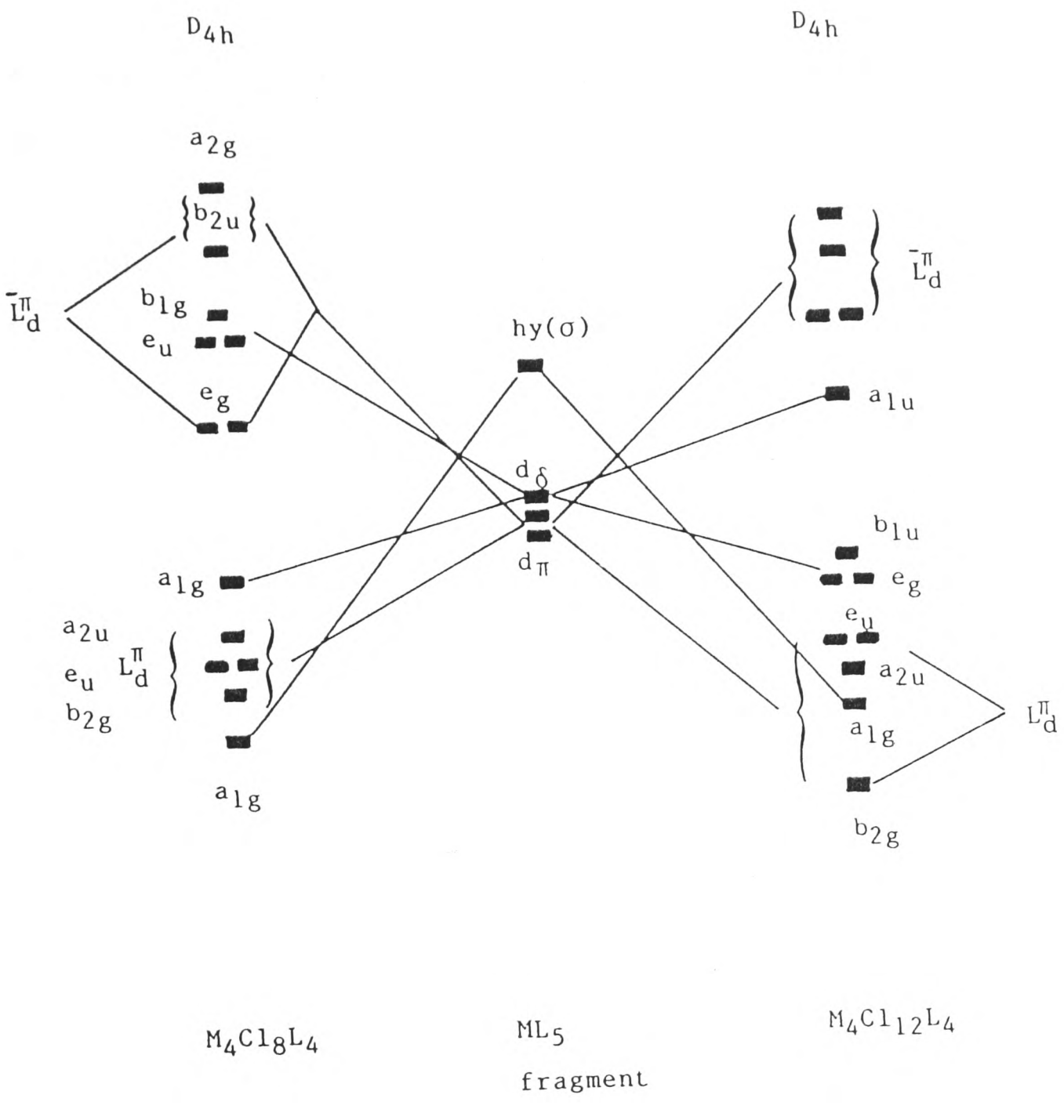


Figure 4.6 The correlation MO diagram of the arachno chloride-bridged clusters derived from (**10**) and (**11**).

Ceulemans and Fowler [23] have previously noted that L_d^{π}/L_d^{δ} and $\bar{L}_d^{\pi}/\bar{L}_d^{\delta}$ mixings have to be taken into account to rationalise the relative energies of the $t_{2u}(D_d^{\delta})$ and t_{2g} (D_d^{δ}) components illustrated in the Figure (see ref. 20). They classified the symmetries of L_d^{π}, $\bar{L}_d^{\pi}$ and those derived from the single d_{δ} component in the O_h finite point group and then took into account the interactions between equisymmetric orbitals. The ideas of Ceulemans and Fowler are extended to the nido and arachno structures in Figure 4.2. Tables 4.4 and 4.5 list the symmetries of molecular orbitals derived from the d_{π} pair, $\delta(x^2-y^2)$ and $\delta(xy)$ basis set for nido (square pyramid) and arachno (square) derivatives of (**10**) and (**11**).

Table 4.4. Symmetries of skeletal molecular orbitals in nido (C_{4v}) structures derived from (**10**) and (**11**) (see Figure 4.2). The $\delta(x^2-y^2)$ bases are needed in face-bridged cluster $M_5Cl_8L_5$. The $\delta(xy)$ bases are needed in edge-bridged cluster $M_5Cl_{12}L_5$.

	$\pi_{xz,yz}$	$\delta(x^2-y^2)$	$\delta(xy)$
bonding	$P^{\pi}(a_1+e)$, $D_{2s}^{\pi}(b_2)$	$D_o^{\delta}(a_1)$, $D^{\delta}(b_1)$	$D^{\delta}(e)$, $F^{\delta}(b_2)$
non-bonding	$D^{\pi}/\bar{D}^{\pi}(e)$		
antibonding	$\bar{P}^{\pi}(a_2+e)$, $\bar{D}_{2s}^{\pi}(b_1)$	$\bar{D}^{\delta}(e)$, $\bar{F}^{\delta}(b_1)$	$\bar{D}_o^{\delta}(a_2)$, $\bar{D}^{\delta}(b_2)$

Table 4.5. Symmetries of skeletal molecular orbitals in square structures derived from (**10**) and (**11**) (see Figure 4.2). The $\delta(x^2-y^2)$ bases are needed in $M_4Cl_8L_4$. The $\delta(xy)$ bases are needed in $M_4Cl_{12}L_4$.

	$\pi_{xz,yz}$	$\delta(x^2-y^2)$	$\delta(xy)$
bonding	$P^{\pi}(a_{2u}+e_u)$, $D^{\pi}_{2s}(b_{2g})$	$D^{\delta}_{O}(a_{1g})$	$D^{\delta}(e_g)$, $D^{\delta}(b_{1u})$
antibonding	$\bar{P}^{\pi}(a_{2g}+e_g)$, $\bar{D}^{\pi}_{2s}(b_{2u})$	$\bar{D}^{\delta}(e_u)$, $\bar{D}^{\delta}(b_{1g})$	$\bar{D}^{\delta}_{O}(a_{1u})$

The nido structure $M_5Cl_8L_5$ has been derived from the face-bridged cluster (**10**) (see Table 4.4). The d_{δ} component, available for cluster bonding, is $\delta(x^2-y^2)$. The non-bonding $D^{\pi}/\bar{D}^{\pi}(e)$ set becomes strongly bonding as a result of interaction with $D^{\delta}(e)$ derived from the $\delta(x^2-y^2)$ basis. The other two e (i.e. P^{π}_{d} and $\bar{P}^{\pi}_{d}$) similarly repel each other but this does not affect the bonding pattern. As a net result 9 bonding orbitals are obtained, $S^{\sigma}(a_1)$, $P^{\pi}_{d}(a_1+e)$, $D^{\pi}_{2s}(b_2)$, $D^{\pi}_{d}/\bar{D}^{\pi}_{d}(e)$ and $D^{\delta}_{d}(a_1)$, $D^{\delta}_{d}(b_1)$ (see the lefthand side of Figure 4.5). For the nido structure $M_5Cl_{12}L_5$ derived from the edge-bridged cluster (**11**) (see Table 4.4), the δ component is $\delta(xy)$. The strong mixing between $D^{\pi}/\bar{D}^{\pi}(e)$ and $D^{\delta}_{d}(e)$ leads to one e bonding and the other e antibonding (see the righthand side of Figure 4.5). Therefore, 8 bonding orbitals are obtained, $S^{\sigma}(a_1)$, $P^{\pi}_{d}(a_1+e)$, $D^{\pi}_{2s}(b_2)$, $D^{\pi}_{d}/\bar{D}^{\pi}_{d}(e)$ and $F^{\delta}_{d}(b_2)$.

In the square clusters $[M_4Cl_8L_4]$ and $[M_4Cl_{12}L_4]$ (see Table 4.5), the mixing between the equisymmetric d_{π} and d_{δ} orbitals does not affect the bonding pattern (see Figure 4.6). Both structures have one S^{σ} and four L^{π}_{d} bonding molecular orbitals and the molecular orbitals

derived from the single d_δ components. The parity operation relates the bonding components in one conformer to the antibonding components in the second conformer.

The following points can be noted from the above discussion.

1. The skeletal molecular orbitals for clusters based on ML_5 fragments are derived from the interactions of one hy(σ), a pair of d_π and one d_δ component.
2. The skeletal molecular orbitals derived from hy(σ) and d_π pair are entirely equivalent to those derived from the three frontier orbitals of $M(CO)_3$ and B-H fragments.
3. The molecular orbitals derived from the single d_δ components are one subset of $L_d^\delta/\bar{L}_d^\delta$ spectrum and are not related by the parity operator Γ_u^o. The parity operator does relate the $L_d^\delta/\bar{L}_d^\delta$ orbitals of face-bridged and edge-bridged clusters which are interconverted by a local rotation of 45° at each ML_5 fragment.
4. L_d^π/L_d^δ and $\bar{L}_d^\pi/\bar{L}_d^\delta$ mixings have to be taken into account in order to rationalise the energies of the $L_d^\delta/\bar{L}_d^\delta$ molecular orbitals. The mixings do not affect the conclusions 2 and 3 because the L_d^π/L_d^δ and $\bar{L}_d^\pi/\bar{L}_d^\delta$ mixings occur simultaneously.

References for Chapter Four

1. K.Wade, *Adv. Inorg. Chem. Radiochem.*, **18**, 1(1976).
2. D.M.P.Mingos, *Nature (London), Phys. Sci.*, **236**, 99(1972).
3. A.J.Stone, *Mol. Phys.*, **41**, 1339(1980).
4. A.J.Stone, *Inorg. Chem.*, **20**, 563(1981).
5. R.L.Johnston and D.M.P.Mingos, *J. Organomet. Chem.*, **280**, 407(1985).
6. R.L.Johnston and D.M.P.Mingos, *J. Organomet. Chem.*, **280**, 419(1985).
7. D.M.P.Mingos, *J. Chem. Soc., Chem. Commun.*, 706(1983).
8. D.M.P.Mingos, *J. Chem. Soc., Chem. Commun.*, 1353(1985);
9. A.Ceulemans, *Mol. Phys.*, **54**, 161(1985).
10. P.W.Fowler, *Polyhedron*, **4**, 2051(1985).
11. P.W.Fowler and C.M.Quinn, *Theor. Chim. Acta.*, **70**, 333(1986).
12. D.B.Redmond, C.M.Quinn and J.G.R.McKiernan, *J. Chem. Soc., Faraday Trans.* 2, **79**, 1791(1983).
13. R.L.Johnston and D.M.P.Mingos, *Polyhedron*, **5**, 2059(1986).
14. R.L.Johnston and D.M.P.Mingos, *Inorg. Chem.*, **25**, 3321(1986).
15. R.L.Johnston and D.M.P.Mingos, *J. Chem. Soc., Dalton Trans.*, 647(1987).
16. R.L.Johnston and D.M.P.Mingos, *J. Chem. Soc., Dalton Trans.*, 1445(1987).
17. D.G.Evans and D.M.P.Mingos, *J. Organomet. Chem.*, **240**, 321(1982).
18. D.G.Evans and D.M.P.Mingos, *Organometallics*, **2**, 435(1983).
19. R.B.Woodward and R.Hoffmann, "The conservation of orbital symmetry", Academic Press, New York, 1970.
20. M.R.Churchill and B.G.DeBoer, *Inorg. Chem.*, **16**, 878(1977).

21. D.Gregson, J.A.K.Howard, M.Murray and J.L.Spencer, *J. Chem. Soc., Chem. Commun.*, 716(1981).

22. (a) R.E.McCarley, *Philos. Trans. R. Soc. London*, **A308**, 141(1982).
(b) R.Chevrel, M.Hirrien and M.Sergent, *Polyhedron.*, **5**, 87(1986).

23. A.Ceulemans and P.W.Fowler, *Inorg. Chim. Acta.*, **105**, 75(1985).

24. R.L.Johnston and D.M.P.Mingos, *Inorg. Chem.*, **25**, 1661(1986).

Chapter 5 A Theoretical Analysis of High Nuclearity Metal Carbonyl Clusters

5.1 Introduction

In recent years, a very large number of high nuclearity cluster compounds have been synthesized and structurally characterized [1-4]. A comprehensive review has been recently given by Vargas and Nicola [3]. In a preliminary communication [5a], Mingos rationalized the bonding patterns in these high nuclearity metal cluster compounds with 13-44 metal atoms (see Tables 5.1-5.3) and found that these clusters are generally characterized by $12n_s+\Delta$ valence electrons, where n_s is the number of surface atoms and Δ is characteristic of the interstitial group of atoms. For instance, if the interstitial group of atoms is an octahedron, Δ is equal to 86; a tetrahedron, Δ=60; and a triangle, Δ=48; etc. In this Chapter, we give a more detailed theoretical analysis of this electron counting rule using Stone's methodology [6]. This model which is based on a particle on a sphere free electron model is relevant because the observed structures of high nuclearity clusters (Tables 5.1-5.3) can be described in terms of multi-concentric spheres [7].

The simplest type of high nuclearity cluster is one where the central metal polyhedron is capped by one or more metal atoms. The theoretical aspects of these clusters have been discussed in some detail elsewhere [8]. The capping principle [9] states that capping a face of a polyhedron leads to no change in the number of skeletal bonding orbitals. Therefore, capping with a transition metal atom leads only to an increase in cluster valence electron count of 12. Consequently, the general formula for the electron count in high nuclearity capped clusters can be expressed as $12n_c+\Delta$, where n_c is the number of capping atoms and Δ is the electron count characteristic of the central cluster. A more complicated situation

arises when the capping atoms are sufficiently numerous for metal-metal bonds to be formed between them. The bonding in this type of cluster is discussed in this Chapter.

Table 5.1 Examples of high nuclearity clusters with one intersititial atom based on the $12(n_s+n_c)+2n_s+2$ rule [a]

compounds	n_i	n_s	n_c	electron count. obs.	calc.	
$[Rh_{13}(CO)_{24}H_5]$	1	12	0	170	170	
$[Rh_{12}Pt(CO)_{24}]^{4-}$ [b]	1(Pt)	12	0	170	170	
$[Rh_{15}(CO)_{30}]^{3-}$	1	14	0	198	198	
$[Ru_6C(C0)_{17}]$	1(C)	6	0	86	86	$12(n_s+n_c)+2n_s+2$
$[Rh_{10}S(CO)_{22}]$	1(S)	10	0	142	142	
$[Rh_{12}Sb(CO)_{27}]$	1(Sb)	12	0	170	170	
$[Os_{10}C(C0)_{24}]^{2-}$	1(C)	6	4	134	134	

n_i: the number of intersititial atoms.

n_s: the number of suface atoms which are connected directly to the intersititial atoms.

n_c: the number of capping atoms.

a. D.M.P.Mingos, J.Chem.Soc.,Chem.Commun., 1353(1985).

b. A.Fumagalli, S.Martinengo, and G.Ciani, J.Chem.Soc.,Chem.Commun.,1381(1983).

Table 5.2 Examples of high nuclearity cluster compounds based on the $12n_s+\Delta_i$ electron counting rule [a]

compounds	n_i	n_s	n_c	electron count. obs.	calc.	
$[Au_9(PPh_3)_8]^+$	1	8	0	114	114	$12n_s+18$
$[Au_{11}I_3(PPh_3)_7]$	1	11	0	138	138	
$[Au_{13}Cl_2(PR_3)_{10}]^{3+}$	1	12	0	162	162	
$[Pt_{15}H_x(CO)_8(PBu_3)_6]$ [b]	1	12	2	178+x	186	$12(n_s+n_c)+10+x$*
$[Pt_{19}(CO)_{22}]^{4-}$	2	17	0	238	238	$12(n_s+n_c)+34$
$[Rh_{22}(CO)_{35}H_{5-q-m}]^{q-}$	2	16	4	273+m	274	
$[Au_{13}Ag_{12}Cl_6(PPh_3)_{12}]^{m+}$	3	22	0	317-m	314	$12n_s+50$
$[Ni_{38}Pt_6(CO)_{48}H_{6-n}]^{n-}$	6(Pt)	32	6	542	542	$12(n_s+n_c)+86$
$[Pt_{38}(CO)_{44}H_m]^{2-}$	6(Pt)	32	0	470+m	470	
$[Ni_{34}H(CO)_{38}(C)_4]^{5-}$ [c]	4(Ni)+4(C)	30		438	438	$12(n_s+n_c)+78$
$[Ni_{35}(CO)_{39}(C)_4]^{6-}$ [c]	4(Ni)+4(C)	31		450	450	
$[Ni_{38}H(CO)_{42}(C)_6]^{5-}$ [d]	8(Ni)+6(C)	30		494	492	$12(n_s+n_c)+132$

a. D.M.P.Mingos, J.Chem.Soc.,Chem.Commun., 1353(1985).

b. J.A.K.Howard, J.L.Spencer, and D.G.Turner, J.Chem.Soc.,Dalton.,259(1987).

c. A.Ceriotti, A.Fait, G.Longoni, G.Piro, L.resconi, F.Demartin, M.Manassero, N.Masciocchi, M.Sansoni, J.Amer.Chem.Soc.,**108**,5370(1986).

d. A.Ceriotti, A.Fait, G.Longoni, G.Piro, F.Demartin, M.Manassero, N.Masciocchi, M.Sansoni, J.Amer.Chem.Soc., **108**,8091(1986).

*. the predicted value x=8.

Table 5.3 Examples of high nuclearity clusters deviating from the electron counting rules

compounds	n_i	n_s	n_c	electron count. obs.	comments
$[Pd_{23}(CO)_{22}(PEt_3)_{10}]^a$	1	18	4	294 =12×(16+6)+30	occupation of 6 L^{π}_{pd} in Figure 5.2
$[Pd_{23}(CO)_{20}(PEt_3)_8]^b$	1	14	8	286 =12×(14+18)+22	occupation of 2 L^{π}_{pd} in Figure 5.2
$[Pt_{24}(CO)_{30}]^c$	1	23	0	276 =12×23+24	occupation of 3 L^{π}_{pd} in Figure 5.2
$[Pt_{26}(CO)_{32}]^c$	3	23	0	326 =12×23+50	$>12n_s+48$
$[Pd_{38}(CO)_{28}(PEt_3)_{12}]^b$	4	22	12	460 =12×(22+12)+52	$<12(n_s+n_c)+60$

a. E.G.Mednikov, N.K.Eremendo, Yu.L.Slovokhotov, and Yu.T.Struchkov, J.Organomet. Chem., **301**,035(1986).

b. E.G.Mednikov, N.K.Eremendo, Yu.L.Slovokhotov, and Yu.T.Struchkov, J.Chem.Soc., Chem.Commun.,218(1987).

c. D.M.P.Mingos, J.Chem.Soc.,Chem.Commun., 1353(1985).

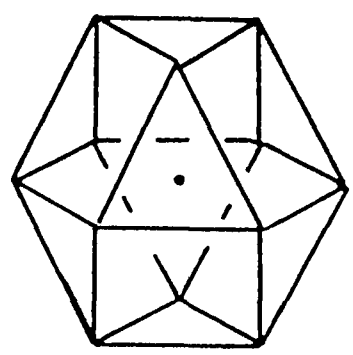
5.2 Bonding Analysis

5.2.1 The bonding in high nuclearity clusters with one interstitial atom.

Some examples of deltahedral and four-connected clusters with transition metal and main group interstitial atoms are summarised in Table 5.1. Deltahedral clusters have a total of n_s+1 bonding skeletal molecular orbitals [10a,b] and $6n_s$ orbitals which are either non-bonding or involved in metal-ligand bonding. Therefore such clusters are

characterised by $12n_s+2(n_s+1)$ valence electrons, i.e. $14n_s+2$ [10b]. In terms of Stone's notation the metal-ligand bonding occurs primarily through $n_sL^{\pi}_{pd}$, $n_sL^{\sigma}_{sp}$ and $n_s\bar{L}^{\pi}_{dp}$ out-pointing hybrid orbitals and the $n_sL^{\delta}_{d}$, $n_s\bar{L}^{\delta}_{d}$ and $n_sL^{\sigma}_{d}$ are essentially non-bonding. For ML_3 fragments the latter correspond to the "t_{2g}" like orbitals of an octahedral fragment [10c]. From Table 5.1, it is apparent that the total number of valence electrons in such clusters does not depend on whether the interstitial atom is a transition metal or a main group atom. For example, although the interstitial atom is Pt in $[Rh_{12}Pt(CO)_{24}]^{4-}$ [11], the cluster has the same number of valence electrons ($170=12n_s+26$, i.e., 13 skeletal bonding orbitals) as $[Rh_{13}(CO)_{24}H_5]$ [12] and $[Rh_{12}Sb(CO)_{27}]^{3-}$ [13]. Similarly the two octahedral clusters, $[Ru_6C(CO)_{17}]$ [14] and $[Rh_6(CO)_{16}]$ [15] have the same electron count of 86 although the former has an interstitial carbon atom.

It has been shown [16] that the anti-cuboctahedron and the cuboctahedron have the same number and pattern of skeletal bonding orbitals. Therefore the results of extended Huckel molecular orbitals calculations on the higher symmetry structure have been used to develop the principal theoretical arguments. Specifically calculations on $Rh_{12}H_{36}$ (ML_3 fragment) and $Rh_{13}H_{36}$ (with one central Rh) as shown in (1) have been completed.



(1)

The Rh_{13} cluster was chosen as a model because the interstitial atom is a transition metal with s, p and d valence orbitals. Figure 5.1 shows the important interactions between the interstitial atom and the outer sphere cluster, Rh_{12}. The non-bonding "t_{2g}" orbitals and the M-L bonding molecular orbitals of the outer sphere cluster have been ommitted from the figure for reasons of clarity. There are a total of $6n_s$ orbitals of this type. The skeletal molecular orbitals for Rh_{12} lie in a narrow energy range and comprise F^{π}, D^{π}, $P^{\sigma/\pi}$, S^{σ} and F^{π}_{3c}. There are a total of 13 skeletal bonding orbitals. This is a general characteristic of 4-connected clusters and this aspect has been discussed in some detail elsewhere.[8] When the central atom is inserted into the Rh_{12} cluster, the three p orbitals of the central atom stabilize the $P^{\sigma/\pi}$ orbitals slightly. The s and d orbitals interact strongly with the S^{σ} and D^{π} orbitals of the outer sphere, and give rise to the in-phase combinations S^{σ} +s and D^{π}+d bonding orbitals, and the out-phase combinations S^{σ}-s and D^{π}-d which are antibonding. The F^{π} orbitals are essentially unaffected by the introduction of the central atom . Consequently, the interaction between s, p and d orbitals of the interstitial atom and the skeletal bonding orbitals of outer sphere leads to no change in the total number of the skeletal bonding orbitals. It is apparent that in the cluster with a main group interstitial atom, the D^{π} orbitals of the outer sphere are still in the bonding region and fully-occupied. Therefore, the clusters with one main group interstitial atom have the same electron count as the clusters with a transition metal atom at the centre if both clusters have the same structure. A more detailed analysis of such clusters has been presented elsewhere.[20]

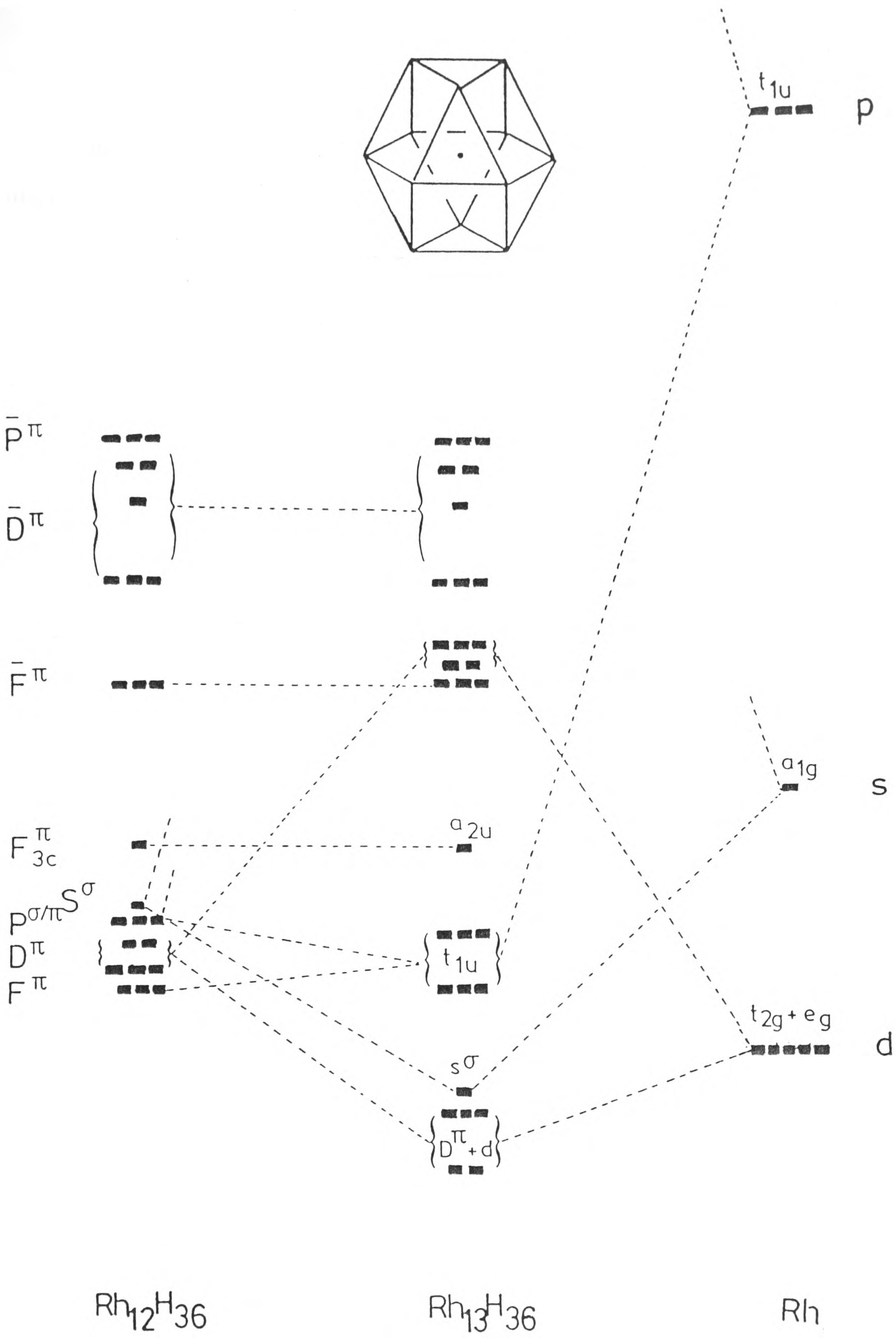


Figure 5.1 MO interaction diagram for a centred cuboctahedral cluster.

Figure 5.2 gives a generalised interaction scheme for high nuclearity clusters with a single interstitial atom. If the metal atoms are evenly distributed on the surface of the sphere then there are always a set of nine S^{σ} , $P^{\sigma/\pi}$ and D^{π} skeletal molecular orbitals capable of interacting with the nd, (n+1)s and (n+1)p valence orbitals of the interstitial atom. In addition there are $(n_s\text{-}8)$ $L^{\pi/\sigma}_{pd}$ (L>2) tangential molecular orbitals with a significant proportion of p orbital character. As the number of metal atoms increases the energy difference between the L^{π}_{pd} and $\bar{L}^{\pi}_{pd}$ orbitals decreases and the energy gap between the L^{π}_{pd} and $\bar{L}^{\pi}_{pd}$ orbitals becomes smaller.[5b] For a close packed arrangement of metal atoms the interstitial atom is surrounded by 12 to 14 metal atoms on a spherical surface and the additional atoms behave as capping atoms and lie on a second concentric spherical surface. It follows therefore from the capping principle [9] that for a close packed arrangement there is a limiting number of between four and six $L^{\pi/\sigma}_{pd}$ (L>2) skeletal molecular orbitals. Furthermore, when there are a large number of atoms on the first and second spherical surfaces the energy differences between alternative c.c.p., h.c.p. and b.c.c. close packed arrangements are small and not-predictable from symmetry based arguments of the type developed in this Chapter.

From Figure 5.2 it is apparent that if the orbitals are filled up to level L_1 the total number of available skeletal molecular orbitals is n_s+1 for $n_s<14$ and 15 if $n_s>14$. Some examples of such high nuclearity clusters are summarised in Table 5.1. The structures of $[Rh_{13}H_5(CO)_{24}]$ and $[Rh_{12}Pt(CO)_{24}]^{4-}$ are based on h.c.p., $[Os_{10}C(CO)_{24}]^{2-}$ on f.c.c. and $[Rh_{15}(CO)_{30}]^{3-}$ on b.c.c.

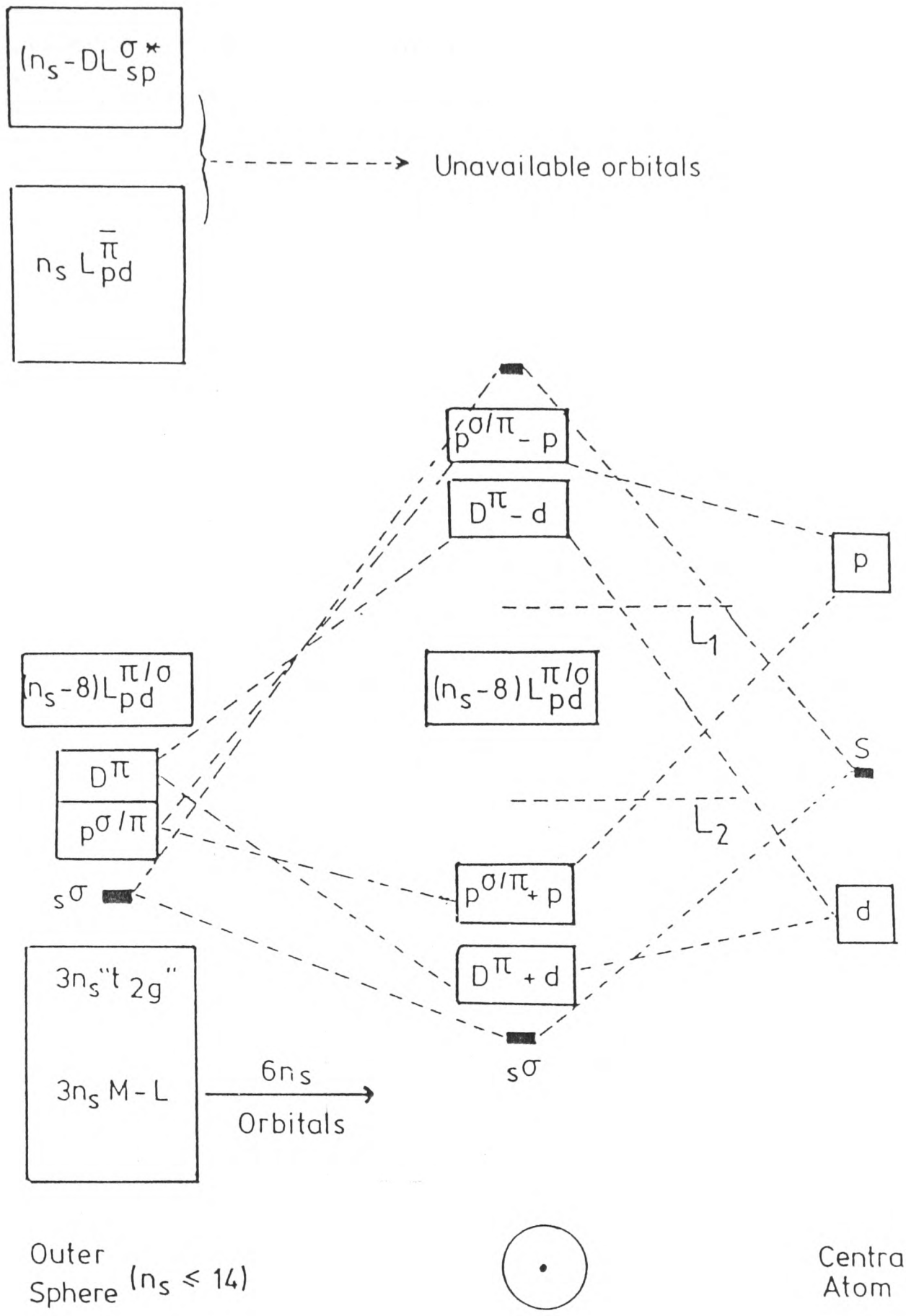


Figure 5.2 MO interaction scheme for a centerd spherical cluster

For the late transition metals and the heavier post transition metals the nd valence orbitals become more core-like and (n+1)s valence orbitals experience a relativistic contraction and consequently the (n+1)p valence orbitals are not as accessible for skeletal and metal-ligand bonding. The molecular orbitals in Figure 5.2 are filled only to the level L_2 because the $(n_s\text{-}8)$ $L^{\pi/\sigma}_{pd}$ orbitals are much less strongly bonding than the nine S^{σ}, $P^{\sigma/\pi}$ and D^{π} skeletal m.o.s. Such spherical clusters are characterised by a total of $12n_s+18$ valence electrons. Examples of such clusters are summarised in Table 5.2. The metal atoms in $[Au_9(PPh_3)_8]^+$ adopt a cubic arrangement, and those in $[Au_{11}I_3(PPh_3)_7]$ and $[Au_{13}Cl_2(PMe_2Ph)_{10}]^{3+}$ close packed arrangements based on an icosahedron. In $[Pt_{15}H_x(CO)_8(PBu_3)_6]$ there are 12 atoms cuboctahedrally arranged on the first spherical surface and an additional four capping atoms. This bonding analysis predicts that the number of unlocated hydrido-ligands equals 8.

In those clusters described above the metal atoms on the first spherical surface are evenly distributed and therefore have a spherical topology. For reasons that have been discussed in some detail elsewhere [5c] if these atoms have a toroidal topology then one of $P^{\sigma/\pi}$ skeletal m.o.'s is no longer bonding and such clusters are characterised by a total of $12n_s+16$ valence electrons, e.g. $[Au_9(PPh_3)_8]^{3+}$.

The compounds described above represent clear cut situations where the $(n_s\text{-}8)L^{\pi/\sigma}_{pd}$ orbitals are either all utilised or not utilised at all. In Table 5.3 some examples of clusters which represent intermediate situations are given. In $[Pd_{23}(CO)_{22}(PEt_3)_{10}]$ the central atom is surrounded by 18 metal atoms which are part of a f.c.c. lattice. Six of the metal atoms are at the vertices of an octahedron, 12 additional metal atoms are located at the mid-points of the edges of this octahedron and

the remaining four metal atoms cap the faces of octahedron. The total number of valence electrons is 294, i.e. $12n_s+30$, corresponding to the occupation of the six $L_{pd}^{\pi/\sigma}$ (L>2) skeletal molecular orbitals for close packed arrangements as noted above.

In $[Pd_{23}(CO)_{20}(PEt_3)_8]$ and $[Pt_{24}(CO)_{30}]^{2-}$ only two and three $L_{pd}^{\pi/\sigma}$ orbitals are occupied and therefore they represent an intermediate situation in Figure 5.2, where an electron occupation between the L_1 and L_2 levels is occurring. The occurrence of these exceptions is not too surprising in view of the way in which the d-p promotion energies of Pd and Pt lead to 18 and 16 electron mononuclear complexes.

5.2.2 The bonding in high nuclearity clusters with a deltahedral interstitial moiety

The molecular orbital calculation on $Rh_{13}H_{36}$ with one interstitial atom indicated that the d orbitals of the central atom play an important bonding role by interacting with D^{π} functions of the atoms on the outer sphere. This suggests that the d orbitals in the inner bare cluster will also play important role for the higher nuclearity clusters. The "t_{2g}" sets of the inner polyhedron in a high nuclearity transition metal cluster include L_d^{σ}, L_d^{δ} and $\bar{L}_d^{\delta}$. As an isolated cluster , these orbitals are effectively metal-metal non-bonding. But as an interstitial moiety they can accept electrons from the outer sphere metal atoms. The outer sphere metal atoms therefore behave like ligands towards the inner sphere polyhedron.

Figure 5.3 gives a schematic fragment orbital interaction diagram for the outer sphere and inner sphere interactions in such a high nuclearity cluster. n_s Indicates the number of atoms on the surface of the outer sphere; n_i is the number of atoms on the surface of the inner sphere. Figure 5.3(c) shows the molecular orbital level diagram of the inner bare cluster which has a deltahedral geometry. From the Stone Tensor Surface Harmonic analysis [6], it has been shown that there are $2n_i$-1 unavailable orbitals and $7n_i$+1 available orbitals in deltahedral clusters [5b]. Of the $7n_i$+1 available orbitals,[5b,6b] The $n_iL_{dp}^{\pi}$ orbitals are inwardly hybridised bonding orbitals, i.e., the skeletal bonding orbitals; $n_iL_{pd}^{\pi}$, $n_iL_{sp}^{\sigma}$ and $n_i\bar{L}_{dp}^{\pi}$ (total $3n_i$) are out-pointing orbitals which are the acceptor orbitals for ligand electron pairs and lead to M-L bonding molecular orbitals in low nuclearity clusters. The $n_iL_d^{\sigma}$, $n_iL_d^{\delta}$ and $n_i\bar{L}_d^{\delta}$ ($3n_i$) orbitals represent the "t_{2g}" set. When interactions with the outer sphere are introduced, the $6n_i$ orbitals, $3n_i$ out-pointing and $3n_i$ "t_{2g}" set of orbitals, are very important for interacting with the symmetry-adapted orbitals of the outer sphere. The $n_iL_{dp}^{\pi}$ skeletal bonding orbitals will be less important because they are inwardly hybridised.

Figure 5.3(a) illustrates the orbital pattern of the outer sphere cluster with ML_3 fragments. The $3n_s$ M-L and $3n_s$ "t_{2g}" sets are out-pointing orbitals in a similar fashion to those discussed above and are less important for interacting with the inner sphere metal atoms. Occupation of these $6n_s$ orbitals leads to a contribution of $12n_s$ electrons to the total number of valence electrons. The primary bonding interactions with the inner sphere polyhedron occur through the n_s $L_{pd}^{\pi/\sigma}$ and S^{σ} skeletal bonding orbitals shown in Figure 5.3(a).

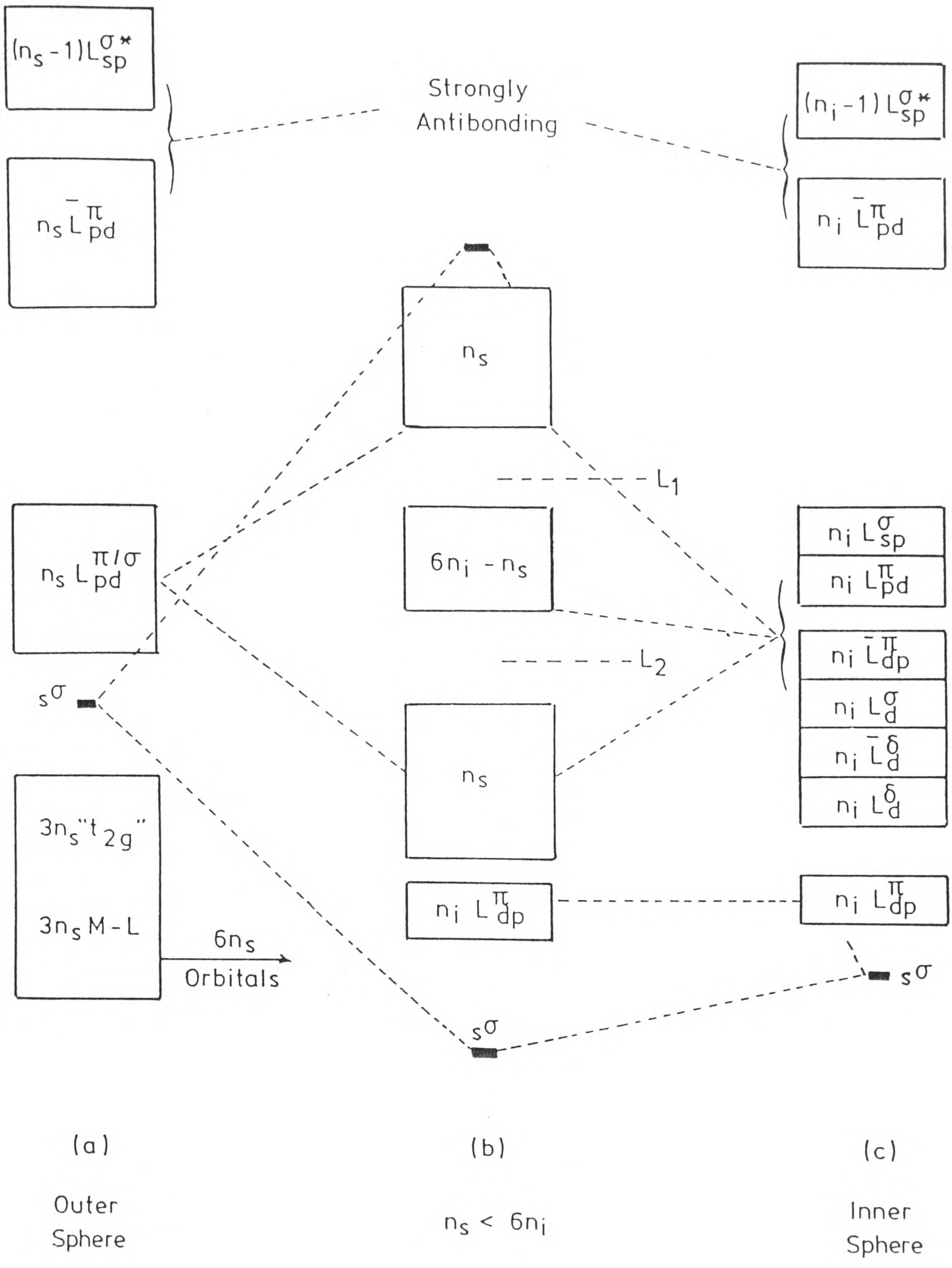


Figure 5.3 MO interaction scheme for a high nuclearity cluster based on two cocentric spheres when $n_s<6n_i$

When the inner and outer spheres are allowed to interact together to form a bi-spherical cluster, the results depend on whether $n_s>6n_i$ or $n_s<6n_i$. If $n_s>6n_i$ then there are a sufficient number of metal atoms in the outer sphere to formally donate electrons into the $3n_i$ out-pointing and $3n_i$ "t_{2g}" like orbitals of the inner polyhedron. Figure 5.3(b) illustrates the results of the interaction between inner and outer spheres when $n_s<6n_i$. The figure indicates that the S^{σ} orbital of the outer sphere interacts strongly with S^{σ} of inner sphere and gives rise to one antibonding and one strongly bonding orbital; the $n_s L_{pd}^{\pi/\sigma}$ orbitals of the outer sphere interact strongly with n_s orbitals from the $6n_i$ group with the same symmetry and give rise to n_s bonding and n_s antibonding orbitals. The $(6n_i-n_s)$ orbitals from the inner sphere remain essentially non-bonding. If the inner sphere is not covered completely by the atoms in the outer sphere, the $(6n_i-n_s)$ orbitals may be stabilized by interactions with bridging carbonyl ligands and are stabilized sufficiently to be occupied. Consequently, if the molecular orbitals are filled up to the L_1 line in Figure 5.3, the total number of valence electrons required is $2(6n_s+7n_i+1)=12n_s+14n_i+2$, where $14n_i+2$ corresponds to the characteristic number of electrons for the interstitial deltahedral moiety. If the interstitial group is not deltahedral , the $14n_i+2$ component is replaced by an alternative number which reflects the structure of the interstitial moiety. This analysis therefore provides a theoretical justification for Mingos' $12n_s+\Delta_i$ electron counting rule for high nuclearity clusters. Examples of clusters following this electron counting rule are listed in Table 5.2. If the $(6n_i-n_s)$ orbitals are not completely filled, the electron count will be less than $12n_s+\Delta_i$, for example $[Pd_{38}(CO)_{28}(PEt_3)_{12}]$ [17] in Table 5.3, where the interstitial moiety is a tetrahedron, has $12n_s+52$ valence electrons rather than $12n_s+60$.

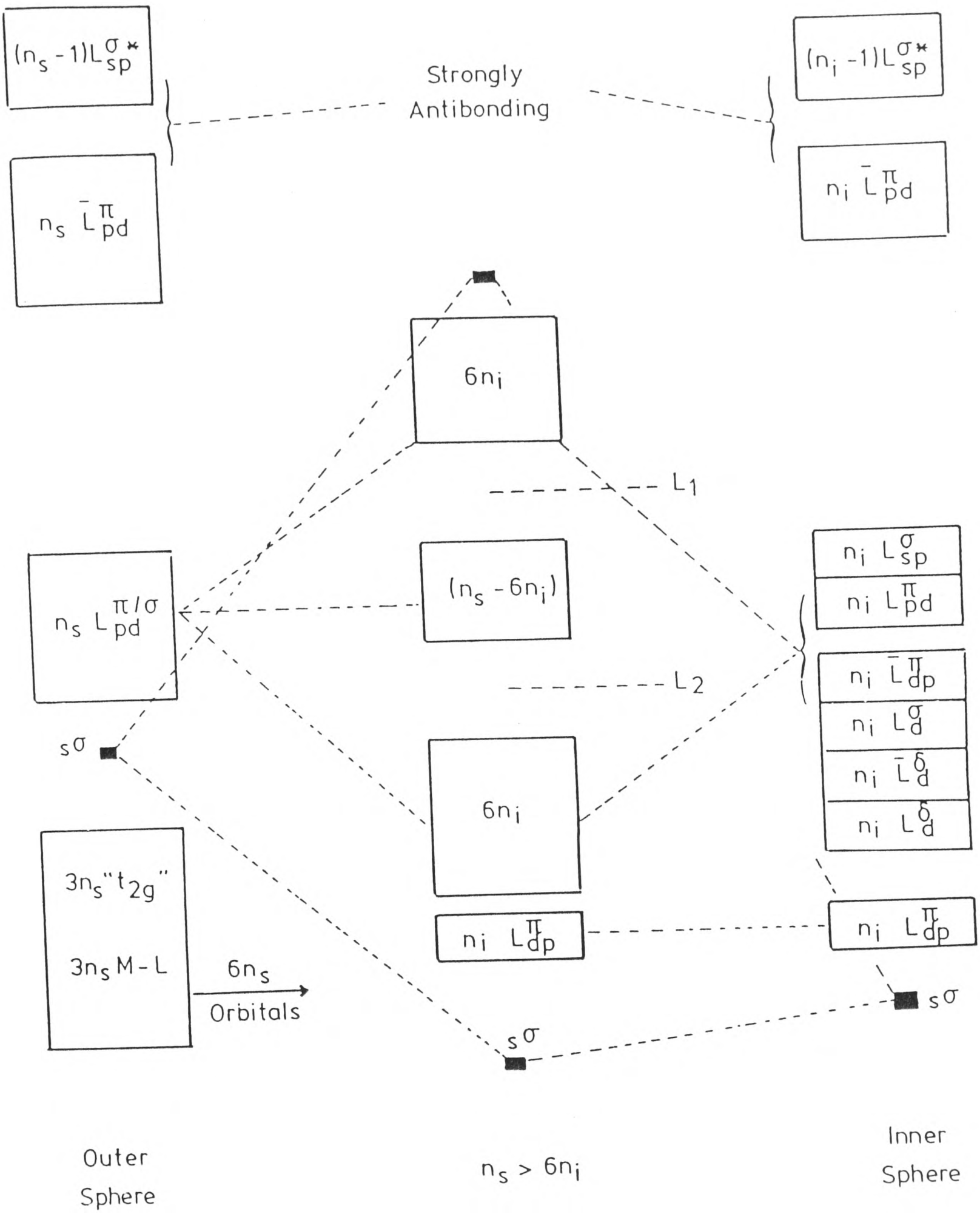


Figure 5.4 MO interaction scheme for a high nuclearity cluster based on two cocentric spheres when $n_s > 6n_i$

Figure 5.4 shows the interactions between the outer sphere atoms and the inner sphere deltahedron when $n_s > 6n_i$. This differs from Figure 5.3 because there are now $6n_i$ rather than n_s molecular orbitals stabilized by the inner and outer sphere interactions. When the molecular orbitals are filled up to the L_1 line, the electron count is $2[6n_s+(n_i+n_s+1)]$. When the electrons are filled up to the L_2 line, the electron count is again the $12n_s+\Delta_i$ derived above in Figure 5.3. The situation illustrated in Figure 5.4 is not commonly observed in cluster compounds because for purely geometric reasons the condition $n_s > 6n_i$ is not satisfied for those atoms lying on the second sphere in a close packed structure.

5.2.3 The bonding in high nuclearity clusters with two or three interstitial atoms.

When the interstitial moiety in a high nuclearity cluster is a triangular fragment, there are 21 acceptor orbitals for interacting with the outer sphere rather than 18 ($6n_i$), because there are 12 orbitals out-pointing. Each metal atom has four orbitals capable of accepting electrons from ligands. In the isolated cluster this leads to triangular cluster based on ML_4 fragments. In addition each metal atom has a "t_{2g}" set, leading to 9 non-bonding orbitals. Occupation of these 21 acceptor orbitals and the a_1 and e skeletal bonding molecular orbitals leads to the 48 electron count commonly associated with triangular clusters, such as $[Os_3(CO)_{12}]$. The interaction diagram for a triangular bare cluster with a large polyhedron is illustrated in Figure 5.5. The molecular orbitals of the inner triangle shown on the right-hand side of the Figure include a_1+e metal-metal bonding orbitals, 21 acceptor orbitals and a_2+e metal-metal anti-bonding orbitals (27 in total number). Interaction with the metal atoms on the outer sphere leads to the stabilization of 24 orbitals

through the S^{σ} and n_s $L_{pd}^{\pi/\sigma}$ inpointing orbitals. In addition there are (n_s-21) approximately non-bonding orbitals derived from this set. The occupation of orbitals up to the L_2 line in Figure 5.5 leads to an electron count of $12n_s+48$, i.e. they also conform to the pattern $12n_s+\Delta_i$. In $[Pt_{26}(CO)_{32}]^{2-}$ [2] the total number of valence electrons is 326, i.e., $12n_s+50$, and Δ_i is 50 rather than 48 for a triangular interstitial moiety. A detailed analysis of the bonding in raft-clusters has shown that the addition of edge-bridging metal atoms to a triangular cluster leads to a stabilization of the a_2 ($\bar{P}_O^{\pi}$) antibonding skeletal molecular orbital. This orbital is sufficiently stabilized in a planar 6 atom cluster to be occupied by an additional electron pair.[18] Therefore, we propose that in high nuclearity clusters with an interstitial triangular moiety the a_2 orbital is utilised in bonding leading to a characteristic electron count of $12n_s+50$ rather than $12n_s+48$ if there are more than 3 surface atoms coplanar with the triangle.

When the geometry of the three interstitial atoms is linear, the bonding scheme is slightly different from Figure 5.5. The a_1+e three metal-metal bonding orbitals on the right hand side of Figure 5.5 are replaced by two metal-metal bonding orbitals (one is S^{σ}, the other is P_z^{σ} if the z axis is defined along the M-M-M bonding direction) there are now 23 acceptor orbitals because the terminal metal atoms each have an additional out-pointing orbital. Interaction with the metal atoms on the outer sphere leads to a stabilization of the 25 orbitals. In addition there are (n_s-23) approximately non-bonding orbitals derived from the outer sphere. Consequently, the occupation of orbitals up to the L_2 line leads to an electron count of $12n_s+50$, i.e., $12n_s+\Delta_i$. $[Au_{13}Ag_{12}Cl_6(PPh_3)_{12}]^{m+}$ provides an example of such a cluster (see Table 5.2), but unfortunately it has not been sufficiently well

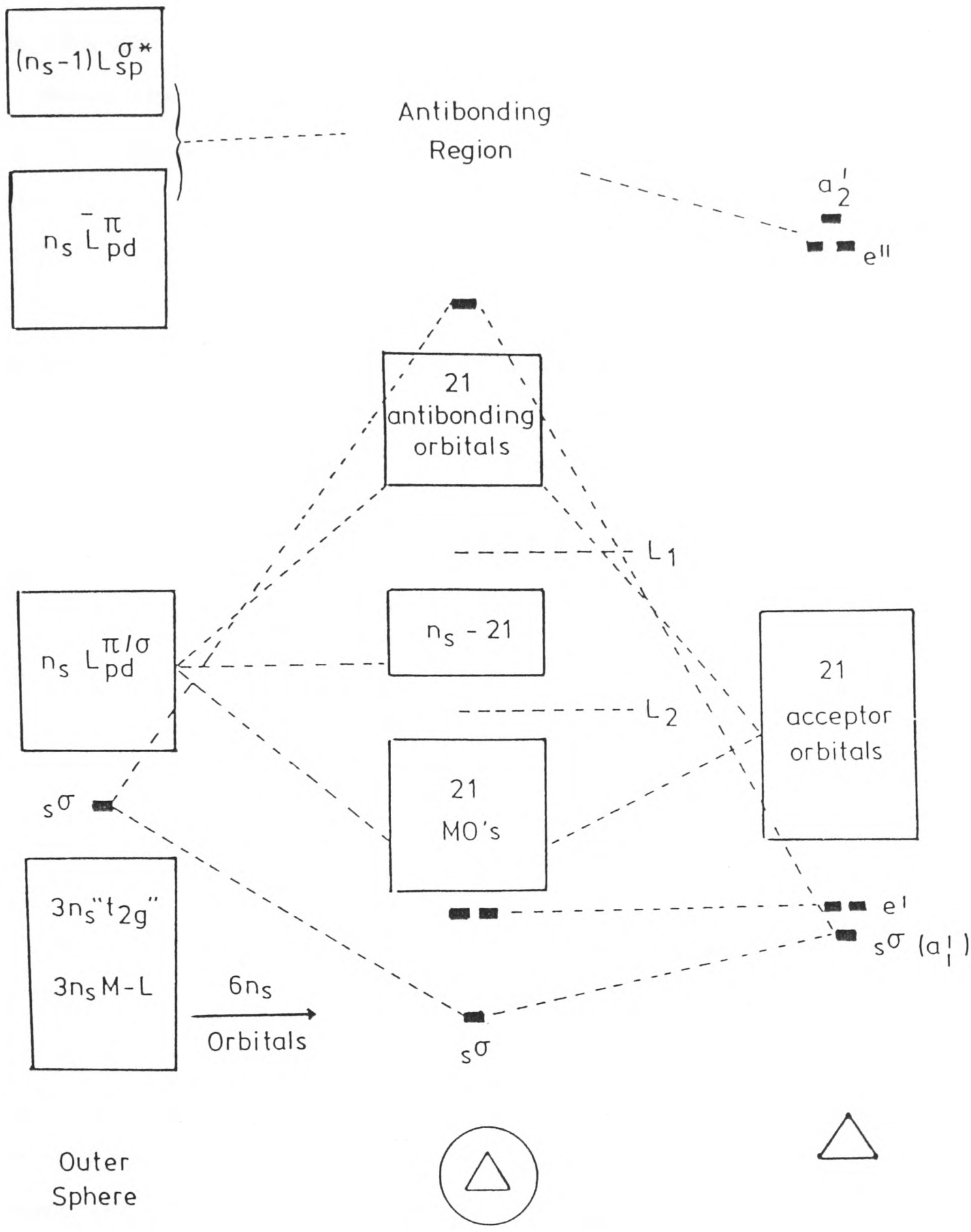


Figure 5.5 MO interaction scheme for a high nuclearity cluster with a triangular interstitial moiety

characterized to provide unambiguous support for the predicted electron count. If the orbitals are filled up to L_1 line, the electron count is $12n_s+2(n_s+2)$.

When the interstitial moiety in a high nuclearity cluster is a diatomic fragment, there are 16 acceptor orbitals for interacting with the outer sphere rather than 12 ($6n_i$), because there are 10 out-pointing orbitals in which each metal atom has 5 orbitals capable of accepting electrons from ligands. In the isolated cluster, this leads to a diatomic cluster based on two ML_5 fragments, such as $Mn_2(CO)_{10}$. In addition each metal atom has a "t_{2g}" set, leading to 6 non-bonding orbitals. Occupation of these 16 orbitals and the S^{σ} metal-metal bonding orbital leads to the 34 electron count. The interaction scheme between the interstitial diatomic fragment and outer sphere is different from Figure 5.5. Now there is only one S^{σ} metal-metal bonding orbital rather than three metal-metal bonding orbitals for the triangular moiety. The interaction between S^{σ} from the interstitial moiety and S^{σ} from the outer sphere leads to one bonding and one antibonding orbitals. The 16 acceptor orbitals interact with 16 symmetry-adapted orbitals from n_s $L_{pd}^{\pi/\sigma}$ set of outer sphere. Consequently, the number of skeletal molecular orbitals below the L_2 level (comparing with Figure 5.5) is 17. In additon, there are (n_s-16) skeletal molecular orbitals present between the L_1 and L_2 levels. Therefore, occupation of orbitals up to the L_2 level leads to 17 skeletal bonding orbitals, corresponding to $12n_s+34$, i.e. $12n_s+\Delta_i$. There are two examples of clusters following this electron count, $[Pt_{19}(CO)_{22}]^{4-}$ and $[Rh_{22}(CO)_{35}H_{5-q-m}]^{q-}$, listed in Table 5.2. If the orbitals are filled up to the L_1 level, the number of skeletal bonding orbitals is n_s+1, corresponding to the $12n_s+2(n_s+1)$ electron counting rule which is the same as the case where there is only one

interstitial atom. In $[Rh_{22}(CO)_{35}H_{5-q-m}]^{q-}$, the two interstitial atoms are surrounded by 16 metal atoms lying on the first spherical surface. The remaining four metal atoms cap the square faces of the polyhedron. Therefore, for $[Rh_{22}(CO)_{35}H_{5-q-m}]^{q-}$ there are no $L_{pd}^{\pi/\sigma}$ orbitals between the L_1 and L_2 levels and its n_s+1 (17) skeletal bonding orbitals are consistent with both the $12n_s+2(n_s+1)$ rule and the $12n_s+\Delta_i$ rule.

Summary of conclusions for high nuclearity transition metal clusters.

The analyses developed above have indicated two limiting types of bonding in high nuclearity clusters. The majority of high nuclearity clusters have electron counts which can be summarised by the $12n_s+\Delta_i$ rule. In terms of the Stone Spherical Harmonic notation this corresponds to the occupation of a set of molecular orbitals which can be correlated with the skeletal (s_i) and acceptor (a_i) orbitals of the interstitial cluster [$\Delta_i=2(s_i+a_i)$] and $6n_s$ metal-ligand and non-bonding orbitals of the outer sphere metal atoms. Previously this mode of bonding has been described as radial in order to emphasise the donation of electrons from orbitals of the outer sphere atoms to the available orbitals of the interstitial cluster.

The molecular orbital schemes in Figures 5.2 and 5.4 also suggest alternative electron counts corresponding to filling up to the L_1 level. The additional number of orbitals lying between the L_2 and L_1 levels depends on the number of metals contained in the interstitial moiety and their geometry. In general there are (n_s-a_i) $L_{pd}^{\pi/\sigma}$ molecular orbitals which are localised predominantly on the outer sphere atoms and are tangential in nature. These additional tangential molecular orbitals are only significant for those clusters of metals with low d-p promotion

energies and low nuclearities. The number of orbitals lying between L_1 and L_2 begins to approach zero as the nuclearity increases. The L quantum number of the relevant orbitals also increases and the corresponding $L_{pd}^{\pi/\sigma}$ orbitals become less strongly bonding.

For this second category of cluster the electron count can also be expressed as

$$12n_s+2(s_i+a_i)+2(n_s-a_i)$$
$$=12n_s+2(s_i+n_s)$$

The outer sphere contains a large number of atoms distributed evenly on the surface of the sphere and is characterised by a total of n_s+1, i.e. s_s, skeletal bonding molecular orbitals. Therefore, these clusters where tangential bonding on the surface is significant are associated with the following total number of valence electrons

$$12n_s+2(s_i+s_s-1)$$

The results of these alternative bonding modes are summarised in Table 5.4. The occurrence of significant tangential bonding is particular important for smaller clusters with main group interstitial moieties.

Table 5.4 Summary of Electron Count Rules.

Intersititial moieties		Rule 1 Radial bonding	Rule 2 Radial + tangential bonding
1 intersititial atom		$12n_s+18$	$12n_s+2(n_s+1)$
2 intersititial atoms		$12n_s+34$	$12n_s+2(n_s+1)$
3 intersititial atoms	triangle	$12n_s+48$(or 50)	$12n_s+2(n_s+3)$ *
	linear M-M-M	$12n_s+50$	$12n_s+2(n_s+2)$ *
	linear M=M=M	$12n_s+46$ *	$12n_s+2(n_s+4)$
	linear X=M=X	$12n_s+26$ *	
Deltahedral moiety		$12n_s+14n_i+2$	$12n_s+2(n_s+n_i+1)$ *
General cases		$12n_s+\Delta_i$	$12n_s+2(s_s+s_i-1)$

*. No example of those electron counts.

5.2.4 The bonding in high nuclearity clusters with more complex interstitial moieties.

The interstitial moiety in high nuclearity clusters is not limited to transition metals. There are clusters with interstitial main group atoms linked together and combinations of main group and transition metals. When the interstitial moiety is a group of main group atoms, then the situation is similar to Figure 5.4 because the number of orbitals contributed by the surface atoms greatly exceeds the number of acceptor orbitals associated with the interstitial moiety. For main group fragments there are only n_i acceptor orbitals rather than $6n_i$ if the interstitial moiety is either deltahedral or 3-connected since each vertex has one out-pointing orbital capable of accepting one pair of electrons from a ligand (for example, in a closo-borane cluster each B atom forms a single bond with H atom). Therefore, the bonding scheme is similar to that shown in Figure 5.4 but the $6n_i$ acceptor orbitals are replaced by n_i acceptor orbitals. Consequently, there are $(2n_i+1)$ (i.e. Δ_i) orbitals below the L_2 line and (n_s-n_i) orbitals between the L_1 and L_2 lines.

The resulting electron counts for a cuboctahedral interstitial moiety are either $12n_s+\Delta_i$ or $12n_s+2(n_s+n_i+1)$. For a cuboctahedral or icosahedral fragment inside a truncated octahedron of nickel atoms, this would correspond to electron counts of 434 $(12n_s+\Delta_i)$ or 474 $[12n_s+2(n_s+n_i+1)]$ and could be realised in the following clusters: $[Ni_{32}B_{12}(CO)_{39}]$ and $[Ni_{32}B_{12}(CO)_{59}]$. The latter results in the occupation of surface tangential molecular orbitals on the metal sphere in addition to the tangential borane L_p^{π} orbitals, but requires an unsatisfactory large number of carbonyl ligands. therefore, for large interstitial main group fragments the $12n_s+\Delta_i$ electron counting rule is likely to be more relevant. However, for small interstitial main group fragments, e.g. C_2, the $12n_s+2(s_i+s_s-1)$ rule is likely to predominate. In

the dicarbido- transition metal clusters, the s_i for the interstitial C_2 fragment is formally equal to 1. The electron count $12n_s+2(s_i+s_s-1)=12n_s+2s_s$ is the same as the situation discussed above for high nuclearity clusters with only one interstitial atom. Therefore the electron count is independent of the interactions between the two interstitial carbon atoms. For example, in the cluster $[Ni_{16}(CO)_{23}C_4]^{4-}$ [21], the interstitial moiety is the four carbon atoms consisting of two C_2 fragments with a separation of 2.88A. The total number of valence electrons is 226=12*16+2(16+1) with the n_s+1 skeletal electron pairs, corresponding to the occupation of skeletal molecular orbitals up to the L_1 line for the high nuclearity clusters with two interstitial atoms discussed in Section 3. A more detailed theoretical analysis has indicated [20] that the C-C separation in the dicarbido- clusters depends critically on the geometric constraints imposed by the metal cage, and the number of skeletal bonding orbitals is independent of the distance between the two carbon atoms.

When the interstitial moiety contains both main group and transition metals it is necessary to calculate the number of available orbitals (the total of s_i and a_i) associated with the total fragment. In general this can be derived from that calculated for the interstitial transition metal fragment and substracting five orbitals for each main group atom. For example in $[Ni_{38}H(CO)_{42}(C)_6]^{5-}$ [23], the interstitial moiety is a cube of nickel atoms capped on each face by μ_4-carbido-ligands. A hexacapped-cubic transition metal cluster is associated with 12 skeletal bonding molecular orbitals [8] and 192 valence electrons, i.e. it has 96 valence orbitals available. The related Ni_8C_6 fragment has 66 available orbitals. Therefore the corresponding cluster is calculated to have $12n_s+132$ valence electrons, i.e. 492, very close to the observed electron count of

494. The additional electron pair probably resides in a second S^{σ} orbital which is out-of-phase between carbon and the interstitial atoms

In $[Ni_{34}H(CO)_{38}C_4]^{5-}$ and $[Ni_{35}(CO)_{39}C_4]^{6-}$ [22], the interstitial moiety is a rhombus of nickel atoms with four edge bridging μ_2-carbido-ligands. A rhombic transition metal cluster has 62 valence electrons, e.g. $[Re_4(CO)_{16}]^{2-}$ and a tetra-edge bridged rhombus, 62+14×4=118 valence electrons, i.e. 59 available orbitals [18]. The corresponding Ni_4C_4 moiety has 39 available orbitals. The following electron counts are therefore calculated $[Ni_{34}H(CO)_{38}C_4]^{5-}$ 438 and $[Ni_{35}(CO)_{39}C_4]^{6-}$ 450 in complete agreement with the observed electron counts (see Table 5.2). In these high nuclearity nickel clusters the radial bonding model is again dominant and the $12n_s+\Delta_i$ rule is applicable. However, for lower nuclearity clusters the occupation of tangential orbitals on the outer sphere can also occur. For example the $[Rh_{17}S_2(CO)_{32}]^{3-}$ [19] cluster has a 4-connected Rh_{16} outer sphere polyhedron and an interstitial SRhS moiety. The Rh-S bond length in the interstitial moiety is 2.168Å which is substantially shorter than the Rh-S single bond length of 2.34Å suggesting substantial multiple Rh-S bonding in the former. The total number of valence electrons in the cluster is 232, $12n_s+40$, corresponding to 20 skeletal electron pairs. The relevant orbital interaction diagram for $[Rh_{17}S_2(CO)_{32}]^{3-}$ is shown in Figure 5.6. The orbitals on the right hand side associated with the S=Rh=S moiety consist of S^{σ} and P^{σ} Rh-S σ-bonding orbitals and two S-Rh-S π-bonding orbitals, which are matched by a set of four antibonding molecular orbitals. There remain a set of 9 acceptor orbitals associated with the SRhS fragment. The molecular orbitals characteristic of a four-connected cluster are shown on the left hand side of the Figure. The interaction between these two sets of orbitals leads to nine stable molecular orbitals localised predominantly on the interstitial moiety (radial) and (n_s-9) $L_{pd}^{\pi/\sigma}$

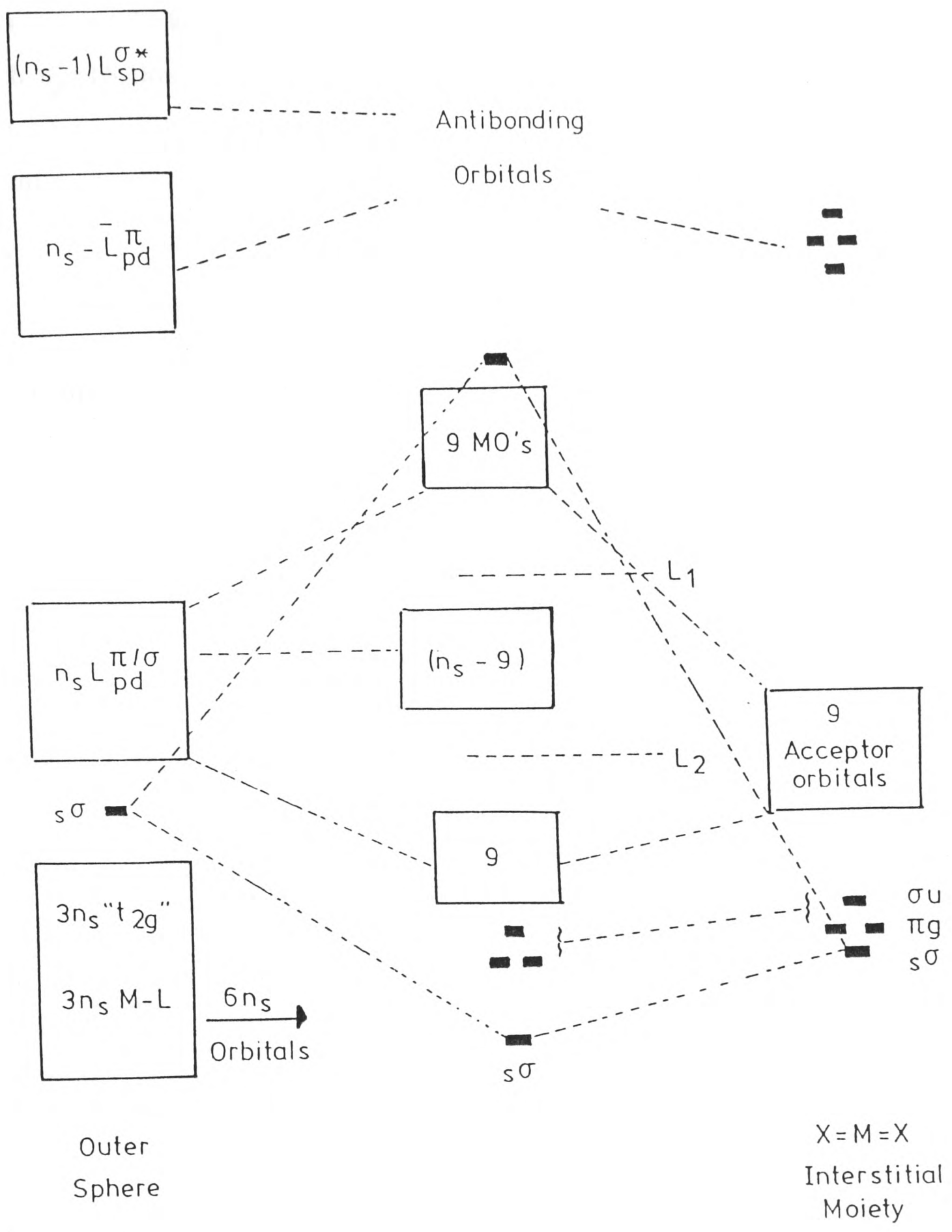


Figure 5.6 MO interaction scheme for a high nuclearity cluster with a X=M=X moiety

tangential orbitals localised predominantly on the outer sphere. Occupation of the tangential and radial molecular orbitals leads to a total of n_s+4 skeletal bonding molecular orbitals. For $[Rh_{17}S_2(CO)_{32}]^{3-}$ with n_s=16 this leads to a total of 20 skeletal bonding molecular orbitals and an electron count in complete agreement with the observed electron count.

5.3 Conclusions

This Chapter has demonstrated that it is possible to apply the Spherical Harmonic Methodology to high nuclearity transition metal carbonyl cluster compounds. It is remarkable how the closed shell requirements of these extremely complex chemical entities can be rationalised in terms of a simple model based on the development of a particle on a sphere problem. The high nuclearity clusters provide a reasonable approximation for this analysis because the metal atoms lie on concentric spheres and the pseudo-spherical symmetry labels can be used to identify the important interactions between atoms on successive layers. The majority of high nuclearity clusters conform to two electron counting rules which are summarised in Table 5.4. If radial and tangential bonding interactions are important for the metal atoms lying on the outer sphere and there is more than one interstitial atom, the relevant electron counting rule can be expressed as:

$$12n_s+2(s_s+s_i-1)$$

where s_s and s_i are the number of skeletal bonding molecular orbitals associated with the surface (s_s) and interstitial (s_i) moieties. This rule is particularly relevant to clusters of rhodium with 12-20 surface atoms and main group interstitial fragments.

For the late transition metals and clusters containing several interstitial metal atoms the radial interactions in the cluster are particularly important and the surface atoms donate electron density to the acceptor orbitals of the interstitial moiety. These clusters are characterised by the electron counting rule

$$12n_s+\Delta_i$$

where Δ_i is the electron count associated with the interstitial moiety. Some examples of such clusters are given in Table 5.2. The interstitial moiety has a set of skeletal bonding molecular orbitals which are similar to those for the isolated cluster. In addition the $6n_i$ orbitals which are either non-bonding or metal-ligand bonding are involved in metal-metal bonding interactions with the surface metal atoms.

5.4 Appendix

The calculations were performed within the extended Hückel method.[24] The exponents of the Rh atom were taken from the literature.[25] For the Rh atoms $H_{ii}(s)$=-9.59ev and $H_{ii}(p)$=-4.57ev. For the surface Rh atoms $H_{ii}(d)$=-12.5ev and $H_{ii}(d)$=-11.0ev for the central Rh atom. This distinction compensated for the approximation of using hydrogen atoms to replace the carbonyl ligands in the real molecules and led to satisfactory highest occupied molecular orbital (h.o.m.o.) - l.u.m.o. energy gaps. The following bond lengths were used in the calculations: Rh-Rh 2.75Å and Rh-H 1.80Å.

References for Chapter Five

1. P.Chini, G.Longoni, and V.G.Albano, *Adv. Organomet. Chem.*, **14**, 285(1976).
2. P.Chini, *J. Organomet. Chem.*, **200**, 37(1980).
3. M.D.Vargas, and J.N.Nicholls, *Adv. Inorg. Chem. Radiochem.*, **30**, 123(1986).
4. A.Ceriotti, F.Demartin, G.Longoni, M.Manassero, M.Marchionna, G.Piva, and M.Sansoni, *Angew. Chem. Int. Ed. Engl.*, **24**, 697(1985).
5. (a) D.M.P.Mingos, *J. Chem. Soc., Chem. Commun.*, 1353(1985);
   (b) D.M.P.Mingos, *Chem. Soc. Rev.*, **15**, 31(1986);
   (c) K.P.Hall, D.I.Gilmour, and D.M.P.Mingos, *J. Organomet. Chem.*, **268**, 275(1984).
6. A.J.Stone, (a) *Mol. Phys.*, **41**, 1339(1980);
   (b) *Inorg.Chem.*, **20**, 256(1981);
   (c) *Polyhedron.*, **3**, 1299(1984).
7. B.K.Teo, and N.A.J.Sloane, *Inorg. Chem.*, **24**, 4545(1985).
8. R.L.Johnston, and D.M.P.Mingos, *J. Chem. Soc., Dalton Trans.*, 647; 1445(1987).
9. D.M.P.Mingos, and M.I.Forsyth, *J. Chem. Soc., Dalton Trans.*, 610(1977).
10. (a) K.Wade, *Adv. Inorg. Chem. Radiochem.*, **18**, 1(1976).
    (b) D.M.P.Mingos, *Nature (London), Phys. Sci.*, **236**, 99(1972).
    (c) M.Elian, M.M.L.Chen, D.M.P.Mingos, and R.Hoffmann, *Inorg. Chem.*, **15**, 1148(1976).
11. A.Fumagalli, S.Martinengo, G.Ciani, *J. Chem. Soc., Chem. Commun.*, 1381(1983).
12. V.G.Albano, G.Ciani, S.Martinengo, and A.Sironi, *J. Chem. Soc., Dalton Trans.*, 978(1979).

13. J.L.Vidal, and J.M.Troup, *J. Organomet. Chem.*, **213**, 351(1981).

14. A.Sirugi, M.Bianchi, and E.Benedetti, *J. Chem. Soc., Chem. Commun.*, 596(1969).

15. E.R.Corey, L.F.Dahl, and W.Beck, *J. Am. Chem. Soc.*, **85**, 1202(1963).

16. D.M.P.Mingos, and Lin Zhenyang, *J. Organomet Chem.* **341**, 523(1988).

17. E.G.Mednikov, N.Y.Eremenko, Y.L.Slovokhotov, and Y.T.Struchkov, *J. Chem. Soc., Chem. Commun.*, 218(1987).

18. D.G.Evans, and D.M.P.Mingos, *Organometallics*, **2**, 435(1983).

19. J.L.Vidal, R.A.Fiato, L.A.Cosby, and R.L.Pruett, *Inorg. Chem.*, **17**,2574(1978).

20. J.-F.Halet, and D.M.P.Mingos, *Organometallics*, 7, 51(1988).

21. A.Ceriotti, G.Longoni, M.Manassero, N.Masciocchi, G.Piro, L.Resconi, and M.Sansoni, *J. Chem. Soc., Chem. Commun.*, 1402(1985).

22. A.Ceriotti, A.Fait, G.Longoni, G.Piro, L.Resconi, F.Demartin, M.Manassero, N.Masciocchi, M.Sanaoni, *J.Amer.Chem.Soc.*, **108**, 5370(1986).

23. A.Ceriotti, A.Fait, G.Longoni, G.Piro, F.Demartin, M.Manassero, N.Masciocchi, M.Sansoni, *J. Amer. Chem. Soc.*, **108**, 8091(1986).

24. R.Hoffmann, *J. Chem. Phys.*, **39**, 1397(1963); R.Hoffmann and W.N.Lipscomb, *ibid.*, **36**, 2179; 3189; **37**, 2827(1962).

25. R.H.Summerville and R.Hoffmann, *J. Am. Chem. Soc.*, **98**, 7240(1976).

Chapter 6 Theoretical Analysis of Cluster Compounds with Cylindrical Topologies

6.1 Introduction

The Tensor Surface Harmonic Theory developed by Stone[1] has proved to be particularly useful for defining the closed shell requirements of main group and transition metal cluster compounds.[2] Although this methodology was initially applied to *closo, nido* and *arachno* deltahedral molecules, it has been subsequently extended to three- and four-connected polyhedral molecules, and condensed and polyspherical high nuclearity cluster compounds.[3-7] This free electron model which is based on the solutions of the Schrödinger equation for the particle on a sphere problem has proved to be successful because it correctly identifies the nodal characteristics of the relevant molecular orbitals, and simplifies the complex valence problem substantially by using the pseudo-spherical symmetry of the polyhedra. From these analyses it is also apparent that the *isolobal* analogies[8] between main group and transition metal polyhedral molecules exist because they both have characteristic "unavailable" molecular orbitals which have a high proportion of p orbital character and are unsuitable either for skeletal bonding or accepting electron pairs from ligands. For a deltahedral metal cluster there are (2n-1) of these orbitals and in the Stone's notation they are described as L^{σ}_{sp} ($L \geq 2$) and L^{π}_{pd}($L \geq 1$).

The metal cluster compounds illustrated in Figure 6.1 do not have analogues in main group chemistry, and their closed shell requirements are not satisfactorily explained within the Tensor Surface Harmonic methodology. It is apparent from Figure 6.1 that the topologies of these clusters more closely resemble cylinders than spheres, and therefore it is inappropriate to attempt to describe them in terms of a spherical electron

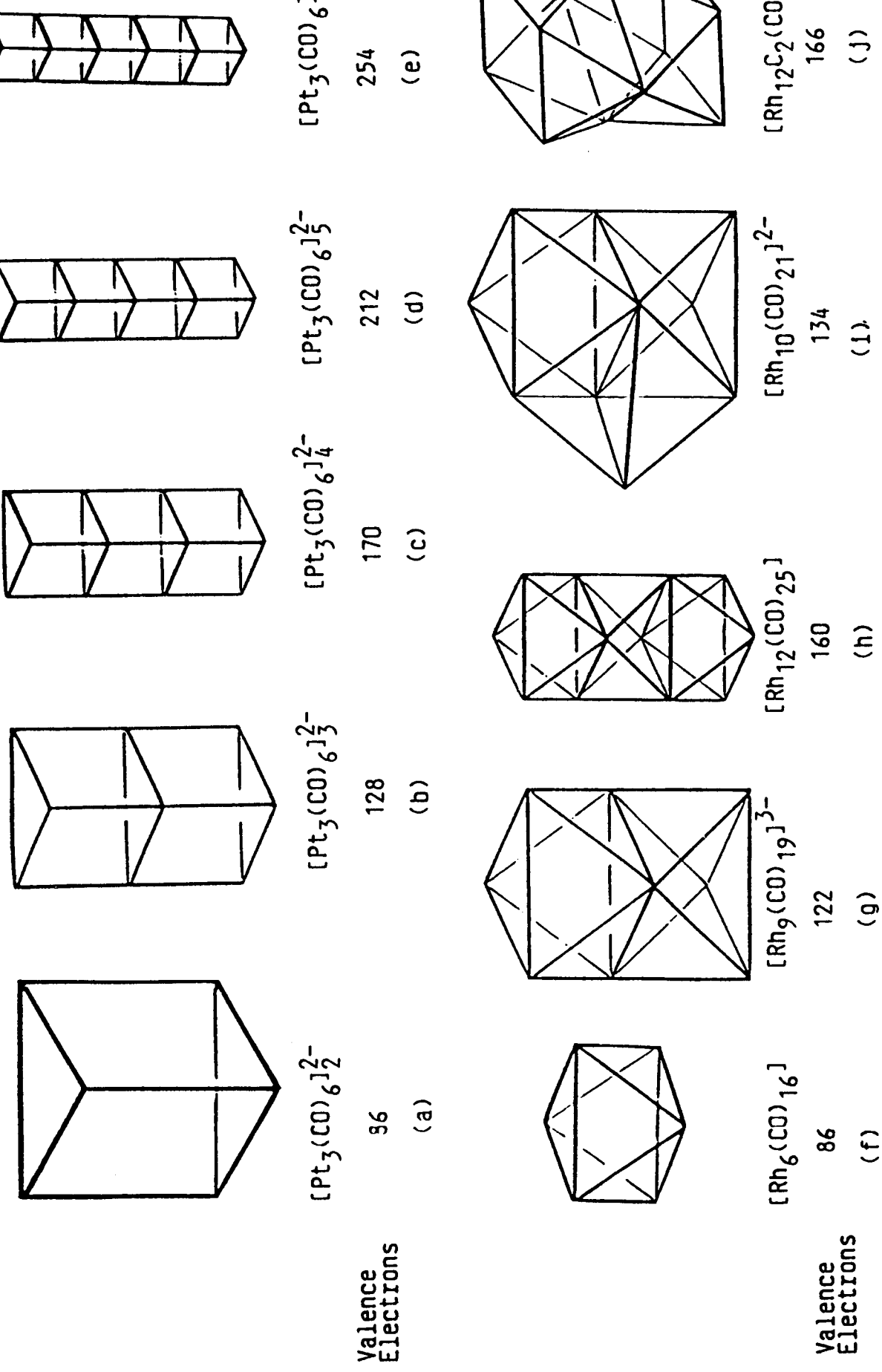


Figure 6.1 Some examples of columnar carbonyl clusters and their characteristic valence electron counts

density model. We have thus developd the solutions in the Schrödinger equation for the particle on the cylinder problem in order to account for the bonding in this type of cluster. Complete details of this theoretical analysis will be given in this Chapter.

6.2 MO wave functions and energies for columnar clusters

6.2.1 MO wave functions

The solution of the Schrodinger equation for a particle on a ring is:

$$\varphi_\lambda = 1/(2\pi)^{1/2}\exp(i\lambda\phi) \qquad \text{----------(1)}$$

where ϕ is the angular co-ordinate and the quantum number λ takes the values 0, ±1, ±2, ... The molecular orbitals ψ_λ can be expressed by the following expansion:

$$\psi_\lambda = (2\pi/n_r)^{1/2} \sum_{j=1}^{n_r} \varphi_\lambda(\phi_j)\, \rho_j \qquad \text{--------(2)}$$

where ϕ_j and ρ_j represent the angular co-ordinate and the basis function of atom j and n_r is the number of atoms in the cycle.

$$\psi_\lambda = 1/(n_r)^{1/2} \sum_{j=1}^{n_r} \exp(i\lambda\phi_j)\, \rho_j \qquad \text{----(3)}$$

When $\lambda \neq 0$ the real forms of these wave functions are:

$$\psi_\lambda^c = (2/n_r)^{1/2} \sum_{j=1}^{n_r} (\cos(\lambda\phi_j))\, \rho_j \qquad \text{------(4)}$$

$$\psi_\lambda^s = (2/n_r)^{1/2} \sum_{j=1}^{n_r} (\sin(\lambda\phi_j))\, \rho_j \qquad \text{-----(5)}$$

$\lambda_{max}=n_r/2$ if n_r is even and $\psi^s_{\lambda max}=0$

$\lambda_{max}=(n_r-1)/2$ if n_r is odd.

The wave functions of a particle on a cylinder can be obtained by taking the products of solutions for a particle on a ring and a particle

on a line. Therefore, for n_z layers of rings of atoms, the product of (3) and the solution for a line of n_z atoms (6) give the required equation (7).

$$\psi_k = [2/(n_z+1)]^{1/2} \sum_{l=1}^{n_z} \sin[kl\pi/(n_z+1)]\ \rho_l \quad \text{----(6)}$$

Where k=1, ..., n_z and refers to the numbering of the layers.

$$\psi_{k,\lambda} = [2/(n_r(n_z+1)]^{1/2} \sum_{l=1}^{n_z} \sum_{j=1}^{n_r} \sin[kl\pi/(n_z+1)]\exp(i\lambda\phi_{lj})\ \rho_{lj} \quad \text{---(7)}$$

where now ϕ_{lj} and ρ_{lj} represent the angular co-ordinate and the basis function of atom j in the lth layer.

For $\lambda \neq 0$ the real forms of these eqations are:

$$\psi^c_{k,\lambda} = [4/(n_r(n_z+1)]^{1/2} \sum_{l=1}^{n_z} \sum_{j=1}^{n_r} \sin[kl\pi/(n_z+1)]\cos(\lambda\phi_{lj})\ \rho_{lj} \quad \text{----(8)}$$

$$\psi^s_{k,\lambda} = [4/(n_r(n_z+1)]^{1/2} \sum_{l=1}^{n_z} \sum_{j=1}^{n_r} \sin[kl\pi/(n_z+1)]\sin(\lambda\phi_{lj})\ \rho_{lj} \quad \text{----(9)}$$

In $D_{\infty h}$ the symmetries of the molecular orbitals for a cylindrical molecule can be defined in terms of the numbers of phase changes along the vertical direction $|\lambda|$ and along the horizontal direction (k-1). Therefore, we introduce the notation whereby $\psi_{\kappa,\lambda}$ is represented by $k\Lambda$, $\Lambda = \Sigma, \Pi, \Delta, \ldots$, for $\lambda = 0, \pm1, \pm2, \ldots$

The basis function ρ bear the following correspondence to the orbital designations used in the spherical problem.

p_σ:	p_σ
p_π:	p_z and p_ϕ
d_π:	$d_{\sigma z}$ and $d_{\sigma\phi}$
d_δ:	$d_{z\phi}$ and $d_{z^2-\phi^2}$

The coordinate system for the cylindrical problem is defined in Figure 6.2.

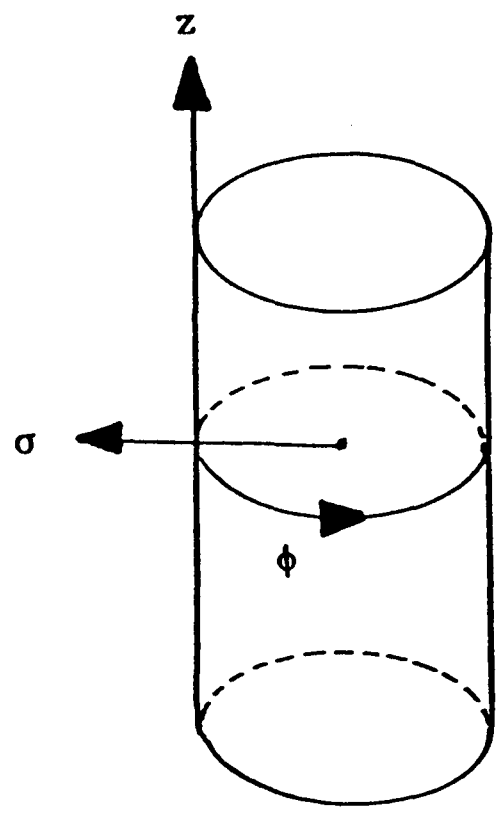


Figure 6.2 Coordinate system for the particle on the cylinder problem

6.2.2 MO energies

The energies of the molecular orbitals based on the wavefunctions in equation (7) can be evaluated by

$$E_{k,\lambda} = (\int \psi_{k,\lambda}^{*} \hat{H} \psi_{k,\lambda} \, d\tau) / (\int \psi_{k,\lambda}^{*} \psi_{k,\lambda} \, d\tau)$$

$$= [2/n_r(n_z+1)] < \sum_{l=1}^{n_z} \sum_{j=1}^{n_r} \sin(kl\pi/(n_z+1)) \exp(i\lambda\phi_{lj}) \, \rho_{lj} \, | \hat{H} |$$

$$\sum_{l=1}^{n_z} \sum_{j=1}^{n_r} \sin(kl\pi/(n_z+1)) \exp(i\lambda\phi_{lj}) \, \rho_{lj} > \text{-------(10)}$$

For illustrative purposes, the Hückel approximations are made for the evaluations of the $E_{k,\lambda}$. If the $\beta(z)$ and $\beta(\phi)$ indicate the resonance integrals of two basis functions between the adjacent atoms along the z

and ϕ directions, then the energies of the molecular orbitals $k\Lambda$ under the Hückel approximations can be expressed in the following formula:

$$E_{k,\lambda} = \alpha + 2\,\beta(z)\cos(k\pi/(n_z+1)) + 2\,\beta(\phi)\cos(2\lambda\pi/n_r) \qquad \text{------(11)}$$

The energies depend on the signs of the $\beta(z)$ and $\beta(\phi)$. The following four different situations illustrated in Figure 6.3 are encountered.

(a) $\beta(z)=\beta$, $\beta(\phi)=\beta$

$$E_{k,\lambda} = \alpha + 2\beta[\cos(k\pi/(n_z+1)) + \cos(2\pi\lambda/n_r)] \qquad \text{--------(12)}$$

The basis functions of s, p_σ, d_σ and $d_z2_{-\phi}2$ are covered by this equation.

(b) $\beta(z)=-\beta$, $\beta(\phi)=\beta$

$$E_{k,\lambda} = \alpha + 2\beta[-\cos(k\pi/(n_z+1)) + \cos(2\lambda\pi/n_r)] \qquad \text{--------(13)}$$

This applies to the p_z basis functions.

(c) $\beta(z)=\beta$, $\beta(\phi)=-\beta$

$$E_{k,\lambda} = \alpha + 2\beta[\cos(k\pi/(n_z+1)) - \cos(2\lambda\pi/n_r)] \qquad \text{--------(14)}$$

This applies to the p_ϕ basis functions.

(d) $\beta(z)=-\beta$, $\beta(\phi)=-\beta$

$$E_{k,\lambda} = \alpha + 2\beta[\cos(k\ /(n_z+1)) + \cos(2\lambda\pi/n_r)] \qquad \text{--------(15)}$$

The $d_{z\phi}$ basis functions follow this equation.

In the right-hand side of Figure 6.3, the MO energy levels of stacked triangle structures based on the approximations above are illustrated. It can be seen that there is parity relationship between (a) and (d) and also between (b) and (c).

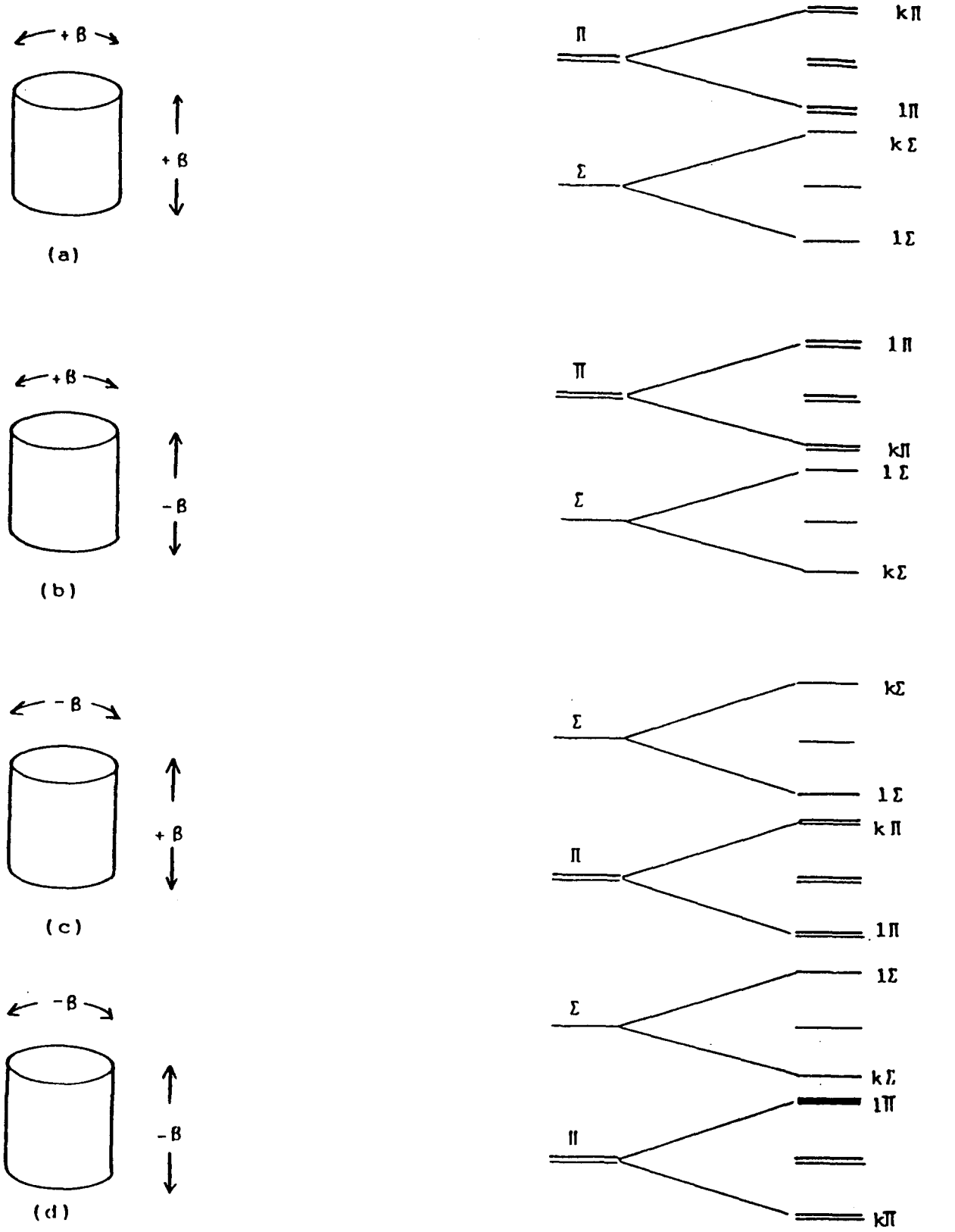


Figure 6.3 The schematic MO energy levels for four different types of situation

6.3 Orbital interactions

From the wave functions (7), (8) and (9), the basis set ρ can be any of the 9 atomic orbitals (s, p and d). If p_z is taken as a basis set, then the linear combinations of p_z's can be obtained from (7)-(9). The same procedure applies to the other basis sets. The energy levels to first order in perturbation theory can be approximately calculated according to equations (11)-(15) and in addition, the simplification $|\beta(\phi)| = |\beta(z)|$ can be made. The mixing between molecular orbitals from different sets of basis functions can be evaluated from second order perturbation theroy.

As in the spherical case, the 9 atomic valence orbitals of each transition metal atom can be classified into σ, π and δ types according whether they have none, one node and two nodes when viewed along the σ axis. The resultant classifications are as follows:

σ: s, p_σ and d_σ;

π: p (p_ϕ, p_z), d ($d_{\sigma z}$, $d_{\sigma\phi}$);

δ: d ($d_z2_{-\phi}2$, $d_{z\phi}$).

6.3.1 σ orbitals

For the three σ atomic orbitals on each atom in the cylindrical cluster, only the in-pointing hybrid combinations of orbitals make major contributions to the skeletal bonding. The other two hybrid orbitals are out-pointing and capable of accepting electron pairs from ligands or are non-bonding. Occupation of these orbitals leads to a contribution of 4n (n is the total number of metal atoms in the cylindrical cluster) electrons to the total electron count.

The number and symmetries of the in-pointing Σ^σ, Π^σ, ..., Λ^σ, ... molecular orbitals for a ring depends on the number of atoms (n_r) in the ring. For example, there are Σ^σ, Π^σ orbitals for a triangular cluster.

For the cluster based on stacked triangles, the molecular orbitals develop a 'band like' structure based on the Σ^{σ} and Π^{σ} orbitals of the parent triangle. The corresponding energy level scheme as a function of n_z (the number of rings) is shown in Figure 6.4. The Σ^{σ} and Π^{σ} bands begin to overlap when n_z is greater than 3. As the number of atoms in the ring (n_r) increases. There are more bands derived from Λ^{σ} besides the molecular orbitals which derived from Σ^{σ} and Π^{σ}.

6.3.2 π-interactions

For the p_{π} orbitals , the resonance integral β_{σ} is approximately equal to the β_{π}. Therefore, the energies of the molecular orbitals derived from p_{ϕ} and p_z components of p_{π} are given by the equation (13) and (14) above. The MO wave functions derived from the p_{ϕ} basis sets are related to the MOs derived from the p_z basis sets by the parity transformation, (P), involving a local rotation of 90° at each atom along the σ axis (see equations (7)-(9) for the explicit forms of these wave functions). It can be seen also from (13) and (14) that the energies of these m.o.s are symmetrical above $\alpha=0$ because of parity relationship.

Figure 6.5 illustrates schematically the energy bands for the stacked triangles. The Σ^{ϕ} band is centred about -2β and Σ^{z} about $+2\beta$ and as n_z approaches ∞ their band widths approach 4β. Therefore, no crossing occurs for these two bands, and one is always in the bonding region and the other in the antibonding region. Moreover, there is no mixing between them because they have different symmetries. The Π^{ϕ} band is centred about $+\beta$ and Π^{z} about $-\beta$, and as n_z increases they overlap in the region from $+\beta$ to $-\beta$. Since many components of the Π^{ϕ} and Π^{z} bands have the same symmetry they mix extensively. However, because of the parity relationships which apply to the wave functions and their energies, the

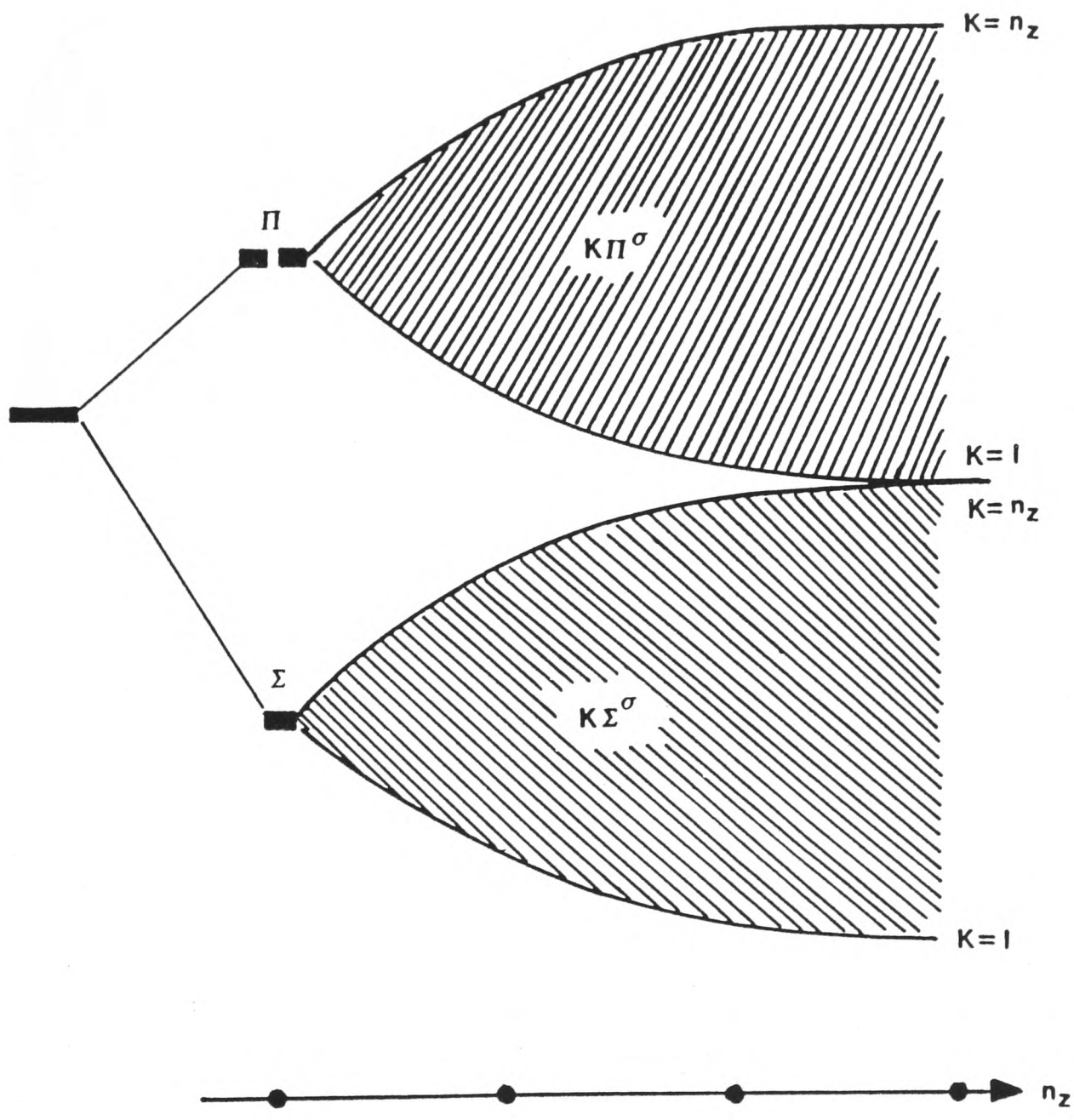


Figure 6.4 The energy level scheme of σ-type for n_z layers based on triangles

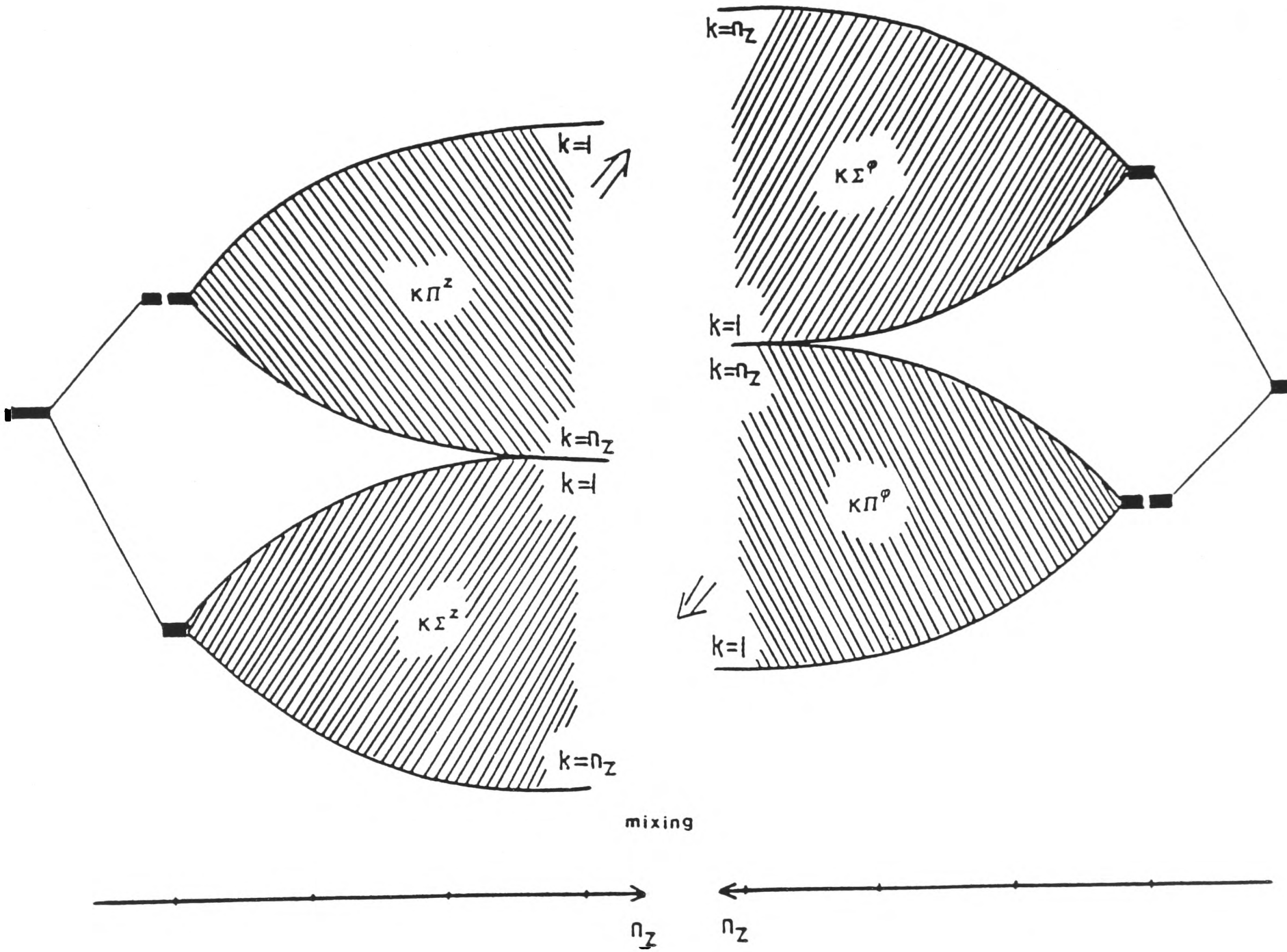


Figure 6.5 The energy level scheme of π-type for n_z layers based on triangles

net result is one bonding band $k\Pi^{\phi/z}$($k=1, ..., n_z$) and second antibonding band $k\Pi^{z/\phi}$. Consequently, the total number of the tangential p_π bonding molecular orbitals for a column of triangles is n. There are also n antibonding π tangential orbitals derived from the p_z and p_ϕ basis sets. As n_r increases the molecular orbitals develop Λ^z and Λ^ϕ bands for $\lambda>1$ as well as the Σ and Π bands. Since the Λ^z and Λ^ϕ bands are also parity related half become bonding and half antibonding. In summary, the tangential p_π orbitals (p_z, p_ϕ) give, after the relevant orbital mixings are taken into account, n bonding and n antibonding skeletal molecular orbitals localised predominantly on the surface of the cylinder.

The d_π ($d_{\sigma z}$, $d_{\sigma\phi}$) orbitals of the metal atoms in a cylindrical cluster have the same symmetry properties as the p_π (p_z, p_ϕ) and mix extensively with them to give equal numbers of in-pointing and out-pointing hybrid orbitals. The former increase the interactions between skeletal molecular orbitals and give rise to no change in the bonding pattern. The latter can either be classified as non-bonding or used in metal-ligand bonding. Since the situation is entirely analogous to that in spherical clusters, the d_π orbitals in a cylindrical cluster do not generate any additional unavailable molecular orbitals .

6.3.3 σ and π mixings

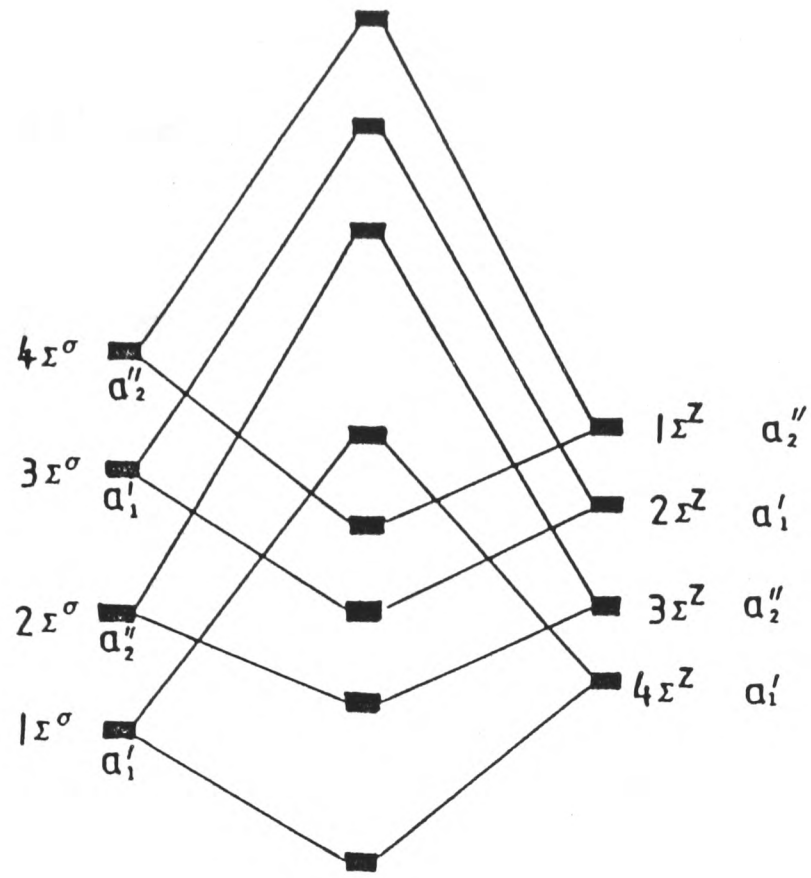
The molecular orbitals Λ^σ ($\lambda\geq1$, Π, Δ, ...) can mix extensively with the Λ^π tangential bonding orbitals ($\Lambda^{\phi/z}$, $\lambda\geq1$). The net result of this mixing is a stabilisation of the π tangential bonding orbitals and a destablisation of the Λ^σ orbitals. This mixing therefore does not increase the number of skeletal bonding orbitals. It is analogous to the σ/π mixing in spherical clusters.

The $k\Sigma^\sigma$ band does make a major contribution to the skeletal bonding

because of its lower energy (see Figure 6.4). The k Σ^{σ} orbitals mix extensively with all the n_z bonding orbitals of the $k\Sigma^{z}$ band since they have the same symmetry, but they do not mix at all with $k\Sigma^{\phi}$ antibonding orbitals which have different symmetry properties.

For columns with an even number of layers, the $1\Sigma^{\sigma}$ and $n_z\Sigma^{z}$ molecular orbitals have matching symmetries and comparable energies. The resultant mixing is illustrated for n_z=4 in Figure 6.6, and results in a pair of molecular orbitals which are both bonding. The in-phase combination is strongly bonding in the outer prisms and the out-of-phase combination is strongly bonding in the middle prism. The remaining pairs of $k\Sigma^{\sigma}$-$(n_z-k+1)\Sigma^{z}$ ($k=2,\ldots,n_z$) molecular orbitals result in combinations which are skeletal bonding and antibonding respectively. Consequently for n_z even the Σ^{σ} and Σ^{z} orbitals mix extensively and result in n_z+1 bonding and n_z-1 antibonding molecular orbitals, i.e. the n_z $k\Sigma^{\sigma}$ and n_z $k\Sigma^{z}$ mixing creates one additional strongly bonding m.o., $1\Sigma^{\sigma/z}$ which corresponds to the S^{σ} orbitals of a spherical cluster.

When n_z is odd the mixings follow a different pattern because the symmetries of the molecular orbitals do not follow a 1:1 mapping. Figure 6.7 illustrates the relevant molecular orbitals for a column of three triangles, i.e., $1\Sigma^{\sigma}(a_1')$, $2\Sigma^{\sigma}(a_2'')$ and $3\Sigma^{\sigma}(a_1')$, and $3\Sigma^{z}(a_2'')$, $2\Sigma^{z}(a_1')$ and $1\Sigma^{z}(a_2'')$. Mixing between $1\Sigma^{\sigma}$, $2\Sigma^{z}$ and $3\Sigma^{\sigma}$ can be represented by the conventional three orbital pattern of bonding, non-bonding and antibonding and $1\Sigma^{z}$, $2\Sigma^{\sigma}$ and $3\Sigma^{z}$ give rise to a similar set. In total this results in a set of 4 molecular orbitals which are either bonding or non-bonding between the rings and strongly bonding within the rings. Calculations for different values of n_z have confirmed that the result of such mixings are (n_z+1) $\Sigma^{z/\sigma}$ bonding skeletal molecular orbitals.



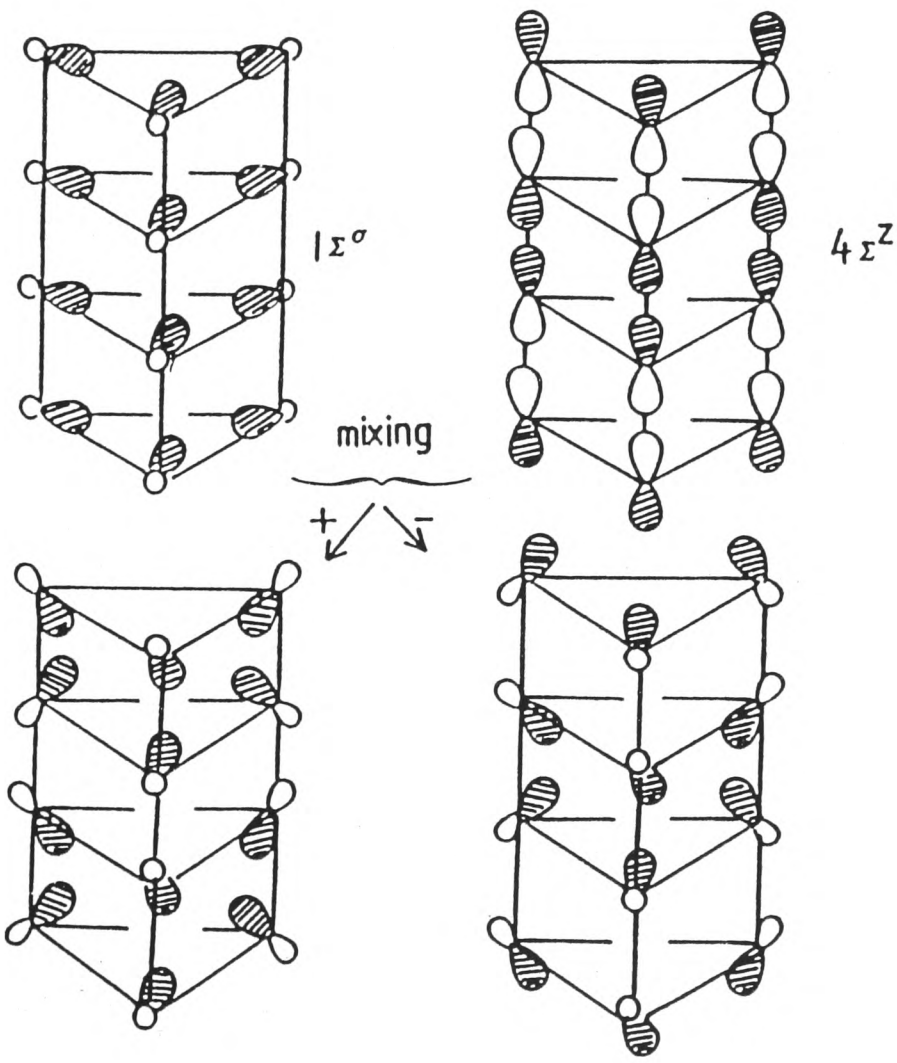
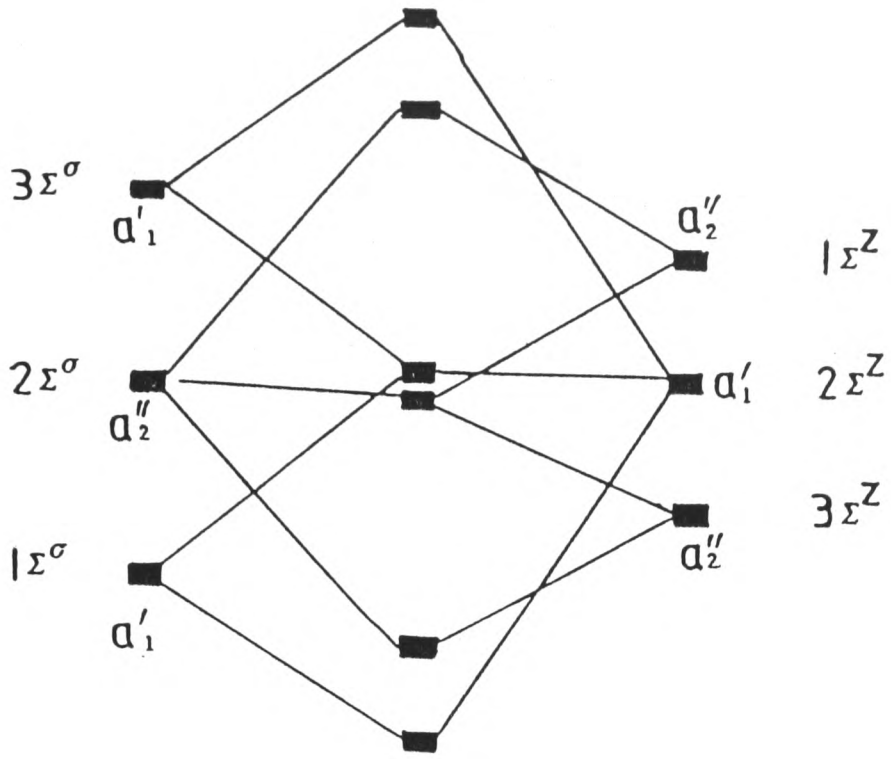


Figure 6.6 The mixings between $k\Sigma^z$ and $k\Sigma^\sigma$ when n_z is even



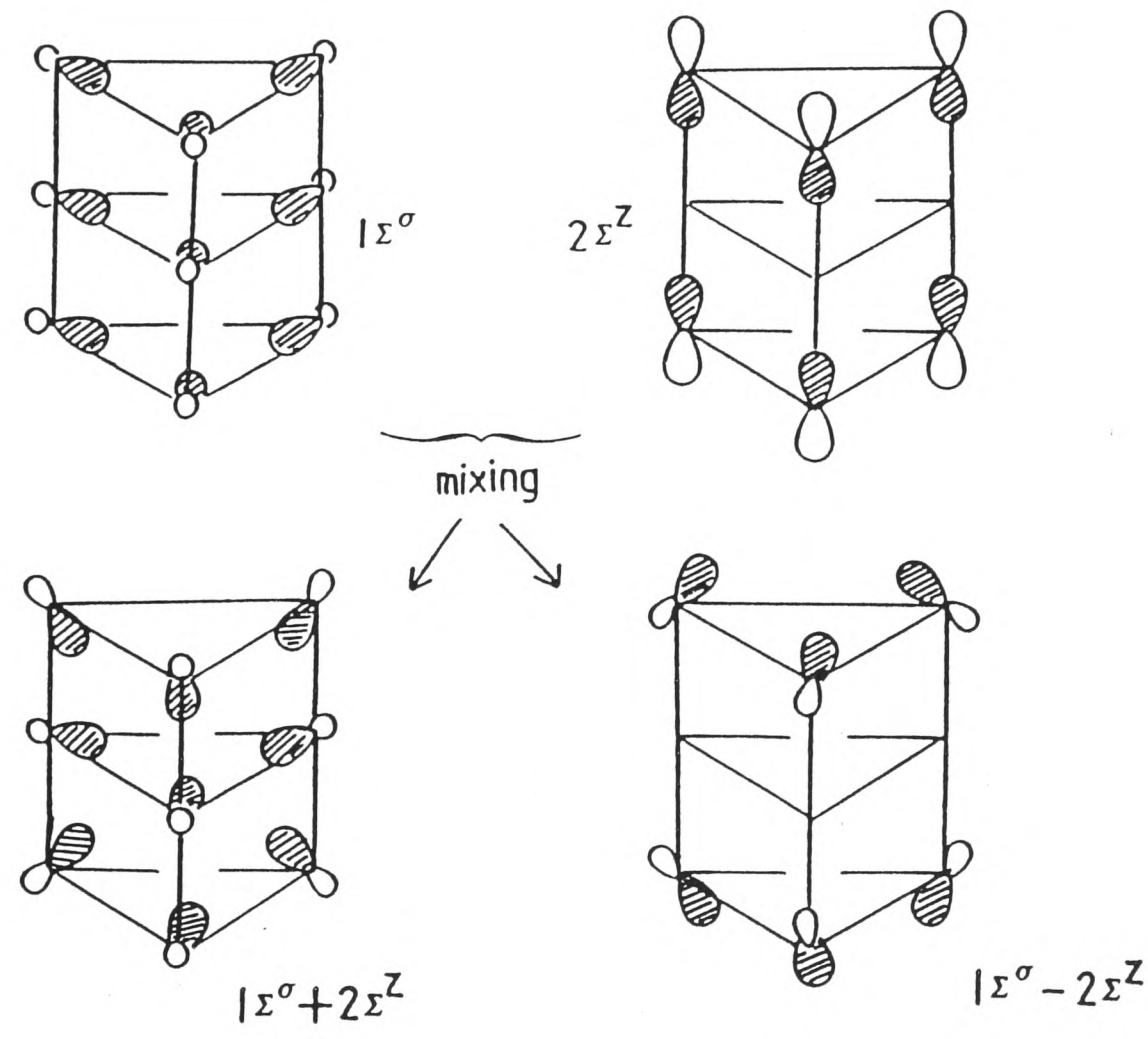


Figure 6.7 The mixings between $k\Sigma^{z}$ and $k\Sigma^{\sigma}$ when n_z is odd

In summary, for a cylindrical cluster of main group atoms with s and p valence orbitals, the in-pointing sp (σ) hybrid orbitals give rise to one very strongly bonding $1\Sigma^{\sigma}$ radial molecular orbital, which has neither vertical nor horizontal nodes. The tangential p orbitals, which for the cylinder problem are defined as p_z and p_{ϕ}, give, after the relevant orbital mixings are taken into account, n bonding and n antibonding skeletal molecular orbitals localised predominately on the surface of the cylinder. Although p_z and p_{ϕ} have been separated the molecular orbitals derived from them are still related by the parity transformation ($\hat{P}$) involving a local rotation of 90° at each atom and along the σ axis. The energies of parity related molecular orbitals are approximately equally bonding and antibonding as long as $\beta_{\sigma} \approx \beta_{\pi}$. Consequently for a cylindrical cluster of this type there are a total of (n+1) bonding and (2n-1) "unavailable" skeletal molecular orbitals, i.e. the same number as that observed for spherical deltahedral clusters. The nodal characteristics of the radial and tangential molecular orbitals are also related to those for a spherical cluster with the same number of atoms. This relationship can be illustrated by reference to specific calculations on $B_9H_9^{2-}$ with either a spherical (**1a**) or cylindrical (**1b**) topology. The tricapped trigonal prism (**1a**) and the face sharing octahedron (**1b**) both belong to to the D_{3h} point group and their bonding skeletal molecular orbitals span the same irreducible representations (see Figure 6.8). In this Figure, the pseudo-symmetry labels of a particle on a cylinder are also given in order to give a correlation between the alternative methodologies.

In Figure 6.8 the computed total energies, overlap populations and computed atomic charges (derived from extended Hückel molecular orbital calculations) are summarised. Although both **1a** and **1b** are

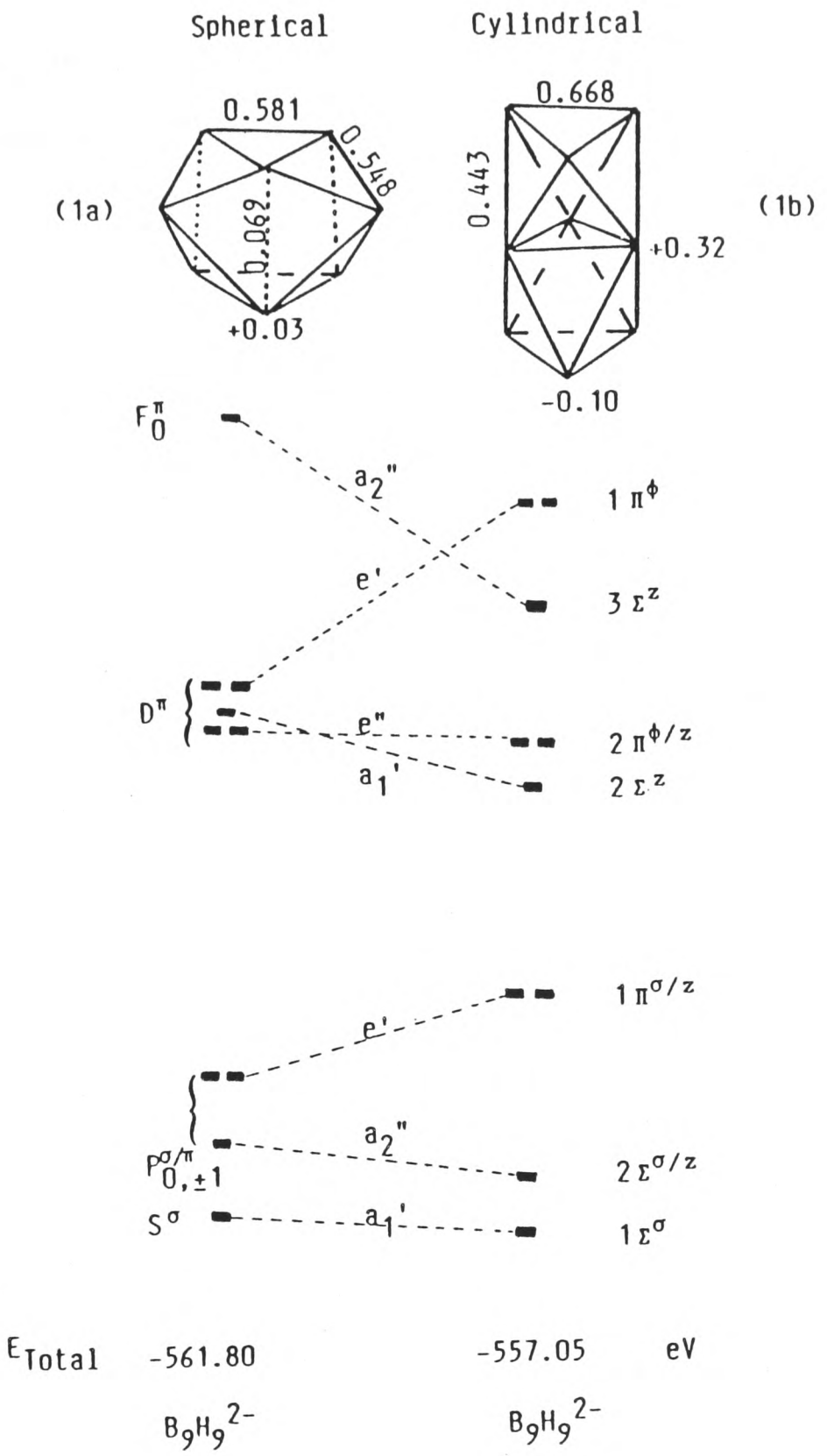


Figure 6.8 The total energies, overlap populations and charges for $B_9H_9^{2-}$ with spherical and cylindrical geometries

characterised by a total of (n+1) skeletal bonding molecular orbitals their computed total energies differ by more than 4.5ev. The spherical geometry is the more stable because it permits more favourable bonding interactions for the radial and tangential molecular orbitals and a more even distribution of charge and bonding electron densities. The latter conclusions are clearly supported by the computed atomic charges on the boron atoms and the overlap populations. In the light of these calculations it is not surprising that main group polyhedral moleules do not in general adopt cylindrical topologies.

The stacked platinum triangular clusters **a-e** in Figure 6.1 provide a reasonable approximation to the bonding situation described above because although they have d valence electrons their d^{10} configurations lead to cancellation of the bonding effects associated with the d shell. All the clusters $[Pt_3(CO)_6]_n^{2-}$ (n=2-6)[9] are characterised by a total of 42n+2 valence electrons which corresponds to the (n+1) skeletal electron pairs calculated for main group cylindrical molecules. Detailed calculations on these clusters [10-11] have indicated that the primary bonding interactions occur within the triangles. The interactions between triangles are much weaker and the resulting single bonding molecular orbital is an in-phase combination of platinum $6p_z$ orbitals ($n\Sigma^z$) with a substantial contribution from the carbonyl π^* orbitals. These interactions slightly outweight the repulsive interactions between the rings arising from the filled d shells.

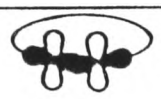
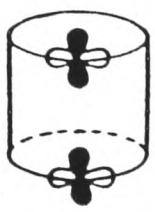
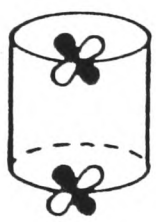
6.3.4 d_δ interactions

The $d_z2_{-\phi}2$ and $d_{z\phi}$ orbitals are the pair of d_δ orbitals in the cylinder problem. The molecular orbitals based on either $d_z2_{-\phi}2$ ($k\Lambda^{z2-\phi2}$) or $d_{z\phi}$ ($k\Lambda^{z\phi}$) basis set can be obtained from (7)-(9). The $k\Lambda^{z2-\phi2}$ and $k\Lambda^{z\phi}$ molecular orbitals are related by a parity operation

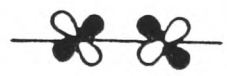
involving a local rotation of 45° along the σ axis. The energies of parity related m.o.s depends on the resonance integrals between the adjacent atoms within the ring $\beta(\phi)$ and between rings $\beta(z)$. Figure 6.9(a) illustrates the $\beta(z)$ and $\beta(\phi)$ for $d_z2_{-\phi}2$ and $d_{z\phi}$ basis sets based on β_σ, β_π and β_δ, where the β_σ, β_π and β_δ are the conventional definition of σ, π and δ overlaps of d orbitals (shown in Figure 6.9(b)). In the right-hand side of Figure 6.9(b), the overlap integrals from Mo-Mo are given. Unlike the p_π orbitals, the parity energy relationship is not precise, because the resonance integrals $\beta_\sigma \neq \beta_\pi \neq \beta_\delta$, unless n_r is very large. Consequently, the energy levels give a more complicated pattern. The energies of the band structures for the $k\Lambda^{z\phi}$ and $k\Lambda^{z2-\phi2}$ can be obtained from (12) and (15) if β_σ, β_π and β_δ are approximately equal. Their patterns are illustrated in Figures 6.3(a) and 6.3(d).

6.3.5 Discussion

In a spherical transition metal carbonyl cluster the Stone methodology leads to a considerable simplification because the pesudo-spherical symmetry of the problem is utilised. In addition the characteristic closed shell electron requirements of a cluster can be identified in terms of a set of molecular orbitals which are designated as "unavailable" by virtue of their strong skeletal antibonding character and their inwardly hybridised nature. In a spherical cluster with n atoms these "unavailable" orbitals have a high proportion of p orbital character and are : n $\bar{L}^{\pi}_{pd}$ and (n-1) L^{σ}_{sp}. Both sets are in-pointing by virtue of d-p (and s) mixing, the former by L^{π}_{p}/L^{π}_{d} mixing and the latter from $L^{\sigma}_{p}/L^{\sigma}_{s}/L^{\sigma}_{d}$ (L≥1) mixing. Consequently a deltahedral transition metal cluster is characterised by a total of (2n-1) unavailable orbitals since the remaining 7n+1 orbitals can be utilised either in metal-ligand or metal-metal bonding or are non-bonding.

	Resonance Integrals β	if $\beta_\sigma = \beta_\pi = \beta_\delta$
	$\beta(\phi)=1/32[(15+6\cos\theta+3\cos^2\theta)\beta_\sigma$ $+(9-6\cos\theta+5\cos^2\theta)\beta_\delta+8\sin^2\theta\,\beta_\pi]$	β
	$\beta(z)=3/4\,\beta_\sigma+1/4\,\beta_\delta$	β
	$\beta(\phi)=-\cos^2(\theta/2)\,\beta_\pi-\sin^2(\theta/2)\,\beta_\delta$	$-\beta$
	$\beta(z)=-\beta_\pi$	$-\beta$
	$\theta = 2\pi/n_r$	
	(a)	

Overlap integrals between Mo and Mo

β_σ		0.0893
β_π		0.0868
β_δ		0.0200

(b)

Figure 6.9 (a) Four different types of d-d resonance integrals
(b) The definition of β_σ, β_π and β_δ

In a cylindrical transition metal cluster, there are a similar set of (2n-1) unavailable orbitals with a high proportion of p orbital character as discussed above, i.e. $n\Lambda^{\pi*}$ and $(n-1)\Lambda^{\sigma*}$. Both sets are in-pointing hybridised antibonding molecular orbitals, the former by the hybridisation of (p_z, p_ϕ) and $(d_{\sigma z}, d_{\sigma\phi})$ and the latter by the hybridisation of s, p_σ and d_σ.

For a spherical cluster, the L_d^δ and $\bar{L}_d^\delta$ molecular orbitals derived from $d_\theta 2_{-\phi} 2$ and $d_{\theta\phi}$ are both filled by a total of 4n valence electrons because the overlap integrals between the d_δ basis sets on the spherical surface are not large and furthermore the L_d^δ can be stablised by the strongly interaction with π^*(CO).

In a cylindrical transition metal cluster, the d $(d_z 2_{-\phi} 2, d_{z\phi})$ basis sets on the surface of cylinder experience a very different situation from that on the surface of a sphere. The situations of the d_δ sets depend on whether the inner or outer ring atoms are considered. The d_δ basis sets from the two outer rings are the same as in the spherical case and are non-bonding because they experience the same interaction as on the surface of a sphere. The d_δ orbitals of the metal atoms belonging to the (n_z-2) rings experience a particularly strong interaction even though they rehybridise with p_π orbitals (see Figure 6.10). It is the d_δ interactions between the (n_z-2) inner rings that create extra "unavailable" orbitals.

When n_r is very large, the resonance integrals $\beta(\phi)$ and $\beta(z)$ for the δ basis set (see Figure 6.9) become approximately equal and their energies reflect the parity relationship, half bonding and half antibonding. Therefore, the total number of "unavailable" orbitals will be the 2n-1 from the σ and π interactions and the additional d_δ from the inner rings $n_r(n_z-2)$ (i.e. the number of atoms in the inner rings). Therefore, the total number of the unavailable orbitals is

$$(2n-1) + n_r(n_z-2) \qquad \text{----------(16)}$$

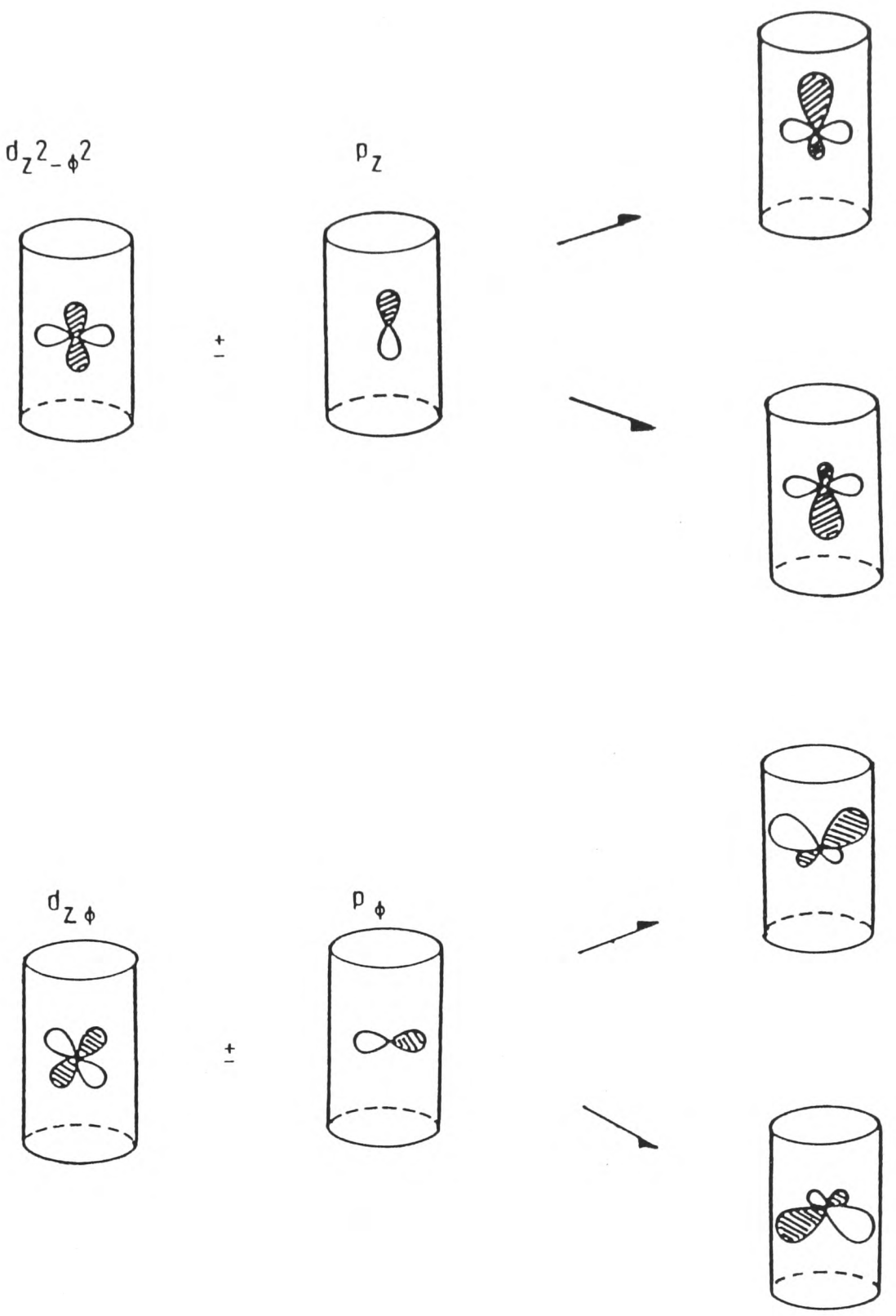


Figure 6.10 the rehybridisation between d_δ and p_π basis sets

However, there are no examples of columnar cluster based on large rings. For small ring, the number of the unavailable d_δ orbitals from the inner rings is less than $n_r(n_z-2)$ because the energy relationship between parity related orbitals is not satisfied. Therefore, the total number of unavailable orbitals can be formulated as:

$$(2n-1) + n_r(n_z-2) - \text{DELTA} \qquad \text{------(17)}$$

Where DELTA depends on the number of atoms in the ring (i.e. n_r).

The smallest ring of a column cluster is the triangle stacked structure which comprise of Σ and Π "band like" molecular orbitals. If we assume $\beta_\sigma=\beta_\pi=4\beta$ (see Figure 6.9(b)), the "band like" molecular orbitals are shown in Figure 6.11(a) and 6.11(b).

Figure 6.11(a) illustrates the $k\Pi^{z\phi}$ and $k\Pi^{z2-\phi2}$ bands. They have the same symmetries (e′ or e") and mix extensively to give one bonding $k\Pi^{z\phi/z2-\phi2}$ band and the other antibonding $k\Pi^{z2-\phi2/z\phi}$ band. This leads to no change of parity properties, i.e. no contribution to the DELTA in (17). The $k\Sigma^{z\phi}$ and $k\Sigma^{z2-\phi2}$ bands are shown in Figure 6.11(b) and no mixing occurs between them because they have different symmetries. As a result, the energy parity does not hold. This leads to a contribution to the DELTA in (17). It can be seen from Figure 6.11(b) that all orbitals from $k\Sigma^{z2-\phi2}$ band are in the bonding region and nearly half of the $k\Sigma^{z\phi}$ band is in the bonding or non-bonding regions. If all the orbitals from $k\Sigma^{z\phi}$ were unoccupied, there would be no effect to the energy parity relationship. The occupation of the half band from $k\Sigma^{z\phi}$ leads to more available orbitals. This give the DELTA for stacked triangles a value of $[(n_z-2)/2]$. Therefore, the number of unavailable orbitals for the column clusters of stacked triangles can be formulated as follow:

$$(2n-1) + 3(n_z-2) - [(n_z-2)/2] \qquad \text{------(18)}$$

(where [x] is the integer contribution of x, e.g. if x=2.5 [x]=2)

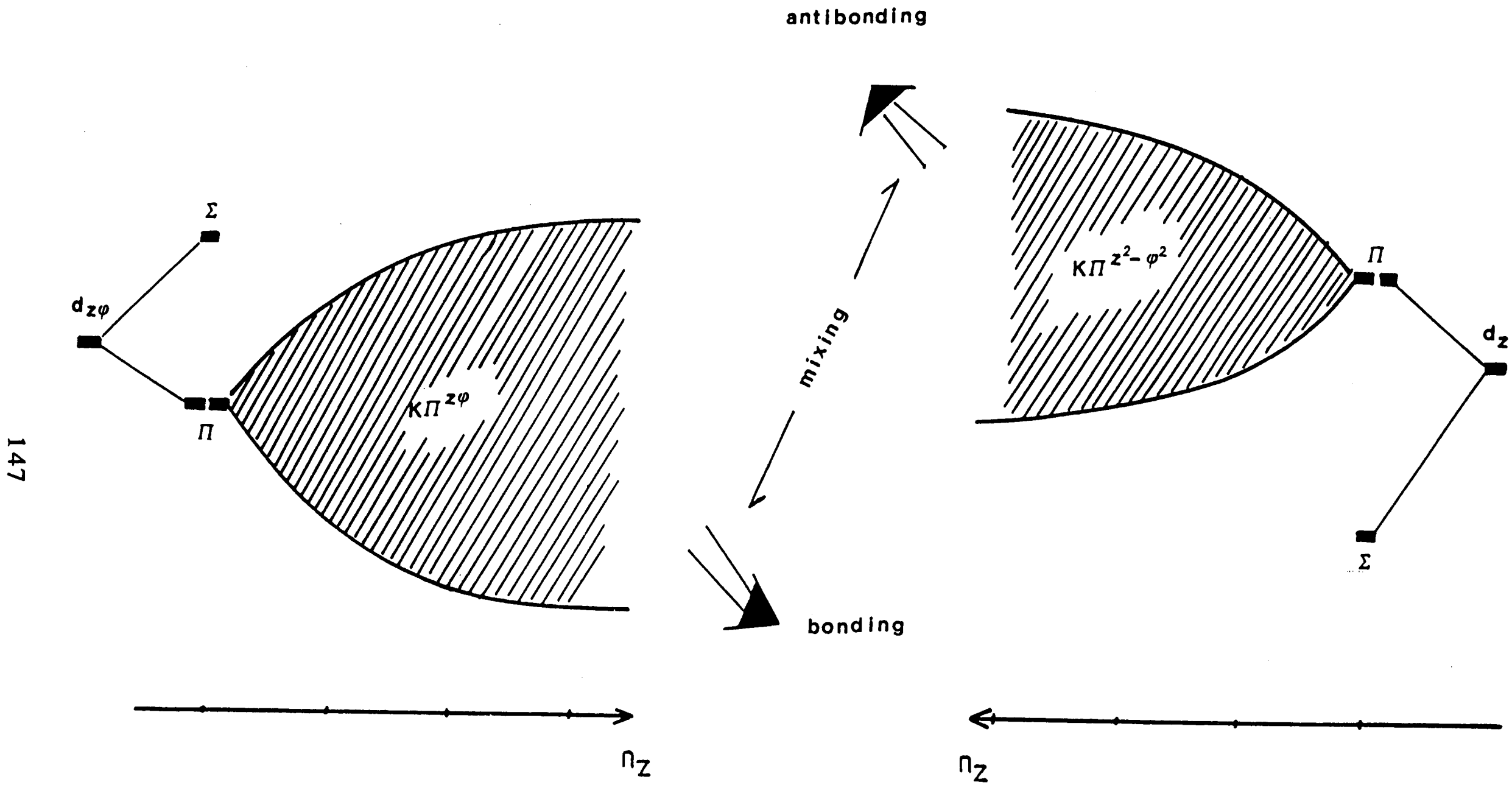
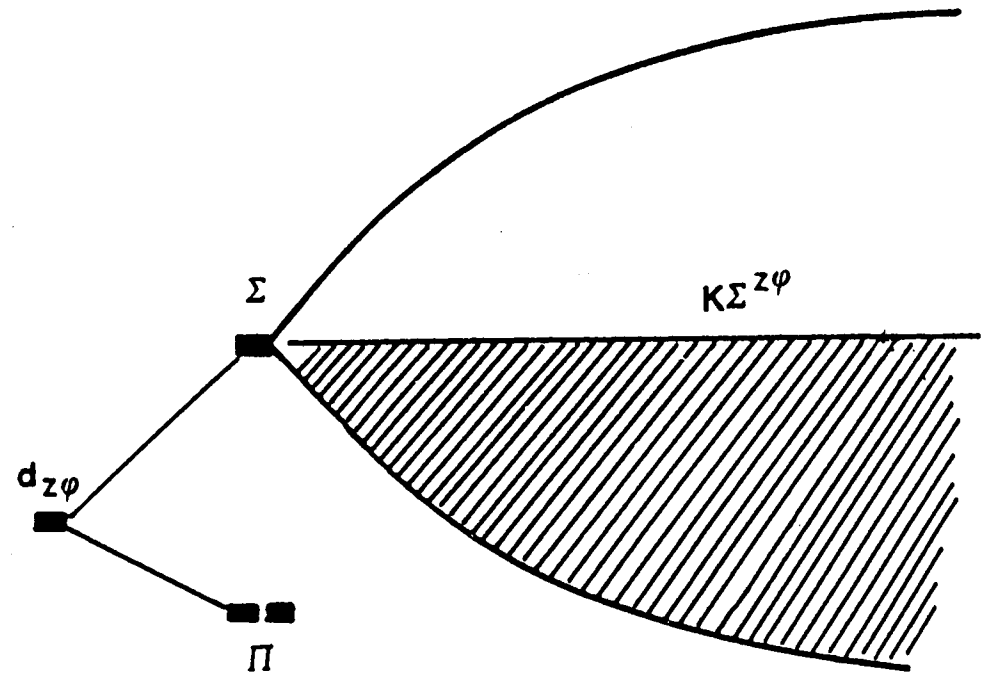
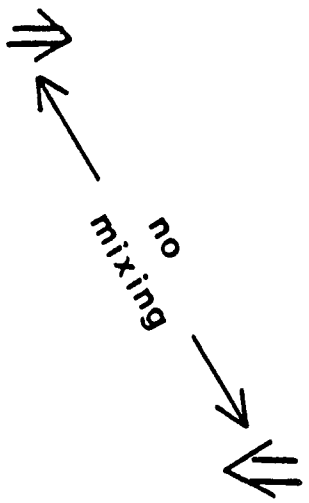


Figure 6.11(a) The energy level scheme of Π band based on d_δ basis set





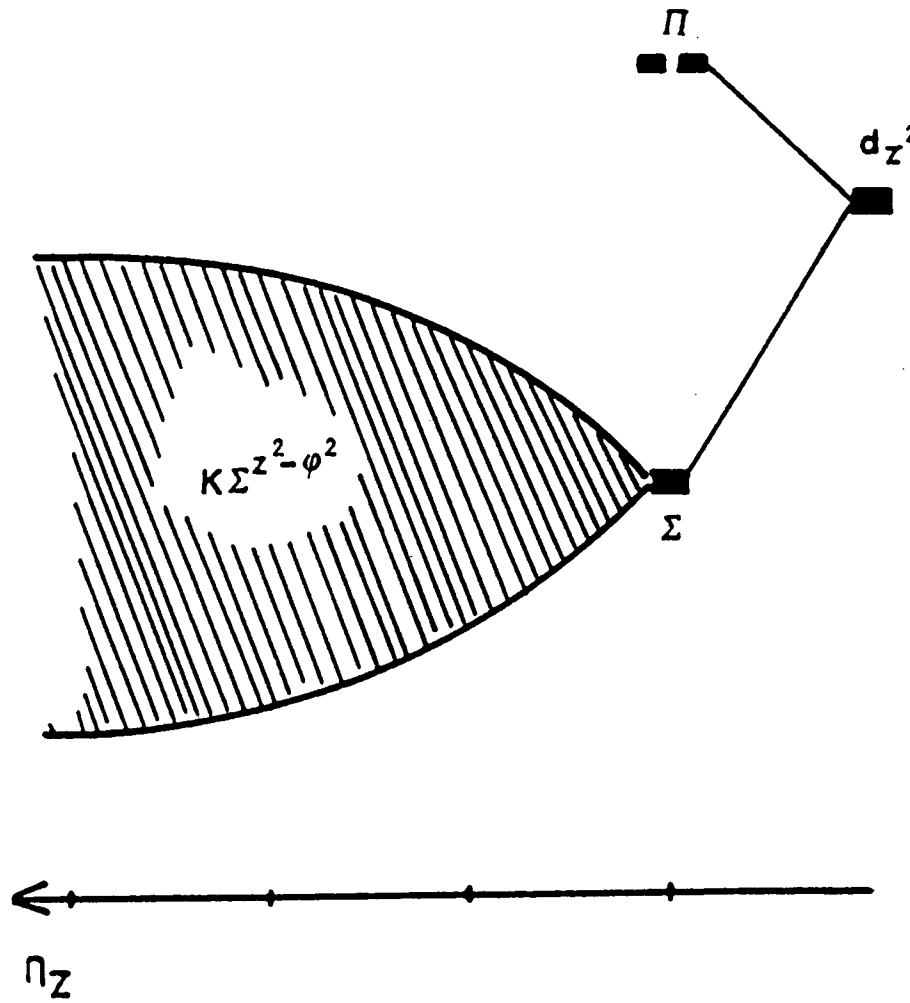


Figure 6.11(b) The energy level scheme of Σ band based on d_δ basis set

The equation (18) accounts for the electron counts in the following series of rhodium carbonyl clusters based on staggered triangles.

$[Rh_6(CO)_{16}]$ [12] (see Figure 6.1(f)) octahedral (n_z=2) 86 valence electrons

$[Rh_9(CO)_{19}]^{3-}$ [13] (see Figure 6.1(g)) face sharing octahedra (n_z=3) 122 valence electrons

$[Rh_{12}(CO)_{25}]$ [14] (see Figure 6.1(h)) three face sharing octahedra (n_z=4) 160 valence electrons

$[Rh_{10}(CO)_{21}]^{2-}$ [15] (see Figure 6.1(i)) is derived from the face sharing octahedra by the introduction of an additional capping atom and is electronically related to the latter by the capping principle,[16] i.e. it has a total of 122+12=134 valence electrons

When n_r increases, the total number of unavailable orbitals in the columnar cluster is between (16) and (18). The electron count depends on the d-d overlap integrals. Although a generalised electron count can not be obtained the methodology developed above gives a clearly classification of the molecular orbitals.

6.4 MO calculations on cylindrical clusters

To confirm the arguments developed above, we have completed extended Hückel molecular orbital calculations on three cylindrical clusters whose structures are based on three, four triangles and three squares staggered with ML_3 fragments. The MO diagrams for these three clusters are illustrated in Figures 6.12, 6.13 and 6.14. For reasons of clarity, we developed energy levels of molecular orbitals through ML_3 fragment ---> single ring ---> cluster MO's, and seperated the π (and σ) basis set and the δ basis set.

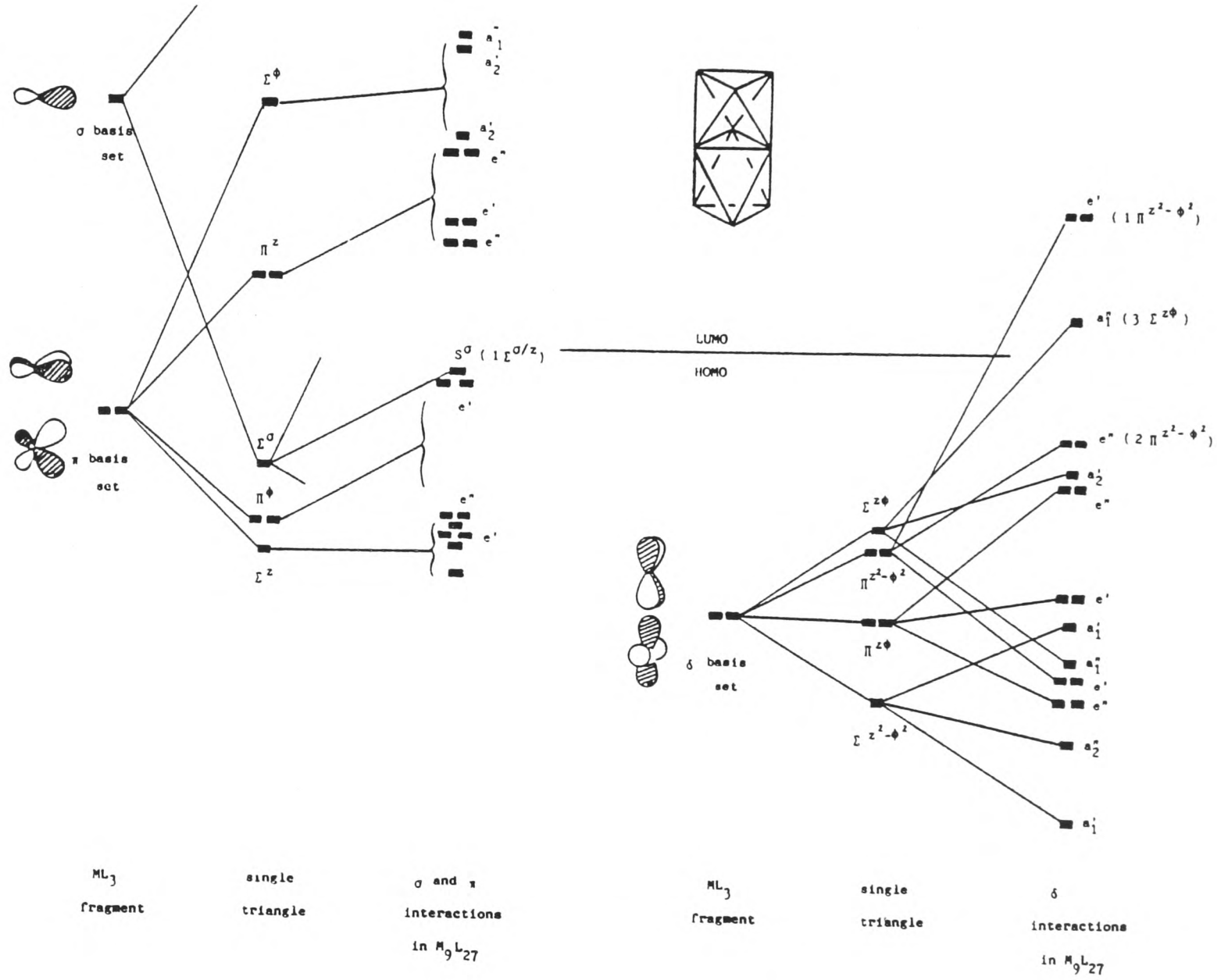


Figure 6.12 The MO diagram for M_9L_{27} with ML_3 fragments based on three staggered triangles

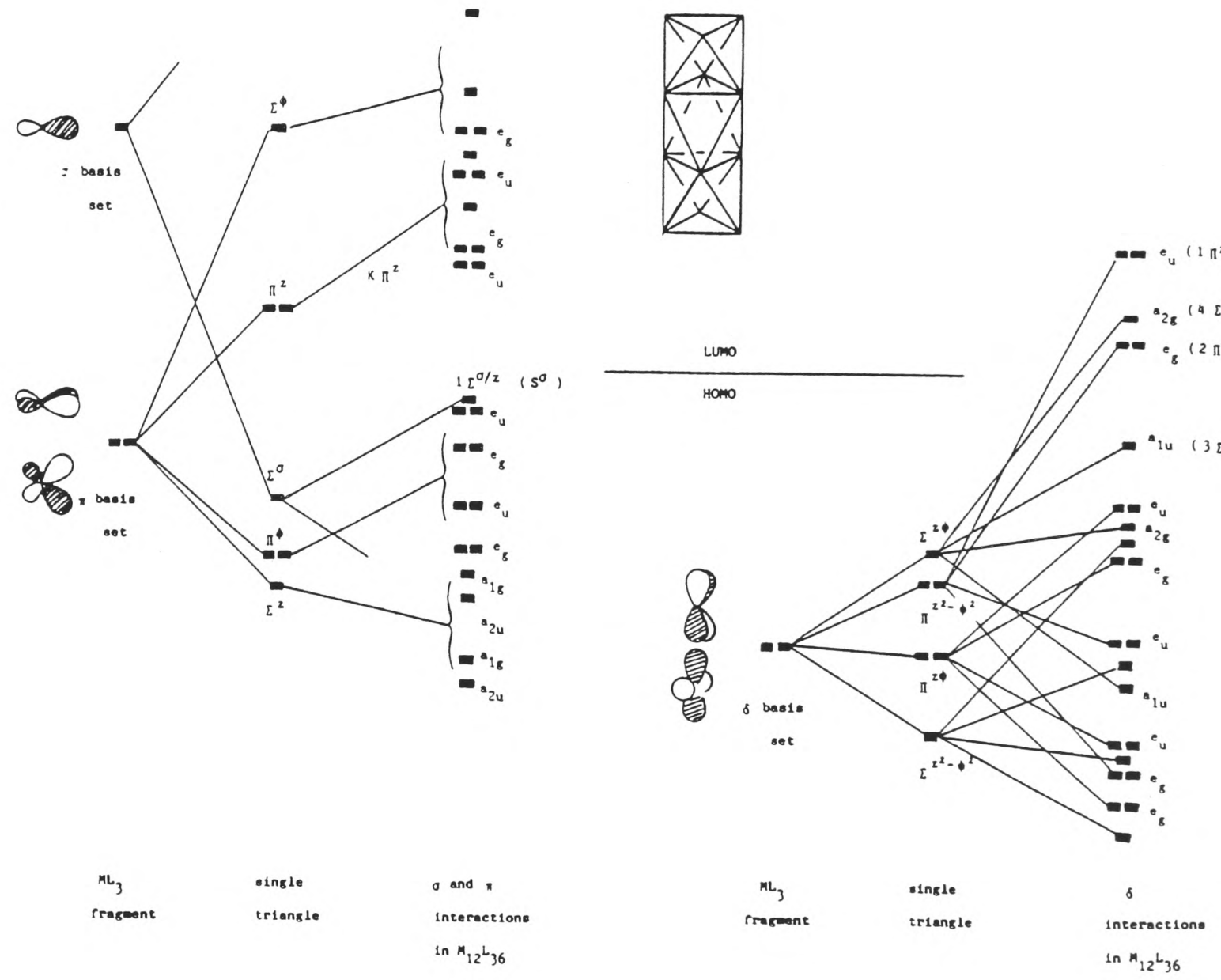


Figure 6.13 The MO diagram for $M_{12}L_{36}$ with ML_3 fragments based on four staggered triangles

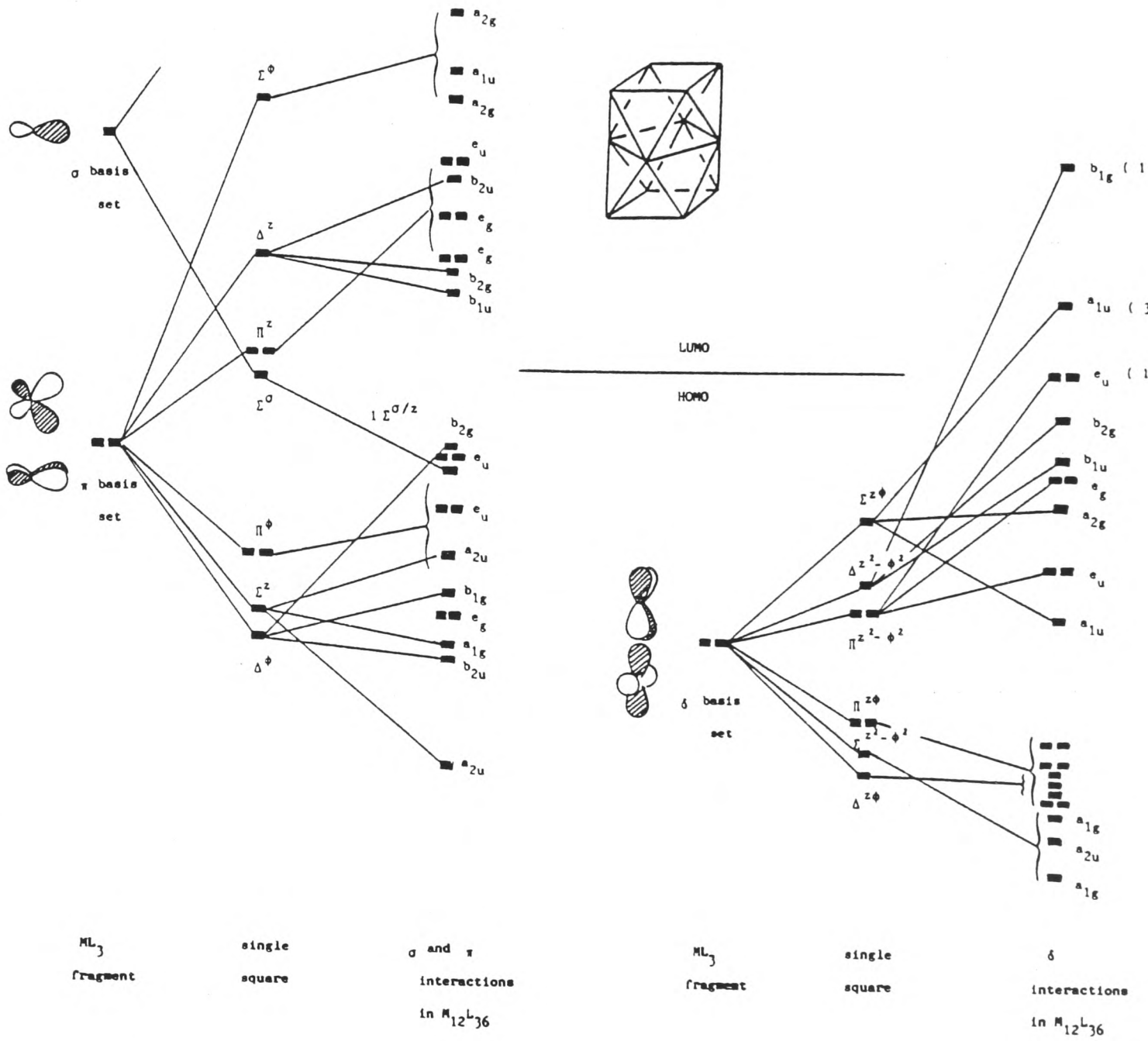


Figure 6.14 The MO diagram for $M_{12}L_{36}$ with ML_3 fragments based on three staggered squares

Figure 6.12 shows the MO interactions of a three-triangle staggered cluster. From the σ and π interactions it is apparent that there are 10 (n+1) skeletal bonding molecular orbitals which are developed by Π^{ϕ} and Σ^{z} orbitals from a single triangle. The σ molecular orbitals developed by Σ^{σ} mix extensively with the orbitals developed by Σ^{z}, and there remains only one $1\Sigma^{\sigma/z}$ extra orbital corresponding to S^{σ} orbital in a spherical cluster in the bonding region. This pattern is similar to that in a spherical case. For the four layer triangle staggered cluster (see Figure 6.13) and three layer square staggered cluster (see Figure 6.14), n+1 skeletal bonding molecular orbitals result from the σ and π interactions. These results confirm the arguments about σ and π interactions above. From Figure 6.14 it can be seen that the higher quantum number state ($1\Delta^{z2-\phi2}$) occurs when n_r=4.

The d_{δ} interactions in the Figures present a clear pattern in which the molecular orbitals develop "band like" structures through the Σ, Π and Δ states based on the d_{δ} ($d_{z}2_{-\phi}2$, $d_{z\phi}$) basis set. The discussion above notes that it is the d_{δ} basis in the inner layers of the cylinder which experience very large interactions that result in extra d_{δ} unavailable orbitals. Figure 6.12 presents 3 unavailable d_{δ} orbitals $1\Pi^{z2-\phi2}$ and $3\Sigma^{z\phi}$ for a three-triangle staggered cluster where there is only one inner triangle; and Figure 6.13 indicates 5 unavailable d_{δ} orbitals $1\Pi^{z2-\phi2}$, $2\Pi^{z2-\phi2}$ and $4\Sigma^{z\phi}$ for a four-triangle staggered cluster with two inner triangles. These orbitals which are illustrated in Figure 6.15 are derived from the out-of-phase combinations of the d_{δ} basis sets on the inner triangles and are also out-of-phase combinations with respect to the outer triangles. The orbitals derived from the out-of-phase combinations of d_{δ} basis on the inner triangles but in-phase combinations with respect to the outer triangles lying in the non-bonding

or bonding regions indicate that the d_δ interactions in the two outer layers are similar to that in a spherical case and are non-bonding. Therefore, this gives a support to the discussion above for the d_δ interaction in the cylindrical problem where the d_δ interaction in the two outer layers are neglected. The $4\Sigma^{z\phi}(a_{2g})$ orbital in the antibonding and $3\Sigma^{z\phi}$ in the bonding region in Figure 6.13, where there are two inner layers, gives a support to that there is half band of $k\Sigma^{z\phi}$ can be occupied for the staggered triangle clusters which is illustrated in Figure 6.11(b). The extra unavailable d_δ orbitals for the three square staggered cluster are $1\Delta^{z2-\phi2}(b_{1g})$ and $3\Sigma^{z\phi}(a_{1u})$ (see Figur 6.14). There is in addition a pair of orbitals which are approximately non-bonding ($1\Pi^{z2-\phi2}(e_u)$). These unavailable d_δ orbitals are illustrated in Figure 6.15.

The three calculations above give a clear picture for the theoretical argument which is developed by a particle on a cylinder problem, and also explain the electron counts for $[Rh_9(CO)_{19}]^{3-}$ and $[Rh_{12}(CO)_{25}]^{2-}$ based on 3 and 4 triangle staggered structures.

$[Rh_{12}C_2(CO)_{24}]^{2-}$ has a structure based on two square-antiprisms sharing a square face (Figure 6.1(j))[17] and has a total of 166 valence electrons. This corresponds to the 11 skeletal bonding molecular orbitals and 25 "unavailable" molecular orbitals. 23 of these (i.e. 2n-1) are associated with the high energy p orbitals and the additional pair correspond to $3\Sigma^{z\varphi}$ and one component of $1\Delta^{z2-\varphi2}$ derived from d_δ. This clearly suggests that in this cluster the non-bonding e_u molecular orbitals are fully occupied.

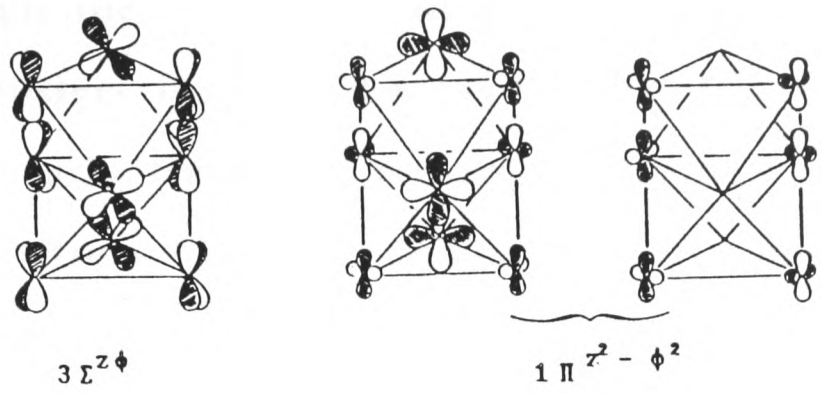


Figure 6.15 Schematic illustrations of the additional "unavailable" molecular orbitals derived from d_δ orbitals of the inner layers:
(a) n_z=3, n_r=3; (b) n_z=4, n_r=3 and (c) n_z=3, n_r=4

6.5 Applications

Although the arguments developed above have concentrated on carbonyl clusters they can be easily extended to halide and sulphide clusters of early transition metals. It has been argued that the major electronic diffrence between octahedral clusters with π-acceptor and π-donor ligands arises from the unavailability of some components of L_d^{δ} molecular orbitals.[18] In a metal carbonyl cluster all the L_d^{δ} and $\bar{L}_d^{\delta}$ orbitals are occupied, whereas in $[Mo_6Cl_8L_6]^{4+}$ there is an additional unavailable molecular orbital F_d^{δ} (a_{2u}). This molecular orbital retains its unavailable character, and is joined in the columnar clusters $[Mo_9S_{11}]^{4-}$, $[Mo_{12}S_{14}]^{6-}$, etc.[19] by an additional $3(n_z\text{-}2)\text{-}[(n_z\text{-}2)/2]$ d_{δ} unavailable molecular orbitals.

The existence of these molecular orbitals accounts for the close shell requirements of the sulphido-columnar clusters. The conclusions based on this analysis are summarised in Table 6.1 and are consistent with a more detailed theoretical analysis.[20]

6.6 Summary

The isolobal analogies which have proved so useful in correlating the structural chemistries of main group and transition metal carbonyl polyhedral molecules are based on the assumption that the molecular orbitals derived from d_{δ} do not make a significant contribution to skeletal bonding. Whilst this assumption is valid for clusters with spherical topologies it is necessary to evaluate the bonding effects associated with the d_{δ} orbitals in cylindrical clusters. The unavailable skeletal molecular orbitals derived from d_{δ} have been evaluated using a particle on a cylinder model.

The observed difference between spherical and cylindrical clusters

has a broader significance in the interpretation of the structures of the elements themselves. Boron does not form close packed metallic structures, but prefers complex arrangements based on the linking of spherical icosahedra. In contrast, transition metals adopt close packed arrangements based on face and edge shared octahedra. Clearly, the d interactions between adjacent metal atoms must make a significant contribution to this observation.

Table 1. Comparison between carbonyl- and sulphido-columnar clusters based on staggered metal triangles

Carbonyl compound	Electron count	Unavailable orbitals 2n-1+(extra d_δ)
$[Rh_6(CO)_{16}]$	86	2×6-1
$[Rh_9(CO)_{19}]^{3-}$	122	2×9-1+(3)
$[Rh_{12}(CO)_{25}]^{2-}$	160	2×12-1+(5)

Sulphido compound	number of d electrons	Electron count: valence electrons + n electron pairs *	Unavailable orbitals 2n-2+(extra d_δ) **
$[Mo_6S_8]^{4-}$	24	72 + (12) = (84)	2×6-2
$[Mo_9S_{11}]^{4-}$	36	102 + (18) = (120)	2×9-2+(3)
$[Mo_{12}S_{14}]^{6-}$	50	134 + (24) = (158)	2×12-2+(5)

* The sp hybridised outpointing orbital of each metal which is available for one terminal ligand is unoccupied in this series of clusters.

** There is one more unavailable orbital (F_d^δ) in $Mo_6S_8L_6$ discussed in ref 18.

6.7 Appendix

The following extended Hückel parameters for M (metal) and L (ligand) are used:

orbital	H_{ii}(ev)	exponents
M 4d	-10.50	4.54(0.58998) 1.90(0.58998)
5s	-9.50	1.96
5p	-5.24	1.90
L 1s	-13.60	1.625

The bonding distances are M-M=2.75Å and M-L=1.80Å. We use the deletion card to avoid the strongly interactions between L ligands if L-L distance is less than 2.4Å.

References for Chapter Six:

1. A.J.Stone, *Mol. Phys.*, **41**, 1339(1981); *Inorg. Chem.*, **20**, 563(1981); *Polyhedron*, **3**, 2051(1984).
2. D.M.P.Mingos, *Chem. Rev.*, **15**, 31(1986).
3. R.L.Johnston and D.M.P.Mingos, *J. Organomet. Chem.*, **280**, 407(1985).
4. R.L.Johnston and D.M.P.Mingos, *J. Organomet. Chem.*, **280**, 419(1985).
5. D.M.P.Mingos, *J. Chem. Soc. Chem. Commun.*, 106(1983).
6. R.L.Johnston and D.M.P.Mingos, *J. Chem. Soc. Dalton Trans.*, 647(1987).
7. R.L.Johnston and D.M.P.Mingos, *J. Chem. Soc. Dalton Trans.*, 1445(1987).
8. M.Elian, M.M.L.Chen, D.M.P.Mingos and R.Hoffmann, *Inorg. Chem.*, **15**, 1148(1976).
9. P.Chini, *J. Organomet. Chem.*, **200**, 37(1980).
10. D.J.Underwood, R.Hoffmann, K.Tatsumi, A.Nakamura and Y.Yamamoto, *J. Amer. Chem. Soc.*, **107**, 5968(1985).
11. D.W.Bullet, *Chem. Rev. Lett.*, **115**, 450(1985).
12. E.R.Corey, L.F.Dahl and W.Beck, *J. Amer. Chem. Soc.*, **85**, 1202(1963).
13. S,Martinengo, A.Fumagalli, R.Bonfichi, G.Ciani and A.Sironi, *J. Chem. Soc. Chem. Commun.*, 825(1982).
14. G.Ciani, A.Sironi and S.Martinengo, *J. Chem. Soc. Chem. Commun.*, 1757(1985).
15. S.Martinengo, G.Sironi and G.Ciani, *J. Chem. Soc. Chem. Commun.*, 1282(1986).

16. D.M.P.Mingos and M.I.Forsyth, *J. Chem. Soc. dalton Trans.*, 610(1977).

17. V.G.Albano, D.Braga, P.Chini, D.Strumolo and S.Martinengo, *J. Chem. Soc. Dalton Trans.*, 249(1983).

18. R.L.Johnston and D.M.P.Mingos, *Inorg. Chem.*, **25**, 1661(1986).

19. R.Cheverel, M.Hirrien and M.Sergent, *Polyhedron*, **5**, 87(1986).

20. T.Hughbanks and R.Hoffmann, *J. Amer. Chem. Soc.*, **105**, 1150(1983).

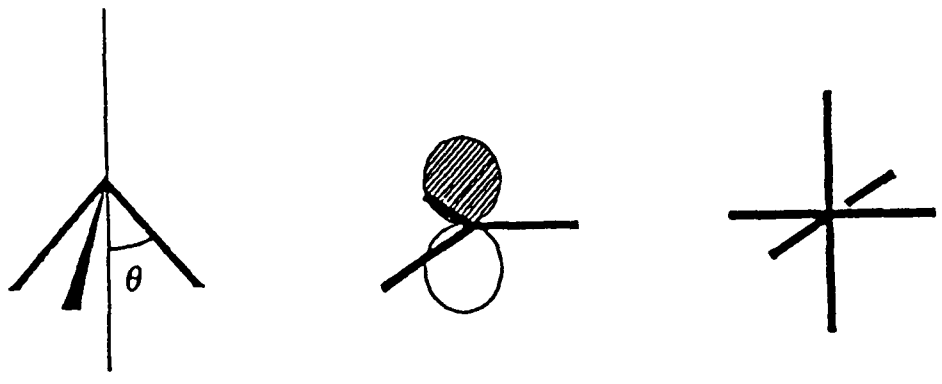
Chapter 7 Non-bonding orbitals in coordination, hydrocarbon and cluster compounds

7.1 Introduction

Phrases such "lone pairs", "empty non-bonding orbitals", "stereochemically active (or non-active) lone pairs", and "electron rich molecules" are part of the language of modern chemistry and their frequent use is a testimony to their usefulness in chemical communication. In common with electronegativity they are very dificult to define precisely and this imprecision can at times lead to heated debate. In this Chapter we shall not attempt to define these terms rigorously, but to codify the situations where "non-bonding orbitals" occur and attempt to provide some general principles for understanding the stereochemical and chemical consequences of these concepts.

Historically the concept of non-bonding electron pairs can be traced to Lewis classic work on the definition of a covalent bond in terms of sharing electrons between atoms.[1] The electrons not involved in such bonds were considered independently and described as 'lone pairs'. He recognised that although such electron pairs did not contribute at all to the bonding within the molecule they could be donated to a second molecule with an incomplete octet and thereby form a dative bond. These ideas were given a quantum mechanical interpretation in Pauling's Valence Bond Theory.[2] He showed how molecules could be built up by using the concept of hybridisation. Linear combinations of atomic orbitals that were directed towards the vertices of regular polyhedra maximised the overlap between orbitals on the central atom and the orbitals at the vertices.[3] If each of these orbitals contained a single electron then an electron pair bond resulted. 'Lone pairs' in molecules such as ammonia (1) also utilised hybrid orbitals which had been

constructed for the tetrahedron and were populated by an electron pair from the nitrogen. The non-bonding nature of this orbital was assured, because it was defined as being orthogonal to the other sp^3 hybrid orbitals of the NH_3 molecule. Within the framework of valence bond theory it is also possible to have non-bonding vacant orbitals based either on hybrids or on unhybridised orbitals that have nodal planes coincident with the positions of the peripheral atoms of the molecule. For example, the p_z orbital in planar BX_3 (2) has a nodal plane coincident with the positions of the X atoms. Similarly the d_{xz}, d_{yz} and d_{xy} orbitals of an octahedral molecule are non-bonding because they have nodal planes that are coincident with the octahedral bond directions (3). The relative energetics of utilising an unhybridised orbital in preference to a hybridised one was not clearly made in the initial valence bond formulations. Furthermore, the deviations from the idealised hybridisation angles required that the lone pair contain a different proportion of s character than the idealised hybrids. The geometric and electronic consequences of these differences in hybridisation were effectively developed by Bent.[4]



(1) (2) (3)

The **Valence Shell Electron Pair Theory**[5-7] returned to the classical Lewis description of the chemical bond, but introduced a three-

dimensional aspect to it by calculating the preferred polyhedra for n electron pairs using a point charge repulsion model. This, when combined with some simple rules defining the relative importance of lone-pair – lone-pair and lone-pair – bond pair repulsions, provides a pedagogically useful way of accounting for the geometries of main group molecules. It does, however, have serious limitations when applied to transition metal complexes.

In the molecular orbital method [8] the bonding is described in terms of linear combinations of atomic orbitals and the localised description of the chemical bond is lost, but as Mulliken [9] showed it is possible to partition the electron density and thereby get an estimate of the spatial distribution and bonding character of an orbital. The procedure can be illustrated by the simple case of a diatomic molecule with one basis function per atom containing N electrons in a molecular orbital. Let the molecular orbital be written as:

$$\phi = a\phi_A + b\phi_B$$

where ϕ_A and ϕ_B are atomic orbitals of atoms A and B. The total population of the MO is:

$$Na^2\int\phi_A^2 d\tau + Nb^2\int\phi_B^2 d\tau + 2Nab\int\phi_A\phi_B d\tau$$

Mülliken described Na^2 the net electron population in ϕ_A on A, Nb^2 that in ϕ_B on B and $2Nab\langle\phi_A|\phi_B\rangle$ the overlap population, since $\int\phi_A\phi_B d\tau$ occupies the region of overlap of the two atomic orbitals.

A chemist also wants to know the gross populations on each atom. The gross population on A or B certainly includes the respective net population, but for each atom one must also include a part of the overlap population. The simplest procedure is to proportion the two parts equally to A and B, even when a and b are unequal, i.e $Nab\langle\phi_A|\phi_B\rangle$ to each atom. Adding this to the net population of either atom gives a gross

population N(A) or N(B), such that N(A)+N(B)=N. Therefore a specific molecular orbital can be described as non-bonding either because N(A)≈N, i.e. it is localised almost exclusively on one centre, or N(A) and N(B) are both significant but the overlap population $2Nab<\phi_A|\phi_B>$is approximately equal to zero.

In this Chapter we will describe the bonding in main group and transition metal compounds in terms of a molecular orbital framework and attempt to define more precisely those situations where the conditions for non-bonding character are met. Such a discussion will focus primarily on the nodal characteristics of the molecular orbitals since the overlap populations between atoms in the non-bonding character approach zero and the analysis of the overlap populations reflect this fact. Such a definition is useful for discussing the stereochemical role of orbitals within an isolated molecule, but does not provide a guide to the ability of that orbital to interact with orbitals on other molecules. This is influenced by the ionisation energy of the non-bonding orbital and its radial characteristics. We are mindful of this and will make passing references to the availability of 'non-bonding orbitals' for intermolecular bond formation. Our initial discussion will focus on the bonding in spherical co-ordination compounds where it is convenient to express the linear combinations of atomic orbitals as a spherical harmonic expansion.

7.2 Non-bonding orbitals in molecular and coordination compounds, ML_n

In the majority of co-ordination and molecular compounds the number of ligands is not equal to the number of valence orbitals on M and it is necessary to establish the factors that influence the resultant pattern of molecular orbitals. It will be demonstrated below that ML_n is

generally characterised by m-n non-bonding molecular orbitals where m is the number of the valence orbitals in the central atom. Before the discussion of this "m-n rule", the symmetry adapted linear combinations of ligand σ orbitals are discussed.

7.2.1 Expansion of the ligand set as spherical harmonic functions

In the Complementary Spherical Electron Density Model,[10-12] the symmetry adapted linear combinations of σ_i ligand orbitals for ML_n compound can be expressed in terms of a spherical harmonic expansion:

$$\psi_{lm} = N' \sum_i C_{l,m}(\theta_i,\phi_i)\sigma_i$$

$$= L^{\sigma}_{m}, \qquad m=0,1c,1s,... \qquad L=S,P,D,...$$

where θ_i and ϕ_i represent the locations of the ligand nuclei in spherical polar coordinates, N′ is a normalising constant, and $C_{l,m}$ is a modified spherical harmonic wavefunction, $C_{l,m}=[4\pi/(2l+1)]^{1/2}Y_{l,m}$. The modified spherical harmonic functions are given in Table 1.1. For those functions with imaginary solutions the real solutions are obtained by taking linear combinations of complementary components, i.e.

$$C^{c}_{l,m} = 1/(2)^{1/2}\ [(-1)^{m}C_{l,m} + C_{l,-m}]$$

$$C^{s}_{l,m} = 1/i(2)^{1/2}\ [(-1)^{m}C_{l,m} - C_{l,-m}]$$

In this fashion the linear combinations are assigned quantum numbers l and m which are related to those which have been defined for the S, P and D functions derived for the particle on the sphere problem. Furthermore, their nodal characteristics mimic those of the atomic wavefunctions of the central atom. The spherical harmonic expansion described above will provide its most accurate description of the symmetry adapted linear combinations when the polyhedral vertices are symmetry equivalent. For example, octahedral ML_6 has S^{σ}, $P^{\sigma}_{0,\pm1}$ and $D^{\sigma}_{0,2s}$ a total of 6 symmetry adapted linear combinations. They are

$$S^{\sigma} = 1/(6)^{1/2} (\sigma_1 + \sigma_2 + \sigma_3 + \sigma_4 + \sigma_5 + \sigma_6)$$

$$P_0^{\sigma} = 1/(2)^{1/2} (\sigma_1 - \sigma_6)$$

$$P_{1c}^{\sigma} = 1/(2)^{1/2} (\sigma_2 - \sigma_4)$$

$$P_{1s}^{\sigma} = 1/(2)^{1/2} (\sigma_3 - \sigma_5)$$

$$D_0^{\sigma} = 1/(3)^{1/2} (\sigma_1 - 1/2\sigma_2 - 1/2\sigma_3 - 1/2\sigma_4 - 1/2\sigma_5 + \sigma_6)$$

$$D_{2c}^{\sigma} = 1/2 (\sigma_2 - \sigma_3 + \sigma_4 - \sigma_5)$$

They are shown schematically in Figure 7.1. This spherical expansion improves as an approximation as n increases. When there is more than one linear combination with the same symmetry then an orthogonalisation problem can arise which will be discussed in more detailed below. In the following sections the utilisation of these spherical harmonic expansions are summarised for a range of common ligand co-ordination geometries.

7.2.1.1 Planar ML_n, Bipyramidal ML_{n+2}, Prismatic and Anti-prismatic ML_{2n} Complexes.

In the planar structure, ML_n, if all the ligands are defined to lie in the xy plane, those functions that possess a nodal plane coincident with the xy plane are systematically excluded. Therefore, the ligand orbitals span the S^{σ}, $P_{\pm1}^{\sigma}$, $D_{\pm2}^{\sigma}$, ..., $L_{\pm L}^{\sigma}$, ... spherical harmonic expansions and there are total of n wavefunctions. For example, the L_3 moiety has S^{σ}, and $P_{\pm1}^{\sigma}$ wavefunctions. For L_4 the additional function generated is a D function, i.e. it is characterised by S^{σ}, $P_{\pm1}^{\sigma}$ and D_{2s}^{σ}.

In the bipyramidal (ML_{n+2}) compounds, the two additional vertices which are located in the +z and -z directions generate two more L^{σ}'s, i.e. P_0^{σ} and D_0^{σ}, besides the n L^{σ}'s generated by the S^{σ}, $P_{\pm1}^{\sigma}$, $D_{\pm2}^{\sigma}$, ..., $L_{\pm L}^{\sigma}$, ...series for the planar geometry which belong to different irreducible representations. They are all orthogonalised with the

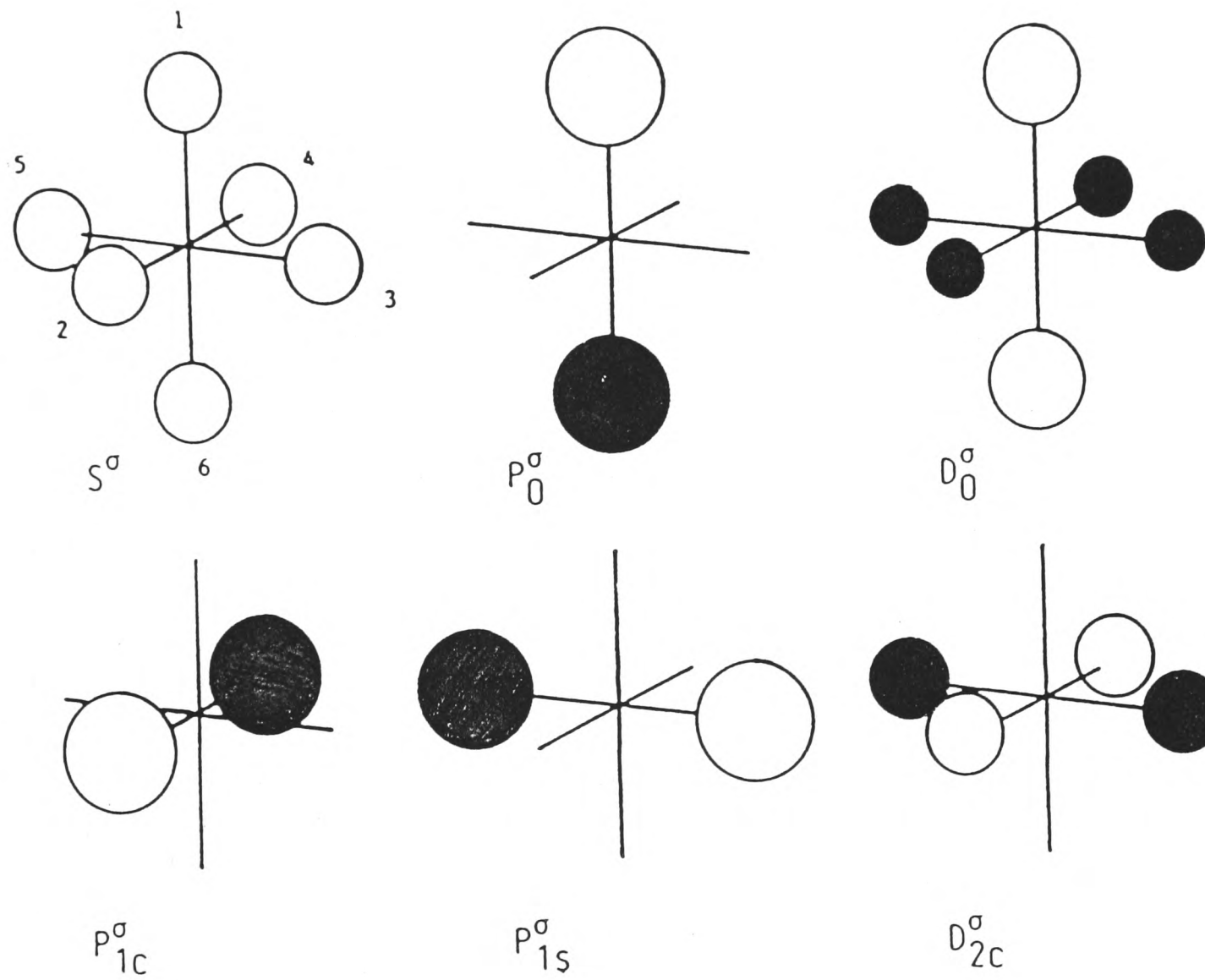


Figure 7.1 The illustrations of the linear combinations of ligand σ orbitals in an octahedral compound

exception of the S^{σ} and D_0^{σ}. The re-orthogonalisation of S^{σ} and D_0^{σ} can be achieved by assuming $\psi_1 = S^{\sigma}$ and $\psi_2 = aS^{\sigma} + bD_0^{\sigma}$. The a and b parameters can be obtained by solving the following equations

$$\begin{cases} \langle\psi_1|\psi_2\rangle = 0 \\ \langle\psi_2|\psi_2\rangle = 1. \end{cases} \quad \text{----->} \quad \begin{cases} a + b\langle S^{\sigma}|D^{\sigma}\rangle = 0 \\ a^2 + b^2 + 2ab\langle S^{\sigma}|D_0^{\sigma}\rangle = 1 \end{cases}$$

For example, the σ ligand orbitals in a trigonal bipyramid ML_5 span S^{σ}, $P_{0,\pm1}^{\sigma}$ and D_0^{σ} functions. S^{σ} and D_0^{σ} are

$$S^{\sigma} = 1/(5)^{1/2}\,(\sigma_1 + \sigma_2 + \sigma_3 + \sigma_4 + \sigma_5)$$
$$D_0^{\sigma} = 1/(11)^{1/2}(2\sigma_1 - \sigma_2 - \sigma_3 - \sigma_4 + 2\sigma_5)$$

where the two axial vertices are defined as positions 1 and 5.

$$\langle S^{\sigma}|D_0^{\sigma}\rangle = 1/(55)^{1/2}\,(2 - 1 - 1 - 1 + 2) = 1/(55)^{1/2}$$

Therefore, $a=1/(54)^{1/2}$ and $b=-(55/54)^{1/2}$ are obtained by solving the above equations. It is noteworthy that the spherical approximation is a reasonable one even in such cases.

In the prismatic structures ML_{2n}, the 2n ligands are taken as the combinations of two n-planar moieties. The L^{σ}'s in ML_{2n} are the linear combinations of the two subsets in the two planes, i.e. $\psi^{\sigma}_{plane1} \pm \psi^{\sigma}_{plane2}$. Since the ψ^{σ}_{plane1} and ψ^{σ}_{plane2} span the same series of $S^{\sigma}, P^{\sigma}_{\pm1}, D^{\sigma}_{\pm2}, ..., L^{\sigma}_{\pm L}, ...,$ one of the combinations, i.e. $\psi^{\sigma}_{plane1} + \psi^{\sigma}_{plane2}$, has the same characteristics as that of the individual plane, ψ^{σ}_{plane1} or ψ^{σ}_{plane2}. The other, $\psi^{\sigma}_{plane1} - \psi^{\sigma}_{plane2}$, generates one more horizontal nodal plane between the two planes. Therefore, $\psi^{\sigma}_{plane1} - \psi^{\sigma}_{plane2}$ is obtained by the multiplication rule developed by Johnston and Mingos.[13]

$$\{ S^{\sigma}, P^{\sigma}_{\pm1}, D^{\sigma}_{\pm2}, ..., L^{\sigma}_{\pm L}, ... \} \otimes P^{\sigma}_0$$
$$\text{----->}\{ P^{\sigma}_0, D^{\sigma}_{\pm1}, F^{\sigma}_{\pm2}, ..., (L+1)^{\sigma}_{\pm L}, ... \}$$

For example, for the pentagonal prism, ML_{10}, the ligand orbitals span S^{σ}, $P^{\sigma}_{\pm1}$ and $D^{\sigma}_{\pm2}$ which are the same as the L^{σ}'s for pentagonal planar ML_5, and P^{σ}_{0}, $D^{\sigma}_{\pm1}$, $F^{\sigma}_{\pm2}$ which are generated by the above multiplication.

The anti-prismatic structures ML_{2n} are constructed from two n-planar moieties which are staggered with respect to each other. For odd n, all of the L^{σ} functions generated by an anti-prism are the same as those generated by the corresponding prism because the L^{σ}'s of the two n-planar moieties span the same series of L^{σ}'s. The situation for even n, however, is different. In this case, the expansions of the L^{σ} wavefunctions for the upper and lower n-planar moieties are different in the final term. If the L^{σ}'s of the upper n-planar moiety span the S^{σ}, $P^{\sigma}_{\pm1}$, $D^{\sigma}_{\pm2}$, ..., $(\Lambda\text{-}1)^{\sigma}_{\pm(\Lambda-1)}$, Λ^{σ}_{c} (where $\Lambda=L_{max}=n/2$), the L^{σ}'s of the lower one span the S^{σ}, $P^{\sigma}_{\pm1}$, $D^{\sigma}_{\pm2}$, ..., $(\Lambda\text{-}1)^{\sigma}_{\pm(\Lambda-1)}$, Λ^{σ}_{s}. Therefore, all the L^{σ}'s for anti-prisms when n is even are:

$$S^{\sigma}, P^{\sigma}_{\pm1}, D^{\sigma}_{\pm2}, \ldots, (\Lambda\text{-}1)^{\sigma}_{\pm(\Lambda-1)}$$

and $\{S^{\sigma}, P^{\sigma}_{\pm1}, D^{\sigma}_{\pm2}, \ldots, (\Lambda\text{-}1)^{\sigma}_{\pm(\Lambda-1)}\}\otimes P^{\sigma}_{0}$ plus Λ^{σ}_{c} and Λ^{σ}_{s}.

7.2.1.2 Deltahedra

In a deltahedral ML_n compound, the linear combinations of the n ligand orbitals are built up in such a way that the n lowest L quantum states are always used before higher L quantum states. For example, ML_4 with a tetrahedral arrangement of four ligands generates S^{σ} and three P^{σ} wavefunctions, and an octahedral ML_6 has S^{σ}, three P^{σ} and two D^{σ} wavefunctions. Unlike the previous classes of polyhedra, F^{σ} functions are not used prior to the completion of the D shell. This property can be related to the ability of deltahedra to give the best

coverage on a spherical surface.[11]

The spherical harmonic expansion methodology developed above provides a method of defining non-bonding orbitals that are localised exclusively on the ligand atoms. In particular if the ligands have an L^{σ} function which is not matched by a valence orbital on the central atom in terms of quantum numbers or point group symmetry then it is strictly non-bonding. For example, in an ML_8 co-ordination compound, which has a cubic arrangement of ligands the L^{σ} ligand linear combinations are S^{σ}, $P^{\sigma}_{\pm 1}$, D^{σ}_{2s}, P^{σ}_{0}, $D^{\sigma}_{\pm 1}$ and F^{σ}_{2c}. If M is a transition metal atom the s, p and d valence orbitals cannot match the F^{σ}_{2s} function which in the O_h point group transforms as a_{2u}. Consequently there is a non-bonding orbital which is localised exclusively on the ligands because of its symmetry and pseudo-spherical symmetry characteristics. The situation is slightly less well defined if the L^{σ} linear combination does not match the pseudo-spherical symmetry requirements but has the same symmetry as one of the valence orbitals of the central atom. For example, a first row main group atom which has s and p valence orbitals might form a trigonal bipyramidal complex in a transition state. The relevant L^{σ} linear combinations are S^{σ}, $P^{\sigma}_{0,\pm 1}$ and D^{σ}_{0}. The latter transforms as a_1' in the D_{3h} point group, i.e. the same irreducible representation as s. Therefore, some overlap between s and D^{σ}_{0} can occur, but it is likely to be small because the D^{σ}_{0} and s functions have different pseudo- symmetries. In particular the D^{σ}_{0} function is doubly noded and the s function is un-noded. Pseudo-symmetry arguments of this type are very important for simplifying the bonding problems in co-ordination compounds.

7.2.2 The m-n rule

In an n-coordinate compound, we assume that there are in total m atomic orbitals (s, p, d, ...) (m=4 or 9 for great majority of situations) associated with the central atom. The new linear combinations of the n σ_i ligand orbitals, ψ_1^σ, ψ_2^σ, ..., ψ_n^σ, which are normalised and orthogonal to each other (i.e., $<\psi_i^\sigma|\,\psi_j^\sigma>=\delta_{ij}$), can always be derived from group theoretical methods and the spherical harmonic classification illustrated above. If the Coulomb integrals for the m atomic orbitals of the central atom are assumed to have the same α_c, the corresponding secular determinant in the Hückel approximation is:

$$\begin{array}{c} \\ n \\ \\ \\ m \\ \\ \end{array} \begin{array}{c} \begin{array}{cc} n & \quad m \end{array} \\ \begin{vmatrix} \alpha_1\text{-}E & & & \\ & \ddots & & \mathbf{R} \\ & & \alpha_1\text{-}E & \\ & & & \alpha_c\text{-}E \\ \mathbf{R^t} & & & \ddots \\ & & & & \alpha_c\text{-}E \end{vmatrix} \end{array} = 0 \qquad \text{(B-1)}$$

where α_1 is the Coulomb integral for the ligand σ orbitals and **R** is the n×m matrix representing the interactions between n ligands and the central atomic orbitals ($\mathbf{R^t}$ is the transpose of **R**). Solving equation (B-1), we get m+n eigenvalues. In mathematical terms this corresponds to obtaining the eigenvalues of matrix A:

$$\begin{pmatrix} \alpha_1 & & & \\ & \ddots & & \mathbf{R} \\ & & \alpha_1 & \\ & & & \alpha_c \\ \mathbf{R^t} & & & \ddots \\ & & & & \alpha_c \end{pmatrix} \qquad \text{(B-2)}$$

$|A - EI| = 0$, I is the identity matrix. Changing the form of (B-2), we get

$$A = \begin{pmatrix} \alpha_1-\alpha_c & & & R & \} n \\ & \ddots & & & \\ & & \alpha_1-\alpha_c & & \\ R^t & & & O & \} m \\ \underbrace{\quad}_{n} & & & \underbrace{\quad}_{m} & \end{pmatrix} \qquad \text{(B-3)}$$

where **O** is an (m×m) zero matrix. The relationship between the eigenvalues of (B-3) and (B-2) is

$$E' = E + \alpha_c \qquad \text{(B-4)}$$

E′ and E are the eigenvalues of (B-2) and (B-3) respectively.

The number of zero eigenvalues of (B-3) (i.e, the number of non-bonding orbitals) is equal to or larger than (m-n) when m≥n.

Proof: The more general form of (B-3) is:

$$A = \begin{pmatrix} B_{n,n} & C_{n,m} \\ D_{m,n} & O_{m,m} \end{pmatrix} \qquad \text{(B-5)}$$

where $O_{m,m}$ is an (m×m) zero matrix.

According to the expansion of the characteristic equation,[14]

$$\det(A-EI) = E^{(n+m)} - G_1(A)E^{(n+m)-1} + G_2(A)E^{(n+m)-2} - \ldots \pm G_{(n+m)}(A) \qquad \text{(B-6)}$$

where the $G_k(A)$ is the sum of the k-by-k principal minors of matrix A. The k-by-k principal minor is the determinant of k-by-k principal submatrix. A k-by-k principal submatrix of A is one lying in the same set of k rows and columns in A ($k \leq n+m$). For example, the largest k-by-k principal minor $G_{(n+m)}(A)$ is det(A).

All the k-by-k principal minors of matrix (B-5), when k>2n+1, are zero because any one ofthe k-by-k principal minors can be rearranged in the following form:

$$B_k = \begin{pmatrix} B_1 & B_2 \\ B_3 & O_{(k-n,k-n)} \end{pmatrix} \qquad \text{(B-7)}$$

where $O_{(k-n,\ k-n)}$ is a zero matrix.

The expansion of the determinant of B_k is

$$\det(B_k) = \sum_{\sigma} \operatorname{sign}(\sigma) \prod_{i=1}^{k} b_{i\sigma(i)}$$

where $b_{i\sigma(i)}$ is the element of the matrix B_k. The sum runs over all k! permutations of the k items {1,2,...,k} and the sign is +1 or -1 according to whether the mininum number of transpositions necessary to achieve it starting from {1,2,...,k} is even or odd. Each product in the summation is of the form

$$b_{1\sigma(1)}b_{2\sigma(2)}\cdots b_{k\sigma(k)} \qquad \text{(B-8)}$$

If $k \geq 2n+1$, there is at least one zero element involved in (B-8). Thus $\det(B_k)=0$. Therefore, $G_k(A)=0$ as well when $k \geq 2n+1$. Now,

$$\begin{aligned} &\det(A-EI) \\ &= E^{(n+m)} - G_1(A)E^{(n+m)-1} + G_2(A)E^{(n+m)-2} - \ldots \pm G_{2m}(A)E^{(n+m)-2n} \\ &= E^{(m-n)}[E^{2n} - G_1(A)E^{2n-1} + G_2(A)E^{2n-2} - \ldots \pm G_{2n}(A)] \end{aligned}$$

So the multiplicity of E=0 eigenvalues is equal to or larger than (m-n). From (B-4), we say that there are at least (m-n) orbitals with the energy of α_c which are localised on the central atom.

Similarly, if n>m, we get at least (n-m) orbitals with the energy of α_l which are localised on the ligands, i.e. n-m non-bonding orbitals.

The following generalisation can be derived when the proof above is combined with the arrangement of the ligand shell in ML_n. The number

of non-bonding orbitals in ML_n systems is exactly equal to m-n if the n ligands define a three dimensional arrangement. This is because the ligand orbitals span the S^{σ}, P^{σ}, D^{σ}, ..., functions, giving a total of n wavefunctions while the D^{σ} functions are not used prior to the completion of the P^{σ} functions. Therefore, there is a one-to-one pseudo-symmetry matching between s,p (and d)orbitals on the central atom and the ligand orbitals, leaving m-n redundant wavefunctions. The most important implication from the m-n rule is that the number of non-bonding orbitals is independent of the geometry of ML_n if the arrangement of the ligand shell retains three or two dimensions. A change in geometry only leads to a change in the character of the non-bonding orbitals, i.e, the ratio of s, p and d character.

7.2.3 The Pairing Theorem

When $\alpha_c=\alpha_l=\alpha$, the pairing theorem which has been widely used in discussion of alternant conjugated organic molecules [15-19] is applicable to the system above because the magnitude of each element in **R** of (B-2) does not affect the generalisation of this proof. This theorem states that if $\alpha+E_k$ is an eigenvalue of (B-2), $\alpha-E_k$ is also an eigenvalue of (B-2). Therefore, the molecular orbitals of such a system are perfectly paired in the Hückel approximation. The corresponding paired molecular orbitals are:

$$\psi_k^+ = \sum_i c_{ik}\phi_i + \sum_l \sum_m c_{lm(k)} L_m^{\sigma} \qquad \text{(B-9)}$$

$$\psi_k^- = \sum_i c_{ik}\phi_i - \sum_l \sum_m c_{lm(k)} L_m^{\sigma} \qquad \text{(B-10)}$$

where ϕ_i are the valence atomic orbitals on the central atom and c_{ik} and $c_{lm(k)}$ are the coefficients of ϕ_i and L_m^σ in the kth molecular orbital respectively. More precisely, the approximation $\langle L_m^\sigma | \phi_{lm'} \rangle = 0$ (unless L=l and m=m′) leads to a diagonalised secular matrix which can be separated into sets of 2 by 2 matrices in which the ϕ_{lm} and L_m^σ are involved. The resonance integral $\langle L_m^\sigma | H | \phi_{lm} \rangle = \beta_{lm}$ for a specific value of l and m leads to pairs of molecular orbitals:

$$\psi_+ = \phi_{lm} + L_m^\sigma \qquad \text{(B-11)}$$

$$\psi_- = \phi_{lm} - L_m^\sigma \qquad \text{(B-12)}$$

with orbital energies of $\alpha+\beta_{lm}$ and $\alpha-\beta_{lm}$ corresponding the in-phase and out-of-phase combinations of the central atom ϕ_{lm} and ligand L_m^σ orbitals. (B-11) and (B-12) are simplifications of (B-9) and (B-10).

The octahedral ML_6 is an example where the approximation is perfect. The resonance integrals, $\langle L_m^\sigma | H | \phi_{lm} \rangle$, can be obtained by using the following equations:

$$\psi^\sigma_{l,m} = N' \sum_i^n C_{l,m}(\theta_i,\phi_i)\, \sigma_i$$

$$\langle \psi^\sigma_{l,m} | \phi_{l,m} \rangle = N' \langle \sum_i^n C_{l,m}(\theta_i,\phi_i)\, \sigma_i | \phi_{l,m} \rangle$$

$$= N' \sum_i^n C_{l,m}(\theta_i,\phi_i) \langle \sigma_i | \phi_{l,m} \rangle$$

$$= N' \sum_i^n C_{l,m}(\theta_i,\phi_i) \times C_{l,m}(\theta_i,\phi_i)\, S_\sigma(l)$$

(where $S_\sigma(l)$ is defined in (4))

$$= N' \sum_i^n C_{l,m}^2(\theta_i,\phi_i)\, S_\sigma(l)$$

$$= [\ \sum_{i}^{n} C_{l,m}^{2}(\theta_i,\phi_i)\ ]^{1/2}\ S_{\sigma}(l)$$

$$\text{(because } N' = 1/[\sum_{i}^{n} C_{l,m}^{2}(\theta_i,\phi_i)\ ]^{1/2}\ )$$

The overlap integrals between the L^{σ}'s and atomic orbitals of central atom in ML_6 octahedral structure are:

$$\langle S^{\sigma}|\, s\rangle = (6)^{1/2} S_{\sigma}(s)$$

$$\langle P_m^{\sigma}|\, p_m\rangle = (2)^{1/2} S_{\sigma}(p) \qquad m = 0, \pm 1$$

$$\langle D_m^{\sigma}|\, d_m\rangle = (3)^{1/2} S_{\sigma}(d) \qquad m = 0,\ 2c.$$

$$\text{and } \langle D_m^{\sigma}|\, d_m\rangle = 0 \qquad m = \pm 1,\ 2s$$

Therefore,

$$\langle L_m^{\sigma}|\, H|\, \phi_{l,m}\rangle = k\langle L_m^{\sigma}|\, \phi_{l,m}\rangle^2$$

$$= \sum_{i} C_{l,m}^{2}(\theta_i,\phi_i)\ kS_{\sigma}^{2}(l)$$

$$= \sum_{i} C_{l,m}^{2}(\theta_i,\phi_i)\ \beta_{\sigma}(l)$$

These lead to the following results:

$$\langle S^{\sigma}|\, H|\, s\rangle = 6\beta_{\sigma}(s)$$

$$\langle P_m^{\sigma}|\, H|\, p_m\rangle = 2\beta_{\sigma}(p) \qquad m=0,\pm 1$$

$$\langle D_m^{\sigma}|\, H|\, d_m\rangle = 3\beta_{\sigma}(d) \qquad m=0,2c$$

$$\text{and} \quad \langle D_m^{\sigma}|\, H|\, d_m\rangle = 0 \qquad m=\pm 1,2s$$

It is noteworthy that the stabilisation energies are always $N\beta^{\sigma}$/Degeneracy where N = Number of ligand atoms. When the assumption $\beta_{\sigma}(s)=\beta_{\sigma}(p)=\beta_{\sigma}(d)$ has been made, the orbital interaction diagram for this idealised situation ($\alpha_s=\alpha_p=\alpha_d=\alpha_l$) is shown in Figure 7.2.

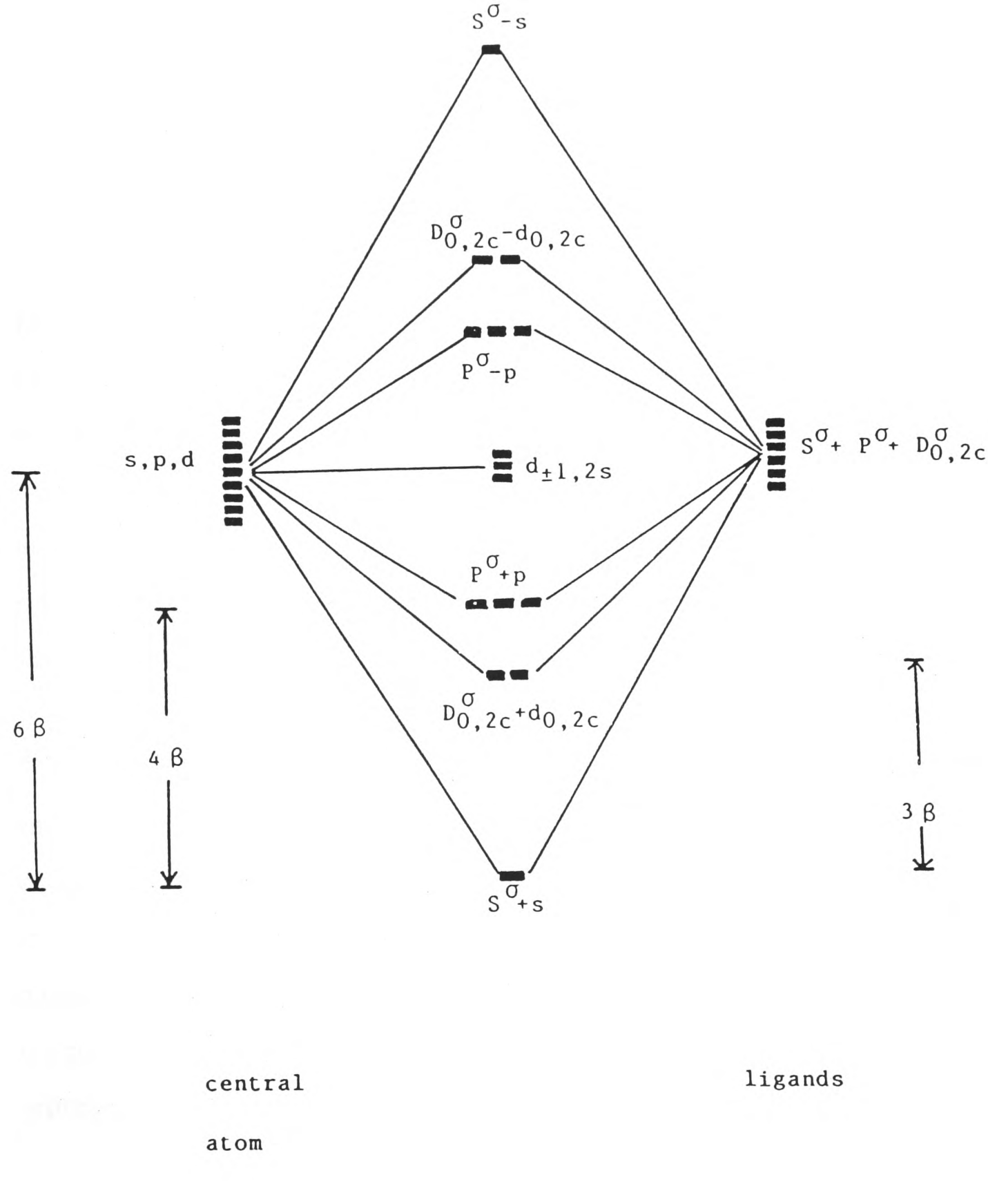


Figure 7.2 The orbital interaction diagram for an octahedral ML_6 compound

7.2.4 Group theoretical aspects

A conjugate organic system is described as alternant if the atoms in it can be divided into two sets starred and unstarred in such a way that no two atoms in the same set are directly linked. In the Hückel approximation, this definition implies that all the p_π atomic orbitals in the starred or unstarred set are orthogonal to each other (i.e. no interaction occurs between the p_π's in the same group) and there are interactions between the two groups. Therefore, the secular determinant describing the orbital interactions of an alternant system have the same form as equation (B-1), except α_c and α_l are set to be α and the resonance integrals are β or 0. Consequently, the orbital interactions in an ML_n compound can be described in a similar fashion to those of an alternant hydrocarbon if the m valence orbitals on the central atom are starred and the ligand orbitals are unstarred because the valence orbitals on the central atom are orthogonal to each other and have zero resonance integrals among them. The ligand orbitals behave likewise.

In a discussion of the group theoretical aspects of alternant systems [20] given in Section 7.3, we have defined an alternant operator, $\hat{A}$, which interconverts the starred and unstarred atomic positions. Since the central atom must lie on the principal axis the alternant operator belongs to the totally symmetric representation in the ML_n system. Therefore, the paired molecular orbitals ψ_k^+ (B-9) and ψ_k^- (B-10) belong to the same irreducible representations which are called self-conjugate representations, i.e. the in-phase (bonding) and the corresponding out-of-phase (antibonding) combinations must belong to the same irreducible representations: the bonding and antibonding combinations differ by the addition of a radial rather than an angular node.

Group theory can be used to resolve the secular determinant (B-1) into a block-diagonalised matrix. Each block matrix represents the interactions between the basis sets belonging to the same irreducible representation.

When the arguments developed above are combined with the **pairing theorem** and the **m-n rule**, the following important generalisation which applies to all simple mono-nuclear compounds ML_n can be derived.

The non-bonding molecular orbitals in ML_n compounds always arise from the presence of an odd number of irreducible representations with the same symmetry. The number of such non-bonding orbitals is equal to the sum of the degeneracies of the irreducible representations which occur in odd numbers. For example, if one system has odd numbers of a and e irreducible representations, the number of non-bonding orbitals is 1+2. ML_n compounds where the number of valence electron pairs is m have $|m-n|$ non-bonding molecular orbitals.

The occurrence of these non-bonding orbitals can be associated with either spherical or non-spherical co-ordination polyhedra. The choice of co-ordination polyhedra depends on several factors and notably:

(a) The relative energies of the valence orbitals

(b) The population of the non-bonding orbitals

(c) Multiple bonding effects

(d) Steric effects.

The relative importance of these factors are described in more detailed in the subsequent Sections. The group theoretical conclusion above can be illustrated by the following examples.

Simple co-ordination and main group molecules with no non-bonding molecular orbitals (i.e. n=m), e.g., $[ReH_9]^{2-}$ [21] and CH_4, have pairs of

self-conjugate bonding and antibonding molecular orbitals, e.g. a_1,t_2, a_1^*, t_2^* for CH_4. When n-m=1, e.g. BH_3, NH_3, $[H_4Mo(PPh_3)_4]$ (dodecahedron), $[H_4W(CN)_8]$ (square antiprism)[22] there is one non-bonding molecular orbital resulting from an odd number of self-conjugate representations, i.e. a_2'' (BH_3), a_1 (NH_3), b_1 $[H_4Mo(PPh_3)_4]$, a_1 $[H_4W(CN)_8]$. When n-m=2, e.g. BeH_2, OH_2, $[Mo(CNBu^t)_7]^{2+}$ (capped trigonal prism), $[V(CN)_7]^{4-}$ (pentagonal bipyramid), and $W(CO)_4Br_3$ (capped octahedron)[22] there must either be a odd number of self-conjugate e representations or a pair of orbitals with different symmetries each of which arises from an odd number self-conjugate representations. For example, BeH_2 (π_u, e_{1u}), OH_2(a_1 and b_2), $[Mo(CNBu^t)_7]^{2+}$ (a_1, b_2), $[V(CN)_7]^{4-}$ (e_1''), and $W(CO)_4Br_3$ (e).

When n-m=3, e.g. $Mo(CO)_6$(octahedral), $Mo(S_2C_2H_2)_3$ (trigonal prism) the three non-bonding orbitals must be either an odd number of self-conjugate t representations, or e and a_1 representations or three singly degenerate representations with different symmetries, e.g. $Mo(CO)_6$ (t_{2g}), $Mo(S_2C_2H_2)_3$ (e′ and a_1'). The full utilisation of the bonding molecular orbitals and the non-bonding molecular orbitals defined above leads naturally to the inert gas rule for co-ordination and organometallic compounds. The non-bonding nature of these orbitals in transition metal compounds is confirmed by the partial occupation of these orbitals. Some specific examples of complexes illustrating this point are summarised in Table 7.1. Clearly the arguments can be extended to hypervalent compounds where n>m and there are n-m non-bonding orbitals localised on the ligand sphere. Such compounds exceed the inert gas rule by 2(m-n) valence electrons. For example, in PF_5 and SF_6 there are 1(a_1) and 2(e_g) non-bonding L^σ orbitals respectively localised on the fluorine ligands.

Table 7.1 Examples of co-ordination compounds with variable occupations of the non-bonding orbitals.

Example	Co-ordination geometry (number)	d^n
$TiCl_4(diars)_2$	dodecahedron (8)	0
$NbCl_4(diars)_2$	dodecahedron (8)	1
$MoH_4(PH_3)_4$	dodecahedron (8)	2
$[ZrF_7]^{2-}$	pentagonal bipyramid (7)	0
$[VF_7]^{4-}$	pentagonal bipyramid (7)	2
$OsH_4(PMe_2Ph)_3$	pentagonal bipyramid (7)	4
$[TiF_6]^{2-}$	octahedron (6)	0
OsF_6	octahedron (6)	2
PtF_6	octahedron (6)	4
$Cr(CO)_6$	octahedron (6)	6

7.2.5 The effects of geometric changes

In this section the effect of a geometrical distortion on the character and energies of the non-bonding molecular orbitals will be considered by reference to specific examples. In the main group, molecule MH_3 (2) with a planar D_{3h} geometry the m-n rule suggests the occurrence of 1 non-bonding orbital and this can be readily be identified as p_z (see (2)). If the molecule is distorted to give a pyramidal C_{3v} geometry (1) then the s and p_z orbitals belong to the same a_1 irreducible representation of the C_{3v} point group. The energies of the resultant a_1 molecular orbitals are obtained by solving the following determinant:

$$A = \begin{array}{c|ccc|c} & s & p_z & \psi^{\sigma} & \\ & \alpha\text{-}E & 0 & \beta_s & s \\ & 0 & \alpha\text{-}E & \beta_p & p_z \\ & \beta_s & \beta_p & \alpha\text{-}E & \psi^{\sigma} \end{array}$$

$$\beta_s = \langle \psi^{\sigma} | H | s \rangle$$

$$\beta_p = \langle \psi^{\sigma} | H | p_z \rangle$$

$$\psi^{\sigma} = 1/(3)^{1/2} (\sigma_1 + \sigma_2 + \sigma_3)$$

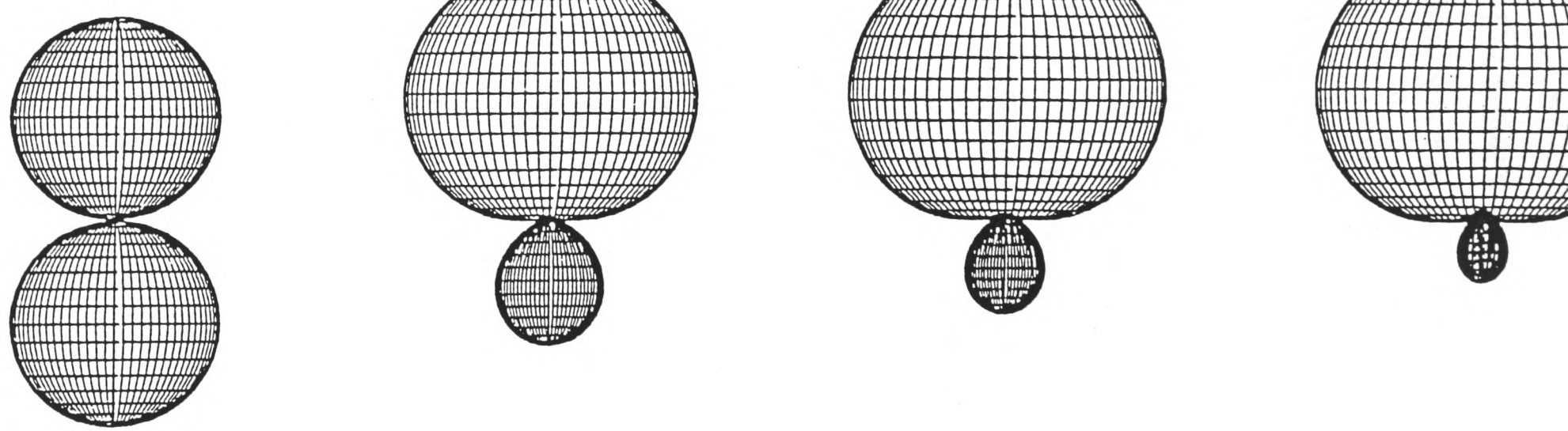
$$\det(A) = (\alpha\text{-}E)^3 - (\alpha\text{-}E)\beta_s^2 - (\alpha\text{-}E)\beta_p^2 = 0$$

This determinant leads of course to a non-bonding orbital with energy, α, confirming the (m-n) rule, but the wavefunction of this molecular orbital now has the following form:

$$\psi_{n.b} = \psi(2a_1) = \beta_p/(\beta_s^2 + \beta_p^2)^{1/2}\, s \; - \; \beta_s/(\beta_s^2 + \beta_p^2)^{1/2} p_z$$

This non-bonding orbital is illustrated in Figure 7.3 for angles θ=90°-54.73°.It is noteworthy that the overlap integral between $\psi_{n.b}$ and the ligand orbital ψ^{σ} is zero, i.e,

$$\langle \psi_{n.b} | \psi^{\sigma} \rangle = 0 \qquad \text{(B-12)}$$



nodal cone angle	90.00°	70.53°	63.44°	54.73°

Figure 7.3 The a_1 non-bonding orbital for MH_3 (1) with different θ angles

Clearly as the hydrogen atoms move away from the original MH_3 plane the s and p orbitals mix to produce a nodal cone coincident with the M-H bond directions. In this way the non-bonding character is maintained. The computed s and p characters as a function of θ are summarised in Table 7.2 for the situation where

Table 7.2 The bonding and non-bonding molecular orbitals in MH_3 as a function of θ angle for the situation where $\beta_\sigma(s)=\beta_\sigma(p)$.

θ(degree) [bond angle]	symmetry	bonding and non-bonding molecular orbitals
90.00°	a_2'':	p_z
[120.00°]	1e':	$0.707p_x+0.707P_x^\sigma$, $0.707p_y+0.707P_y^\sigma$
	a_1':	$0.707s+0.707S^\sigma$
70.53°	$2a_1$:	$0.316s+0.949p_z$
[109.47°]	1e :	$0.707p_x+0.707P_x^\sigma$, $0.707p_y+0.707P_y^\sigma$
	$1a_1$:	$0.685s-0.224p_z + 0.685S^\sigma-0.224P_O^\sigma$
68.00°	$2a_1$:	$0.351s+0.936p_z$
[106.80°]	1e :	$0.707p_x+0.707P_x^\sigma$, $0.707p_y+0.707P_y^\sigma$
	$1a_1$:	$0.662s-0.248p_z + 0.662S^\sigma-0.248P_O^\sigma$
63.44°	$2a_1$:	$0.408s+0.913p_z$
[101.54°]	1e :	$0.707p_x+0.707P_x^\sigma$, $0.707p_y+0.707P_y^\sigma$
	$1a_1$:	$0.645s-0.299p_z + 0.645S^\sigma-0.299P_O^\sigma$
54.73°	$2a_1$:	$0.500s+0.866p_z$
[90.00°]	1e :	$0.707p_x+0.707P_x^\sigma$, $0.707p_y+0.707P_y^\sigma$
	$1a_1$:	$0.612s-0.354p_z + 0.612S^\sigma-0.354P_O^\sigma$

$\beta_\sigma(s) = \beta_\sigma(p)$ (as defined in (4))

$\beta_s = \langle 1/(3)^{1/2}(\sigma_1+\sigma_2+\sigma_3)| H| s\rangle = (3)^{1/2}\beta_\sigma(s)$

$\beta_p = \langle 1/(3)^{1/2}(\sigma_1+\sigma_2+\sigma_3)| H| p_z\rangle = -(3)^{1/2}\cos\theta\ \beta_\sigma(p)$



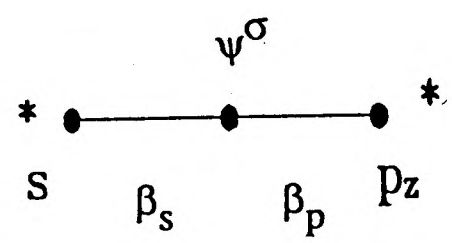
(4)

The alternant nature of the non-bonding molecular orbital problem as represented in (5) means that the coefficients at the starred positions multiplied by the relevant resonance integrals must add up to zero at the unstarred position:

$\beta_s C_s + \beta_p C_p = 0$ i.e. $C_s/C_p = -\beta_p/\beta_s$

Specifically for this problem:

$C_s/C_p = [\beta_\sigma(p)/\beta_\sigma(s)]\cos\theta = \cos\theta$



(5)

This result conforms with the computed coefficients given in Table 7.2.

The energies of the bonding and antibonding molecular orbitals can also be evaluated from the secular determinant. They are:

$$E(1a_1) = \alpha - (\beta_s^2 + \beta_p^2)^{1/2}$$

$$E(3a_1) = \alpha + (\beta_s^2 + \beta_p^2)^{1/2}$$

and the relevant wavefunctions are:

$$\psi(1a_1) = 1/(2)^{1/2}[1/(\beta_s^2 + \beta_p^2)^{1/2} (\beta_s s + \beta_p p_z)] + 1/(2)^{1/2}\psi^{\sigma}$$

$$\psi(3a_1) = 1/(2)^{1/2}[1/(\beta_s^2 + \beta_p^2)^{1/2} (\beta_s s + \beta_p p_z)] - 1/(2)^{1/2}\psi^{\sigma}$$

The energies and wavefunctions emphasise the alternant nature of the problem. If we express ψ^{σ} in terms of a linear combination of S^{σ} and P_z^{σ} weighted according to their overlap integrals:

$$\psi^{\sigma} \propto \langle\psi^{\sigma}|\, s\rangle\, S^{\sigma} + \langle\psi^{\sigma}|\, p_z\rangle\, P_z^{\sigma}$$

$$= 1/(\beta_s^2 + \beta_p^2)^{1/2} [(\beta_s S^{\sigma} + \beta_p P_z^{\sigma})]$$

Therefore,

$$\psi(1a_1)=1/(2)^{1/2}[1/(\beta_s^2+\beta_p^2)^{1/2}(\beta_s s+\beta_p p_z)]+1/(2)^{1/2}[1/(\beta_s^2+\beta_p^2)^{1/2}(\beta_s S^{\sigma}+\beta_p P_z^{\sigma})]$$

$$\psi(2a_1)= 1/(\beta_s^2+\beta_p^2)^{1/2}(\beta_p s-\beta_s p_z)$$

From these equations it is apparent that the sum of the squares of the coefficients associated with s, S^{σ}, p_z and P_z^{σ} for all the bonding and non-bonding orbitals have following relationships:

$$C_s^2 + C_S^2\sigma = 1$$

$$C_p^2 + C_P^2\sigma = 1$$

These relationships are confirmed in Table 7.2.

This represents a justification of the Spherical Electron Density Model [11] which suggests that in molecules that conform to the inert gas

rule the total electron density is pseudo-spherical.

The corresponding molecular orbitals derived from p_x and p_y have the following energies and wavefunctions:

$$E_{bonding}(1e) = \alpha + \beta(p_{x,y})$$

$$\beta(p_{x,y}) = \langle p_x | H | P_x^{\sigma} \rangle = \langle p_y | H | P_y^{\sigma} \rangle = (6)^{1/2}/2 \sin\theta \, \beta_{\sigma}(p)$$

$$1e_x = 1/(2)^{1/2} (p_x + P_x^{\sigma}) \qquad P_x^{\sigma} = 1/(6)^{1/2} [2\sigma_1 - (\sigma_2 + \sigma_3)]$$

$$1e_y = 1/(2)^{1/2} (p_y + P_y^{\sigma}) \qquad P_y^{\sigma} = 1/(2)^{1/2} (\sigma_2 - \sigma_3)$$

$C_p^2 + C_P^2\sigma = 1$ for $1e_x$ and $1e_y$ bonding orbitals.

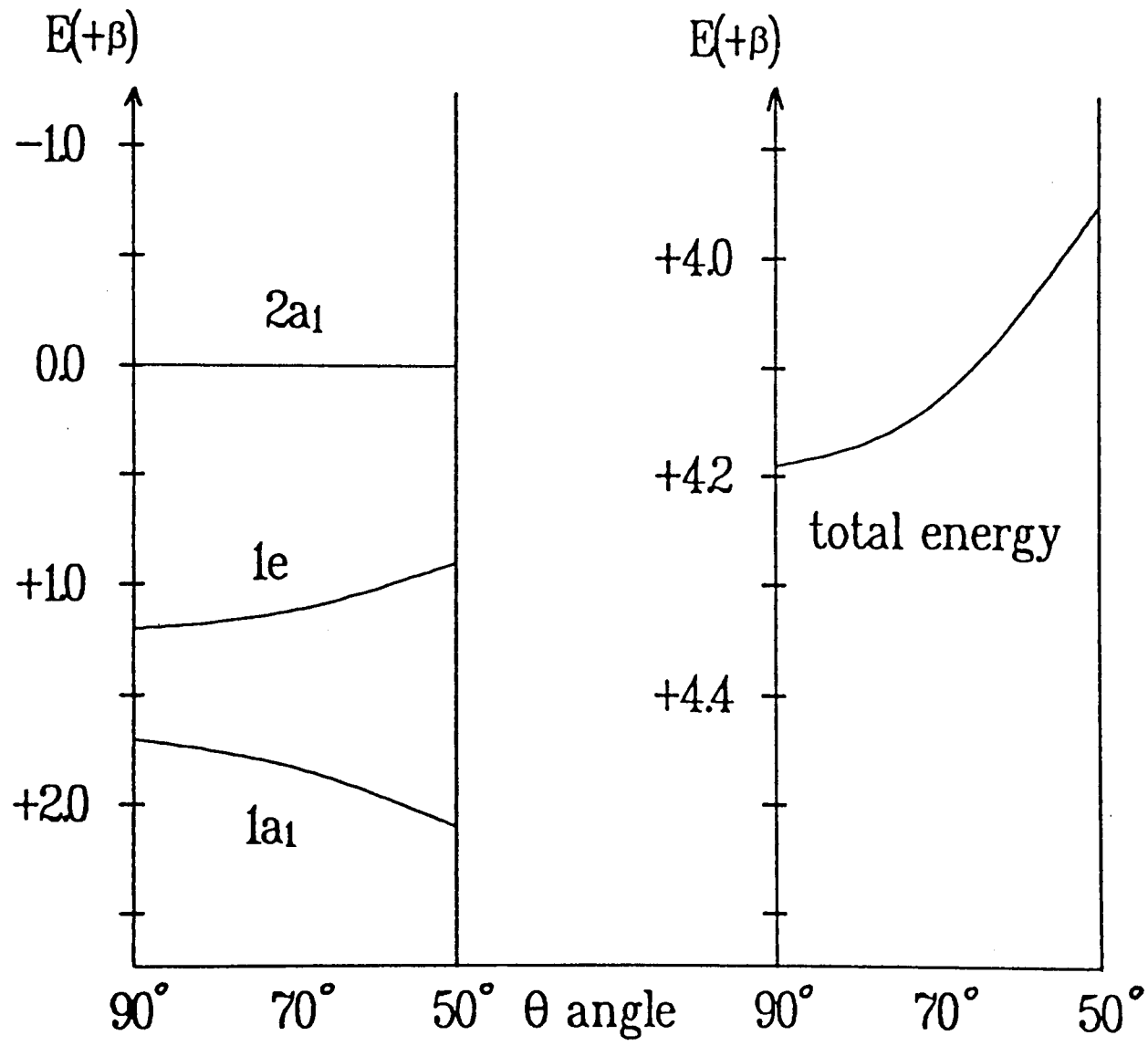


Figure 7.4 The energies of molecular orbitals in MH_3 (1) as a function of θ angle

In Figure 7.4 the energies of the molecular orbitals as a function of θ are illustrated for the situation where $\alpha=0$, $\beta_\sigma(s)=\beta_\sigma(p)=\beta$ and represent a "Walsh diagram" for the distortion co-ordinate. The validity of the pairing theorem along the distortion co-ordinate is nicely illustrated in the diagram. It is significant that except for the situation where the lowest energy bonding molecular orbital only is filled the planar geometry is preferred for all remaining electron counts up to the inert gas configuration. The more symmetrical geometry is preferred because the destabilisation energies associated with 1e bonding orbitals are larger than the stabilisation energy associated with $1a_1$.

The overlap integrals between the hydrogen atoms and the s orbitals of the central atom are independent of the θ angle and therefore cannot contribute to a geometric preference. The p_x and p_y overlap integrals decrease by $\sin\theta$ as a result of the change in geometry and the destabilisation which results outweighs the increased stabilisation associated with the p_z orbital whose overlap integral increases by a factor of $\cos\theta$. Therefore, for the hypothetical situation when $\alpha_s=\alpha_p$ a spherical co-ordination geometry is preferred because it maximises the overlaps between the ligand orbitals and the central atomic valence orbitals.

Interestingly, the geometric change causes a redistribution of electron density between the s and p_z orbitals, which belong to the same a_1 representation of the C_{nv} point group. The electron density associated with the p_x and p_y orbitals remains constant, however, because they belong to a different (e) irreducible representation. The redistribution of electron density associated with s and p_z is illustrated in Figures 7.5a and 7.5b for 6 and 8 electron pyramidal molecules. For the 6 electron molecule the initial populations when $\theta=90°$ are $s^1p_z^0$ and

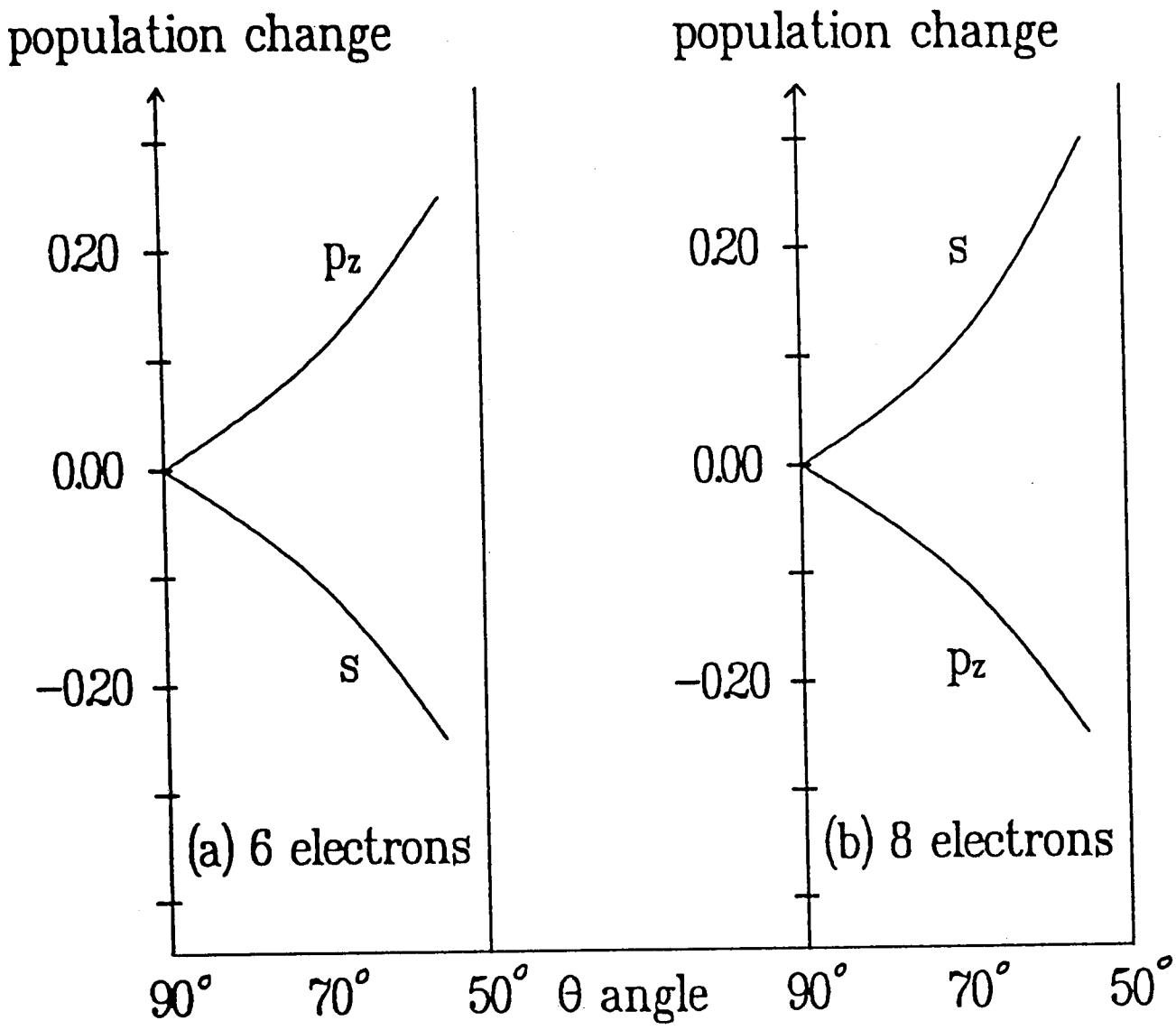


Figure 7.5 The redistribution in MH_3 (1) molecular orbitals of the electron density associated with s and p_z orbitals for 6 electrons (a) and 8 electrons (b) as a function of θ angle

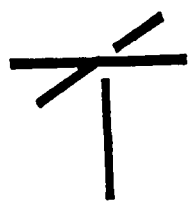
change to $s^{0.75}p_z^{0.25}$ when θ=54.73°. In contrast for the 8 electron molecule the populations change from $s^1p_z^2$ (θ=90°) to $s^{1.25}p_z^{1.75}$ when θ=54.73°. This is a very important result because it suggests that a geometric distortion which results in a low symmetry molecule belonging to a C_{nv} point group causes a transfer of electron density from s to p_z if an empty non-bonding orbital is created and a transfer of electron density from p_z to s if a filled non-bonding hybrid orbital is created. This has no energetic consequences if $\alpha_s=\alpha_p$, however in real main group

molecules $\alpha_s \neq \alpha_p$ and this transfer of electron density has important geometric consequences. In particular if the valence s orbitals are more stable than the valence p orbitals this means that the higher symmetry geometry is preferred unless the non-bonding orbital is occupied. Therefore, the important stereochemical activity of lone pairs in main group chemistry is intimately connected with the redistribution of electron density between s and p_z and the relative ordering of the valence orbitals. This aspect will be discussed in a more quantitative fashion below.

The a_1 non-bonding orbital in a square pyramidal ML_5(6) behaves in an analogous manner. The wavefunction of this a_1 non-bonding orbital can also be obtained in the Hückel approximations. In the square pyramid, the 5 L^σ's are $P^\sigma_{\pm 1}$, D^σ_{2c} (which are the same as in the octahedron) and two a_1 representations,

$\psi_2 = (1/6)^{1/2} S^\sigma - (1/2)^{1/2} P^\sigma_o + (1/3)^{1/2} D^\sigma_o$ (localised on position 6)

$\psi_3 = (2/3)^{1/2} S^\sigma - (1/3)^{1/2} D^\sigma_o$ (localised on the square)



(6)

where S^σ, P^σ_o and D^σ_o represent the ligand L^σ functions of an

octahedron. These two a_1 ligand orbitals interact with the s, p_z and d_z2 orbitals of the central atom.

We assume that the resonance integrals $\beta_\sigma(s)$, $\beta_\sigma(p)$ and $\beta_\sigma(d)$ (see (4)) are the same and equal to unity. The latter assumption does not affect the coefficients of the molecular orbitals because they define only the orbital energies. Using all the assumptions above and the resonance integrals in Section B.3, the resonance integrals between s, p_z and d_z2 on the central atom and ligand orbitals ψ_2 and ψ_3 can be calculated and are listed in the Table below.

$\langle\psi_i\vert H\vert\phi_i\rangle$	s	p_z	d_z2
ψ_2	1	-1	1
ψ_3	2	0	-1

Let $H_{ii}(s)=H_{ii}(p)=H_{ii}(d)=\alpha_c$ (c:central atom) and $H_{ii}(\text{ligand})=\alpha_l$ (l: ligand). Then the secular determinant is,

$$\begin{vmatrix} \alpha_l-E & 0 & 1 & -1 & 1 \\ 0 & \alpha_l-E & 2 & 0 & -1 \\ 1 & 2 & \alpha_c-E & 0 & 0 \\ -1 & 0 & 0 & \alpha_c-E & 0 \\ 1 & -1 & 0 & 0 & \alpha_c-E \end{vmatrix} = 0$$

Obviously, there is one eignvalue with $E=\alpha_c$. This means this orbital with α_c orbital energy is the non-bonding orbital. The non-bonding orbital is:

$$\psi_{nb}= 1/(14)^{1/2}s + 3/(14)^{1/2}p_z + 2/(14)^{1/2}d_z2$$

localised on the central atom with a maximum density in the direction of the missing vertex (position 1). It can be checked that

$$\langle\psi_{nb}|\psi_2\rangle=\langle\psi_{nb}|\psi_3\rangle=0 \qquad \text{(B-13)}$$

The corresponding bonding molecular orbitals of a_1 symmetry are:

$$\phi_1 = -0.070s + 0.406p_z - 0.575d_z2 + \text{ligand contributions}$$
$$E = \alpha + 1.608\beta$$
$$\phi_2 = 0.678s - 0.116p_z - 0.164d_z2 + \text{ligand contributions}$$
$$E = \alpha + 2.327\beta$$

In addition there are the following molecular orbitals of b_2 and e symmetry:

$$\phi(b_2) = 0.707d_{x^2-y^2} + 0.707D^{\sigma}_{2c} \qquad E = \alpha + 1.7321\beta$$

$$\phi(e_x) = 0.707p_x + 0.707P^{\sigma}_x$$
$$\phi(e_y) = 0.707p_y + 0.707P^{\sigma}_y \qquad E = \alpha + 1.414\beta$$

The occupation of the five bonding molecular orbitals leads to the following orbital occupations:

$$s^{0.92}p^{2.36}d^{1.72}$$

When the non-bonding orbital is occupied these orbital populations become:

$$s^{1.06}p^{3.64}d^{2.29}$$

For a square pyramidal ML_5 complex, where M is a transition metal, there are in addition three non-bonding orbitals, d_{xy}, d_{xz}, d_{yz} localised exclusively on the central metal atom. The complete molecular orbital splitting diagram for such a complex is illustrated in Figure 7.6.

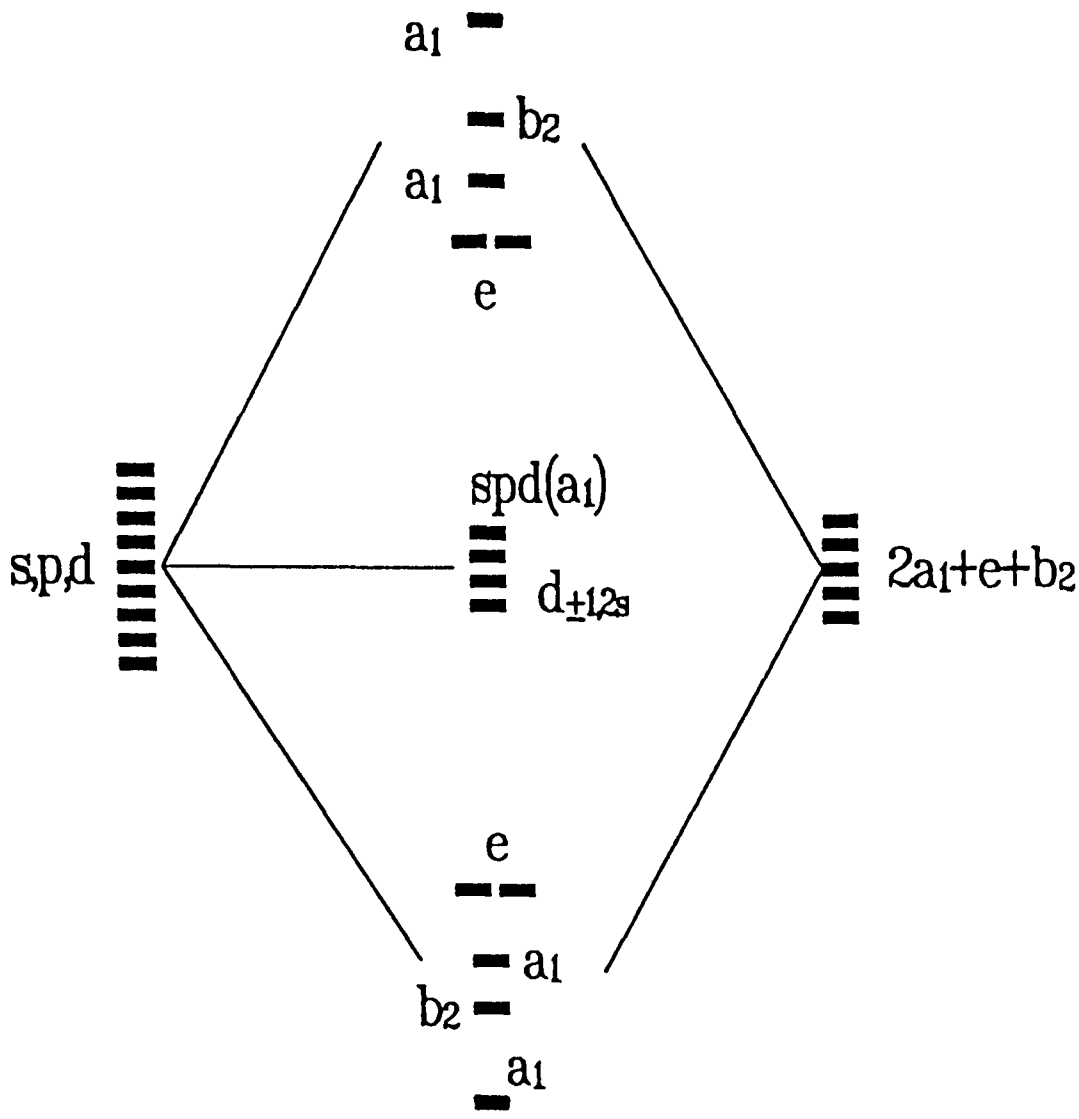


Figure 7.6 The orbital interaction diagram for a square pyramidal transition metal ML_5 complex

In a transition metal trigonal bipyramidal complex the corresponding five bonding molecular orbitals are:

$$\phi(1a_1') = 0.707s + 0.707S^{\sigma} \qquad E = \alpha + 2.236\beta$$

$$\phi(2a_1') = 0.707d_z2 + 0.707D_0^{\sigma} \qquad E = \alpha + 1.658\beta$$

$$\phi(a_2'') = 0.707p_z + 0.707P_0^{\sigma} \qquad E = \alpha + 1.414\beta$$

$$\phi(e_x') = 0.707[(4/7)^{1/2}p_x + (3/7)^{1/2}d_{x^2-y^2}] + 0.707P_x^{\sigma}$$

$$\phi(e_y') = 0.707[-(4/7)^{1/2}p_y + (3/7)^{1/2}d_{xy}] + 0.707P_y^{\sigma}$$

$$E = \alpha + 1.620\beta$$

In addition there are the following non-bonding orbitals:

$$\phi_{nb}(e_x') = -(3/7)^{1/2}p_x + (4/7)^{1/2}d_{x^2-y^2}$$

$$\phi_{nb}(e_y') = (3/7)^{1/2}p_y + (4/7)^{1/2}d_{xy} \qquad E = \alpha$$

and pure d orbitals d_{xz} and d_{yz}. It is significant that in the D_{3h} point group that s and p_z belong to different irreducible representations and therefore cannot mix to create a non-bonding a_1 molecular orbital. However, (p_x, p_y) and ($d_{x^2-y^2}$, d_{xy}) both transform as e′ and create linear combinations which either have maxima in the equatorial bond directions leading to $\phi(e_x')$ and $\phi(e_y')$ above or are noded in these directions $\phi_{nb}(e_x')$ and $\phi_{nb}(e_y')$. The relevant molecular orbital diagram is illustrated in Figure 7.7.

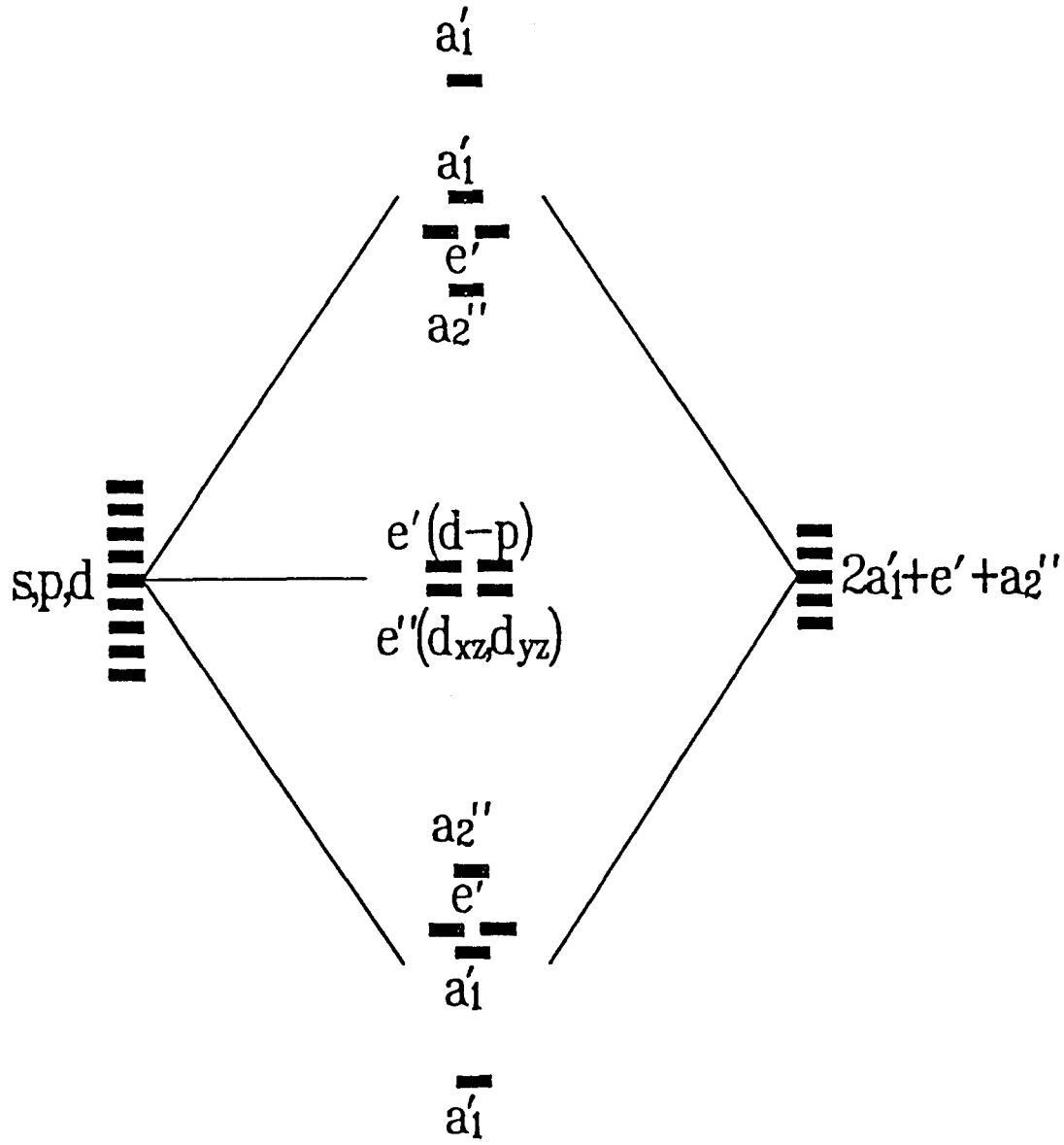


Figure 7.7 The orbital interaction for a trigonal bipyramidal transition metal ML_5 complex

If only the bonding electron pairs are occupied the relevant orbital populations are:

$$s^{1.00}d^{1.86}p^{2.14}$$

If the bonding orbitals are all doubly occupied by electrons the corresponding total energies are identical for the trigonal bipyramid and square pyramid, i.e. 8.55β. This is consistent with the observation that the potential energy surface for the interconversion of trigonal bipyramidal and square-pyramidal molecules is very soft.[23]

The orbital populations are also very similar, i.e. $s^{1.00}d^{1.86}p^{2.14}$ for the trigonal bipyramid and $s^{0.92}d^{1.72}p^{2.36}$ for the square pyramid. Therefore, for molecules where the assumption $\alpha_s \neq \alpha_p \neq \alpha_d$ is not valid there will be little change in the relative stabilities of the two geometries.

The observed atomic energies for transition metals $|\alpha_d| > |\alpha_s| >> |\alpha_p|$ will lead to a slight preference for the trigonal bipyramidal geometry. For main group atoms where $|\alpha_s| > |\alpha_p| >> |\alpha_d|$ there will be a corresponding slight preference for the trigonal bipyramid which has a somewhat larger s orbital population.

When the ML_5 molecules have more than five electron pairs the geometric preferences depend on the number of electron pairs and the relative energies of the valence orbitals. For a transition metal where $|\alpha_d| > |\alpha_s| >> |\alpha_p|$ the following conclusions are pertinent:

d^0-d^4 (low spin) the two geometries will have similar energies.

d^6 (low spin) the square pyramid is energetically preferred because the six electrons can be accommodated in pure d orbitals, whereas for a trigonal bipyramid there is an electron pair in a d-p hybrid.

d^8 (low spin) The structures will be finely balanced because for

both geometries there are electrons occupying hybrids which have higher orbital energies than pure d orbitals, i.e. for a square-pyramid there is one electron pair in an spd hybrid and for a trigonal bipyramid two electron pairs in p-d hybrids.

In a square-planar geometry, the ψ_1 and ψ_2 are localised on positions 1 and 6 respectively, where

$$\psi_1=(1/6)^{1/2}S^{\sigma}+(1/2)^{1/2}P_o^{\sigma}+(1/3)^{1/2}D_o^{\sigma}.$$

The remaining ψ_3 should be taken into account. Now the secular determinant is:

$$\begin{vmatrix} \alpha_1-E & 2 & 0 & -1 \\ 2 & \alpha_c-E & 0 & 0 \\ 0 & 0 & \alpha_c-E & 0 \\ -1 & 0 & 0 & \alpha_c-E \end{vmatrix} = 0$$

There are two eigenvalues $E_1=E_2=\alpha_c$, i.e., two non-bonding orbitals. They are:

$$\psi_1= p_z$$

$$\psi_2= 1/(5)^{1/2}s + 2/(5)^{1/2}d_z2$$

localised on the central atom. The overlap integrals between these two non-bonding orbitals and ligand orbital ψ_3 are zero, i.e.,

$$\langle\phi_1|\psi_3\rangle=\langle\phi_2|\psi_3\rangle=0. \qquad \text{(B-14)}$$

The discussion presented above illustrates the form of the non-bonding orbitals in main group compounds and transition metal complexes. Particularly striking is the fact that **all the non-bonding orbitals localised on the central atom have zero overlaps with all the ligands.**

7.2.6 More quantitative analysis of the effects of s-p-d separations ($\alpha_s \neq \alpha_p \neq \alpha_d$)

In molecules such as ammonia the energy of the 2p orbital of nitrogen is similar to that of the hydrogen 1s orbital but the 2s orbital is considerably more stable (by ca. 10.00ev). A first order correction [24-25] to the wavefunctions arising from a change in Coulomb integral from α to $\alpha + \delta\alpha$ is given by:

$$\psi_i' = \psi_i^o + \sum_j t_{ji}^{(1)} \psi_j^o$$

$$t_{ij} = (C_{\alpha i}^o C_{\alpha j}^o \delta\alpha)/(e_i^o - e_j^o)$$

where ψ_j^o and e_j^o are the zeroth order orbital and energy, and t_{ij} is the mixing coefficient.

For ammonia which has a bond angle of 106.8° and θ=68.0°,the relevant wavefunctions of a_1 symmetry are:

	Energy
$\psi^o(3a_1) = 0.662s - 0.248p_z - 0.707\psi^\sigma(a_1)$	$\alpha + (\beta_s^2+\beta_p^2)^{1/2}$
$\psi^o(2a_1) = 0.351s + 0.936p_z$	α
$\psi^o(1a_1) = 0.662s - 0.248p_z + 0.707\psi^\sigma(a_1)$	$\alpha - (\beta_s^2+\beta_p^2)^{1/2}$

consider the $1a_1$ orbital:

$$t_{2a1,1a1} = 0.662\times0.351\times[-\delta\alpha/(\beta_s^2+\beta_p^2)^{1/2}]$$

$$t_{3a1,1a1} = 0.662\times0.662\times0.5\times[-\delta\alpha/(\beta_s^2+\beta_p^2)^{1/2}]$$

Making the simplifying assumption that

$$\delta\alpha = -(\beta_s^2+\beta_p^2)^{1/2}$$

$$t_{2a1,1a1} = 0.232$$

$$t_{3a1,1a1} = 0.219$$

$$\psi'(1a_1) = 1/N\ [(1a_1) + t_{2a1,1a1}\ (2a_1) + t_{3a1,1a1}\ (3a_1)]$$
$$= 0.803s - 0.077p_z + 0.591\psi^{\sigma}(a_1)$$

Under these conditions the corresponding wavefunctions for $3a_1$ is:

$$\psi'(3a_1) = 1/N\ [(1a_1) - t_{2a1,1a1}\ (2a_1) - t_{3a1,1a1}\ (3a_1)]$$
$$= 0.415s - 0.391p_z - 0.821\psi^{\sigma}(a_1)$$

For the non-bonding $2a_1$ orbital the corresponding perturbation theory correction is:

$$t_{1a1,2a1} = -0.232 \qquad t_{3a1,2a1} = 0.232$$
$$\psi'(2a_1) = 0.333s + 0.889p_z - 0.312\psi^{\sigma}(a_1)$$

It can be seen that the 1st order perturbation correction leads to the mixing of ligand character into the non-bonding orbital ($2a_1$). No change in the C_s/C_p ratio in the modified wavefunction ($2a_1$) occurs because $t_{1a1,2a1}=-t_{3a1,2a1}$. The change of the s and p characters is a result of the re-normalisation. Therefore, the nodal cone angle in the non-bonding orbital does not change even when mixing of ligand character occurs. Since there is no s contribution to the e orbitals, the energies and wavefunctions of the e orbitals are unchanged.

These modified wavefunctions together with those derived from ab initio calculations[26] are summarised in Table 7.3. The agreement between the two is remarkably good although the time of computation is several orders of magnitude different.

The 1st order correction to the orbital energies is given by:

$$\delta E = (C_{\alpha i}^{0})^2 \times \delta\alpha$$

More accurate orbital energies can be calculated from the modified wavefunctions $\psi'(1a_1)$, $\psi'(2a_1)$ and $\psi'(3a_1)$:

$$E = \langle\psi'(na_1)|\ H|\ \psi'(na_1)\rangle$$

Table 7.3 The wavefunctions and orbital energies for NH_3 derived from our approximation and ab initio calculations.

ab initio*:	orbital	energy(ev)	wavefunction
	$2a_1$	-11.22	$0.30s+0.94p_z-0.07[H_{1s}(1)+H_{1s}(2)+H_{1s}(3)]$
	1e	-16.97	$0.80p_y+0.43[H_{1s}(2)-H_{1s}(3)]$
	$1a_1$	-31.16	$0.87s-0.18p_z+0.19[H_{1s}(1)+H_{1s}(2)+H_{1s}(3)]$

this approximation:

orbital	energy(ev)		1st order modified wavefunction
	1st order correction	from modified mos	
$2a_1$	-17.51	-17.33	$0.33s+0.89p_z-0.18[H_{1s}(1)+H_{1s}(2)+H_{1s}(3)]$
1e	-20.13	-20.13	$0.71p_y+0.50[H_{1s}(2)-H_{1s}(3)]$
$1a_1$	-30.62	-26.63	$0.80s-0.08p_z+0.34[H_{1s}(1)+H_{1s}(2)+H_{1s}(3)]$

*. Only 2s and 2p atomic orbitals are considered.

These are computed with α=-14.00ev, $\delta\alpha$=-10.00ev, β_s=-9.35ev and β_p=3.50ev (because $\delta\alpha=-(\beta_s^2+\beta_p^2)^{1/2}$ and $\beta_s=(3)^{1/2}\beta_\sigma$, $\beta_p=-(3)^{1/2}\cos\theta\ \beta_\sigma$) and contrasted with the ab initio results [26] in Table 7.3. The agreement is less good. This emphasises the fact that semi-quantitative molecular orbital methods like the Hückel and extended Hückel do yield reasonably accurate wavefunctions but the energies of the molecular orbitals are less reliable.

The same methodology can be applied to H_2O which has a bond angle of 104.5°, θ=52.25°. When $\alpha_s=\alpha_p=\alpha_H$

$$C_s/C_p = -\beta_\sigma(p)\cos\theta/\beta_\sigma(s)$$

for the non-bonding orbital ($2a_1$). Using $\beta_\sigma(p)=\beta_\sigma(s)$

$$\psi_{nb}(2a_1) = 0.522s + 0.853p_z$$

The resultant wavefunctions derived from first order perturbation theory with $\delta\alpha=-(\beta_s^2+\beta_p^2)^{1/2}=-15.00$ev ($\alpha=-14.00$ev) are given in Table 7.4 and contrasted with those derived from ab initio calculations.[27]

Table 7.4 The wavefunctions and orbital energies for H_2O derived from our approximation and ab initio calculations.

ab initio*: orbital	energy(ev)	wavefunction
$1b_1$	-10.95	p_y
$2a_1$	-12.68	$0.52s+0.79p_z-0.26[H_{1s}(1)+H_{1s}(2)]$
$1b_2$	-16.97	$0.62p_x+0.42[H_{1s}(1)-H_{1s}(2)]$
$1a_1$	-34.95	$0.84s-0.13p_z+0.15[H_{1s}(1)+H_{1s}(2)]$

this approximation:

orbital	energy(ev)		1st order modified wavefunction
	1st order correction	from modified mos	
$1b_1$	-14.00	-14.00	p_y
$2a_1$	-21.83	-21.17	$0.48s+0.78p_z-0.24[H_{1s}(1)+H_{1s}(2)]$
$1b_2$	-24.12	-24.12	$0.71p_x+0.50[H_{1s}(1)-H_{1s(2)}]$
$1a_1$	-38.00	-32.48	$0.79s-0.14p_z+0.42[H_{1s}(1)+H_{1s}(2)]$

*. Only 2s and 2p atomic orbitals are considered.

It is apparent from earlier calculations on NH_3 that the preferred geometry was planar ($\theta=90°$) when $\alpha_s=\alpha_p=\alpha_H$. The effect of

introducing a s-p separation by first order perturbation theory is illustrated in Figure 7.8. Clearly a pyramidal geometry is now preferred. Particularly influential is the greater stabilisation of the $2a_1$ (non-bonding molecular orbital).

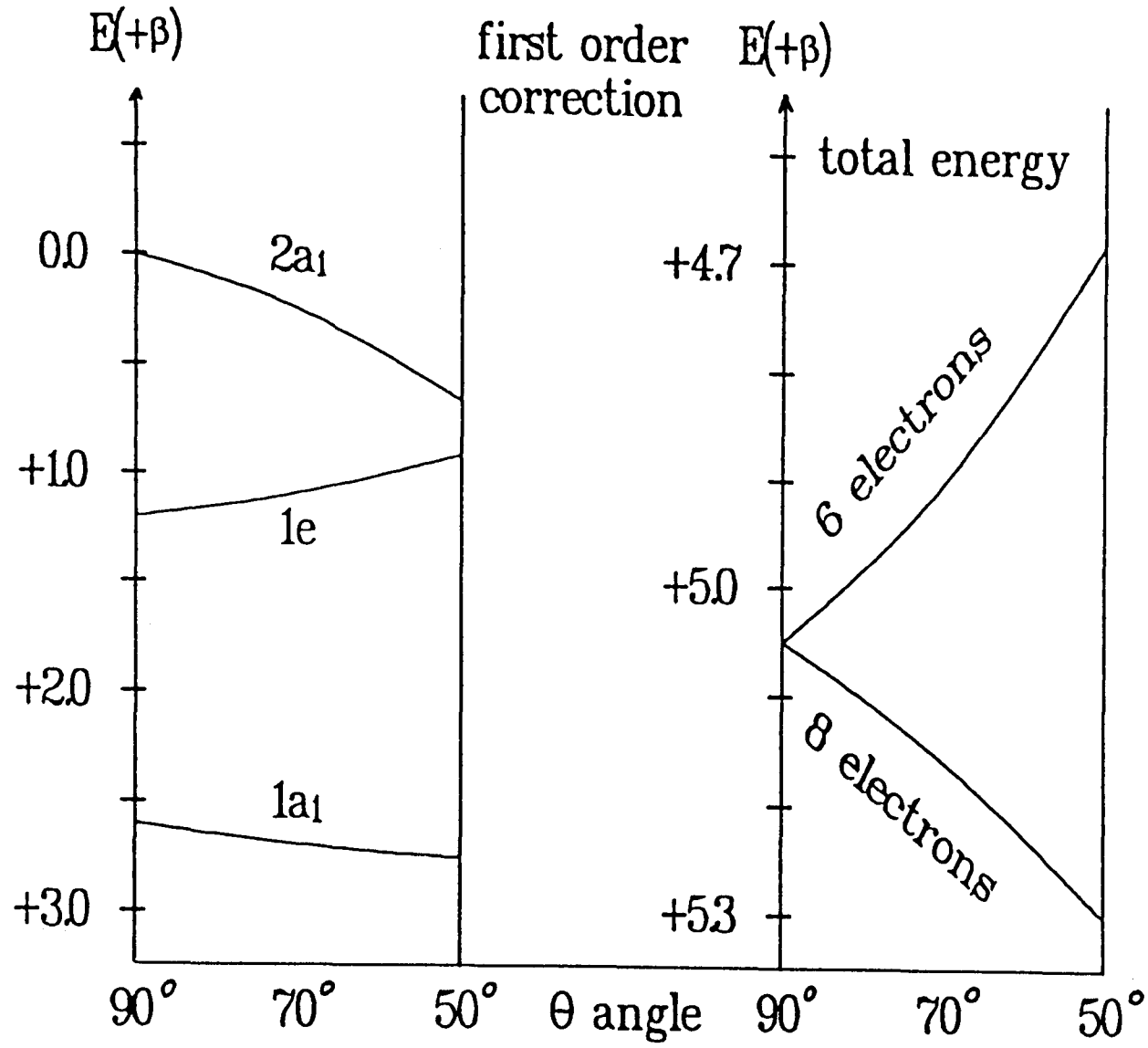


Figure 7.8 The energies of molecular orbitals in MH_3 (1) as a function of θ angle after the first-order perturbation correction

How can a non-bonding orbital exert such a strong stereochemical influence? Since the first order stabilisation is equal to $C_s^2\delta\alpha$ those orbitals which experience the largest changes in s character as θ is altered gain the greatest stabilisation. Particularly for θ values of 90° and 54.73° the following changes in s character (C_s^2) occur:

	θ		ΔC_s^2
	90.00°	54.73°	
$1a_1$	0.707^2	0.612^2	-0.125
$2a_1$(non-bonding)	0.000	0.500^2	0.250

These trends are clearly illustrated in Figure 7.5.

In molecules such NF_3 the energy of the 2s orbital of nitrogen is similar to that of the 2p orbitals which are responsible for forming the σ bond with nitrogen, but that of the 2p orbitals of nitrogen is considerably higher (ca. 10ev).[28] In this case the same methodology (first order perturbation theory) can be used to improve those wavefunctions and orbital energies associated with 2p atomic orbital of nitrogen. From the zero order wavefunctions of $1a_1$ and $2a_1$ developed above, the destabilisation energy from the first order correction is:

$$[1/(\beta_s^2+\beta_p^2)]\times(\beta_s^2/2+\beta_p^2)$$

Since the β_s is constant from our approximation, the destabilisation energy derived from raising the α_p depends on only β_p and consequently only on the cone angle θ in (1). The larger the magnitude of β_p the smaller destabilisation energy. Therefore, as θ is decreased the destabilisation energy decreases. Since the 2p character in e orbitals are independent of θ angle, the destabilisation energies (first order correction) are constant.

The arguments developed above show that the trends in geometric effects are the same regardless of raising α_p or lowering α_s as a perturbation.

In the transition metal complexes, the methodogy can be used to evaluate the effect of $\alpha_s \neq \alpha_p \neq \alpha_d$ by lowering α_d as a perturbation. In this case, the first order stabilisation energy is equal to $C_d^2\delta\alpha$. Therefore the non-bonding orbital(s) which experience the largest changes in d

character as the geometry is changed gain the greatest stabilisation and exert a stronger stereochemical influence.

7.2.7 Generation of non-bonding orbitals

The discussion given in the previous sections has provided a methodology for defining the non-bonding orbitals. The equations (B-12), (B-13) and (B-14) showed that the ligands are always located on the nodal lines of the non-bonding orbitals. The nodal properties of the non-bonding orbitals do not change even though the first order correction from $\alpha_s \neq \alpha_p \neq \alpha_d$ is included. A more general method for defining the non-bonding orbitals can be formulated in the following equation:

$$\langle \psi_{\text{non-bonding}} | \sigma_i \rangle = 0 \qquad \text{(B-15)}$$

where $\psi_{\text{non-bonding}}$ is a linear combination of valence orbitals on the central atom,

$$\psi_{\text{non-bonding}} = \sum_{l,m} a_{lm} \psi_{lm}$$

e.g., as+bp+cd. Since the wavefunctions of the valence orbitals in the central atom are represented in terms of spherical harmonic functions of the form:

$$\psi_{l,m} = R_{nl}(r) Y_{lm}(\theta,\varphi)$$

the $\langle \psi_{\text{non-bonding}} | \sigma_i \rangle$ can be formulated in the following equation:

$$\langle \psi_{\text{non-bonding}} | \sigma_i \rangle$$

$$= \sum_{l,m} a_{lm} \langle R_{nl}(r) | \sigma \rangle Y_{lm}(\theta_i,\varphi_i) \qquad \text{(B-16)}$$

$$= \sum_{l,m} a_{lm} \langle R_{nl}(r) | \sigma \rangle [(2l+1)/4\pi]^{1/2} C_{lm}(\theta_i,\varphi_i) \qquad \text{(B-17)}$$

(because $C_{lm} = [4\pi/(2l+1)]^{1/2} Y_{lm}$)

The assumption of $S_\sigma(s)=S_\sigma(p)=S_\sigma(d)$ (see (4)) (S indicates the overlap integral) in fact is equivalent to that $[(2l+1)/4\pi]^{1/2}<R_{nl}(r)|\,\sigma>$ is equal for s, p and d. Under this assumption, the following equation is obtained:

$$\sum_{l,m} a_{lm}\, C_{lm}(\theta_i,\varphi_i) = 0 \qquad \text{(B-18)}$$

Therefore, the wavefunction of the non-bonding orbital can be determined by solving equation (B-18). For example, the a_1 non-bonding orbital in a square pyramid is:

$$as+bp_z+cd_z2$$

Inserting the wavefunctions C_{lm} into above equation, we obtain:

$$a + b\cos\theta + c/2(3\cos^2\theta-1)$$

Replacing θ by 180° and 90°, we have:

$$a - b + c = 0$$

$$a - c/2 = 0$$

Combining this with the normalisation condition, we obtain:

$$\psi_{\text{non-bonding}} = (1/14)^{1/2}s + (9/14)^{1/2}p_z + (4/14)^{1/2}d_z2$$

which is exactly the same as the one we obtained in Section B.5

In the square planar ML_4 complex, the a_{1g} non-bonding orbital is a linear combination s and d_z2, i.e.

$$as + bd_z2$$

Following the same methodology, we have:

$$a + b \times 1/2(3\cos^2\theta-1)\,|_{\theta=90°} = 0$$

Therefore $a - 1/2\ b = 0$. The a_{1g} non-bonding orbital which has zero overlap with the four ligands has the form of

$$(1/5)^{1/2}s + (4/5)^{1/2}d_z2$$

which is also the same as the one given in Section B.5.

In a discussion of hybridisation schemes,[29] only the angular function Y_{lm} were used in (B-18) instead of C_{lm} to determine the non-bonding

orbitals. That corresponds to the approximation that $<R_{nl}(r)|\sigma>$ is the same for s, p and d. It can be correlated to the molecular orbital method by assuming $S_\sigma(s):S_\sigma(p):S_\sigma(d)=1:(3)^{1/2}:(5)^{1/2}$. It is apparent that the Y_{lm} approximation tends to overemphasise the overlap of d orbitals with ligands. Nevertheless, the relative sign of the orbital mixings in the non-bonding orbitals are reproduced as are the trends associated with the variation of the nodal characteristics as the d, s and p contributions are varied. For a spherical co-ordination compound, the effect of the above assumptions on the solutions of the non-bonding orbitals is limited since the non-bonding orbitals do not involve much admixture between s, p and d.

The other method to generate a non-bonding orbital is based on the spherical and complementary nature of the electron density in co-ordination compounds and the localisation procedure described previously.[11] The linear combination of the octahedral symmetry adapted ligand linear combinations $(1/6)S^\sigma+(1/2)P_O^\sigma+(1/3)D_O^\sigma$ is localised exclusively at position 1 of the octahedron (see Figure 7.1) and the remaining five linear combinations are delocalised over the other five locations and may be constructed to be equivalent to the symmetry adapted linear combinations for a square pyramid. The localisation procedure was developed by Mingos and Hawes [11]. The linear combination $as+bp_z+cd_z2$ produces a region of electron density in the position 1 of the octahedron. When the coefficients a, b and c are equal to those $(1/6)S^\sigma+(1/2)^{1/2}P_O^\sigma+(1/3)^{1/2}D_O^\sigma$ gives $a=(1/6)^{1/2}$, $b=(1/2)^{1/2}$ and $c=(1/3)^{1/2}$. The orbital $(1/6)^{1/2}s+(1/2)^{1/2}+(1/3)^{1/2}d_z2$ maximises the electron density in the position 1. An electron pair occupying this orbital localised on the central atom will be essentially non-bonding with respect to the bonding molecular orbitals associated with the square pyramidal co-ordination polyhedron.

7.2.8 Summary

The arguments developed above provide some fundamental principles governing the nature of the molecular orbitals of ML_n compounds. Although the **m-n rule** and the **pairing theorem** are based on the assumption of $\alpha_s=\alpha_p=\alpha_d$ (and $=\alpha_l$ for the latter), the effects of unequal Coulomb integrals ($\alpha_s\neq\alpha_p\neq\alpha_d$) can be treated using a perturbation correction and most conclusions derived from them retain their generality. The following general points can be made from the discussions of the previous sections.

(1) The number of non-bonding orbitals in ML_n complexes is equal to $|m-n|$ if the number of valence orbitals in the central atom is m.

(2) The group theoretical aspects for defining the number of non-bonding orbitals can be applied to any ML_n compound.

(3) The ligands are always located on the nodal lines, planes or cones of the non-bonding orbitals. The nodal properties do not change even when the first order correction arising from $\alpha_s\neq\alpha_p\neq\alpha_d$ is included.

(4) The non-bonding orbitals can be classified into following categories:

(a) pure atomic orbitals when the ligands are all located on their nodal planes or cones, e.g. $BH_3(p_z)$ and $ML_6(d_{xz},d_{yz},d_{xy})$. Further examples of these types of non-bonding orbitals are tabulated in Table 7.5.

Table 7.5 Non-bonding orbitals localised on the central atom and not hybridised

Geometry	p orbitals	d orbitals
Linear ML_2	p_x, p_y	$d_x2_{-y}2, d_{xy}, d_{xz}, d_{yz}$
Trigonal ML_3	p_z	d_{xz}, d_{yz}
Tetrahedral ML_4		$d_x2_{-y}2, d_z2$
Square planar ML_4	p_z	d_{xy}, d_{xz}, d_{yz}
Trigonal bipyramidal ML_5		d_{xz}, d_{yz}
Octahedral ML_6		d_{xy}, d_{xz}, d_{yz}
Pentagonal bipyramidal ML_7		d_{xz}, d_{yz}
Dodecahedral ML_8		$d_x2_{-y}2$

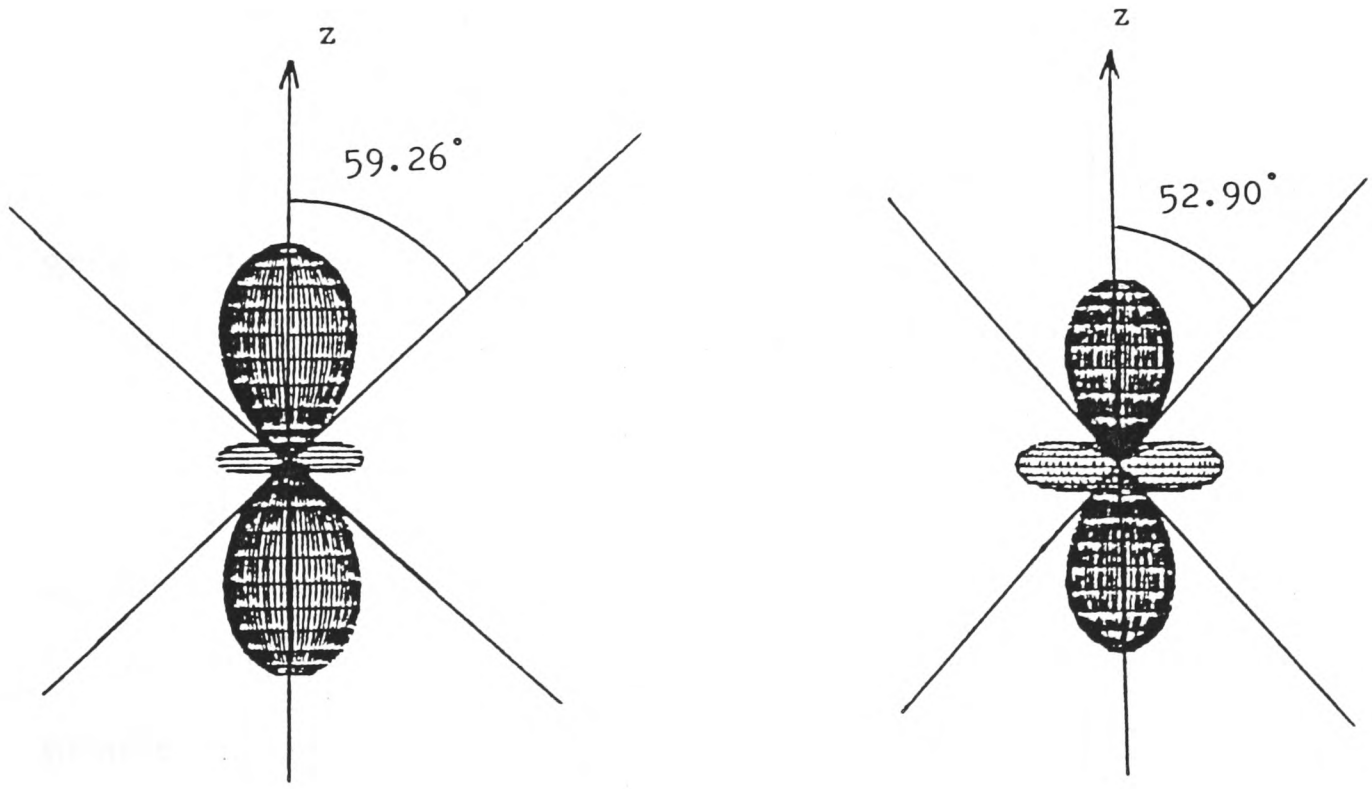
(b) hybrids (mixing of spd, sp or dp) whose nodal lines or planes coincide with the metal-ligand bond directions. In molecules belonging to C_{nv} point groups, where s, p_z and d_z2 belong to the a_1 irreducible representation a hybrid $s+\lambda p_z+\lambda" d_z2$ can be defined which has nodes in the ligand directions. Such a hybrid points towards the vacant co-ordination site of the polyhedron. In main group chemistry the hybrid is generally occupied by an electron pair, whereas in transition metal compounds it is generally vacant. This difference can be traced back to the relative energies of the valence orbitals, i.e. $|\alpha_s| > |\alpha_p| >> |\alpha_d|$ in the former and $|\alpha_d| > |\alpha_s| >> |\alpha_p|$ in the latter. All main group molecules that have a stereochemically active non-bonding orbital have geometries belonging to the C_{nv} point groups. Specific examples include NH_3 (C_{3v}), SF_4 (C_{2v}), PbO (C_{4v}) and BrF_5 (C_{4v}). For higher co-ordination molecules (n>3) the adoption of these C_{nv} geometries in preference to higher symmetries (more spherical geometries) also avoids the necessity of occupying a metal-ligand antibonding molecular orbital. For example,

in tetrahedral SH_4 molecule the additional electron pair would occupying a M-L σ antibonding molecular orbital which if $|\alpha_s| >> |\alpha_p|$ is of a_1 symmetry, and an out-of-phase combination of s and S^{σ}. Consequently, the T_d--->C_{2v} geometric distortion has the effect of converting an antibonding interaction into a non-bonding interaction. This is an important and ubiquitous driving force for geometric distortions not only in simple molecules but also in infinite solids.[30] However, the driving force is only a significant one if the highest occupied molecular orbital is strongly antibonding. If it is not then the greater stabilisation energy associated with the transformation of an antibonding into a non-bonding orbital does not out-weigh the greater destabilising ligand-ligand interactions which result from the lower symmetry structure.

As the co-ordination number increases the antibonding character of the s-S^{σ} molecular orbital becomes smaller and there are many examples of molecules with 6, 8 and 12 co-ordination which do not exhibit the stereochemical activity of the lone pair. Specific examples include $[SbX_6]^{3-}$ (X=Cl, Br or I); $[MX_6]^{2-}$ (M=Se or Te; X=Cl, Br or I) which have seven electron pairs but remain octahedral and $[XeF_8]^{2-}$ which has nine electron pairs and is square-antiprismatic. As Ng and Zuckerman[30] have noted the absence of a stereochemical effect with the lone pair orbital is particularly prevalent for infinite structures with high co-ordination numbers and octahedral, cubic or dodecahedral geometries. In such situations although the additional electron pair is occupying an s-S^{σ} antibonding orbital it is unlikely to be strongly antibonding if $|\alpha_s| >> |\alpha_p|$ and the β_s resonance integral is small because of the core like nature of the s orbital.

In the dihedral point groups s and p_z no longer have the same symmetry transformation properties and $s \pm \lambda d_z 2$ non-bonding hybrids

only can be generated. In the linear molecules (see Table 7.6) the hybrids concentrate density in the direction perpendicular to the metal-ligand bond directions. In the trigonal prism and the square antiprism the ligands lie near the cone of the hybrid. These hybrids which are obtained from equation (B-18) are illustrated in Figure 7.9.



$0.107s+0.994d_{z^2}$

(a)

$0.046s-0.999d_{z^2}$

(b)

Figure 7.9 The a_1 non-bonding orbital for a square antiprismatic transition metal ML_8 complex

Table 7.6 Non-bonding hybrids in dihedral point groups

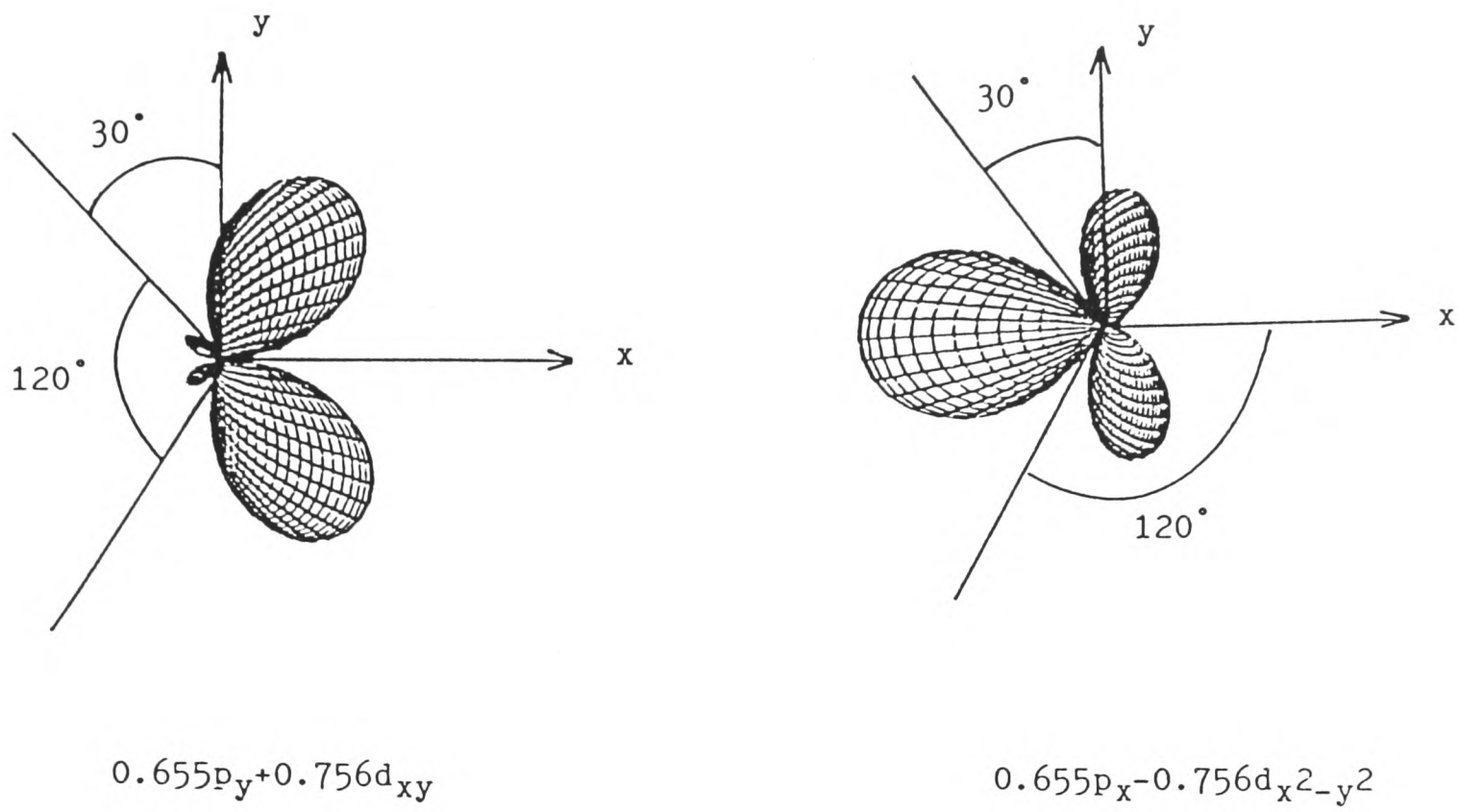
	$s \pm \lambda d_z 2$	$d_x 2_{-y} 2 \pm \lambda p_x$	$d_{xy} \pm \lambda p_y$
Linear ML_2	yes		
Trigonal planar ML_3	yes	yes	yes
Squrae planar ML_4	yes		
Trigonal bipyramidal ML_5		yes	yes
Trigonal prismatic ML_6	yes	yes	yes
Square antiprismatic ML_8	yes		

In finite dihedral point groups $d_x 2_{-y} 2$ and d_{xy} transform in the same manner as p_x and p_y and, for example, in trigonal planar and trigonal bipyramidal molecules hybrids of the type illustrated in Figure 7.10 are generated.

In the tetrahedral point group (d_{xz}, d_{yz}, d_{xy}) and (p_x, p_y, p_z) both transform according to the t_2 irreducible representation and generate three d-p hybrids which point towards the vertices of a cube not utilised by the tetrahedron (see Figure 7.11).

(c) The non-bonding orbitals are localised on the ligands when the number of ligand orbitals is larger than that of valence orbitals in the central atom, e.g. PF_5 and SF_6. This localisation limits the occurrence of such non-bonding orbitals to molecules with very electronegative ligands, e.g., F and O.

(d) π-localised non-bonding orbitals on the ligands can also occur, e.g. MnO_4^{2-} (T_d point group) since the 12 p orbitals in oxygen transform as $a_1+2t_2+e+t_1$ and the valence orbitals on the central atom as a_1+2t_2+e, t_1 are the π-localised non-bonding orbitals.



$0.655p_y+0.756d_{xy}$ $0.655p_x-0.756d_{x^2-y^2}$

Figure 7.10 The e pair of d-p hybrid non-bonding orbitals for the trigonal plannar and the trigonal bipyramidal molecules

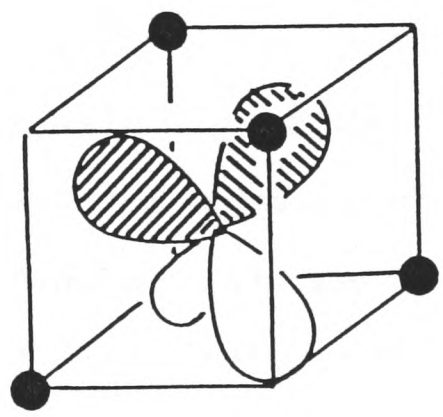


Figure 7.11 p_z-d_{xy} hybrid orbital in the tetrahedral point group

(5) The comparision between Figures 7.4 and 7.8 indicates that a filled non-bonding orbital(s) does exert a very strong stereochemical influence, when $|\alpha_s| > |\alpha_p|$. This stereochemical activity is associated with the redistribution of s and p electron density which accompanies the geometric distortion. Although the discussion above has focussed on the occurrence of non-bonding orbitals in molecular compounds it should be noted that the non-bonding character has been defined with respect to the σ-radial orbitals. Such non-bonding orbitals which have nodes in the metal-ligand directions are ideally suited for forming π-bonds with orbitals of the appropriate symmetry. These types of interactions are maximised when the non-bonding orbital has a minimal contribution from the s orbital. For example, in planar MX_3 the maximum π-bonding is achieved for the planar molecule which has a non-bonding p_z orbital on M rather than the pyramidal molecule where the non-bonding orbital is a s-p_z hybrid. The superior p_z-X_π ligand overlap integrals for the planar geometry reinforce this preference.

In transition metal complexes similar arguments apply to d-s hybrids, but d_{xz}-p_x hybrids can result in very favorable π-bonding effects between the metal and the ligand.

In molecules where m-n=2 there are, by the "n-m" rule , two non-bonding orbitals. These can be a degenerate e set resulting from the occurrence of an odd number of e representations in the point group. Alternatively the two non-bonding orbitals must belong to different irreducible representations. If they belonged to the same they would interact strongly especially since they have similar energies to produce a bonding and an antibonding orbital. In main group molecules with two non-bonding electron pairs the first is accommodated in an orbital of a_1 ($s+\lambda p_z+\lambda' d_z 2$) symmetry and the second in a p_y orbital orthogonal to the ligand plane. For example, OH_2, ClF_3 and XeF_4 all have planar

geometries which satisfy this condition, although in the latter example the first electron pairs occupies $s+\lambda d_z 2$ rather $s+\lambda p_z+\lambda' d_z 2$.

(6) Effects associated with the radial parts of the wavefunctions

The discussion presented above has emphasised the importance of the nodal characteristics of the molecular orbitals and many of the conclusions have depended on the assumption that $\beta_s \approx \beta_p \approx \beta_d$. This is a good approximation when the radial parts of the wavefunctions lead to comparable overlaps with the ligand orbitals, but for many real molecules this approximation begins to break down. For example, for a first row main group atom $\beta_s \approx \beta_p$ but for heavier atoms $|\beta_s| < |\beta_p|$ and this has important consequences for the geometries of molecules with stereochemically active lone pair. In particular there is more s character in the non-bonding orbital and the geometries show greater distortions. Furthermore, for molecules such as the inert gas molecules, XeF_2, XeF_4 and XeF_6, the s orbitals on the central atom are effectively core-like because of their high ionisation potential, i.e. $|\beta_s| << |\beta_p|$.

For transition metal atoms the nd, (n+1)s and (n+1)p valence orbitals have very different radial distribution functions. In particular the nd orbitals are much more contracted than (n+1)s and (n+1)p. Therefore, the nd orbitals do not overlap strongly with the ligand orbitals unless the metal-ligand distances are short. This is achieved either with small ligands, e.g. H, or ligands which form multiple bonds with the metal, e.g. CO, O or N. When the ligands do not overlap very strongly then the d orbitals approximate to non-bonding. Chemically this is reflected in the occurrence of high-spin and low-spin complexes and variable occupations of the d-manifold orbitals. In lanthanide complexes the 4f orbitals are also very contracted and almost core-like. Consequently, their overlap with ligands is small and they exert no stereochemical influence.

7.3 Non-bonding orbitals in hydrocarbons

7.3.1 Alternant Hückel hydrocarbons

A conjugated organic system is described as alternant if the atoms in it can be divided into two groups starred and unstarred in such a way that no two atoms of like parity, i.e. which belong to the same group, are directly linked. Some typical examples of even and odd alternant hydrocarbons are illustrated in Figure 7.12. When the number of atoms in the two sets differ, the more numerous set is call the starred set. Within the Hückel approximation such alternant systems having the following important properties which collectively are described as the Coulson-Rushbrooke Pairing Theorem.[19]

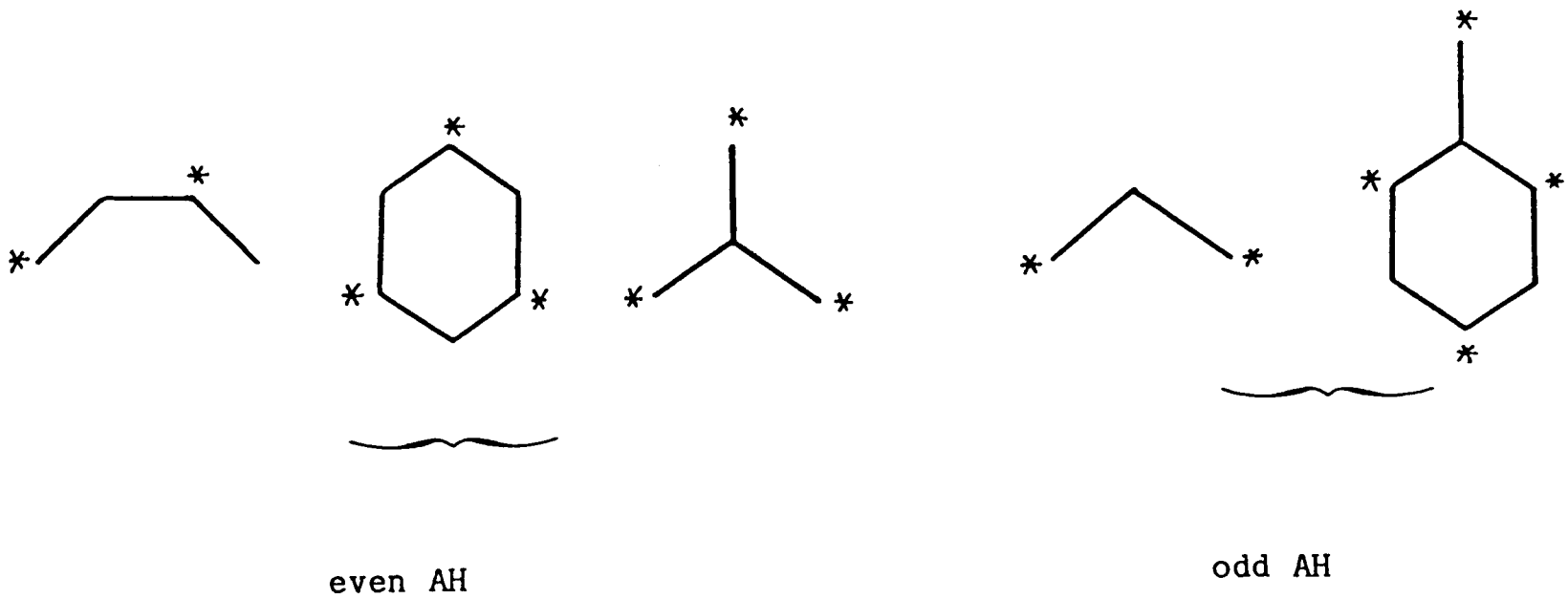


Figure 7.12 Some typical examples of even and odd alternant hydrocarbons

(1). The molecular orbitals of an even AH (AH, alternant hydrocarbon) occur in pairs with energies $\alpha \pm E_\mu$, α being the Coulomb integral for carbon.[15]

(2). If one of the MO's Φ_μ^+ of a pair (energy $\alpha+E_\mu$) is given by:

$$\Phi_\mu^+ = \sum_i^* a_{\mu i}^* \phi_i^* + \sum_j^o a_{\mu j}^o \phi_j^o$$

where ϕ_i^* is the p atomic orbital of a starred atom and ϕ_j^o that of an unstarred atom then the twin MO Φ_μ^- (energy $\alpha-E_\mu$) is given by:

$$\Phi_\mu^- = \sum_i^* a_{\mu i}^* \phi_i^* - \sum_j^o a_{\mu j}^o \phi_j^o$$

Therefore, the coefficients of the paired molecular orbitals are numerically the same, but the signs of one set of MO's is reversed in going from one MO to the other.

(3). In an odd AH where the total number of MO's is correspondingly odd, all but one of the MO's is paired as in (1) and (2) above. The odd MO has energy α and is confined to the starred atoms.

$$\Phi_O = \sum_i^* a_{Oi}^* \phi_i^*$$

These conclusions can also be interpreted in terms of the "m-n rule" developed above and are a direct consequence of the properties of the (B-1) matrix. The Pairing Theorem does not completely define the spectrum of molecular orbitals in an alternant hydrocarbon, because (1) is consistent with the presence of an even number of molecular orbitals. Whilst this might generally mean that the number of non-bonding molecular orbitals is 0, there are instances when there are 2, 4, etc. For example, both butadiene and cyclo-butadiene are even alternant hydrocarbons, but the former has no non-bonding molecular orbitals and the latter 2 (see Figure 7.13).

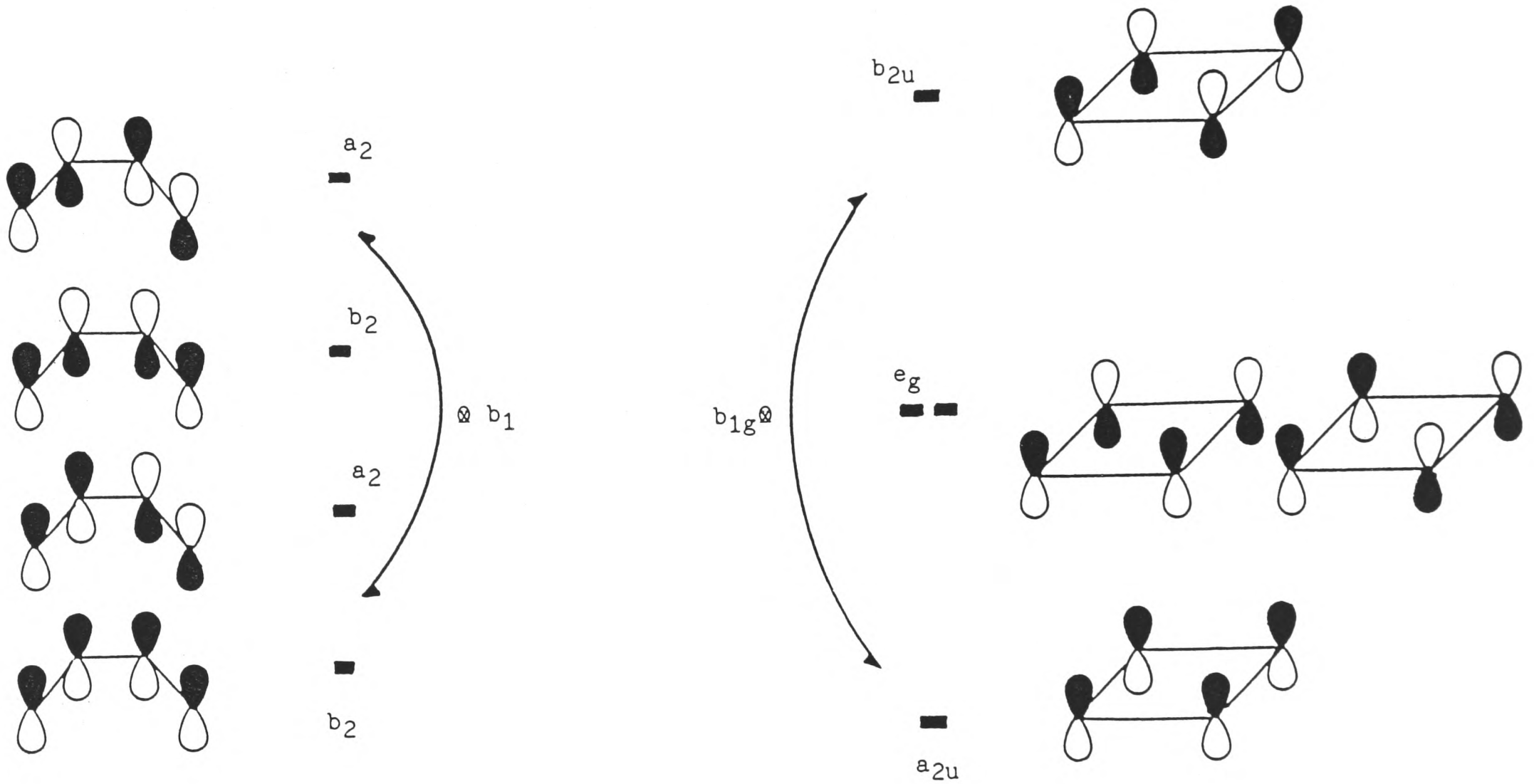


Figure 7.13 Molecular orbitals for cis-butadiene and cyclo-butadiene

Group theory can be used to resolve this distinction, because the sets of paired molecular orbitals defined above are related by specific symmetry relationships. If Φ_{μ}^{+} belongs to the irreducible representation Γ_{+} and Φ_{μ}^{-} belongs to the irreducible representation Γ_{-} they are related by the following direct products:

$$\Gamma_{+} = \Gamma_{A} \otimes \Gamma_{-}$$

$$\Gamma_{-} = \Gamma_{A} \otimes \Gamma_{+}$$

where Γ_{A} is a one dimensional representation which interconverts the starred and unstarred atomic positions. It has the character of +1 for those operations which merely interconvert the positions of starred atoms and -1 for those operations which interconvert starred and unstarred positions.

For example, for cis-butadiene (C_{2v} point group) Γ_{A} corresponds to the b_1 representation (the carbon atoms lie in the xz plane) and the paired molecular orbitals shown in Figure 7.13 are related in the following manner:

$$\Gamma_{-} = \Gamma_{A} \otimes \Gamma_{+}$$

$$\Gamma_{-} = b_1 \otimes b_2 = a_2$$

$$\Gamma_{-} = b_1 \otimes a_2 = b_2$$

Similarly for cyclo-butadiene (D_{4h} point group) Γ_{A} transforms according to the b_{1g} representation and the a_{2u} and b_{2u} bonding and antibonding molecular orbitals shown in Figure 7.13 are related by the following direct product:

$$b_{2u} = b_{1g} \otimes a_{2u}$$

For reasons which will be discussed below it is highly significant that the non-bonding molecular orbitals remain unaffected by the multiplication.

$$e_g = b_{1g} \otimes e_g$$

The Γ_A irreducible representation is not a characteristic of the point group, but reflects the symmetry transformation properties of the starred and unstarred atoms. For example, cis-butadiene and allyl, C_3H_5, both belong to the C_{2v} point group but $\Gamma_A=b_1$ for the former and $\Gamma_A=a_1$ for the latter. Indeed, in any molecule where there is an atom on the principal symmetry axis the Γ_A will correspond to the totally symmetric representation and the paired molecular orbitals will have the same symmetry transformation properties, i.e.

$$\Gamma_- = a_1 \otimes \Gamma_+ = \Gamma_+$$

The examples described above can be generalised to three distinct situations. We define the representations as conjugate when they are transformed by the representation, Γ_A, corresponding to the alternant operator, $\hat{A}$.

(a) Γ_- is always distinct from its conjugate Γ_+. Cis-butadiene provided an example of this behaviour.

(b) Γ_- is always self-conjugate with Γ_+. This occurs when Γ_A belongs to the totally symmetric representation, e.g. allyl.

(c) Some Γ_- are self-conjugate and some are not, e.g. cyclo-butadiene, where b_{2u} and a_{2u} are conjugate and e_g self-conjugate.

These symmetry considerations become highly significant when combined with the pairing theorem, because if the total number of irreducible representations spanned by the atomic basis functions contains an odd number of self-conjugate representations it has a set of non-bonding molecular orbitals equal to the sum of the degeneracies of the self-conjugate representations.

For example, cyclo-butadiene has two non-bonding molecular orbitals arising from the odd number of self-conjugate e_g representations and allyl has one non-bonding molecular orbital of a_2 symmetry deriving

from the odd number (1) of a_2 irreducible representations.

In benzene, the alternant operator, $\hat{A}$, corresponds to the b_{1u} representation, and the paired molecular orbitals shown in Figure 7.14 are related by the following direct products:

$$\Gamma_{-} = \Gamma_{A} \otimes \Gamma_{+}$$

$$b_{2g} = b_{1u} \otimes a_{2u}$$

$$e_{2u} = b_{1u} \otimes e_{g}$$

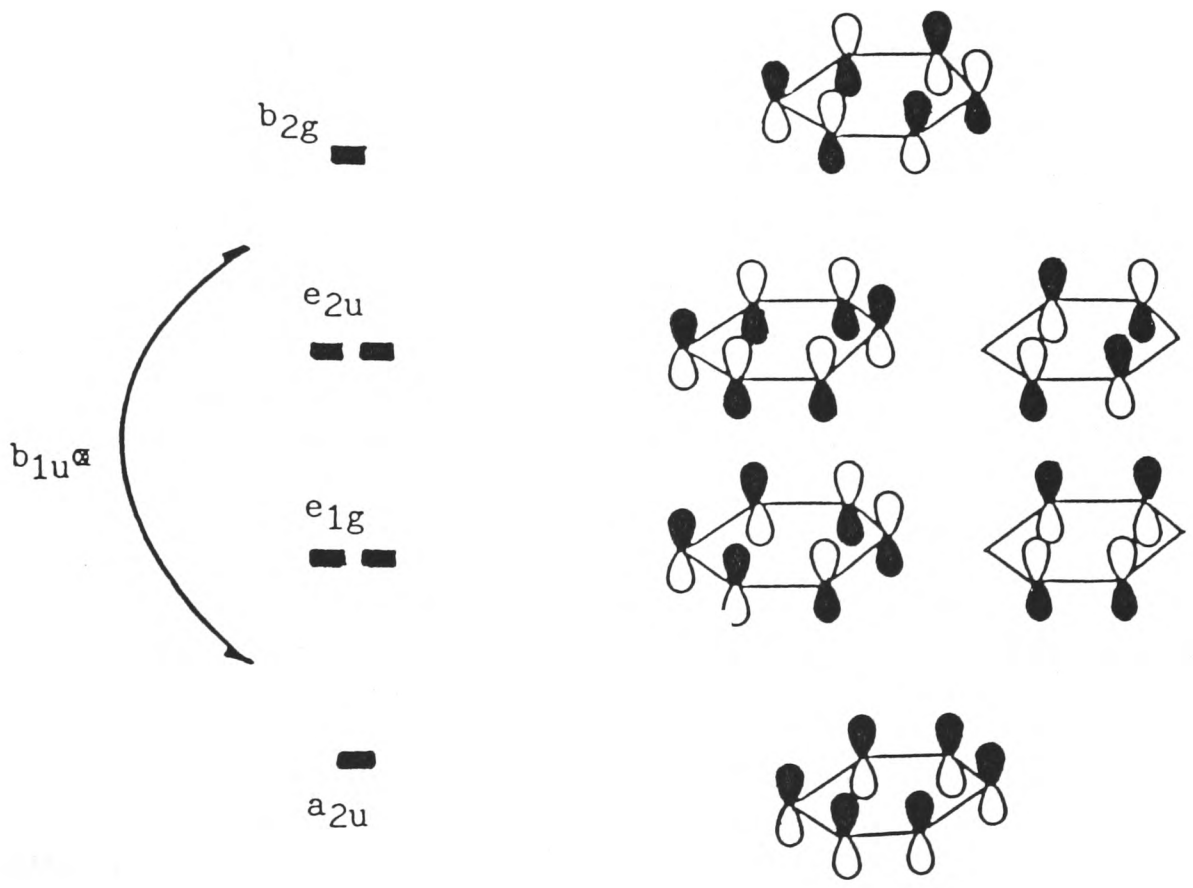


Figure 7.14 Molecular orbitals for benzene

There are no self-conjugate molecular orbitals and therefore no non-bonding molecular orbitals. Without labouring the point it is clear that the pairing theorem together with alternant symmetry operator relationships define the 4n+2 Hückel rule for cyclic delocalisation.

7.3.2 Alternant Möbius hydrocarbons

Alternant Möbius hydrocarbons conform to the pairing theorem even though the topology of the orbital interactions is different. The molecular orbitals of a Möbius ring of π-orbitals are analysed using the double group $C_n \otimes R$, because the n successive $2\pi/n$ and twists of π/n of the p_π basis functions result in $\phi_1 \rightarrow -\phi_1$ after a rotation of 2π, and $\phi_1 \rightarrow \phi_1$ after a total rotation of $4\pi(720°)$. For an even Möbius system the p_π functions generate E′, E", E"′,..., representations, where the total number of E representations is equal to n/2. For example, for Möbius cyclo-butadiene E′ and E" and Möbius benzene E′, E", E"′. The alternant operator $\hat{A}$ transforms as B in this pseudo-cyclic group and leads to the following relationships:

Möbius	Möbius
cyclo-butadiene	cyclo-benzene
$E'' = B \otimes E'$	$E'''= B \otimes E'$
	$E'' = B \otimes E''$
no self-conjugate representations	E" self-conjugate representation

Consequently, the requirement that non-bonding orbitals be either completely filled or empty leads to the Möbius 4n rule for cyclic delocalisation.

The combination of Hückel and Möbius generalisations can be utilised to restate the Woodward-Hoffmann rules,[31] in a manner that has been popularised by Zimmermann.[32]

7.4 Non-bonding orbitals in cluster compounds

Three dimensional polyhedral molecules such as the borane anions, $B_nH_n^{2-}$, are characterised by a total of n+1 skeletal electron pairs or 4n+2 valence electrons in total.[33] The isolobal analogy between the BH and ML_3 fragments has provided a theoretical relationship between the borane and the transition metal cluster compounds.[34] A detailed analysis of the molecular orbitals of deltahedral transition metal clusters showed that they also have a total of n+1 bonding skeletal molecular orbitals, which is the same as that in the borane clusters, and 6n orbitals that are either non-bonding or involved in the metal-ligand bonding. Therefore, such clusters are characterised by 14n+2 valence electrons in total.

It is apparent that deviations from the above electron counts in cluster compounds result from an occurrence of skeletal non-bonding orbitals. The skeletal non-bonding orbitals arise either from topological factors associated with deltahedral geometries or the presence of missing vertices in nido- and arachno- structures.

7.4.1 Expansion of the cluster skeletal molecular orbitals in terms of the Tensor Surface Harmonic functions

The skeletal molecular orbitals are generated from basis sets with $0(\sigma)$ and $1(\pi)$ nodes with respect to a radial vector passing through the atoms.

For a basis set of σ orbitals, the LCAO expansions take a form that is exactly the same as the expansion for ligand σ-orbitals, i.e.

$$\psi_{LM}^{\sigma} = L_M^{\sigma} = N \sum_i C_{LM}(\theta_i,\varphi_i)\, \sigma_i \qquad \text{(D-1)}$$

For a basis set of π-orbitals, the LCAO expansions are derived from the sets of π_i^{θ} and π_i^{φ} orbitals which are defined in Figure 1.4. The even parity functions have the following form:

$$\psi_{LM}^{\pi} = L_M^{\pi} = N \sum_i [V_{LM}^{\theta}(\theta_i,\varphi_i)\pi_i^{\theta} + V_{LM}^{\varphi}(\theta_i,\varphi_i)\pi_i^{\varphi}] \qquad \text{(D-2)}$$

For M>0 the real forms of the Vector Surface Harmonics $V_{LMs}^{\theta,\varphi}/V_{LMc}^{\theta,\varphi}$ are used and listed in Table 1.2. The corresponding odd parity wavefunctions $\bar{\psi}_{LM}^{\pi}$ ($\bar{L}^{\pi}$) are related to ψ_{LM}^{π} (L^{π}) by a 90° anticlockwise rotation of the tangential vectors (π_i^{θ}, π_i^{φ}) about the radial vector, at each vertex. Therefore, the wavefunctions of $\bar{L}^{\pi}$ have the following form:

$$\bar{\psi}_{LM}^{\pi} = \bar{L}_M^{\pi} = N \sum_i [V_{LM}^{\varphi}(\theta_i,\varphi_i)\pi_i^{\theta} - V_{LM}^{\theta}(\theta_i,\varphi_i)\pi_i^{\varphi}] \qquad \text{(D-3)}$$

Stone[35] showed that for deltahedral clusters the L^{π} MOs are generally bonding. The $\bar{L}^{\pi}$ MOs are, therefore, generally antibonding, since the parity inversion operation leads to a reversal of the bonding properties of L^{π} and $\bar{L}^{\pi}$. He used the methodology of Tensor Surface Harmonic theory to derive the n+1 skeletal electron pair rule for deltahedral boranes. Each of the n BH fragments possesses one σ-type sp hybrid, yielding nL^{σ} MOs in total, one of which (S^{σ}) is strongly bonding because it possesses no angular nodes. In addition each fragment has two π-type p orbitals which generate nL^{π} bonding and $n\bar{L}^{\pi}$ antibonding cluster orbitals. Mixing between L^{σ} and L^{π} orbitals with the same L values results in one bonding combination and one antibonding combination for every matched pair of L^{σ}/L^{π} orbitals. In total, therefore, there are n+1 cluster bonding MOs (S^{σ} and nL^{σ}/L^{π}) since there is no S^{π} orbital.

7.4.2 Pairing principle and group theoretical aspects

Stone[35] has shown how every bonding overlap is converted to an antibonding overlap by the parity operation, and vice versa. Thus in the absence of σ–π interaction, there would be a mirror relationship between the energies of the L^{π} and $\bar{L}^{\pi}$ orbitals. This is the pairing principle in TSH theory. Even after σ–π interactions are allowed for it has been shown that an approximate pairing persists in the frontier orbital region.[36] As with the discussion above for coordination compounds, this pairing principle is particularly useful for defining the non-bonding orbitals in cluster compounds especially when combined with the group theoretical aspects of the problem.

In terms of irreducible representations the symmetry of an L^{π} set is converted to that of the $\bar{L}^{\pi}$ set by multiplication by the odd-parity pseudo-scalar representation Γ_u°:[37]

$$\Gamma(\bar{L}^{\pi}) = \Gamma(L^{\pi}) \otimes \Gamma_u^{\circ}$$

Γ_u° is a one dimensional representation with characters +1 under proper rotations and -1 under improper rotations.

Fowler [36] has elegantly demonstrated that for the point groups C_i, C_s, C_{2v}, $D_{(2n+1)d}$, C_{nh}, $S_{(4n-2)}$, D_{nh}, T_h, O_h, I_h and R_{3h} $\Gamma(L^{\pi})$ is always distinct from its conjugate $\Gamma(L^{\pi})$. In contrast in the point groups C_n, D_n, T, O and I, $\Gamma(L^{\pi})$ and $\Gamma(\bar{L}^{\pi})$ are always self-conjugate.

Therefore, in the vast majority of deltahedral clusters which belong to these point groups the total representation $\Gamma_{\pi+\bar{\pi}}$ splits into two distinct sub-shells and there are n bonding and n antibonding molecular orbitals. Since such boranes also have a single radial bonding molecular orbital belonging to the totally symmetric representation they are characterised by a total of n+1 skeletal electron pairs or 4n+2 valence electrons in total.

However, in the point groups $C_{nv}(n>2)$, S_{4n}, D_{2nd} and T_d only some of the L^{π} combinations are self-conjugate. Using reasoning similar to that developed above for co-ordination compounds it can be demonstrated that if $\Gamma_{\pi+\bar{\pi}}$ contains an odd number of self-conjugate e representations then the deltahedron will have a non-bonding e set and the polyhedron will be associated with either n or n+2 skeletal electron pairs.

7.4.3 Non-bonding orbitals in closo deltahedral and three-connected cluster compounds

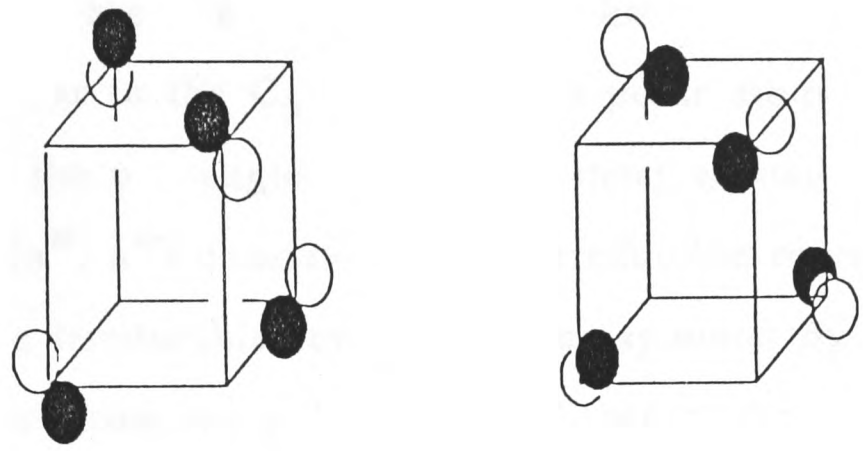
As indicated above, the irreducible representations spanned by the L^{π} and $\bar{L}^{\pi}$ tangential molecular orbitals in closo deltahedral clusters may contain an odd number of self-conjugate representations. For example, for the tetrahedron Γ_u^o transforms as a_2, and the $\Gamma_{\pi+\bar{\pi}}$ tangential molecular orbitals span the representations $t_1 + e + t_2$.

$$\Gamma(\bar{L}^{\pi}) = \Gamma_u^o \otimes \Gamma(L^{\pi})$$

$$t_1 = a_2 \otimes t_2$$

$$e = a_2 \otimes e$$

There is an odd number of self-conjugate e representations and the tetrahedron has a non-bonding e set. The relevant e set of non-bonding orbitals for the tetrahedron is illustrated in Figure 7.15. The two components of the e set are related by the parity operation, P, i.e., a local rotation of 90° in the same sense and are therefore self-conjugate. Since they can be equally well defined as D^{π} or $\bar{D}^{\pi}$ molecular orbitals they must be non-bonding if $\beta^{\sigma}=\beta^{\pi}$.



parity related e pair

Figure 7.15 The e non-bonding molecular orbitals in the tetrahedral cluster

A general group theoretical criterion, based on the pairing principle in TSH theory, has been presented by Fowler[36] and Johnston and Mingos.[38] Fowler concluded that an odd number of self-conjugate e representations in closo deltahedral clusters arise in two cases:

(1) T or T_d clusters with an odd number of sets of four equivalent cage atoms;

(2) C_m or C_{3m}($m \geq 3$) clusters with an odd number of cage atoms on the C_m-axis.

Subsequently, Johnston and Mingos [38] pointed out that it is not geometrically feasible to have a closo-deltahedron with an odd number of cage atoms on the C_m axis with $m>3$, because square, pentagonal and higher faces would be generated. They found that for deltahedra, the occurrence of an odd number of self-conjugate representations occurs as a

consequence of there being one atom on each C_3 rotation axis of a polyhedron belonging to one of the point groups C_3, C_{3v}, T or T_d. These clusters are defined as polar deltahedra with 3p+1 cluster vertices. In such clusters there are p triangles of symmetry related atoms lying in planes perpendicular to the C_3 axis and one polar atom lying on the C_3 axis. For each of the p triangles of the symmetry related atoms the linear combinations of (π^{θ}, π^{φ}) consist of two e irreducible representations. The total number of e irreducible representations spanned by L^{π} and $\bar{L}^{\pi}$ are 2p plus one e pair from the polar atom. Therefore they are characterised by n skeletal bonding molecular orbitals and one e set of non-bonding orbitals and have n or n+2 skeletal electron pairs. Examples illustrating the above conclusion are the tetrahedral clusters (p=1: B_4Cl_4 with n skeletal electron pairs; C_4R_4 with n+2 pairs), capped octahedron (p=2: $Os_7(CO)_{21}{}^{39}$ with n skeletal electron pairs) and the 10-atom metalloborane $[H(PPh_3)(Ph_2PC_6H_4IrB_9H_8)]$ (p=3: with n skeletal electron pairs).[40]

The three-connected cluster compounds are characterised by a total of 3n/2 skeletal electron pairs which correspond to the localisation of each electron pair on an edge of the polyhedron. Johnston and Mingos[41] have shown that in these polyhedra there are (n/2)+2 strongly skeletal bonding molecular orbitals and n-2 approximately non-bonding skeletal molecular orbitals. The latter correspond to a weakly bonding set of (n/2-1)L^{π} MOs, and by the pairing principle an equal number of weakly antibonding $\bar{L}^{\pi}$ MOs. These non-bonding orbitals are not a consequence of an odd number of e representations since most of the three-connected clusters belong to the D_{nh} point groups. In all the prismatic three-connected polyhedra the irreducible representations spanned by the L^{π} and $\bar{L}^{\pi}$ tangential molecular orbitals are always distinguished from each

other and are not self-conjugate. In the prismatic structures, Johnston and Mingos noted that the non-bonding nature of these orbitals arise as a consequence of being antibonding within the upper and lower layers of atoms and bonding across the equator or vice versa. They found that $D^{\pi}_{\pm1}(e'')$ orbitals are non-bonding for a trigonal prism, $D^{\pi}_{\pm1}(e'')$ and D^{π}_{2c} orbitals for a cube, $D^{\pi}_{\pm1}(e''_1)$ and $F^{\pi}_{\pm2}(e''_2)$ for a pentagonal prism and so on. More generally, for a prismatic cluster with n=2k atoms we conclude that when k=odd $D^{\pi}_{\pm1}$, $F^{\pi}_{\pm2}$, $G^{\pi}_{\pm3}$, ..., $\Lambda^{\pi}_{\pm(\Lambda-1)}$ ($\Lambda=L_{max}$) and their counterparts $\bar{L}^{\pi}$ make a total of n-2 approximately non-bonding orbitals. When k=even $D^{\pi}_{\pm1}$, $F^{\pi}_{\pm2}$, $G^{\pi}_{\pm3}$, ..., $\Lambda^{\pi}_{\pm(\Lambda-1)}$, $\Lambda^{\pi}_{\Lambda c}$ ($\Lambda=L_{max}$) and their counterparts $\bar{L}^{\pi}$ again make a total of n-2 approximately non-bonding orbitals.

7.4.4 Non-bonding orbitals in nido structures

The TSH theory is based on a free electron model derived from the solution of the Schrödinger equation for a particle on a sphere. The grossly non-spherical nature of a nido structure means that their skeletal molecular orbitals are no longer adequately described in terms of the equations (D-1), (D-2) and (D-3). However, it is possible to describe them in terms of the wavefunctions of the parent structure. For example, the skeletal molecular orbitals of a nido square pyramidal cluster can be expressed in terms of those of an octahedron. The correlation diagram for the skeletal molecular orbitals of an octahedron and a square pyramid are illustrated in Figure 7.16. It can be seen that P^{π}_{0}, D^{π}_{2s}, $\bar{D}^{\pi}_{2s}$ and $\bar{P}^{\pi}_{0}$ are the same for both structures. Three e tangential molecular orbitals result from the mixings of $D^{\pi}_{\pm1}$, $\bar{D}^{\pi}_{\pm1}$, $P^{\pi}_{\pm1}$ and $\bar{P}^{\pi}_{\pm1}$ of the octahedron. The L^{π} and $\bar{L}^{\pi}$ molecular orbitals of an octahedron are illustrated in Figure 7.17. The two π atomic orbitals at position 1 of an octahedron (π^{θ}_{1}, π^{φ}_{1})

can be expressed in terms of linear combinations of $D^{\pi}_{\pm1}$, $D^{\pi}_{\pm1}$, $P^{\pi}_{\pm1}$ and $P^{\pi}_{\pm1}$ using a localisation procedure developed by Mingos and Hawes:[11]

$$\pi_1^{\theta} = 1/2(P^{\pi}_{1c} + D^{\pi}_{1c} - \bar{P}^{\pi}_{1s} - \bar{D}^{\pi}_{1s})$$
$$\pi_1^{\varphi} = 1/2(\bar{P}^{\pi}_{1c} + \bar{D}^{\pi}_{1c} + P^{\pi}_{1s} + D^{\pi}_{1s})$$

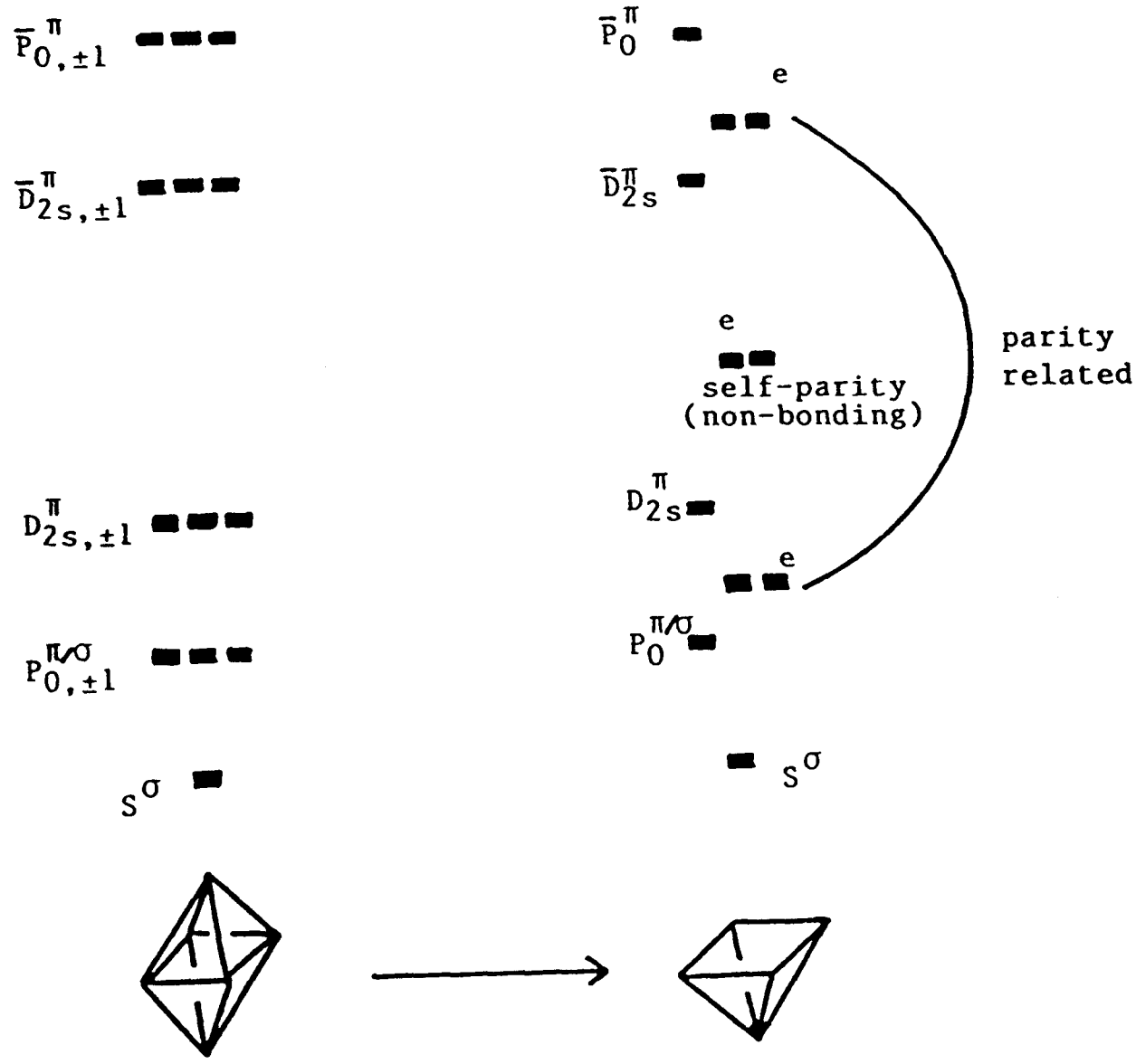


Figure 7.16 The correlation diagram for the skeletal molecular orbitals of an octahedral and a square pyramidal cluster compound

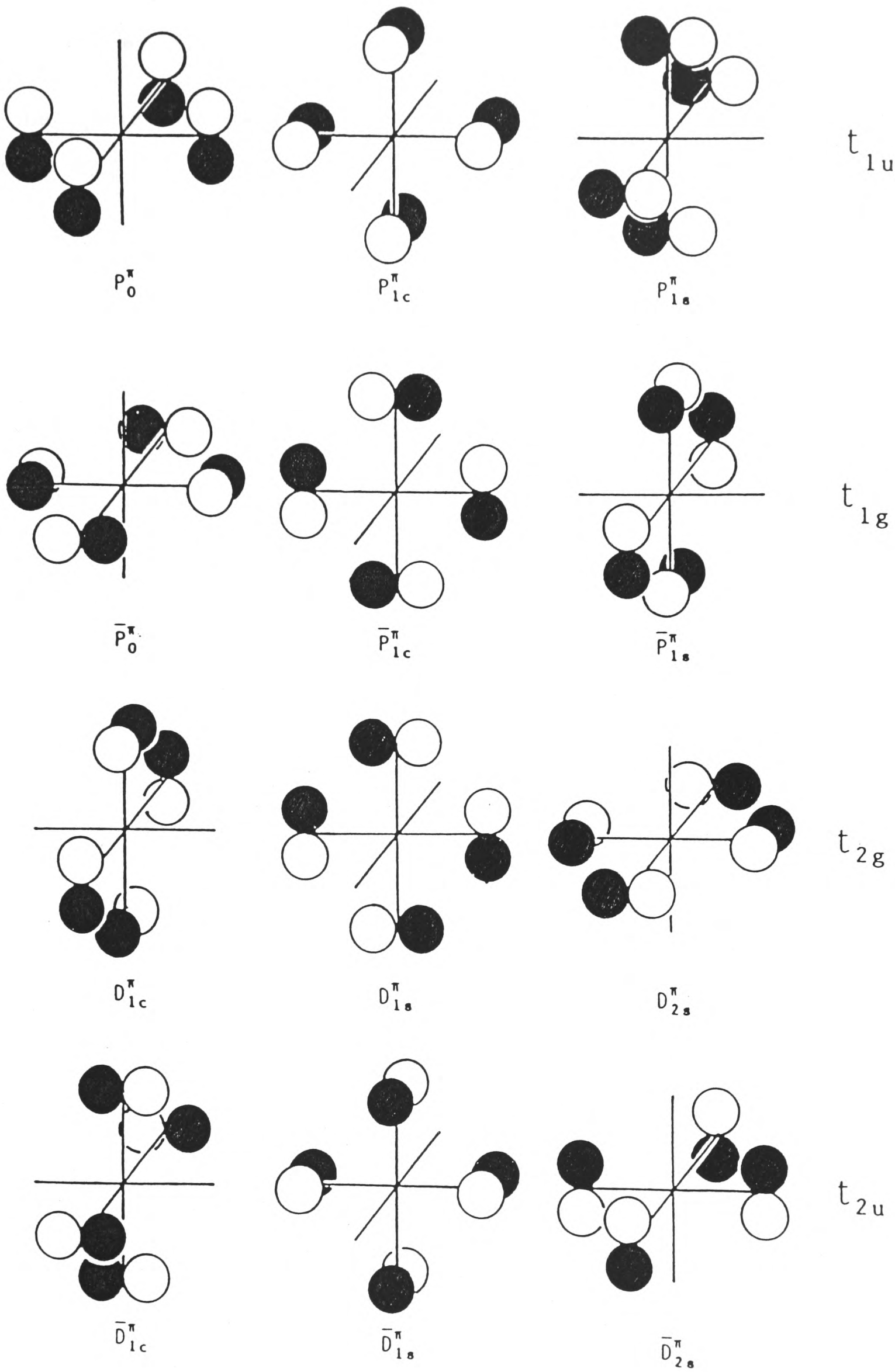


Figure 7.17 The L^{π} and $\bar{L}^{\pi}$ molecular orbitals of an octahedral cluster

In the square pyramidal cluster, the interaction between the remaining three e sets gives rise to one e bonding, one e antibonding and one e non-bonding according to the **pairing principle.**

The expressions for π_1^{Θ} and π_1^{Φ} in terms of the octahedral $L^{\pi}/\bar{L}^{\pi}$ wavefunctions show that the π-tangential skeletal molecular orbitals of a nido structure can be described in terms of the TSH expressions for the parent closo structure.

In coordination compounds, ML_n, a non-bonding orbital that is a linear combination of atomic orbitals on the central atom was defined by using the quantum mechanical requirement that it has zero overlap with ligands. A similar method can be developed for the generation of the tangential non-bonding skeletal molecular orbitals for a nido cluster. In the pyramidal structure, one atom lies on the polar position and the remaining in the equatorial plane. Such a structure has an odd number of e irreducible representations and therefore a self-conjugate $L^{\pi}/\bar{L}^{\pi}$ non-bonding e set. Generally a nido structure is characterised by a total of n+2 skeletal electron pairs, with the e set of non-bonding orbitals. Vector harmonics defining the e non-bonding orbitals in the pyramidal structure can be generated by using the following quantum mechanical requirements.

(1) This e set of non-bonding orbitals is a linear combination of $L^{\pi}_{1s,1c}$ and $\bar{L}^{\pi}_{1s,1c}$.

(2) Symmetry restrictions limit the mixing to occur only between L^{π}_{1s} and $\bar{L}^{\pi}_{1c}$, or L^{π}_{1c} and $\bar{L}^{\pi}_{1s}$.

(3) The mixing between L^{π}_{1s} and $\bar{L}^{\pi}_{1c}$ occurs in equal amount, i.e., the wavefunctions of the non-bonding orbitals have the form $\sum_L c_L(L^{\pi}_{1c}+\bar{L}^{\pi}_{1s})$ because the energy of the non-bonding orbital coincides with the mid-point of the energies of L^{π} and

$\bar{L}^{\pi}$ in the Hückel approximation.

From (D-2), (D-3) and the requirements above

$$\psi^{\pi}_{\pm1}(\text{non-bonding}) = N \sum_i [V^{\theta}_{\pm1(non)}(\theta_i,\varphi_i)\, \pi^{\theta}_i + V^{\varphi}_{\pm1(non)}(\theta_i,\varphi_i)\, \pi^{\varphi}_i]$$

where

$$V^{\theta}_{\pm1(non)} = c_1(p^{\theta}_{\pm1}+\bar{p}^{\theta}_{\pm1}) + c_2(d^{\theta}_{\pm1}+\bar{d}^{\theta}_{\pm1})$$
$$V^{\varphi}_{\pm1(non)} = c_1(p^{\varphi}_{\pm1}+\bar{p}^{\varphi}_{\pm1}) + c_2(d^{\varphi}_{\pm1}+\bar{d}^{\varphi}_{\pm1})$$

In a real form,

$$\psi^{\pi}_{1c,1s}(\text{non-bonding}) = N\sum_i [V^{\theta}_{1c,1s(non)}(\theta_i,\varphi_i)\pi^{\theta}_i + V^{\varphi}_{1c,1s(non)}(\theta_i,\varphi_i)\pi^{\varphi}_i] \qquad \text{(D-4)}$$

and

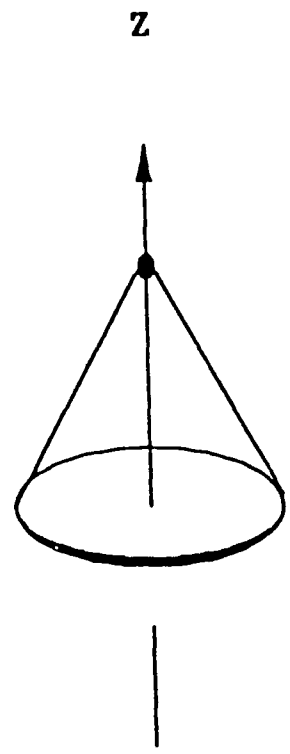
$$V^{\theta}_{1s(non)} = c_1(p^{\theta}_{1s}+\bar{p}^{\theta}_{1c}) + c_2(d^{\theta}_{1s}+\bar{d}^{\theta}_{1c})$$
$$V^{\varphi}_{1s(non)} = c_1(p^{\varphi}_{1s}+\bar{p}^{\varphi}_{1c}) + c_2(d^{\varphi}_{1s}+\bar{d}^{\varphi}_{1c}) \qquad \text{(D-5)}$$

The 1c components can be obtained in a similar way. Inserting the wavefunctions of Table 1.2 into (D-5), we have:

$$V^{\theta}_{1s(non)} = [c_1(\cos\theta+1) + c_2(3)^{1/2}(\cos2\theta+\cos\theta)]\sin\varphi$$
$$V^{\varphi}_{1s(non)} = [c_1(\cos\theta+1) + c_2(3)^{1/2}(\cos2\theta+\cos\theta)]\cos\varphi$$

The wavefunction generated from the above vector harmonics (V^{θ}_{1s},V^{φ}_{1s}) is the 1s component of the e non-bonding orbital which has an orbital energy of α in a nido structure such as that shown in (7). This is true for all c_1/c_2 ratios because the L^{π} and $\bar{L}^{\pi}$ coefficients are equal. The vector can be expressed in the following form:

$$[f(\theta)\sin\varphi,\ f(\theta)\cos\varphi]$$



(7)

where $f(\theta)=c_1(\cos\theta+1)+c_2(\cos2\theta+\cos\theta)$. When θ is defined, e.g., for the equatorial ring, the vector is $c(\sin\varphi, \cos\varphi)$. The relevant vector diagram is illustrated in Figure 7.18. Similarly the 1c component is $[-f(\theta)\cos\varphi, f(\theta)\sin\varphi]$ which relates to the 1s component by the parity relationship. Therefore, the 1s and 1c components are a pair of self-conjugate vector harmonics.

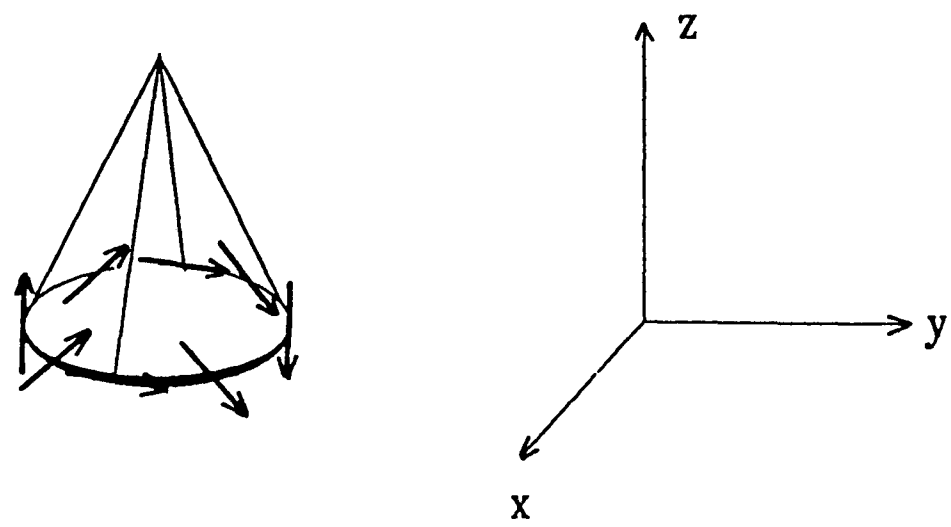


Figure 7.18 The vector for describing the non-bonding orbital in a *nido* structure as shown in (7)

As the c_1/c_2 ratio is defined, the relative coefficients of the polar atom and the equatorial atoms can be determined. This can be achieved by defining some boundary conditions. The non-bonding orbital can be defined by considering the relevant secular determinant for the e representations. The three relevant e_{1s} components for a square pyramid are shown in Figure 7.19. The secular determinant for the three e_{1s} components is:

$$\begin{array}{c|ccc|} & e_{1s}^{(1)} & e_{1s}^{(2)} & e_{1s}^{(3)} \\ e_{1s}^{(1)} & \alpha - E & \beta' & \beta' \\ e_{1s}^{(2)} & \beta' & \alpha - E & 0 \\ e_{1s}^{(3)} & \beta' & 0 & \alpha - E \end{array} = 0$$

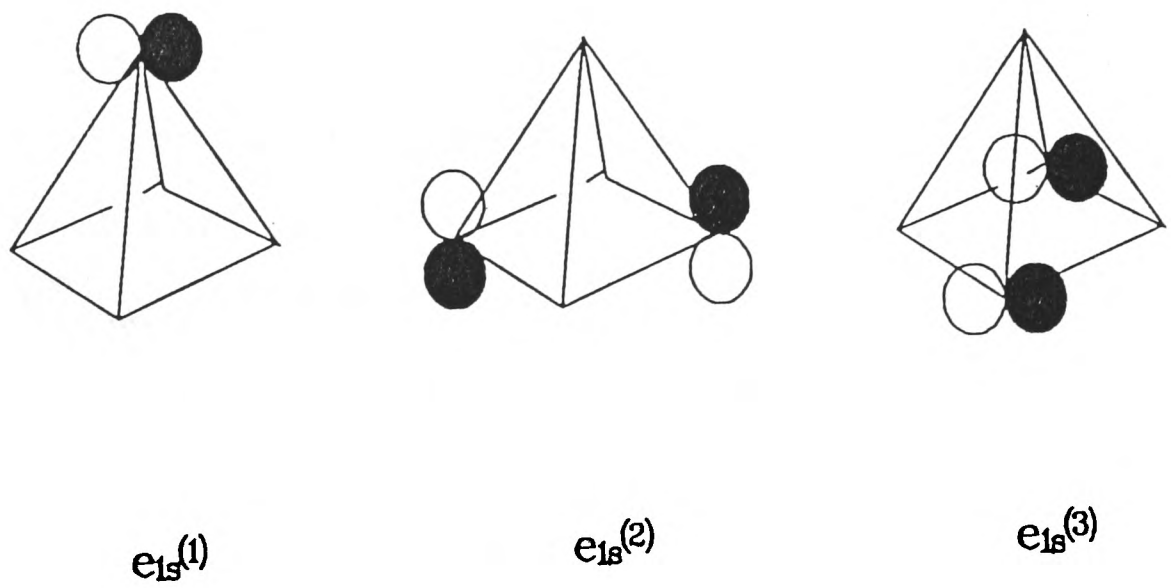


Figure 7.19 The three e_{1s} components for a square pyramidal cluster

where β' indicates the resonance integral between $e_{1s}^{(1)}$ and $e_{1s}^{(2)}$ (or $e_{1s}^{(1)}$ and $e_{1s}^{(3)}$, the assumption of $\beta^{\sigma}=\beta^{\pi}$ has been made). Comparing the above determinant with (B-1), it can be concluded that the non-bonding orbital with an orbital energy of α is localised on the equatorial atoms. Therefore, the assumption that $V^{\theta}_{1s(non)}=V^{\varphi}_{1s(non)}=0$ when $\theta=0$ can be made. However, when the number of atoms in the equatorial ring is increased the above assumption is invalid since the energies of the corresponding $e_{1s}^{(2)}$ and $e_{1s}^{(3)}$ components are not equal to α. The determinant now is:

$$\begin{array}{c|ccc|} & e_{1s}^{(1)} & e_{1s}^{(2)} & e_{1s}^{(3)} \\ e_{1s}^{(1)} & \alpha - E & \beta' & \beta' \\ e_{1s}^{(2)} & \beta' & \alpha+\Delta - E & 0 \\ e_{1s}^{(3)} & \beta' & 0 & \alpha-\Delta - E \end{array} = 0$$

For example $\Delta=\beta$ for a hexagonal planar structure. The corresponding non-bonding orbitals are no longer localised on the equatorial atoms. Fortunately, the open face in most nido clusters contains 4 or 5 atoms. Therefore, the assumption can be taken as an approximate boundary condition. Under this assumption, $c_1/c_2 = -(3)^{1/2}$ and the following results are obtained:

$$\begin{aligned} V^{\theta}_{1s(non)} &= (1-\cos 2\theta)\sin\varphi \\ V^{\varphi}_{1s(non)} &= (1-\cos 2\theta)\cos\varphi \end{aligned} \qquad \text{(D-6)}$$

In a similar way, the 1c components are:

$$\begin{aligned} V^{\theta}_{1c(non)} &= -(1-\cos 2\theta)\cos\varphi \\ V^{\varphi}_{1c(non)} &= (1-\cos 2\theta)\sin\varphi \end{aligned} \qquad \text{(D-7)}$$

The equations (D-6) and (D-7) are a pair of self-conjugate vector

harmonics. The vector harmonics ($V^{\theta}_{1s(non)}$, $V^{\varphi}_{1s(non)}$) in (D-6) are illustrated in Figure 7.18. The 1c component can be obtained by a rotation of the p^{π} orbitals in Figure 7.18 through 90° about the +z axis. A specific example illustrating how the vector harmonics are used to define the non-bonding e_{1s} component for a square pyramid based on the vector diagram is illustrated in Figure 7.20. The important point to emphasise with this e set is that the π^{θ} and π^{φ} components contribute equally and the parity relationship interconverts the e components. This ensures the non-bonding character of this molecular orbital. The effect of the parity relationship is illustrated in Figure 7.20.

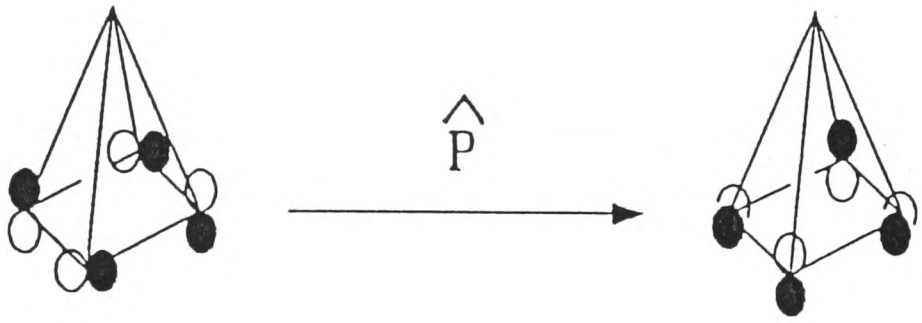
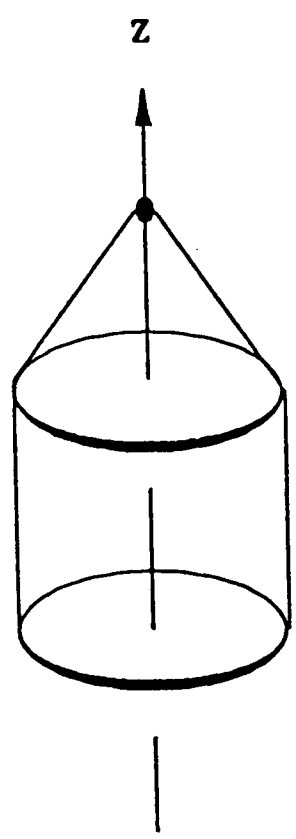


Figure 7.20 The parity related e non-bonding orbitals in a square pyramidal cluster

When the nido structure has three layers of atoms (8), the $f^{\pi}_{\pm 1}$ functions are involved in the non-bonding orbitals since the $F^{\pi}_{\pm 1}$ skeletal molecular orbitals are generated in the parent closo structure. In a similar way, the vector harmonics ($V^{\theta}_{1s(non)}$, $V^{\varphi}_{1s(non)}$) have the following linear combinations:



(8)

$$V^{\theta}_{1s(non)} = c_1(p^{\theta}_{1s}+\bar{p}^{\theta}_{1c}) + c_2(d^{\theta}_{1s}+\bar{d}^{\theta}_{1c}) + c_3(f^{\theta}_{1s}+\bar{f}^{\theta}_{1c})$$

$$V^{\varphi}_{1s(non)} = c_1(p^{\varphi}_{1s}+\bar{p}^{\varphi}_{1c}) + c_2(d^{\varphi}_{1s}+\bar{d}^{\varphi}_{1c}) + c_3(f^{\varphi}_{1s}+\bar{f}^{\varphi}_{1c})$$

Inserting the wavefunctions in Table 1.2 into above equations, we obtain:

$$V^{\theta}_{1s(non)} = \{c_1(\cos\theta+1) + (3)^{1/2}c_2(\cos2\theta+\cos\theta) + (3/8)^{1/2}c_3[\cos\theta(15\cos^2\theta-11)+(5\cos^2\theta-1)]\}\sin\varphi$$

$$V^{\varphi}_{1s(non)} = \{c_1(\cos\theta+1) + (3)^{1/2}c_2(\cos2\theta+\cos\theta) + (3/8)^{1/2}c_3[\cos\theta(15\cos^2\theta-11)+(5\cos^2\theta-1)]\}\cos\varphi$$

Again, the above vector can be expressed as $[f(\theta)\sin\varphi, f(\theta)\cos\varphi]$. Therefore the vector in each ring has the same definition as that in Figure 7.18. Consequently the non-bonding character within each ring is retained. As above for a pyramidal structure, the assumption that $V^{\theta}_{1s(non)}=V^{\varphi}_{1s(non)}=0$ when $\theta=0$ is made again. Another condition is

that when $\theta=90°$, i.e. the equatorial plane between the two rings in (8), $V^{\theta}_{1s(non)}=V^{\varphi}_{1s(non)}=0$. This implies that the vectors in the hemispheres above and below the equatorial plane change their signs. The sign changes ensure a zero overlap of the tangential orbitals between the two rings and retains their non-bonding character. The π^{θ} components have positive overlaps, whereas the π^{φ} components have negative overlaps. The total overlap is zero under the assumption of $\beta(\sigma)=\beta(\pi)$. This cancellation is illustrated schematically in Figure 7.21. Therefore, we have the following equations:

$$c_1 + (3)^{1/2}c_2 + (6)^{1/2}c_3 = 0$$
$$c_1 - (3)^{1/2}c_2 - (6)^{1/2}/4c_3 = 0$$

Solving the above equations, we obtain:

$$c_1:c_2:c_3 = (27/32)^{1/2}:(25/32)^{1/2}:(-1)$$

The final expressions for $V^{\theta}_{1s(non)}$ and $V^{\varphi}_{1s(non)}$ are:

$$V^{\theta}_{1s(non)}=\cos\theta\sin^2\theta\sin\varphi$$
$$V^{\varphi}_{1s(non)}=\cos\theta\sin^2\theta\cos\varphi \qquad \text{(D-8)}$$

The constant in front of the $\cos\theta$ term in the equation above has been ignored since it depends on the normalisation condition. The relevant vector diagram is illustrated in Figure 7.21. The 1c components have the following form:

$$V^{\theta}_{1c(non)} = -\cos\theta\sin^2\theta\cos\varphi$$
$$V^{\varphi}_{1c(non)} = \cos\theta\sin^2\theta\sin\varphi \qquad \text{(D-9)}$$

In summary, the non-bonding e orbitals for nido structures of the type illustrated in (7) or (8) can be obtained from equations (D-4), (D-6) and (D-7) or (D-4), (D-8) and (D-9).

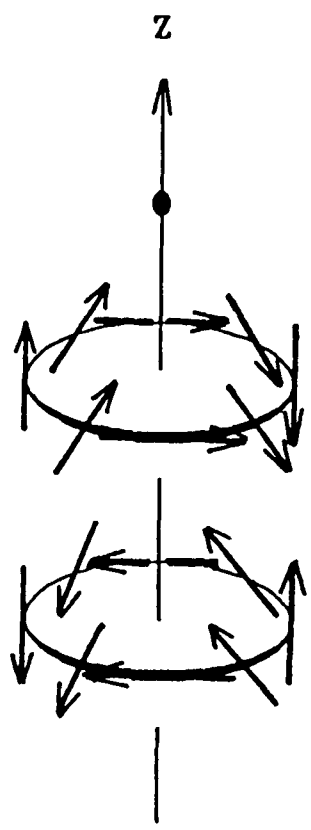


Figure 7.21 The vector for describing the non-bonding orbital in a *nido* structure as shown in (8)

An example illustrating the vector (D-8) to define the e_{1s} component of the e non-bonding orbitals for a capped- square antiprism is shown in Figure 7.22. The non-bonding orbital has the following form according to equation (D-8):

$$\psi_{non}(1s) = 0.353(p_{\varphi 1}-p_{\varphi 3}) + 0.353(p_{\theta 2}-p_{\theta 4}) + 0.250[(-p_{\theta 5}-p_{\varphi 5})+(-p_{\theta 6}+p_{\varphi 6})+(p_{\theta 7}+p_{\varphi 7})+(p_{\theta 8}-p_{\varphi 8})]$$

From an extended Hückel molecular orbital calculation on $[B_9H_9]^{4-}$, this component is:

$$\psi_{non}(1s) = 0.120(p_{\varphi 1}-p_{\varphi 3}) + 0.230(p_{\theta 2}-p_{\theta 4}) + 0.275[(-p_{\theta 5}-p_{\varphi 5})+(-p_{\theta 6}+p_{\varphi 6})+(p_{\theta 7}+p_{\varphi 7})+(p_{\theta 8}-p_{\varphi 8})] - 0.478p_{\varphi 9} + L^{\sigma} \text{ and H contributions}$$

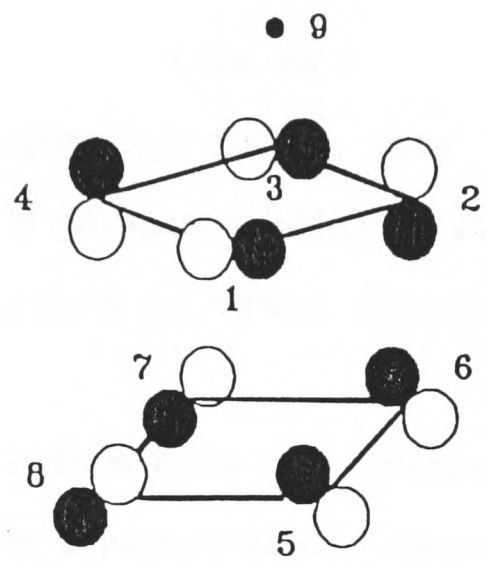


Figure 7.22 The e_{1s} component of the e non-bonding orbitals in a capped square antiprismatic cluster

The above result indicates that there is a contribution from the polar atom in the non-bonding orbitals. This is due to a mixing between L^{σ} and L^{π}. It also means that the assumption of a zero vector in the polar position is not strictly valid. However, the sign of p_{θ} and p_{φ} is exactly matched between both results. Particular striking is the fact that the character contributed from those atoms in the open face is very close in both results.

The methodology developed above can also be used in those polar deltahedral clusters with 3p+1 vertices which have one e set of non-bonding orbitals. Consequently the vector diagram in Figure 7.21 can be used to define the mixing between $L^{\pi}_{\pm 1}$ and $\bar{L}^{\pi}_{\pm 1}$ functions.

The mathematical aspects developed above can be summarised as follows. Whenever a <u>nido</u> polyhedron with C_{nv} ($n \geq 3$) symmetry is

generated from a closo deltahedron it will have a non-bonding e set of molecular orbitals. This e set is localised predominately on the open face of the polyhedron and the π^{Θ} and π^{Φ} components conform to the vector diagrams shown in Figures 7.18 and 7.21. If this e set is filled then the nido polyhedron is characterised by n+2 skeletal electron pairs.

The localisation of this e set on the open face of the polyhedron has two important consequences: firstly, they can be stabilised by overlap with the 1s orbitals of protons leading to the nido boranes B_nH_{n+4}, and secondly they can be used as donor orbitals to transition metals to form closo metalloboranes.

If the nido polyhedron does not belong to a C_{nv} ($n \geq 3$) point group there will no longer be a non-bonding self-conjugate degenerate e set, but a pair of non-degenerate but parity related orbitals, which are approximately non-bonding. For example, for nido $[B_8H_8]^{4-}$ which is generated from a tricapped trigonal prism by the removal of a capping atom there is a frontier orbital set of b_1 and b_2 symmetry which are illustrated in Figure 7.23.

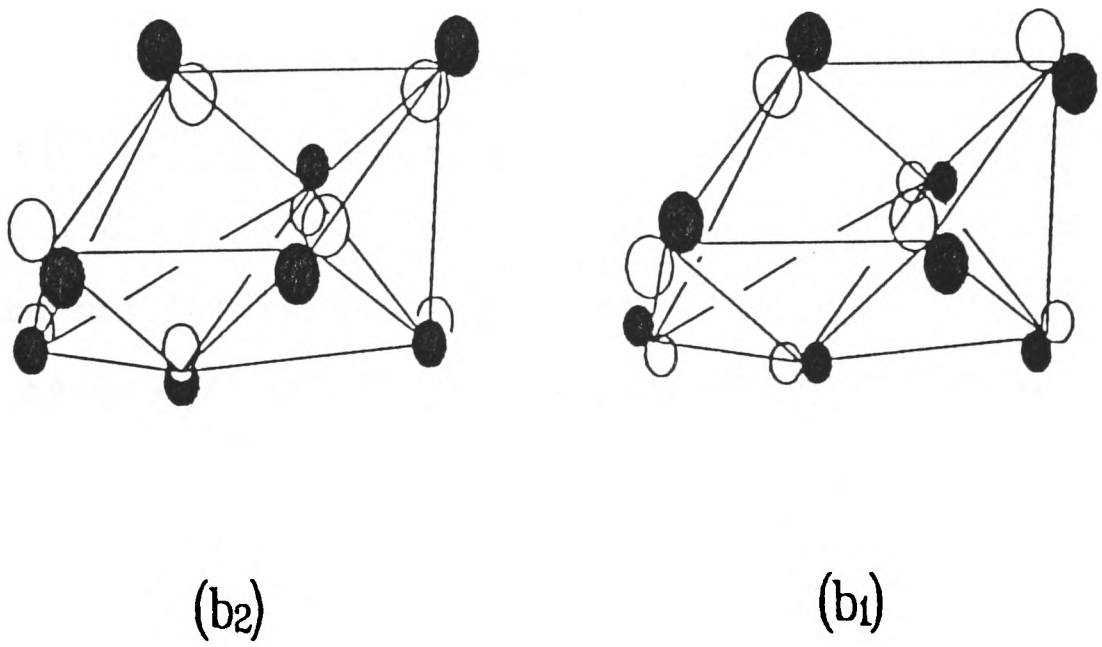
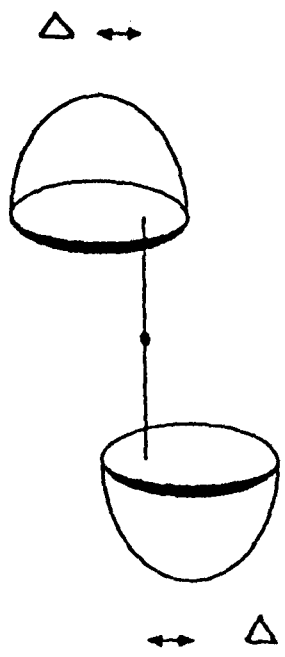


Figure 7.23 The parity related b_1 and b_2 frontier orbitals for a bicapped trigonal prismatic cluster

The relationship between closo $B_nH_n^{2-}$ which have spherical deltahedral structures and nido $B_nH_n^{4-}$ which have C_{nv} structures based on closo $B_{n+1}H_{n+1}^{2-}$ with a missing vertex is reminiscent of that noted previously for MX_n molecules with n electron pairs (spherical deltahedral) and those with n+1 electron pairs which are based on MX_{n+1} polyhedra. In each case the more open C_{nv} structure results in the occupation of a non-bonding orbital in preference to an antibonding orbital in the parent spherical molecule. For MX_n the choice of a C_{nv} structure is required by the necessity of creating a $s+ap_z+bd_z2$ hybrid of a_1 symmetry which is noded in the M-X directions. For $B_nH_n^{4-}$ the C_{nv} geometry forces L^{π} and $\bar{L}^{\pi}$ components with e symmetry to mix to create an e pair of non-bonding tangential molecular orbitals. In the former case there are an odd number of a_1 orbitals and in the latter an odd number of e representations in the $L^{\pi}/\bar{L}^{\pi}$ set.

In sandwich compounds and metallocarboranes an alternative distortion mode is observed which converts an antibonding orbital into a non-bonding orbital. This distortion has been described as a "slip" distortion [42-43] and involves the mutual displacement of the rings or nido polyhedra shown in (9). The manner in which the antibonding character of the d_{xz}-$e_1^{\pi}(x)$ molecular orbital is reduced is illustrated schematically in Figure 7.24. Particularly noteworthy is the manner in which the nodal cones of the metal and ligand orbitals move out of coincidence and thereby reduce their overlap.

Once again it should be emphasised that these distortions will only observed when the initial orbital in the symmetrical structure is strongly antibonding. For example, first row metallocenes, e.g. $Co(\eta\text{-}C_5H_5)_2$ [44] and $Ni(\eta\text{-}C_5H_5)_2$ [45] do not show such distortions, but second and third row examples where the metal-ring overlaps are larger do, e.g. $Ru(\eta^6\text{-}C_6Me_6)(\eta^4\text{-}C_6Me_6)$. [46]



(9)

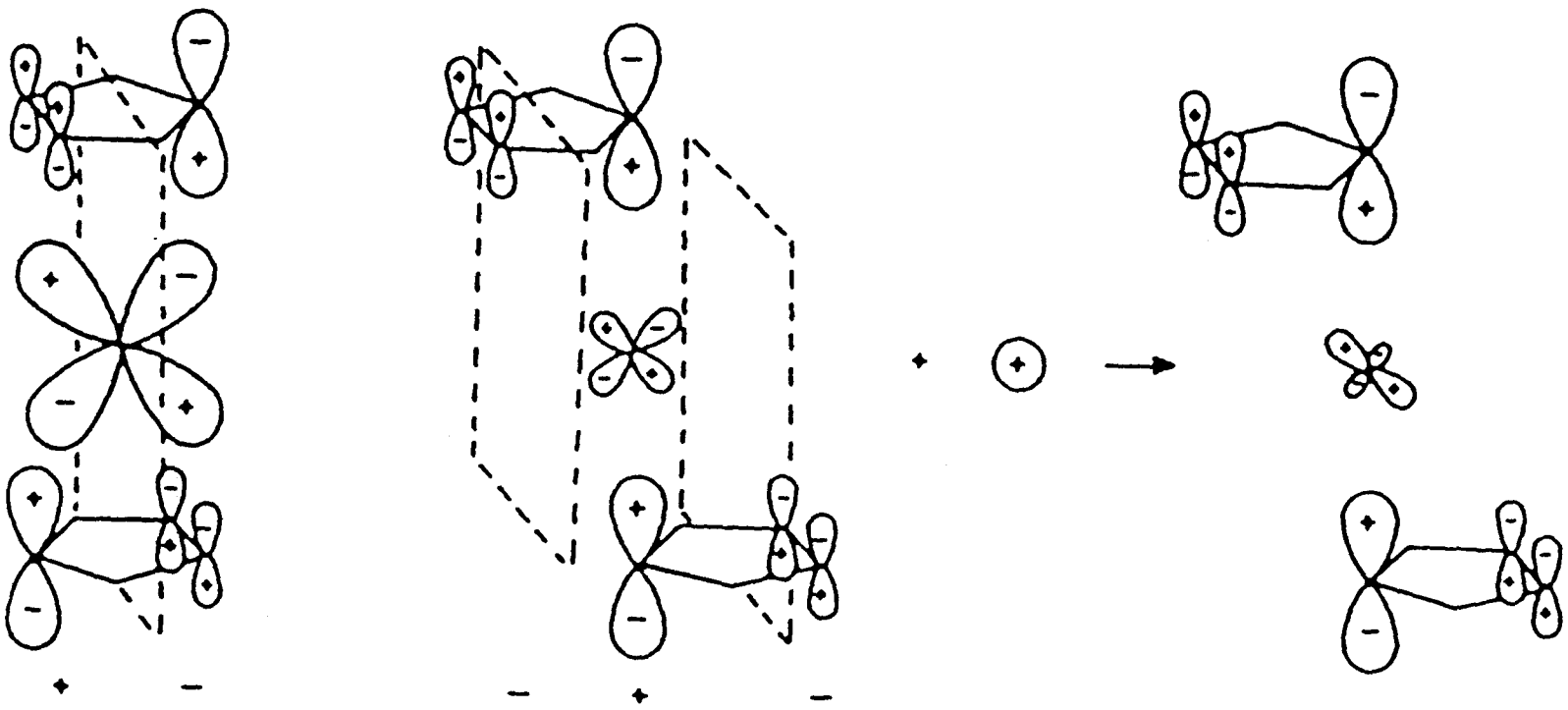


Figure 7.24 The antibonding character of the d_{xz}-$e_1^{\pi}(x)$ molecular orbital in sandwich compounds

In an arachno structure generated by the removal of trans vertices of closo deltahedron the highest point group symmetry that can be achieved is D_{nd}. On each open face a non-bonding e set is generated by a removal of a single vertex. Therefore, the removal of two trans vertices simultaneously generates e_1 and e_3 (D_{4d}) and e_{1g} and e_{1u} (D_{5d}) parity related and approximately non-bonding molecular orbitals. If these orbitals are fully occupied the arachno polyhedron is associated with n+3 skeletal electron pairs. When the two open faces in an arachno structure are adjacent, the symmetry of the cluster is usually C_{2v}. The two e sets in fact transform as $2b_1+2b_2$. Therefore, the L^{π} and $\bar{L}^{\pi}$ molecular orbitals mix extensively but remain approximately non-bonding.

7.5 Summary

The discussion presented above has demonstrated that non-bonding orbitals play an important role in determining the stereochemistries and closed shell requirements of both co-ordination and cluster compounds. In group theoretical terms, whenever there are an odd number of irreducible representations a non-bonding orbital is generated which is either localised exclusively on the central atom, or the peripheral atoms and has nodal characteristics which lead to a zero or minimal overlap with the remaining atoms in the structure.

The structure adopted by a molecule will always try and maximise the number of electron pairs in bonding molecular orbitals. A structure that is able to accommodate electron pairs in non-bonding orbitals will always be preferred to a more symmetrical structure which results in the population of antibonding molecular orbitals. For main group molecules where more than one structure is possible with the same number of non-

bonding orbitals, the one that maximises the character of the most stable atomic orbital is preferred. For example, both planar and pyramidal NH_3 have a non-bonding orbital but the latter has a higher percentage s character and therefore is preferred.

The analysis of non-bonding orbitals presented above provides a basis for understanding some of the important structural similarities between main group molecules and polyhedral compounds. The structures of these two classes of compounds are summarised in matrix form in Figures 7.25 and 7.26. For main group molecules ML_n, these arise when the total number of valence electron pairs is n, and for polyhedral molecules $B_nH_n^{2-}$ when the total number of skeletal electron pairs is n+1. The occurrence of a common structural basis for both classes of molecules is initially rather surprising since the shapes of main group molecules are generally interpreted using the Valence Shell Electron Pair Repulsion Model,[5-7] which emphasises electron-electron repulsion terms, whereas the shapes of polyhedral molecules are interpreted within a molecular orbital framework. However, it is possible to reconcile the structures using the Tensor Surface Harmonic Theory[35] and the Complementary Electron Density Model.[10-12]

The Complementary Spherical Electron Density Model recognises the essential spherical nature of the majority of coordination compounds. In particular the linear combinations of ligand σ orbitals are expressed in terms of a scalar harmonic expansion with each linear combination defined by L and M quantum numbers. A closo ML_n molecule generates S, P and D in its total of n linear combinations, n L_M^{σ}'s. The interaction between these n L_M^{σ} ligand orbitals and the atomic orbitals on the central atom results in, when $n \geq m$ (where m is the number of atomic orbitals on the central atom), m bonding and n-m non-bonding (localised on the

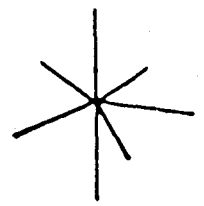
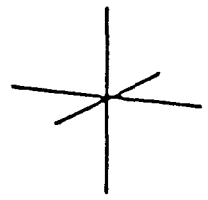
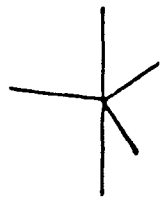
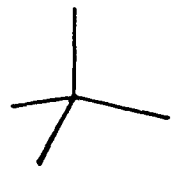
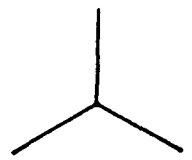
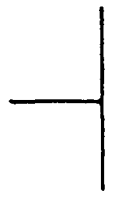
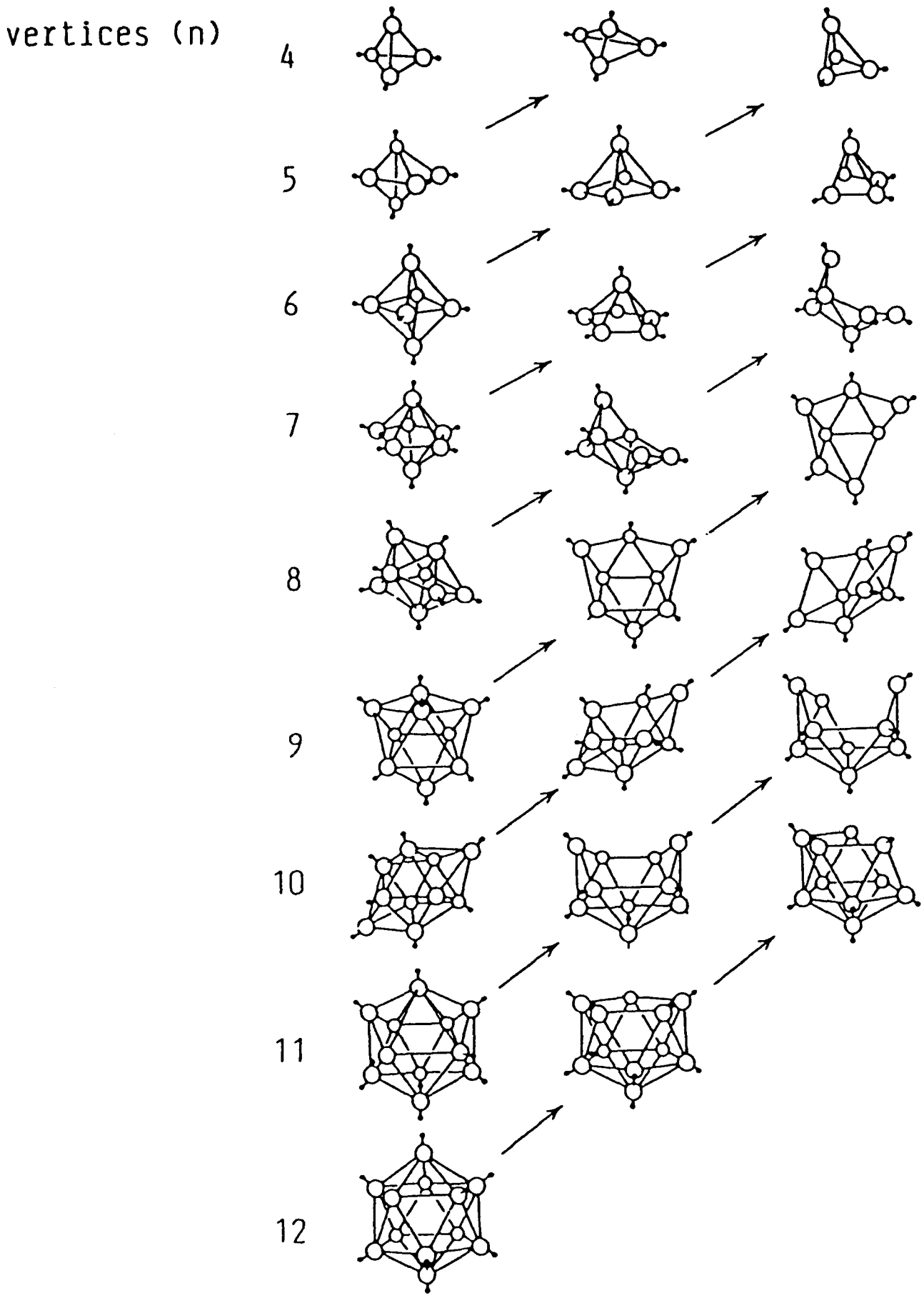
no. of valence electron pairs \ n	7	6	5	4	3	2
closo n	 IF_7	 SF_6	 PF_5	 CH_4	 BF_3	 BeF_2
nido n+1			 BrF_5	 SF_4	 NH_3	 SO_2
arachno n+2				 XeF_4	 ClF_3	 SeH_2

Figure 7.25 Structure-valence electron pair correlation for <u>closo</u>, <u>nido</u> and <u>arachno</u> main group molecules ML_n



Geometry	closo	nido	arachno
No. of SEP's	(n+1)	(n+2)	(n+3)

Figure 7.26 Structure-skeletal electron pair correlation for closo, nido and arachno boranes

ligands) orbitals. The occupation of these bonding and non-bonding orbitals leads to a closed shell of n valence electron pairs. The deltahedral coordination geometries not only provide a means of maximising the separations between the electron pairs, but also provide a set of S, P and D functions which correspond to the atomic orbitals on the central atom.

In a nido co-ordination compound, one ligand, and consequently one σ ligand orbital, is lost from the parent deltahedral closo structure. If the missing vertex lies on the principal axis, the missing σ orbital belongs to the a_1 representation. This results in the presence of odd number of a_1 representations in the system. Therefore, one non-bonding orbital, localised primarily on the central atom, is generated. In the arachno structures, two non-bonding orbitals are generated. These two non-bonding orbitals belong to different irreducible representations and thereby retain their orthogonality. Therefore, n, n+1 and n+2 valence electron pairs in the closo, nido and arachno main group molecules (see Figure 7.25) are related to the fact that the molecules can be represented by a particle on a sphere model and the orthogonality relationships necessary for generating non-bonding orbitals.

For cluster compounds where the tangential bonding predominates, it is necessary to take into account the vector surface harmonic solutions to the particle on a sphere problem. In a closo $B_nH_n^{2-}$ cluster molecule, n L^{σ} radial and 2n π tangential skeletal molecular orbitals are generated. The 2n π tangential orbitals are divided into n L^{π} bonding and n $\bar{L}^{\pi}$ antibonding skeletal molecular orbitals. When the mixing between L^{σ} and L^{π} (L^{π}/L^{σ}) is taken into account, n+1 (S^{σ} and n L^{π}/L^{σ}) skeletal bonding orbitals are generated. The deltahedral structures are adopted because they provide the best coverage of the spherical surface and

thereby stabilise the delocalised bonding molecular orbitals most effectively.

Two and four tangential nonbonding orbitals are generated for nido and arachno molecules respectively since each B-H fragment provides two tangential orbitals for skeletal bonding. The odd number of e molecular orbitals in nido clusters result in na non-bonding e set. In arachno clusters, the odd number of two different irreducible e (e.g e_1 and e_3) sets occurs, and results in two non-bonding e sets. Therefore, the closo, nido and arachno cluster molecules are characterised by n+1, n+2 and n+3 skeletal electron pairs (see Figure 7.26).

References for Chapter Seven

1. G.N.Lewis, Valence and the Structure of Atoms and Molecules, Chemical Catalogue Co., New York 1923; Reprinted by Dover publications, New York 1966
2. L.Pauling, Nature of the Chemical Bond, 3rd Ed., Cornell University Press, Ithaca, New York 1960
3. L.Pauling, *Proc. Nat. Acad. Sci. USA.*, **72**, 4200(1975); **73**, 274,1403(1976)
4. H.A.Bent, *Chem. Rev.*, **61**, 275(1961)
5. N.V.Sidgwick and H.E.Powell, *Proc. Roy. Soc. London*, **A176**, 153(1940)
6. R.J.Gillespie and R.S.Nyholm, *Quart. Rev.*, **11**, 339(1957)
7. R.J.Gillespie, Molecular geometry, Van Nostrand-Reinhold, Princeton, New Jersey 1972
8. C.J.Ballhausen and H.B.Gray, Molecular Orbital Theory, W.A.Benjamin, New York 1964
9. R.S.Mulliken, *J. Chem. Phys.*, **23**, 1833, 1841, 2338, 2343(1955)
10. D.M.P.Mingos and J.C.Hawes, *J. Chem. Soc., Chem. Commun.*, 991(1985)
11. D.M.P.Mingos and J.C.Hawes, *Structure and Bonding*, **63**, 1(1985)
12. D.M.P.Mingos, *Pure & Appl. Chem.*, **59**, 145(1987)
13. R.L.Johnston and D.M.P.Mingos, *Theor. Chim. Acta.* **75**, 11(1989)
14. R.A.Horn and C.R.Johnson, Matrix Analysis, Cambridge University Press 1985
15. D.H.Rouvray, Chemical Application of Graphy Theory, A.T.Balaban (Ed.), Chapter 7, Academic Press, London, New York 1976

16. I.Gutman,and N.Trinajstic, *Topics in Current Chemistry*, **42**, 49(1973)

17. (a) H.C.Longuet-Higgins, *J. Chem. Phys.*, **18**, 265(1953)
(b) M.J.S.Dewar, *J. Amer. Chem. Soc.*, **74**, 3341, 3345, 3350, 3353, 3355, 3357(1952)

18. D.Cvetkovic, I.Gutman,and N.Trinajstic, *Croat. Chim. Acta.*, **44**, 365(1972)

19. C.A.Coulson and S.Rushbrooke, *Proc. Camb. Phil. Soc.*, **36**, 193(1940)

20. D.M.P.Mingos and Lin Zhenyang, *J. New. Chem.*, **12**, 787(1988)

21. S.C.Abrahams, A.P.Ginsberg and K.Knox, *Inorg. Chem.*, **3**, 558(1964)

22. D.L.Keppert, Inorganic Sterochemistry, Spring-Verlag, Berlin Heidelberg, New York 1982

23. (a) E.L.Mutterties and R.A.Shunn, *Quart. Rev., Chem. Soc.*, **20**, 245(1966)
(b) E.L.Mutterties and L.J.Guggenberger, *J. Amer. Chem. Soc.*, **96**, 1748(1974)

24. (a) J.K.Burdett, Molecular Shapes, John Wiley & Sons, New York 1980
(b) T.A.Albright, J.K.Burdett and M.H.Wangbo, Orbital Interactions in Chemistry, John Wiley & Sons, New York 1985

25. J.P.Lowe, Quantum Chemistry, Academic Press, New York, San Francisco, London 1978

26. R.E.Ballard, Photoelectron Spectroscopy and Molecular Orbital Theory, Adam Hilger Ltd., Bristol 1978

27. S.Aung, R.M.Pitzer and S.I.Chan, *J. Chem. Phys.*, **49**, 2071(1968)

28. W.Kutzelnigg, *Angew. Chem. Int. Ed. Engl.*, **23**, 272(1984)

29. D.M.P.Mingos and Lin Zhenyang, *Structure and Bonding*, in press

30. J.-W.Ng and J.J.Zuckerman, *Adv. Inorg. Chem. Radiochem.*, **29**, 297(1985)

31. R.B.Woodward and R.Hoffmann, The Conservation of Orbital Symmetry, Academic Press, New York 1970

32. H.E.Zimmerman, *Acc. Chem. Res.*, **4**, 272(1971)

33. K.Wade, *Adv. Inorg. Chem. Radiochem.*, **18**, 1(1976)

34. (a) D.M.P.Mingos, *Chem. Soc. Rev.*, **15**, 31(1986)

(b) D.M.P.Mingos and R.L.Johnston, *Structure and Bonding*, **68**, 29(1987)

35. A.J.Stone, (a) *Mol. Phys.*, **41**, 1339(1980);

(b) *Inorg. Chem.*, **20**, 256(1981);

(c) *Polyhedron*, **3**, 1299(1984)

36. P.W.Fowler, *Polyhedron*, **4**, 2051(1985)

37. D.B.Redmond, C.M.Quinn and J.G.R.McKiernan, *J. Chem. Soc., Faraday Trans.* 2, **79**, 1971(1983)

38. R.L.Johnston and D.M.P.Mingos, *Polyhedron*, **5**, 2059(1986)

39. C.R.Eady, B.F.G.Johnson, J.Lewis, P.B.Hitchcock and K.M.Thomas, *J. Chem. Soc., Chem. Commun.*, 385(1977)

40. J.Bould, N.N.Greenwood, J.D.Kennedy and W.S.McDonald, *J. Chem. Soc., Chem. Commun.*, 465(1982)

41. R.L.Johnston and D.M.P.Mingos, *J. Organomet. Chem.*, **280**, 407(1985)

42. (a) D.M.P.Mingos and M.I.Forsyth, *J. Organomet. Chem.*, **146**, C37(1978)

(b) M.J.Calhorda, D.M.P.Mingos and A.J.Welch, *J. Organomet. Chem.*, **228**, 309(1982)

43. (a) D.M.P.Mingos, *J. Chem. Soc., Dalton Trans.*, 602(1977)

(b) D.M.P.Mingos, M.I.Forsyth and A.J.Welch, *J. Chem. Soc., Dalton Trans.*, 1363(1978)

44. W.Bunder and E.Weiss, *J. Organomet. Chem.*, **92**, 65(1975)

45. P.Seiler and J.D.Duaitz, *Acta. Cryst.*, **B36**, 2255(1980)

46. G.Huttner and S.Lange, *Acta. Cryst.*, **B28**, 2049(1972)